CHEMICAL BASIS OF DIESEL FUEL STABILIZATION BY TERTIARY ALKYL PRIMARY AMINES

Rajiv Banavali and Bharati Chheda,
Rohm and Haas Company,
Deer Park, Texas 77536

ABSTRACT

The oxidative degradation products, formed under both the prolonged storage and thermal stress, are a problem in the utilization of diesel fuels. There is a continued challenge in developing fuel stabilizers that are increasingly cost-effective, do not degrade the performance of fuel, and are environmentally acceptable. Our interest in highly branched tertiary alkyl primary amines(TAPA) has led to evidence that they are excellent stabilizers for diesel fuels. TAPA possess unique chemical and physical properties. We will present the results of stability experiments for thermal and oxidative degradation of several diesel fuels. The TAPA are evaluated in these stability tests in comparison with other well-known stabilizers. Chemical factors preventing formation of color, insoluble sediments and gums were studied by modeling generally accepted degradation mechanisms. In this paper we will report our mechanistic investigation into the chemical details of the stabilization and effect of the TAPA chemical structure on the activity. Data for acid scavenging, reduction of hydroperoxides, and solubilization/dispersancy mechanisms of stabilization is presented

INTRODUCTION

The oxidative degradation products, formed under both the prolonged storage and thermal stress, continue to be a problem in the utilization of diesel fuels. Fuel-instability reactions are defined in terms of the formation of deleterious products, such as filterable sediment, adherent gums, and peroxides. Sediments and gums which result from the oxidation reactions act to block filters and deposit on surfaces. There may be a relationship between the chemistry of deposit formation during normal long term storage and the deposits obtained by thermal stressing. Fuels containing higher amounts of olefins, certain nitrogen and sulfur compounds, organic acids, or dissolved metals are likely to degrade more and faster. Insolubles in diesel fuels are known to occur through several generally agreed mechanisms[1]. The sediment and gum formation mechanisms have been studied in great details[2,3] and can be summarized as: acid-base reactions involving N, O, and S species, free radical induced polymerization reactions involving unsaturated hydrocarbons, and esterification reactions involving aromatic and heterocyclic species. Previous studies have indicated that certain sulfonic acids[4], organic nitrogen compounds[5], and olefins[6], when added to fuels that are then subjected to thermal or oxidative stress, tend to produce insoluble sediments.

Stabilizing additives are often used to counteract the above mechanisms[2]. Several chemistries may contribute to fuel stabilization. Antioxidants act to inhibit the reactions that form sediment. Most additives control peroxide formation, but do not curb formation of polymerized gum products. Dispersants act to suspend any sediment particles that form and prevent them from agglomerating and becoming a problem. The stability enhancing additives for middle distillate fuels include hindered phenols, alkylated diphenylamines, phenylenediamines, tertiary amines, metal deactivators and dispersants. Amine additives are generally considered as antioxidants(aromatic amines) and to neutralize acidic impurities/by-products(tertiary amines). Tertiary amines are generally considered[2] better than secondary or primary amines as fuel antioxidants. Phenylenediamine type antioxidants are more effective than hindered phenols in neutralizing peroxides. It was found that traditional amine stabilizers fail to control peroxide formation adequately. Also, these amines, while being more effective than hindered phenols in gasoline, are not being used in diesel because they degrade distillate fuel stability[2b]. Recent work has implicated that widely used fuel stabilizers such as hindered phenols are ineffective in reducing sediment formation. Phenylenediamines have been shown to be detrimental in both high and low sulfur diesels, as they participate in side reactions forming sediments[2a] and increasing color body formation[2c]. Thus, a search for better stabilizers continues.

Primary amines are not considered as good radical or peroxide quenchers as secondary or tertiary amines. This is true for typical straight-chain fatty amines. However, we are mainly interested[7] in a special class of primary amines that possess branched alkyl chains with the primary amino group attached to a tertiary carbon[8]. We will refer to these as tertiary alkyl primary amines (TAPA). Branched tertiary alkyl primary amines possess excellent oil solubility[9], superior

thermal and oxidative stability[10], strong basicity, and fluidity over a wide temperature range(See Table I). These benefits find usage in lubricant applications[11] also. We have previously shown[12] that TAPA can be used as fuel stabilizers, and are better than several other common stabilizers. We will describe here the work carried out recently at Rohm and Haas research laboratories with TAPA for their ability to stabilize diesel fuels. An attempt is made to form an interpretation of stabilization mechanisms of TAPA by using stability test methods under various conditions.

EXPERIMENTAL

I. Fuel Samples And Additives: Fresh test samples of diesel fuel without any additives were obtained from commercial sources. The fuel samples were analyzed to ensure conformance with specifications and stored under ambient temperature, in dark, and under nitrogen atmosphere. All tests were started within a month of obtaining the fresh samples. All commercial additives used were as received without further purification. All the C_9, C_{12}, and C_{18} TAPA samples were commercial products sold under the trademark Primene by Rohm and Haas company. Chemicals used for the experimental studies were purchased from Aldrich Chemical Company. The antioxidants used for the experiments included N,N-dimethylcyclohexylamine, 2,6-di-t-butyl-4-methylphenol, N,N'-di-sec-butyl-p-phenylenediamine, and dinonyl diphenylamine. Organic acid co-dopants included dodecylbenzene sulfonic acid. Classes of nitrogen compounds employed included N,N-di-methylaniline, 4-dimethylaminopyridine, and 2,5-dimethylpyrrole. Co-dopants such as metals and t-butylhydroperoxide were also used.

II. Diesel Thermal Stability Tests: A modified Octel/Du Pont F21 test was used as follows. A 50 mL sample of fuel oil in a test tube is stored in a 300°F bath for 90 minutes (or 180 Min.). After removal from the bath it is allowed to cool to room temperature (about 2 hr.). The aged fuel is then filtered through 4.25 cm Whatman No 1 filter paper. The paper is then washed with heptane and the color of the filter paper is compared to a set of standards (1 = No color, 20 = dark brown). The data is given in Tables II and III. Thermal stability tests were also done by using pressurized differential scanning calorimetry.

III. Diesel Oxidation Stability Tests: A modified ASTM D2274 was used for oxidative stability tests as follows. A 350 mL sample of fuel is heated at 95°C for 16 hr. (or 40 hr.) while oxygen is bubbled through at the rate of 3 liters per hour. After aging, the sample is cooled to room temperature and filtered to obtain the filterable insoluble quantity. Adherent insolubles are then removed from the associated glassware with trisolvent (TAM). The TAM is then evaporated to obtain the adherent insolubles. The sum of filterable and adherent insolubles, expressed as milligrams per 100 mL, is reported as total insolubles. The data is given in Table V. In addition, oxidative stability was also measured by DSC experiments and by ASTM D942 test.

IV. Doping Studies: Various fuel samples were doped with precise amounts of additives(inhibitors, peroxides, acids, bases, etc.) The fuel stabilities were then measured as mentioned in the above experiments. In the case of hydroperoxide doping experiments, peroxide numbers were measured by the standard ASTM D3703 method. The results are calculated as milligrams per kilogram (ppm) of peroxide.

V. Solubility: Solubility experiments were carried out with salts of dodecylbenzenesulfonic acid with various basic nitrogen compounds such as 2,5-dimethylpyrrole, 4-dimethylaminopyridine, alkylated-phenylenediamines, and C_{12} TAPA. Solubility of the pure salts was then studied in diesel. The Kauri-butanol value (KB Value, ASTM D1133) was used as a measure of solvent power of TAPA. The KB was calculated by standardization with toluene (assigned KB of 105) and heptane-toluene (assigned KB of 40) blend.

RESULTS AND DISCUSSION

Oxidative and thermal stability of diesel fuels was studied on fuel samples collected from major regions around the world; namely, North America, Latin America, and Asia. The results of the various stability tests as measured by color, sediments and gum formation show clearly that addition of TAPA, at few ppm levels, significantly improves the stability of diesels. Tables II and III show that the thermal stability of both low and high sulfur diesel fuels can be improved by TAPA doping at 8-40 ppm range. It is noteworthy that both sedimentation and color are improved by TAPA. The results of oxidative stability of diesel showing the similar TAPA benefits were shown earlier[12]. Several commercial fuel stabilizers at the same dosage level show similar or worse performance. The data that TAPA are equal or better stabilizers is also seen in comparative experiments with several well-known fuel antioxidants. C_9 TAPA shows the best results for the low sulfur diesel when compared on equal weight basis with other stabilizers. Although diphenylamines improve the stability, hindered phenol was only slightly effective.

However, addition of pheneylenediamine degraded both the filter pad rating and color. The fuel oil stability results using the C_{12} TAPA in combination with a dispersant and/or a metal deactivator have shown that the performance over the TAPA alone is not significantly improved. The diesel data, in addition, shows the differences in activity of various TAPA additives. This data allows both dosage and structure-activity relationships establishment. The mechanism by which TAPA act as antioxidants is not completely understood, but an attempt is made here to form a general interpretation of their stabilization mechanisms. The mechanistic study here is done based on structure-activity relationship of TAPA coupled with results of stability tests under various conditions.

STRUCTURAL ATTRIBUTES OF TAPA

The feature of having a tertiary carbon attached to nitrogen is very beneficial because it imparts important characteristics[8] to these amines. Table 1 lists some of the key TAPA properties of value in diesel stabilization. TAPA with branched alkyl groups have low viscosity and are liquids at room temperature whereas most long chain linear amines are solids[9] at room temperature. Compared to linear alkyl primary amines the branched TAPA are readily soluble in fuel oils. In addition, these amines are also ashless and completely combustible. They are virtually insoluble in water and are not leached from fuels by contact with water during storage and handling. The fact that there are no α-hydrogens attached to nitrogen gives TAPA better oxidative stability because this weak C-H bond is most prone to oxidation. The lack of α-hydrogens also ensures that unstable imines are not formed which can deaminate in the presence of water. This makes TAPA oxidatively more stable than their corresponding linear amines. The oxidative stability of selected TAPA and their linear analogs were comparatively evaluated by DSC measurements[10]. In all cases the corresponding *n*-alkylamines decomposed before the TAPA indicating that the TAPA are oxidatively more stable than corresponding linear primary amines. Oxidation is the most common form of degradation of fuels. Hindered phenols and amines are commonly used as oxidation inhibitors and work by interrupting radical chain reactions. The chain carrying peroxy radical is scavenged by the phenol or amine by hydrogen atom donation. The resulting radicals are resonance stabilized and are eventually destroyed by reaction with another peroxy radical. Hindered amines, such as TAPA, can also react with free radicals to form stable intermediates that do not readily take part in chain reactions. Although they are not as resonance stabilized, they can regenerate by scavenging another hydrogen radical. A common test used to evaluate the antioxidant properties of additives involves heating base fluid in the presence of 0.5 - 1.0 % inhibitor at 120°C in an oxygen pressurized bomb and measuring the oxygen pressure drop as a function of time. We found[11] both C_{12} and C_{18} TAPA inhibited the oxidation of petroleum fluids. These TAPA proved similar to some commercially used phenolic and aminic antioxidants.

ACID SCAVENGING

Hazelett has shown[13] the correlation of carboxylic and sulfonic acids in increasing deposit formation. The reaction of certain acidic compounds, such as naphthalene sulfonic acid, with nitrogen compounds, such as indoles, quinolines, and carbazoles, appears to be one of the mechanisms for fuel insolubles formation. Dodecylbenzenesulfonic acid promotes[4] sediment formation and also may become incorporated into the sediment. Amine based stabilizers can react with acidic species preferentially. For weak acids, the amines exhibit more than 1:1 action and certain amines exert favorable behavior only if they are strong organic bases. TAPA are strong bases[14] and can readily react with acidic species, sacrificing themselves to form salts that are miscible in these liquids and thus do not precipitate. In salt formation, two TAPA attributes are very important. First, the high basicity exhibited by these amines, in non-polar media such as fuels, allows very efficient and complete scavenging of both strong and weak acids. Furthermore, the branched and hindered carbon chain of TAPA helps envelop the salt thereby better solvating it. We have recently done[14] pK_a measurements on these amines using both reaction calorimetry and quantum chemical estimates and find that TAPA are stronger bases than corresponding linear primary amines in non-polar solvents.

REDUCTION OF HYDROPEROXIDES

Sediments that form in diesel fuels are often the direct result of autoxidation reactions involving hydroperoxides[3]. Thus, increasing peroxide concentration is often an indicator of the instability. The peroxides can stimulate insolubles by two processes. One is by converting thiols and aldehydes to sulfonic and carboxylic acids which act as acid catalysts and sediment promoters. The second is by a free-radical mechanism, possibly by oligomerizing olefins and by addition of the thiyl radical to olefins. Induced decomposition of hydroperoxides can be catalyzed by metals, acids, and amines. The catalytic efficiency of the amines generally correlates with their ionization potentials. This correlation supports the mechanistic interpretation that a charge

transfer complex between the amine and the peroxide weakens the O-O bond. Quenching by amines is also subject to steric effects. Tertiary amines have been well-studied as hydroperoxide scavengers, but not much is known about TAPAs. However, oxidation of mercaptans in sour fuels to disulfides by organic hydroperoxides has been shown[15] to be catalyzed efficiently by C_{12} TAPA. We studied the effect of added hydroperoxide to the fuel by measuring both the oxidative stability and concentration of peroxides (See Table IV). As anticipated, addition of hydroperoxide greatly destabilizes the fuel by showing much higher amounts of gum and sediments than in the undoped sample. Also as expected, addition of 2, 5-dimethylpyrrole further increases the sediment formation. However, addition of TAPA greatly increases stability as measured by the reduction in sediment and also reduces the peroxide concentration. The effect of TAPA on reducing sediments is better than that shown by both the secondary and tertiary amines.

SOLUBILIZATION AND DISPERSANCY

For a good stabilizer, it is important not only to mitigate the oxidative process, but also to help resolve problems caused by them. Not only are the TAPAs soluble in base oil but many salts of oil insoluble organic and inorganic acids of these TAPA are completely miscible in base oil. We have studied[10] the solubility of several inorganic and organic salts of TAPA in kerosene and white mineral oil. For example the TAPA salts of EDTA, trichloroacetic acid, molybdic acid, tungstic acid, and sulfuric acid are readily soluble (>20%) in mineral oil compared to their free acid. TAPA can act by forming fuel soluble salts with acidic by-products of oxidation. Furthermore, their complexation with metals and other species can allow suspension of gums and particles. By keeping the sediment particles from agglomerating they can be kept small enough to be dispersed through the fuel filters. Molecular modeling shows that the resulting complexes can effectively shield the metal atoms thereby reducing their ability to catalyze degradative reactions. The role of TAPA in minimizing gums and sediment formation by "solvating ability" of the branched alkyl chains of TAPA is also likely. The high Kauri Butanol values measured are indicative of that. For the C_{18} TAPA the KB value of more than 119 compares well with that of only 30-35 seen for the diesel. The decreased sediment seen, in both the thermal and oxidative tests, is most likely in part due to better solvent properties[16]. To confirm this theory, we prepared salts of model acidic compounds(Dodecylbenzenesulfonic acid) with various amines. The pure salts were then tried to dissolve in diesel fuel at various levels. The results can be seen in Table V. It was noted that acid salts of TAPA were not solids, unlike other amine salts, and could be readily dissolved in the diesel. Furthermore, these salts had much lighter color than the salts prepared from phenylenediamines.

CONCLUSIONS

We have shown that deterioration is delayed, color degradation is inhibited and sludge formation is reduced by addition of TAPA to the diesel fuels. The tertiary alkyl primary amines are highly effective stabilizers for the prevention of sludge and color formation under both thermal and oxidative stress. Their performance is equal or better than many other commonly used fuel stabilizers. They inhibit the reactions responsible for sludge formation and also disperse the gum and sediment from depositing. The additive concentration and structure effect suggest that the stabilization properties of TAPA result from factors such as acid scavenging, hydroperoxide decomposition, dispersing of gums and particulates, or any combination of these factors. The several established fuel degradation mechanisms pathways can be prevented or resolved by the use of these amines.

ACKNOWLEDGMENTS

We would like to thank Rohm and Haas company for providing the support for this work and permission to publish the results.

REFERENCES

1) Beaver, B.; *Fuel Science And Technology Intl.*, **1991**, 9(10), 1287 and **1992**, 10(1), 1.

2) a)Batt, R. J.; Henry, C. P.; Whitesmith, P. R.; *Proceedings of the 5th International Conference on Long Term Storage Stability of Liquid Fuels*, **1995**; Eds.; Giles, H. N.; National Technical Information Service, Springfield, Va, Vol. 2, 761. b)Hazlett, R. N.; Hardy, D. R.; *NRL Letter Report 6180-832*, Naval Research Laboratory, Washington, DC, **1984**. c)Henry, C.; *Proceedings of the 2nd Intl Conf on Long Term Storage Stabilities of Liquid Fuels*, Stavinova, L.L.; Ed.; SWRI, San Antonio, TX; **1986**, p 807.

3) Mushrush, G. W.; Speight, J. G.; In *"Petroleum Products: Instability and Incompatibility"*, Taylor and Francis, Washington, DC; **1995**.

4) Wechter, M. A., Hardy, D. R., *Energy & Fuels*, **1996**, 10, 117.

5) Pedley, J. F., Hiley, R. W., Hancock, R. A., *Fuel*, **1989**, 68, 27.

6) Adiwar, Batts, B. D., *Proceedings of the 5th International Conference on Long Term Storage Stability of Liquid Fuels*, **1995**; Eds.; Giles, H. N.; National Technical Information Service, Springfield, Va, Vol. 2, 649.

7) These TAPA are commercially available from Rohm and Haas Company as Primene® Amines. The C-9 is available as Primene® BC-9, C-12 as Primene® 81-R and C-18 as Primene® JM-T.

8) Banavali, R.; Ellis, M. J.; Piccolini, R. J.; *Resin Review*, Rohm and Haas, Philadelphia, Pa, **1993**, XLIII, 1, 13.

9) Banavali, R.; Chheda, B.; In *International Symposium on Production and Application of Lube Base Stocks*, Singh, H.; Prasada Rao, T.S. R.; Eds.,Tata McGraw-Hill, New Delhi, **1994**; p 318.

10) Banavali, R.; Chheda, B.; Uhran, J.; *In 2nd Brazilian Symposium on Lubricants*, Instituto Brasileiro de Petroleo, **1995**, p 1.

11) Banavali, R.; Karki, S. B.; *Prepr. Pap.- Am. Chem. Soc. Div. Of Pet. Chem.*, **1997**, 42(1), p 232.

12) Banavali, R., Chheda, B., *Prepr. Pap -Am. Chem. Soc., Div. Fuel Chem.*, **1997**, 42(3), 784.

13) Hazlett, R. N.; *Fuel Science and Technology*, 6(2), 185, **1988**.

14) Rohm and Haas Research Laboratory Unpublished Data.

15) S. Wang, G. L. Roof, B.W. Porlier, Nalco Chemical Company, U. S. Patent #4,514,286,**1985**.

16) Westbrook, S. R., Stavinoha, L. L., Present, D. L., *Interim Report BFLRF No. 255*, Southwest Research Institute, San Antonio, TX, **1988**,

Table I. Tertiary Alkyl Primary Amine Properties

Property	TAPA C_9	TAPA C_{12}	TAPA C_{18}
Chemical name	t-nonylamines	t-dodecylamines	t-octadecylamines
Molecular Weight	143 (average)	185 (average)	269 (average)
Boiling Range (°C)	170-180	220-240	265-305
Pour point	-85°C/ -185°F	<-59°C/-74°F	<-40°C/-40°F
Base Strength (pKa)	11	11	11
Water solubility at 25°C	0.53%	1000 ppm maximum	900 ppm max
Kp (Water/Heptane)	0.00772	0.0036	0.0031
Surface tension at 20°C (dynes/cm^2, ASTM D-1331)	27	30	31
Interfacial Tension with water (dynes/cm^2, ASTM D 971)	1.5	2	8
Kauri-Butanol Value (ASTM-1133)	20	35	>119
Thermal Stability by DSC	>500°C	>500°C	>500°C

Table II. Thermal Stability Test Results Using Du Pont F-21 @ 150°C/90 Min.

Additives (ppm)	Diesel #1		Diesel #2		Diesel #3		Diesel #4	
Sulfur Content	0.24%		0.38%		0.56%		0.72%	
	Filter Pad Rating	ASTM Color	Filter Pad Rating	ASTM Color	Filter Pad Rating	ASTM Color	Filter Pad Rating	ASTM Color
None	11	2.5	16	5	16	6	18	5
TAPA C_{12} (8.5)	3	2	4	3.5	3	4	2	3
TAPA C_{12} (17)	2	2	2	3.5	4	3.5	2	2.5
TAPA C_{12}(35)	2	2	3	3	4	3	3	2.5
Commercial AO #1 (8.5)	5	2	2	3	6	4	4	3
Commercial AO #1 (17)	2	2	3	3.5	4	4	4	2.5
Commercial AO #1 (35)	2	2	2	3.5	2	3.5	5	2.5
Commercial AO #2 (8.5)	3	2	11	2	10	3.5	8	2
Commercial AO #2 (17)	3	2	10	2	7	3	8	2
Commercial AO #2 (35)	2	2	7	2	6	2.5	6	2

Table III. Thermal Stability Test Results of Using Du Pont F-21 test @ 150°C /180 Min.

Additives (ppm)	Diesel #5	
Sulfur Content	0.04%	
	Filter Pad Rating	ASTM Color
None	13	1.5
TAPA C_{12} (20)	9	1.5
TAPA C_9 (20)	10	1.5
2,6-di-t-butyl-4-methylphenol (20)	11	1.5
2,6-di-t-butyl-4-methylphenol (40)	12	2
N,N'-di-sec-butyl-p-phenylenediamine (20)	14	2.5
N,N'-di-sec-butyl-p-phenylenediamine (40)	14	2.5
Dinonyl diphenylamine (20)	9	2.5

Table IV Comparative Oxidation Stability (ASTM D2274 @ 40 hr) with Added Peroxide and Stabilizers

Diesel + additives *	Total Insolubles (mg/100 ml)	Peroxide, ppm (before 2274)	Peroxide, ppm (after 2274)
Blank	0.1	0.1	4.5
+ t-BHP	1	99.8	25.6
Dimethylpyrrole + t-BHP	57.6	58.6	2.3
Dimethylcyclohexylamine + t-BHP	1.5	>118	2
Dinonyl diphenylamine + t-BHP	0.6	92.8	5.3
N,N'-di-sec-butyl-p-phenylenediamine + t-BHP	5.4	97.7	8.7
TAPA C_9 + t-BHP	0	97.9	10.9
TAPA C_{12} + t-BHP	0.1	99.1	14
TAPA C_{18} + t-BHP	o	90.8	19

* For the doping experiments, following amounts were used: t-butylhydroperoxide at 100 ppm peroxide and stabilizer at 135 ppm Nitrogen concentration.

Table V. Solubility of Dodecylbenzene Sulfonic Acid Salts of Aminic Bases* in Diesel

Aminic Bases	0.1% in diesel	0.2% in diesel	0.5% in diesel	0.7% in diesel	Comments
TAPA C_{12}	Soluble	Soluble	Soluble	Soluble	The salt is a light colored gum
4-(dimethylamino)-pyridine (solid)	Soluble	Soluble	Soluble	Slightly soluble	The salt was made using diesel as a solvent, light colored paste, and foamy when mixed with diesel
2,5-Dimethylpyrrole	Not soluble	Not soluble	Not soluble	Not soluble	The salt was made using diesel as a solvent, dark colored gum
N,N'-di-sec-butyl-phenylenediamine	Not soluble	Not soluble	Not soluble	Not soluble	The salt was made using diesel, dark colored gum

* Salt was prepared by reacting Dodecylbenzene sulfonic acid and aminic bases at 1:1 equivalent ratio

EFFECT OF INCREASINGLY SEVERE HYDROTREATING ON STABILITY-RELATED PROPERTIES OF NO. 2 DIESEL FUEL

J. Andrew Waynick

Amoco Petroleum Products, 150 West Warrenville Road
Naperville, Illinois 60563-1460, USA

ABSTRACT

This paper reports the effect of increasingly severe hydrotreating on the compositional and stability-related properties of four No. 2 diesel fuels ranging in sulfur level from 222 ppm to 11 ppm. Denitrification was essentially complete when the fuel sulfur level had been reduced to 86 ppm. At 222 ppm sulfur (similar to current U.S. low sulfur diesel fuels), fewer multi-ring but similar total aromatics were present compared with the high sulfur feed. With further sulfur removal, total aromatics were reduced as well, due to removal of mono-ring aromatics. Storage stability was excellent for all four fuels. Hydroperoxide susceptibility appeared adequate to excellent under conditions similar to commercial transport and storage. Additional information concerning diesel fuel instability chemistry was also demonstrated.

INTRODUCTION

Before October 1993, No. 2 distillate fuel sold in the United States contained 0.2-0.4%(wt) sulfur. As of October 1993, No. 2 distillate fuel used for on-highway vehicles was required to have a sulfur level no greater than 0.05%(wt), i.e. 500 ppm(wt). This sulfur level reduction has been achieved by increasing the severity by which diesel fuel feedstocks are hydrotreated.

Limited early data indicated that such low sulfur diesel fuels would have improved storage stability,[1-3] i.e. form less sediment and dark-colored fuel-soluble materials. A more recent study verified this conclusion.[4]

A few studies have been published to date concerning the effect of hydrotreating on No. 2 diesel fuel peroxidation tendency.[7-8] The most significant and most recent study indicated that commercial U.S. low sulfur diesel fuels did have increased hydroperoxide susceptibility compared with commercial U.S. high sulfur diesel fuels under sufficiently accelerated conditions. However, no such tendency was observed under ordinary field conditions of fuel transport and storage.[4]

The primary objective of the work reported in this paper was to evaluate an already available set of four hydrotreated No. 2 diesel fuels made from the same feedstock. Since finished fuel sulfur levels began at 222 ppm and went as low as 11 ppm, trends in fuel properties as a function of hydrotreating severity could be examined. Resulting data could provide useful insight not possible by looking only at commercial U.S. low sulfur (LS) and high sulfur (HS) diesel fuels. Also, the data could provide important information for future U.S. diesel fuel production, which might be required to attain even lower sulfur levels

EXPERIMENTAL

Fuel Samples

Each of the four No. 2 diesel fuel samples used in this work was obtained by a two-stage hydrotreating of a highly aromatic feedstock having the following gross compositional properties as measured by mass spectrometry:

Aromatics, %(wt)	
Total	46.5
Mono	17.6
Di	23.5
Tri	2.9

Stage	First	Second
Catalyst	Co/Mo	Pt/Pd on Mol Sieve
Psig H2	500	900
lhsv	2.1	1.0
Temperature, °F	650	500-550
H2-Circulation Rate, scf/bbl	1,500	5,000

The samples were about one year old when testing began. During that year, they had been stored in clear, sealed glass bottles at ambient laboratory temperature.

Tests

The four additive-free fuel samples were tested for chemical composition and stability using the following procedures:

Chemical Composition

Total Sulfur by Dispersive X-Ray Fluorescence (ASTM D4294)
Total Nitrogen (ASTM D4629, modified)
Basic Nitrogen (ASTM D2896)
SMORS
Phenalenones
Aromatics by Mass Spectrometry

Stability

Oxidative Stability (ASTM D2274)
Nalco Pad Stability
Storage Stability (ASTM D4625)
40-Hour Stability
Initial Peroxide Number (ASTM D3703)
Peroxide Number after ASTM D4625 (ASTM D3703)
Hydroperoxide Potential, CRC Procedure
Hydroperoxide Potential, Oxygen Overpressure (OP) Procedure

The ASTM procedures are well documented and will not be described further here. The Nalco Pad stability procedure measures thermal stability and has been described elsewhere.[5] ASTM D2274 and the Nalco Pad test are known not to correlate with real storage stability. However, they were included since they continue to be used as specification tests by many diesel fuel marketers and customers. The 40-Hour Stability test is a procedure developed and used by Amoco Oil Company and has been shown to correlate well with the reliable ASTM D4625. During this test, a 350 ml sample of distillate fuel is stressed at 80°C for 40 hours in a mineral oil bath while oxygen is bubbled through the sample at a rate of 3 liters/hour. The sample is then removed from the oil bath and allowed to cool for two hours in the dark. After determining the final color, the sample is diluted to 1, 225 ml with N-pentane, mixed thoroughly, and filtered through a tared 0.8 micron filter. After rinsing with N-pentane, the filter is dried and weighed to determine the total insolubles. Initial Peroxide Number should actually be regarded as a Peroxide Potential (susceptibility) test with a one year, ambient temperature storage period. The CRC Hydroperoxide Potential procedure was originally developed for jet fuels[6] and involves heating a 100 ml fuel sample at 65°C and 1 atmosphere air for four weeks. Peroxide number is then determined as an indication of the fuel's hydroperoxide susceptibility. The OP procedure for hydroperoxide potential was adapted from previously documented work involving jet fuels.[7] The procedure involves heating a 50 ml fuel sample at 100°C and 690 kPa (100 psia O2) for 24 hours. The peroxide number is then determined. The modification to the total nitrogen procedure was that the fuel sample was delivered to the combustion tube by a platinum boat rather than by standard syringe injection. SMORS (soluble macromolecular oxidatively reactive species) are believed to be sediment precursors, and the procedure for measuring them has been previously documented.[8] Phenalenones are believed to be SMORS and sediment precursors, and the analytical method for measuring them was based on a previously reported procedure.[9]

RESULTS AND DISCUSSION

Chemical Composition

Chemical composition test results are given in Table I. Total and basic nitrogen levels dropped significantly as the fuel was hydrotreated from 222 ppm to 86 ppm sulfur. Further reductions in sulfur did not result in much further decrease in nitrogen levels. No phenalenones were detected in any of the four hydrotreated diesel fuels. Since phenalenones are formed by the facile oxidation of phenalene, this indicates that the hydrotreating process was probably severe enough to reduce all phenalenes that may have been present in the original feed. Only the 222 ppm sulfur fuel had a high level of SMORS. The other three fuels had SMORS that were similar to the mean values of both LS and HS commercial U.S. diesel fuels.[4] This indicates that by hydrotreating the feed to 86 ppm sulfur, SMORS precursors were nearly removed. Since phenalenones are believed to be SMORS precursors, the absence of phenalenones and the high SMORS level in the 222 ppm sulfur fuel is interesting. It implies that either phenalenones initially present in the feed were not removed by hydrotreating and then completely reacted to form SMORS during the one year storage, or else the SMORS formed in the 222 ppm sulfur fuel were formed from precursors other than phenalenones. As will be shown in the subsequent section on stability, the latter explanation is the more likely one.

Gross hydrocarbon analysis indicated that the main change in going from the feed to the 222 ppm sulfur fuel was to reduce polycyclic aromatics to monocyclic aromatics, with no overall reduction in aromatic content. This is consistent with earlier U.S. commercial diesel fuel survey data.[4] However, as hydrotreating became progressively severe, both poly- and mono-cyclic aromatics significantly decreased.

Stability

Stability test results are given in Table II. All four samples showed excellent thermal and storage stability. As sulfur level decreased, overall results remained constant.

SMORS measured on the filtered samples after D4625 storage showed a decreasing trend with decreasing sulfur level. Only the 222 ppm sulfur and 86 ppm sulfur fuels developed significant additional SMORS relative to the amounts initially present. The 222 ppm sulfur fuel developed a quite high level of SMORS. Since all four fuels prior to D4625 testing contained no measurable phenalenones, the SMORS developed during D4625 testing must have been formed from other precursors. Also, since ASTM color did not darken much during D4625 testing, the SMORS formed must not have been very dark. This is in contrast to HS diesel fuel, where previous work indicates that SMORS contribute to aged color formation[4] and can correlate to aged sediment formation.[10] The major implication of this result is that SMORS formed in LS diesel fuel are different from SMORS formed in HS diesel fuel. In fact, the SMORS formed in HS diesel fuel may include a wide range of compounds beyond the indolyl phenalenes and indolyl phenalenones typically suggested in the literature.[11] This wide range of compounds may include some of the SMORS formed in LS diesel fuels. Although not published, some of these conclusions concerning the diversity of SMORS in diesel fuel have been suggested by one of the researchers who first discovered SMORS.[12]

Hydroperoxide susceptibility of the four progressively hydrotreated fuels was profiled by measuring the peroxide number developed after four increasingly severe storage conditions. Based on the one year ambient data, it appears that "real world" hydroperoxide susceptibility of U.S. LS diesel fuel will improve as sulfur levels are further reduced beyond the current typical levels. Although the 7 meq O/Kg value for the 222 ppm sulfur fuel is within the "problem" range cited in prior jet fuel literature, it is unlikely that much on-highway diesel fuel will be stored for one year. Previous data indicated that commercial U.S. LS fuel (with similar sulfur levels) gave negligible levels of hydroperoxides.[4] Those fuels represented what the end user would likely receive. Whatever level of hydroperoxide stability exists in today's LS diesel fuel, further reductions in required sulfur levels should improve that stability.

Looking at the entire peroxide number data, an interesting trend can be seen. As test storage conditions increased in severity, the maximum peroxide number observed among the four fuels shifted towards lower sulfur diesel fuel. For instance, the initial peroxide number (after one year storage in the laboratory) showed the highest level in the 222 ppm sulfur fuel. A similar pattern was observed for peroxides measured after D4625 storage (43°C, 13 weeks, 1 atm. air), although overall values after D4625 were higher than the initial values. However, after the even more severe CRC conditions (65°C, 4 weeks, 1 atm air), the maximum peroxide level shifted towards the 86 ppm sulfur fuel. After the most severe OP storage condition (100°C, 24 hours, 690 kPa O2), the maximum peroxide number was observed in the 39 ppm sulfur fuel, with much lower values for the other three fuels. These test results can be best understood by remembering that a fuel's peroxide number reflects the difference between the rates of two processes: hydroperoxide formation and hydroperoxide decomposition. Factors promoting hydroperoxide formation are apparently more important under the less severe test storage conditions. One such factor is the concentration of compounds most prone to hydroperoxide formation. As indicated previously,[4] compounds containing benzylic carbon are among the most prone to hydroperoxide formation. As poly-cyclic aromatics are reduced to mono-cyclic aromatics with total aromatic content remaining constant, benzylic carbon content increases. This fact has been proposed as a primary reason why hydroperoxide susceptibility under accelerated conditions is greater in commercial LS diesel fuels compared with HS diesel fuels.[4] However, when hydrotreating is severe enough to reduce all aromatic species, benzylic carbon content will decrease, replaced by carbons less susceptible to hydroperoxide formation. This would explain why peroxide number decreased under lower test severity as the fuel was more severely hydrotreated.

However, as test storage conditions become more severe, factors promoting hydroperoxide decomposition apparently become more important for the less hydrotreated diesel fuels. One factor that may contribute to this effect is the concentration of naturally occurring hydroperoxide decomposers in the fuels. These compounds are removed as the fuel is progressively

hydrotreated. So, at higher test severity, hydroperoxide decomposition by naturally occurring hydroperoxide decomposers will be greater in the less hydrotreated diesel fuels. Also, there is some evidence that benzylic hydroperoxides are somewhat less kinetically stable compared with non-aromatic hydroperoxides. If so, this would also tend to increase the rate of hydroperoxide decomposition in the less hydrotreated diesel fuels.

More data will be required to fully explain how these and other factors contribute to the peroxide number trends evident in the Table II data.

It is interesting to note that the most severely hydrotreated diesel fuel (11 ppm sulfur) gave only about 0.5 meq O/Kg for all test storage conditions. Without further analysis for final oxidation products, it can only be concluded that for that fuel the rates of hydroperoxide formation and decomposition were nearly equal under all test storage conditions.

CONCLUSIONS

The work reported in this paper supports the following conclusions:

1. Current U.S. commercial LS diesel fuel has less multi-ring aromatics than HS diesel fuel, but similar total aromatic levels. With further hydrotreating, total aromatics are reduced as well, due to removal of mono-ring aromatics.

2. As diesel fuels are hydrotreated to and beyond current U.S. commercial LS diesel fuel sulfur levels, storage stability remains excellent.

3. As diesel fuels are hydrotreated to current U.S. commercial LS diesel fuel sulfur levels, hydroperoxide susceptibility remains acceptable under normal conditions of commercial transport and storage. As diesel fuels are further hydrotreated, hydroperoxide susceptibility under those same conditions should improve.

4. SMORS in non-additized LS diesel fuel do not significantly contribute to color darkening. Neither are they sediment precursors. LS diesel fuel SMORS are either chemically distinct from HS diesel fuel SMORS, or they are an innocuous subset of HS diesel fuel SMORS.

ACKNOWLEDGMENTS

The contributions of the following people are gratefully acknowledged: Simon Kukes for providing the diesel fuel samples and the processing conditions used to generate them; Al Novak for providing some of the analytical data on the initial feed and resulting fuels; Susan Taskila for running many of the laboratory tests; Don Porter for graphically treating the data.

REFERENCES

(1) Palmer, L. D.; Copson, J. A. "Hydrotreatment of Light Cycle Oil for Stabilization of Automotive Diesel Fuel"; Proceedings of 2nd International Conference on Long-Term Storage Stabilities of Liquid Fuels, San Antonio, Texas, July 1986.

(2) Martin, B.; Bocard, C.; Durand, J. P.; Bigeard, P. H.; Denis, J.; Dorbon, M.; Bernasconi, C. "Long-Term Storage Stability of Diesel Fuels: Effect of Aging on Injector Fouling; Stabilization by Additives or Hydrotreating"; presented at SAE Fuels and Lubes meeting, Tulsa, Oklahoma, 1990.

(3) Vardi, J.; Kraus, B. J. "Peroxide Formation in Low Sulfur Automotive Diesel Fuels"; SAE Paper No. 920826, 1992.

(4) Waynick, J. A.; Taskila, S. M. "A Comparison of Low and High Sulfur Middle Distillate Fuels in the United States"; Proceedings of the 5th International Conference on Stability and Handling of Liquid Fuels; Rotterdam, the Netherlands, October 1994.

(5) Waynick, J. A. "Evaluation of Commercial Stability Additives in Middle Distillate Fuels"; Proceedings of the 5th International Conference on Stability and Handling of Liquid Fuels; Rotterdam, the Netherlands, October 1994.

(6) Determination of the Hydroperoxide Potential Jet Fuels, CRC Report No. 559, April, 1988.

(7) Black, B. H.; Hardy, D. R. "Comparison of Jet Fuel Phenolic Antioxidants Using A Serial Dilution Technique"; Proceedings of the 4th International Conference on Stability and Handling of Liquid Fuels, Orlando, Florida, November 1991.

(8) Hardy, D. R.; Wechter, M. A. "What Are Soluble Macromolecular Oxidatively Reactive Species (SMORS)?"; ACS National Meeting, Washington, D.C., August 1990.

(9) Marshman, S. J. "Liquid Chromatographic Determination of Phenalenones in Middle Distillate Fuels"; *Fuel* 1990, 69, pp 1558-1560.

(10) Wechter, M. A.; Hardy, D. R. "The Use of Macromolecular Oxidatively Reactive Species (SMORS) to Predict Storage Stability of Mid-Distillate Diesel Fuels"; Proceedings of the 4th International Conference on Stability and Handling of Liquid Fuels, Orlando, Florida, November 1991.

(11) Malhotra, R. "Field Ionization Mass Spectrometric Analysis of Sediments: Chemistry of Insolubles Formation"; Proceedings of the 4th International conference on Stability and Handling of Liquid Fuels; Orlando, Florida, November 1991.

(12) Personal communication with M. A. Wechter, Rotterdam, the Netherlands, October 6, 1994.

TABLE I

CHEMICAL COMPOSITION

Sulfur, ppm (wt)	222	86	39	11
Total Nitrogen, ppm (wt)	75	8	4	<1
Basic Nitrogen, ppm (wt)	12	<5	<5	<5
SMORS, mg/100 ml	2.5	0.4	0.4	0.2
Phenalenones, ppm (wt)	ND[1]	ND[1]	ND[1]	ND[1]
Aromatics by Mass Spec., % (wt)				
Total	53	28	13	7.2
Mono-cyclic	43	24	11	5.3
Di-cyclic	9.7	3.3	1.1	0.8
Tri-cyclic	0.6	0.7	0.9	1.0

[1] Not detected

TABLE II

STABILITY

Sulfur, ppm (wt)	222	86	39	11
Initial Color, ASTM[1]	<1.5	-6[2]	-16[2]	<1.0
Stability, D2274				
Total Insolubles, mg/100 ml	0.2	0.1	0.0	0.0
Final Color, ASTM	<2.0	<0.5	<0.5	<1.0
Nalco Pad Rating	1	1	1	1
40-Hour Stability				
Total Insolubles, mg/100 ml	0.4	0.1	0.0	0.0
Final Color, ASTM	<1.5	-6[2]	-16[2]	<1.0
Stability, D4625				
Total Insolubles, mg/100 ml	0.3	0.2	0.2	0.2
Final Color, ASTM	<2.0	<0.5	0.5	<1.0
SMORS, mg/100 ml				
Initial[3]	2.5	0.4	0.2	0.2
After D4625	11.0	1.0	0.4	0.3
Hydroperoxide Potential, meq O/Kg				
Initial[3]	7.6	1.7	0.43	0.50
After D4625	193	24	1.4	0.55
CRC[4]	26	28	2.0	0.43
OP[5]	1.3	21	199	0.68

[1] ASTM D1500 except where noted
[2] Saybolt color
[3] Measured on fuels after 1 year ambient laboratory temperature storage
[4] CRC Hydroperoxide Potential Method as described in EXPERIMENTAL section
[5] OxygenOverpressure Method as described in EXPERIMENTAL section

EFFECT OF HYDROTREATING ON THE STABILITY OF SYNTHETIC CRUDE FROM WESTERN CANADA

P. Rahimi and C. Fairbridge, National Centre for Upgrading Technology, 1 Oil Patch Drive, Suite A-202, Devon, Alberta, CANADA, T9G 1A8

M. Oballa, C. Wong and A. Somogyvari, NOVA Research and Technology Corporation,2928-16th Street N.E., Calgary, Alberta, CANADA, T2E 7K7

Keywords : hydrocracking, distillates, hydrotreating, colour, storage stability

ABSTRACT

The storage stability of distillates from the hydrocracking of Western Canadian bitumen atmospheric residue was studied over 60 days. naphtha-jet and gas oil fractions of the hydrocracked distillates were shown to be unstable with respect to the formation of existent gum, total insoluble materials and asphaltene. The storage stability was significantly improved when these two fractions were mildly hydrotreated. The data were used to generate correlations that predict the stability of synthetic crudes.

INTRODUCTION

The refining industry in North America is consistently moving towards the utilization of heavier feedstocks for the production of synthetic crude. Current production of synthetic crude oil from oil sands and heavy oils is achieved by hydrogen addition as well as carbon rejection technologies. The primary products from these heavy feedstocks require different degrees of hydrotreating to obtain transportation fuels that meet current specifications. The hydroprocessing of bituminous materials and residues results in coke deposition on the catalyst as well as sludge formation in the product oil [1]. The products obtained are rather unstable, generally described as storage instability. Storage stability of hydrocarbon fuels therefore refers to their tendency to produce coloured species, soluble gums, and insoluble sediment during storage [2]. The storage and thermal stability of liquid stocks, especially diesel and jet fuel, have been topics of intense study especially by the military [3, 4]. To our knowledge, there has been very little study on the stability of hydrocracked products from the residues of Canadian heavy oils or the synthetic crude so blended after hydrotreating the hydrocracked distillate fractions.

The objective of the study was to quantify the rate of deterioration of the hydrocracked material and the hydrotreated distillates in terms of colour change and formation of soluble gums and insoluble materials, as well as to establish the presence or absence of the precursors to instability in the liquid fractions.

EXPERIMENTAL

The feedstock for this study was 50/50 Cold Lake/Llyodminster atmospheric residue (399°C +). The hydrocracking of the residue to distillate fractions was performed on a commercial $NiMo/Al_2O_3$ catalyst using a continuous bench scale stirred tank reactor. The experiments were carried out using the following conditions: Pressure < 20,685 kPa, temperature < 450°C and LHSV < 1 h^{-1}. The catalyst was presulphided and conditioned for 120 hours. To obtain the required amount of distillate products the experiment was continued for another 16 hours. The product samples had to be analyzed as soon as they were generated and distilled to give the fractions required for further processing (hydrotreating) or analysis. Distillation of the hydrocracked materials was carried out in order to obtain fractions which were tested for storage and colour stability and further characterized to identify materials causing instability. The hydrocracked materials were distilled into naphtha, jet-fuel, diesel, gas oil and Residue. The naphtha and jet-fuel fractions were analyzed for both colour and storage stability and then combined as feedstock for hydrotreating. Similarly, diesel and gas oil fractions were analyzed for colour and storage stability and then combined as feedstock for hydrotreating. The catalysts used for naphtha-jet and diesel-gas oil hydrotreating experiments were C-411 and C-424 catalysts respectively. Detailed experimental procedures and equipment are described elsewhere [5].

Analytical Methods and Analyses of Samples

Specific gravities were determined in triplicate at 15.5°C on a Paar DMA 48 instrument. Dynamic viscosities were determined in triplicate at 40°C using a Brookfield DV II instrument. Heptane insoluble asphaltenes were determined using the method of Pearson et.al. [6]. Existent gum was determined by the jet evaporation technique according to ASTM D 381-86. Hydrocarbon-types were determined in low boiling (IBP-249°C) distillates by the fluorescent indicator adsorption

method according to ASTM D 1319-77 and gave the volume percent of saturates, olefins and aromatics. The aniline point of the various distillate fractions was determined according to ASTM D 611-82. Bromine Numbers were determined according to procedures in ASTM D 1159-82. Carbon, hydrogen and nitrogen were determined using a CHN Analyzer. Trace nitrogen was determined on an Antek 771 pyroanalyzer coupled to an Antek chemiluminiscent nitrogen detector. Basic nitrogen was determined according to procedures outlined in UOP Method 269-70T. Sulfur was determined on a Leco SC-132 sulfur analyzer. The colour of the petroleum products was determined by the Lovibond Tintometer method as described in IP 17/52. The oxidation stability of middle distillate fractions was determined according to ASTM D 2274-88 and these procedures have been found useful for estimating the storage stability of distillate fuels boiling between 175 and 370°C. The procedures in ASTM D 4625-87 were followed for the prediction of storage stability. Hydrocarbon-type analyses on the liquid samples were performed using a modified ASTM D 2007-75 and ASTM D 2579-78 procedures. The saturates and the aromatic fractions were analyzed by low resolution mass spectrometry by modifications to procedures in ASTM D 3239 and ASTM D 2786-71. The polars fraction, which contained mostly nitrogen heterocycles, was similarly analyzed via high resolution mass spectrometry.

RESULTS AND DISCUSSION

Effect of Hydrocracking:

The hydrocracking of the feedstock resulted in a 66.7% conversion of material boiling above 524°C (Table 1). The asphaltene content which is more or less a measure of the hydrogen deficiency of an oil was reduced to one third of its original value after hdrocracking and mainly remained in the 524°C+ fraction. The increase in the hydrogen to carbon ratio after hydrocracking was synonymous with the decrease in the asphaltene content. The viscosity and density of the hydrocracked materials decreased as expected. Of particular interest is the ratio of non-basic nitrogen to basic nitrogen in the hydrocracked sample. Some nitrogen compounds have been known to contribute to fuel instability, while others are inert. As shown in Table 1 hydrocracking reduced the total nitrogen in the feed, but the basic nitrogen increased.

Effect of Hydrotreating :

The hydrotreating was carried out on the naphtha-jet fuel fraction as well as on the diesel-gas oil fraction. For simplicity, these hydrotreated fractions are referred to as hydrotreated naphtha-jet and hydrotreated Gas Oil respectively. The hydrotreating step not only removed the heteroatoms (S, N, O), but also refined and stabilized the products. Sulfur was released in the form of H_2S, nitrogen in the form of NH_3, and oxygen in the form of H_2O. The following tests were performed to determine the effect of hydrotreating on the stability of different distillate fractions.

Stability Tests:

Total Insolubles: The oxidation stability results performed on naphtha-jet fraction are shown in Table 1. The data indicate that the total insolubles were much higher in the unhydrotreated material than in the hydrotreated samples. This data confirmed that hydrotreating stabilized the reactive hydrocarbons thereby rendering them less reactive than they otherwise would have been. The effects of hydrotreating on the long term storage stability of different fractions are shown in Table 2 and Table 3. In the unhydrotreated naphtha jet fraction, after 60 days of storage time, the total insolubles increased from 0.03 to 19.2 mg/100ml whereas in the hydrotreated sample, the total insolubles were at 0.25 mg/100 ml after storage for 60 days. In the unhydrotreated gas oil fraction, the total insolubles were 15.9 mg/100 ml after 60 days of storage, while for the hydrotreated sample, the total insolubles were only at 3.6 mg/100 ml after 60 days of storage.

Existent Gum: It is generally believed that the products of initial oxidation, probably peroxides, catalyze the oxidation of normally less reactive hydrocarbons to increase the rate of gum formation. Most of the oxidation products are said to be soluble in naphtha but decompose during evaporation to give gum that is largely composed of acidic material. Some of the studies show a correlation between gum content and total nitrogen content, while in other studies the gum content is said to increase with boiling range. The results in Tables 2 show that the existent gum in the naphtha-jet fraction decreased from 8.8 mg/100 ml before hydrotreating to zero after hydrotreating. After storage of the unhydrotreated fraction for 60 days, the existent gum was 142 mg/100 ml as opposed to a hydrotreated sample stored for the same 60 days which had 0.80 mg/100 ml. Undoubtedly, hydrotreating affects the existent gum content of naphtha -jet fractions.

Colour : The results of the colour test are shown in Table 1. Colour is one of the most distinguishing characteristics of untreated hydrocracked distillates. On distillation after hydrocracking, the naphtha-jet fraction is from clear to pale yellow. However, when exposed to

ordinary room conditions, this hydrocracked fraction will start to darken and also to deposit gum. Colour change is therefore indicative of the aging of the sample. The naphtha-jet fraction before hydrotreating had a colour number of 0.5 to 1.0 and after hydrotreating the colour number was reduced to zero. The gas oil fraction had a colour number of 3.5 to 4.5 before hydrotreating and after hydrotreating the colour number was reduced to 1.5 to 2.

Viscosity : The viscosity of the fractions (Table 2 and 3) is influenced more by storage time than by hydrotreating. Both the naphtha-jet and the gas oil fractions showed an increase in viscosity with storage time.

Aniline Point : There is an inverse relationship between aniline point and aromatic content. Aniline Point is usually increased slightly with the molecular weight and boiling point of a sample, and rapidly with the paraffinicity of oil samples. The higher aniline point value denotes a lower aromatic content and a higher paraffin content. Tables 2 and 3 show a higher aniline content after hydrotreating for both the naphtha -jet and the gas oil fractions. In Table 4, the analyses for paraffins and aromatics confirm the above conclusions. Overall, the monocycloparaffins are being converted to dicycloparaffins, leaving a decrease in the paraffinic content after aging. Both the mono- and di-aromatic constituents of the distillates increased at the expense of the paraffinic components, which suggests that saturated paraffinic components undergo some form of condensation with aromatic constituents.

SUMMARY:

The work presented here was undertaken to address the issue of the storage stability of middle distillates obtained from Western Canadian heavy oil/bitumen. Fuel stability is the general resistance of a fuel to change. Two types of stability were investigated. The first was storage stability, which reckons the ability of the fuel to stay in storage for a long period of time with little deterioration. The second was thermal stability which is the ability of the fuel to resist with little deterioration high temperature stress for a short period. The study results show that the deterioration of the fuel through storage manifested itself in colour change, development of soluble and insoluble gum, and changes in the physical and chemical properties of the fuel, like viscosity, density, nitrogen, sulfur, aromatics and asphaltene content. The results obtained also suggest that hydrocracked or thermally cracked materials should be hydrotreated/processed as quickly as possible. The detail hydrocarbon-type analyses of different fractions before and after hydrotreating showed that hydrotreating reduced refractory materials, including polar compounds, that cause storage instability.

ACKNOWLEDGEMENT :

Our thanks go to the management of NCUT and NOVA Research & Technology Corporation for financing the project and publication of the paper.

REFERENCES

1- M. F. Symoniak and A. C. Frost, Oil & Gas Journal, Mar. 17, 1971, 76.
2- J. Ritchie, J. Inst. Petr., 1965, Vol. 51, 296.
3- O. K. Bahn, D.W. Brinkman, J.B. Green and B. Carley, Fuel, 1987, Vol. 66, 1200.
4- J. V. Cooney, E. J. Beal, M.A. Wechter, G. W. Mushrush and R. N. Hazlett, Preprints, Petroleum Chemistry Division, 1984, Vol. 29, 1003.
5- M.C. Oballa, C. Wong and A. Somogyvari, "Colour and Storage Stability of Synthetic Crudes & Distillates", Final Report, for Energy Mines and Resources Canada, 1992, SCC File No : 06SQ.23440-1-9014
6- C.D. Pearson, G.S. Huff and S.G. Garfeh, Anal-Chem., 1986, Vol. 58, 3265

TABLE 1: COLOUR AND STORAGE STABILITY OF SAMPLES

	FSTK[1]	HC[2]	IBP-249	249-524	After Hydrotreating	
					IBP-249	249-524
Asphaltene Content (wt%)	15.86	5.31	0.02	0.06	0.02	0.05
Viscosity @ 40 deg C (cP)	8.75E+05	22.4	0.69	24.1	0.88	11.4
Density @ 15.5 deg C (g/cc)	1.0266	0.9292	0.7934	0.9295	0.7822	0.889
API Gravity (API)	6.33	20.78	46.85	20.73	49.40	27.67
Sludge (wt%)	-	0.74	-	0	-	0
Bromine No. (mg Br/100 g)	-	17.3	-	10.7	-	1.2
Hydrocarbon Types by FIA						
Aromatics (Vol.%)	-	-	21.1	-	3.4	-
Saturates (Vol. %)	-	-	75.5	-	95.4	-
Olefin (Vol.%)	-	-	3.4	-	1.2	-
Aromatics by Mass Spec.	-	-	-	-	-	-
Colour						
IBP - 177 C	-	-	0-0.5		0	
177 - 249 C	-	-	0.5-1.0		[IBP 249]	
249 - 343 C	-	-	-	3-3.5		1.5-2.0
343 - 524 C	-	-	-	4.5-5		[249-524]
Aniline Point (deg C)	-	-	46.7	61.8	63.4	74.5
Elemental Analysis						
Total Nitrogen (wt%)	0.546	0.410	0.104	0.291	<1 ppm	146ppm
Basic Nitrogen (wt%)	0.117	0.129	0.088	0.125	<1 ppm	25ppm
Non-Basic Nitrogen (wt%)	0.429	0.281	0.016	0.166	<1 ppm	121ppm
C (wt%)	83.15	86.66	85.00	87.14	85.17	87.07
H (wt%)	10.36	12.33	13.03	11.08	13.84	12.50
S (wt%)	5.231	1.043	0.488	1.402	144 ppm	800ppm
H/C Ratio (Atomic)	1.49	1.70	1.83	1.52	1.94	1.71
Oxidation Stability						
Filterable Insolubles (mg/100ml)	-	-	3.23	-	0.11	-
Adherent Insolubles (mg/100ml)	-	-	6.00	-	0.03	-
Total Insolubles (mg/100ml)	-	-	9.23	-	0.14	-
Existent Gum (mg/100ml)	-	-	8.8	-	0	-
Simulated Distillation (wt%)						
IBP - 177 C	0	7.60	40.00	0	44.00	2.50
177 - 249 C	0	8.80	52.50	0.80	48.50	4.30
249 - 343 C	0.50	17.00	6.80	27.50	6.00	34.50
343 - 524 C	32.00	44.10	0.70	69.30	1.30	58.70
524 C+	67.50	22.50	0.00	2.40	0.20	0

(1) Feedstock
(2) Hydrocracked product

TABLE 2 - NAPHTHA-JET FUEL FRACTION - EFFECT OF HYDROTREATING ON STORAGE STABILITY

PROPERTIES	IBP - 249 °C Unhydrotreated		IBP - 249°C Hydrotreated	
	At Time 0	After 60 days storage	At Time 0	After 60 days storage
Aniline Point [°C]	46.7	47	63.4	64.2
Viscosity [CP @ 40°C]	0.69	1.22	0.88	1.03
Asphaltene Content [wt%]	0.02	0.20	0.02	0.14
Existent Gum [mg/100ml]	8.8	142	0	0.80
Storage Stability [mg/100ml]				
Filterable Insolubles	0.03	0.90	0	0.14
Adherent Insolubles	0	18.30	0	0.11
Total Insolubles	0.03	19.20	0	0.25

TABLE 3 - DIESEL - GAS OIL FRACTION - EFFECT OF HYDROTREATING ON STORAGE STABILITY

PROPERTIES	249 - 524°C Unhydrotreated		249 - 524°C Hydrotreated	
	At Time 0	After 60 days storage	At Time 0	After 60 days storage
Aniline Point [°C]	61.8	61.7	74.5	74.6
Viscosity [CP @ 40°C]	24.1	28.3	11.4	14.5
Asphaltene Content [wt%]	0.06	0.25	0.05	0.23
Storage Stability [mg/100ml]				
Filterable Insolubles	0.20	15.33	0.11	3.31
Adherent Insolubles	0	0.63	0	0.29
Total Insolubles	0.20	15.96	0.11	3.60

TABLE 4 - MASS SPECTROMETRY ANALYSIS RESULTS OF THE HYDROCRACKED SAMPLES

HYDROCARBON	NAP-JET Before Storage (wt%)	NAP-JET After Storage (wt%)	GAS-OIL Before Storage (wt%)	GAS-OIL After Storage (wt%)	HT* GAS-OIL Before Storage (wt%)	HT* GAS-OIL After Storage (wt%)
Paraffins	36.40	32.52	17.15	17.17	22.23	19.02
Cycloparaffins	39.93	39.97	29.10	29.18	46.36	47.45
Monoaromatics	22.46	24.78	29.22	27.23	25.72	25.80
Diaromatics	0.73	1.14	14.92	15.14	3.74	4.82
Triaromatics	0	0	2.29	2.52	0.36	0.55
Tetraaromatics	0	0	0	0	0	0
Pentaaromatics	0	0	0.43	0.32	0.24	0.25
Unidentified	0	0	0.03	0.01	0	0
Aromatic Sulfur	0.03	0.43	2.97	3.35	0.97	1.56
Polar Compounds	0.45	1.16	3.89	5.08	0.38	0.55

* Hydrotreated

A COMPARISON OF LOW AND HIGH SULFUR MIDDLE DISTILLATE FUELS IN THE UNITED STATES

J. Andrew Waynick
Amoco Petroleum Products
150 West Warrenville Road
Naperville, Illinois 60563-8460

ABSTRACT

Sixty-nine low sulfur (LS) and twenty-six high sulfur (HS) No. 2 diesel fuel samples were collected from twenty-four marketers throughout the United States in early 1994. Fuel samples were tested for chemical composition and stability. Statistical analysis of the data indicated that other than sulfur and nitrogen levels, the main compositional difference between LS and HS diesel fuels was a partial saturation of poly-aromatics to mono-aromatics in LS fuel. Storage stability via ASTM D4625 was improved in LS fuels compared to HS fuels. Hydroperoxide susceptibility of LS and HS fuels was equivalent and acceptable under conditions of ambient fuel transport and storage. However, under progressively severe thermal and oxidative stress, LS fuels appeared increasingly less stable than HS fuels..

INTRODUCTION

Before October 1993, No. 2 distillate fuel sold in the United States contained 0.2-0.4 %(wt) sulfur. As of October 1993, No. 2 distillate fuel used for on-highway vehicles was required to have a sulfur level no greater than 0.05 %(wt), i.e. 500 ppm(wt). This sulfur level reduction has been achieved by increasing the severity by which diesel fuel feedstocks are hydrotreated.

Limited data indicates that such low sulfur diesel fuels will have improved storage stability[1-3], i.e. form less sediment and dark-colored fuel-soluble materials. However, there have been concerns that resulting low sulfur diesel fuels may be more prone to form hydroperoxides upon storage.

The objective of the work reported in this paper was to compare the storage stability and hydroperoxide susceptibility of a large number of low and high sulfur No. 2 diesel fuels throughout the United States.

EXPERIMENTAL

Fuel Samples

Ninety-five No. 2 diesel fuel samples were collected during the period of February-March 1994. Sixty-nine samples were low sulfur (LS) diesel fuels; twenty-six were high sulfur (HS) fuels. Samples were collected in five geographic areas of the United States: Northern Midwest, Southern Midwest, Texas Gulf Coast, Rocky Mountains, and East Coast. Fuel samples spanned twenty-four marketers of diesel fuel, and were taken from both company-operated terminals and service stations. A few samples were taken directly from product pipelines. No attempt was made to determine if samples had been co-mingled during fungible pipeline shipment, or delivered segregated from the refinery. However, all samples represent diesel fuel being sold by the various marketers in the United States during early 1994.

All samples were shipped to the Amoco Research Center, Naperville, Illinois, by overnight express mail from the sampling points, and were stored at 40°F except when being tested.

Tests

Fuel samples were tested for chemical composition and stability using the following procedures:

Chemical Composition	Stability
Total Sulfur by Dispersive X-Ray Fluorescence (ASTM D4294)	Storage Stability (ASTM D4625)
Total Nitrogen (ASTM D4629, modified)	Initial Peroxide Number (ASTM D3703)
SMORS	Peroxide Number after ASTM D4625 (ASTM D3703)
Paraffins/Aromatics by Mass Spectrometry	Hydroperoxide Potential, CRC Procedure
	Hydroperoxide Potential, Oxygen Overpressure (OP) Procedure

Initial color (ASTM D1500) and ASTM D4625 final color were usually not determined for HS diesel fuel samples, since nearly all of those samples were dyed. The CRC Hydroperoxide Potential Procedure was originally developed for jet fuels[4] and involves heating a 100 ml fuel sample at 65°C and 1 atmosphere air for four weeks. Peroxide number is then determined as an indication of the fuel's hydroperoxide susceptibility. The OP procedure for hydroperoxide potential was adapted from previously documented work involving jet fuels[5]. The procedure involves heating a 50 ml fuel sample at 100°C and 690 kPa (100 psia) O_2 for 24 hours. The peroxide number is then determined. The modification to the total nitrogen procedure was that the fuel sample was delivered to the combustion tube by a platinum boat rather than by standard syringe injection. SMORS (Soluble Macromolecular Oxidatively Reactive Species) are believed to be sediment precursors, and the procedure for measuring them has been previously documented[6].

Statistical Treatment of Data

Data was statistically analyzed using SAS 6.08 for Windows. Statistical analysis was executed in three steps:

1. Distribution analysis
2. Analysis of geographic variance
3. Two sample t-testing of LS and HS fuels

Distribution analysis of the LS and HS results was done to ensure that normal distributions existed before running t-tests. When certain fuel test results gave non-normal distributions, a conversion to their logarithms usually gave the normal distributions required for valid t-testing. For a few tests, large numbers of zeros required the use of a non-parametric procedure known as the Median Scores test instead of the more commonly used t-test. Before t-tests were performed, the variance of data in each geographic area was analyzed to allow a stronger statistical treatment of the entire data pool. Two sample t-testing was then done to determine the statistical probability that a given mean test value was different for LS fuels compared to HS fuels. The confidence level (in percent) that the mean LS test value and mean HS test value is different was calculated. For the purposes of this paper, a difference in LS and HS mean test results was not considered statistically significant unless the confidence level was at least 90%. However, confidence levels that were somewhat lower were not entirely dismissed.

RESULTS AND DISCUSSION

Chemical Composition

Results of the statistical analysis of chemical composition tests are given in Table I. None of the LS fuels significantly exceeded the 500 ppm(wt) maximum allowed value for sulfur. Sulfur and nitrogen values reflected the already demonstrated fact[2] that hydrotreating removes sulfur-containing compounds more easily than nitrogen-containing compounds. Surprisingly, SMORS did not significantly decrease in LS fuels compared to HS fuels. The mass spectrometric data indicated that while LS fuels had more mono-aromatics and less poly-aromatics than HS fuels, they did not have significantly less total aromatics.

Stability

Results of the statistical analysis of stability tests are given in Table II. ASTM D4625 storage stability of all fuels was generally acceptable. LS fuel total insolubles averaged half that of HS fuel total insolubles, a statistically significant difference. This agrees with earlier work indicating that when diesel fuels are hydrotreated to reduce sulfur levels to less than 500 ppm(wt), conventional storage stability improves[3]. Dyeing practices prevented the determination of final color for the HS diesel fuels. However, the mean LS value (1.2, ASTM) appeared to be significantly improved from the typical HS values seen over the years in our laboratory. This also confirms previous observations that increased hydrotreating improves storage stability color, a significant result in view of the general inability of currently available additives to accomplish the same thing[2].

All fuels except one LS fuel gave zero initial hydroperoxides via the ASTM D3703 titrametric procedure. Previous researchers found the same result when examining field samples of HS diesel fuels. They concluded that HS diesel fuels were stable with respect to hydroperoxide formation[3]. Since the sixty-nine LS fuels in this study were also taken from the field, the same line of reasoning would indicate that LS diesel fuels are also stable with respect to hydroperoxide formation under commercial transport and storage conditions.

Differences in peroxide susceptibility between LS and HS diesel fuels varied directly with the severity of the sample storage conditions. Under ASTM D4625 conditions (13 weeks, 43°C, 1 atm. air), LS fuels developed hydroperoxide levels that were higher than HS fuels by a modestly significant amount (C. L. = 83.9%). Under the CRC conditions (4 weeks, 65°C, 1 atm. air), the same trend was observed, but the difference was very significant (C. L. = 99.2%). Under the OP conditions (24 hours, 100°C, 690 kPa O_2), the difference was even more significant (C. L. = 99.9%). It should also be noted that in all three hydroperoxide susceptibility tests, the mean final hydroperoxide level for LS fuels was far above the 1.0 meq O/Kg maximum level imposed on freshly refined JP-5 fuel. Hydroperoxide susceptibility for HS fuels exceeded this limit only for the most severe oxygen overpressure method.

The trend in hydroperoxide susceptibility is exactly what is expected, based on prior reported work and known chemical principles. Hydroperoxides in fuels are known to form via the well known peroxidation chain mechanism[7]. Very often, a slow initial stage of fuel oxidation, the induction period, occurs after which a more rapid rate of hydroperoxide formation is observed[8]. The length of the induction period will be determined by many factors including the level and efficacy of any naturally occurring or intentionally added antioxidants. Removal of those antioxidants by hydrotreating will reduce the induction period at any given set of incubation conditions (temperature, oxygen partial pressure, time). At very mild incubation conditions, the induction period may not be exceeded for most or all fuels. In that case, little or no difference in peroxidation susceptibility would be observed. As the incubation conditions become more severe, eventually the less stable fuels would exceed their induction period and rapid peroxidation would onset. These fuels would then be observed as more unstable. As the incubation conditions continue to become more severe, the separation of less stable and more stable fuels would become increasingly apparent up to a point.

Based on these observations, it appears that LS diesel fuels produced in the United States may be as hydroperoxide stable as HS diesel fuels under conditions they experience while getting to the end user. Also, results suggest that all three hydroperoxide susceptibility procedures used in this study may overpredict actual hydroperoxide levels generated by LS fuels under ambient conditions of fuel transport and storage. However, there is a real decrease in the peroxidation stability of LS diesel fuels compared to HS diesel fuels that could become apparent if the fuel is sufficiently stressed.

CONCLUSIONS

Major conclusions regarding the U.S. diesel fuels evaluated in this paper include the following:

1. Other than reduced sulfur and nitrogen content, the main statistically significant compositional difference between LS and HS diesel fuels was a partial saturation of poly-aromatics to mono-aromatics in LS fuels. There did not appear to be a strong statistical difference in total aromatics between LS and HS fuels.

2. Conventional storage stability as measured by ASTM D4625 was improved by a statistically significant amount in LS diesel fuels compared to HS diesel fuels. Both total insolubles and final color appeared to be improved.

3. Hydroperoxide susceptibility appeared to be equivalent and satisfactory for both LS and HS diesel fuels under the ambient conditions encountered during fuel transport and storage. However, under progressively severe thermal and oxidative stress, LS fuels appeared increasingly less stable than HS fuels.

ACKNOWLEDGMENTS

The contributions of the following people are gratefully acknowledged: Mike Dattalo, Teresa Myczek, and Jack Treadman for running much of the laboratory tests; Don Porter for performing the statistical analysis of data.

REFERENCES

1. Palmer, L. D.; Copson, J. A. "Hydrotreatment of Light Cycle Oil for Stabilization of Automotive Diesel Fuel," Proceedings of 2nd International Conference on Long-Term Storage Stabilities of Liquid Fuels, San Antonio, Texas, July 1986.

2. Martin, B.; Bocard, C.; Durand, J. P.; Bigeard, P. H.; Denis, J.; Dorbon, M.; Bernasconi, C. "Long-Term Storage Stability of Diesel Fuels: Effect of Ageing on Injector Fouling; Stabilization by Additives or Hydrotreating," presented at SAE Fuels and Lubes meeting, Tulsa, Oklahoma, 1990.

3. Vardi, J.; Kraus, B. J. "Peroxide Formation in Low Sulfur Automotive Diesel Fuels," SAE Paper No. 920826, 1992.

4. Determination of the Hydroperoxide Potential of jet Fuels, CRC Report No. 559, April 1988.

5. Black, B. H.; Hardy, D. R. "Comparison of Jet Fuel Phenolic Antioxidants Using A Serial Dilution Technique," Proceedings of the 4th International Conference on Stability and Handling of Liquid Fuels, Orlando, Florida, November 1991.

6. Hardy, D. R.; Wechter, M. A. "What Are Soluble Macromolecular Oxidatively Reactive Species (SMORS)?" ACS National Meeting, Washington, D.C., August 1990.

7. Lundberg, W. O. (Ed.) *Autooxidation and Antioxidants*. Interscience (John Wiley and Sons), 1961.

8. Fodor, G. E.; Naegali, D. W.; Kohl, K. B. "Peroxide Formation in Jet Fuels," *Energy and Fuels* **1988**, *2*, pp 729-734.

Table I
Results of the Statistical Analysis
Chemical Composition

Test	Low Sulfur Mean	Low Sulfur St Dv	High Sulfur Mean	High Sulfur St Dv	Conf. Level for Diff.	Test Metric [1]
Total Sulfur, ppm(wt)	296	92	2082	902	99.9	Log
Total Nitrogen, ppm(wt)	74.3	47.4	156.1	79.5	99.9	Original
SMORS, mg/100ml	.59	.50	.53	.35	35.4	Original
Mass Spectrometry Analysis, %(vol)						
Total Saturates	69.9	5.2	68.7	4.7	68.0	Original
Total Aromatics	30.1	5.2	31.3	4.7	68.0	Original
Mono-Aromatics	23.9	4.4	19.6	3.4	99.9	Original
Poly-Aromatics	6.3	2.2	11.7	3.3	99.9	Original

1. Test Metric indicates whether original data or natural logarithms were used to generate statistical information. See EXPERIMENTAL section for more information.

Table II
Results of the Statistical Analysis
Stability

Test	Low Sulfur Mean	Low Sulfur St Dv	High Sulfur Mean	High Sulfur St Dv	Conf. Level for Diff.	Test Metric [1]
Storage Stability, ASTM D4625						
Total Insolubles, mg/100ml	.30	.31	.67	.67	99.9	Log
Final Color, ASTM	1.20	.514	.750 [2]	--	--	Log
Hydroperoxide Analysis, meq O/Kg						
Initial Peroxide Number, ASTM D3703	.071[4]	.590	0.00	0.00	--	Original
Peroxide Number after ASTM D4625 [3]	21.3	156.0	.78	1.42	83.9	Original
Hydroperoxide Potential, CRC [3]	23.6	131.3	.10	.53	99.2	Original
Hydroperoxide Potential, OP	339	545	19.8	11.2	99.9	Log

1. Test Metric indicates whether original data or natural logarithms were used to generate statistical information. See EXPERIMENTAL section for more information.
2. High sulfur results based on 1 observation
3. Because of the large number of zeros, the Median Scores test results are reported
4. Only one of the sixty-nine LS fuel samples had a non-zero result.

EFFECT OF C_{60} ON OXIDATIVE STABILITY OF FUELS

R. Malhotra
SRI International, Menlo Park, CA 94025

D. R. Hardy, E. J. Beal, R. E. Morris, B. H. Black
Naval Research Laboratory, Code 6180, Washington DC 20036

ABSTRACT

Prompted by the ability of fullerenes to intercept radical chain processes, we investigated their possible application as additives to enhance thermal and storage stabilities of fuels. The thermal stability was evaluated using a gravimetric JFTOT apparatus, and the storage stability was assesses using the oxygen overpressure test. At a doping of 24 ppm, we found a significant beneficial effect of C_{60} in enhancing the thermal stability of jet fuels, but only a marginal effect for the storage stability of diesel fuels. In addition, we found that the presence of fullerenes had no effect on hydroperoxide formation as long as the fuel was kept in the dark. However, exposure to ambient light led to the build up of substantial quantities of hydroperoxides.

INTRODUCTION

Formation of insolubles in the fuel is a general problem. It can happen under various conditions, such as thermal stressing of jet fuels at 250 - 400°C during a flight, or during long term (years) storage of diesels under ambient conditions (10 - 45°C). The formation of insoluble materials can lead to many problems such as plugging of filters or fouling of engine parts.[1,2] In the extreme case when fuel flow is completely blocked, the consequence is extremely serious. Autoxidation has been implicated as a key step in the chemical scheme resulting in insolubles formation. This process involves generation of radical species, which initiate a chain reaction with oxygen to give oxidized hydrocarbons. The scheme, as originally proposed by Hazlett, is shown below:

INITIATION:

$$R\text{-}H + X \xrightarrow{\text{(metal ion or surface)}} R\bullet + XH$$

PROPAGATION:

$$R\bullet + O_2 \rightarrow ROO\bullet$$

$$ROO\bullet + R\text{-}H \rightarrow ROOH + R\bullet$$

TERMINATION:

$$ROO\bullet + ROO\bullet \rightarrow ROH + R'COR'' + O_2$$

$$ROO\bullet + R\bullet \rightarrow ROOR$$

$$R\bullet + R\bullet \rightarrow R\text{-}R$$

In view of the ability of C_{60} to scavenge radicals[3] we decided to test the effect it would have on (i) thermal stability of jet fuels, (ii) storage stability of diesels, and (iii) hydroperoxide formation.

RESULTS AND DISCUSSION

Numerous studies have been conducted on the chemistry leading to insolubles formation in jet fuels at elevated temperatures.[1] Key reactions are the thermal decomposition of alkyl chains by the Rice Herzfeld mechanism and autoxidation. The thermal stability tests were conducted using a gravimetric JFTOT apparatus with two JP-5 fuels (J1 and J2) and commercial Jet A fuel (JA). The JFTOT strip was heated to 260°C and 450 mL of fuels were pumped over it at 3.0 mL/min. The weight of the deposits on the strip as well as those collected on the filter were determined. The strip deposit is often very small (about 5-10%) of the total deposit. However, addition of 24 ppm C_{60} reduced deposit formation on the strip as well as the filtered deposit by about 50%. The data for the total deposits are displayed in Figure 1. The reduction in the fuel J1, which had a commercial additive package in it, is particularly noteworthy, because C_{60} was able to further reduce the very small amount of the deposit. An additive-free jet fuel (J2), which gave 15 mg/L of deposits, gave only 5.5 mg/L when doped with 24 ppm C_{60}. Finally, a commercial jet fuel, Jet A, which also had the additive package in it, showed no beneficial effect upon doping with C_{60}.

The chemistry of insolubles formation during long term storage is fairly complex and involves many different reactions. A possible scenario includes oxidation of sulfur species to sulfonic acids which catalyze the nucleophilic reaction of alkylindoles with phenalenones, which are also formed by autoxidation.[4] Tests on the storage stability of diesels were conducted with two diesel fuels (D1 and D2) by the oxygen over pressure (oop) test developed at the Naval Research Laboratory.[5] Both of the fuels are a 20% light cycle oil blend with the straight run diesel. The fuels were stressed for 16 h at 90°C with 100 psig O_2. The results are shown in Table 1.

Table 1. Effect of C_{60} on the Insolubles formation in diesel fuels during the oxygen overpressure test (90°C, 16 h, 100 psig O_2)

Fuel ID	Neat	+24 ppm C_{60}	% Redn.
D1	56	47	16
D2	44	34	23

At the doping level of 24 ppm both fuels responded to the addition of C_{60}, although the more unstable fuel, Fuel D1, exhibited a modest 16% reduction deposit formation. At a similar level of doping with an alkyl amine additive, these fuels showed a reduction in deposit formation of about 70%. Thus, C_{60} is not a particularly effective agent for enhancing the storage stability of diesel fuels.

Finally development of hydroperoxides in an unstable JP-5 fuel, held in the dark at 102°C under 50 psia air, was monitored over a 150-h duration. The results are illustrated in Figure 2. Initially, C_{60} (@24 ppm) accelerated the hydroperoxide formation, but at the end (~140 hr), both samples—additive free and doped—show the same low values. Experiments were also

conducted with a stable JP-5 at ambient temperatures under a fluorescent light in the presence of 0, 5, 10, and 20 ppm C_{60}. In control experiments, there was no formation of hydroperoxides in the dark, but C_{60} had a profound influence on the formation of hydroperoxides in the light. These results further illustrate the ability of C_{60} to photosensitize the oxidation of other substrates.

These preliminary data show that although C_{60} reduces the deposit formation in jet fuels, it can also have deleterious effects, particularly if the fuel were to be exposed to light. Further work with functionalized fullerenes is currently under way.

REFERENCES

1. R. N. Hazlett, "Thermal Oxidation Stability of Aviation Tubine Fuels," ASTM Publications, Philadelphia, PA, 1991.

2. A. Z. Fathoni and B. D. Batts, *Energy Fuels* **1992**, *6*, 681.

3. C. N. McEwen, R. G. McKay, and B. S. Larsen, *J. Am. Chem. Soc.* **1992**, *114*, 4412-4414.

4. R. N. Hazlett, D. R. Hardy, and R. Malhotra, *Energy Fuels* **1994**, *8*, 774.

5. D.R. Hardy, R.N. Hazlett, E.J. Beal and J.C. Burnett, *Energy Fuels* **1989**, *3*, 20.

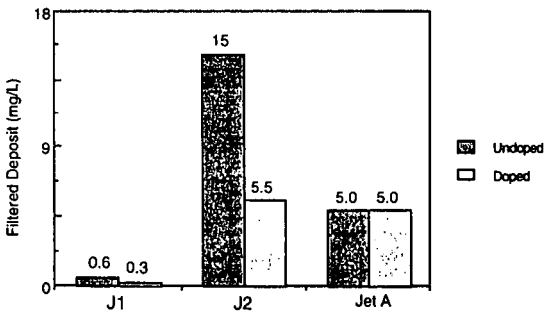

FUELS

J1: JP5 (contains additives)
J2: Fresh blend (unstable)
Jet A: Commercial aviation fuel (contains edditives)

Doping at 24 mg/L

Figure 1. Effect of C_{60} on the thermal stability of jet fuels as determined in a gravimetric JFTOT test conducted at 260°C.

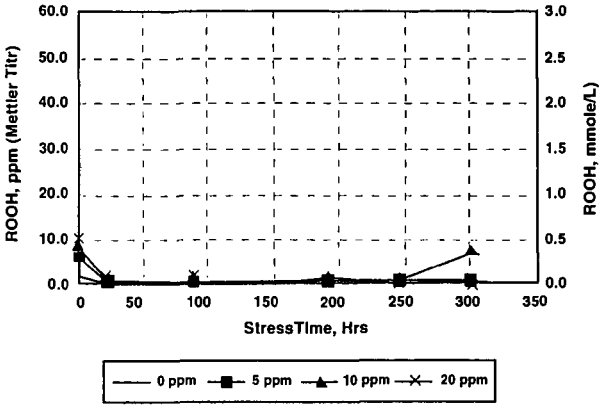

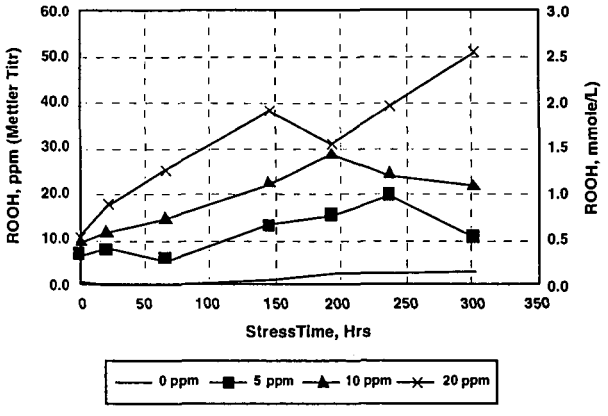

Figure 2. Effect of C_{60} on the peroxide formation at 25°C in aviation fuel 91-7 in (a) dark and (b) in light.

EFFECTS OF CARBON SURFACES ON THERMAL DECOMPOSITION OF HYDROCARBONS

Philip H. Chang and Semih Eser
Fuel Science Program
Department of Materials Science & Engineering
209 Academic Projects Building
The Pennsylvania State University, University Park, PA 16802, USA

INTRODUCTION

Deposition of carbonaceous solids on metal surfaces in the fuel system has been a major concern for the development of advanced aircraft with high thermal loads (Heneghan et al., 1996; Eser, 1996). In our previous studies we showed that the presence of high surface area activated carbon PX-21 prevented solid deposition on reactor walls and reduced the extent of decomposition of *n*-alkanes (Eser et al., 1992; Gergova et al., 1994; Gergova et al., 1996). We have suggested that the active sites of PX-21 carbon act to stabilize the pyrolysis products and enhance the H-transfer reactions. There are other reports on the activity of solid carbons in catalyzing the reactions of hydrocarbons (Szymanski and Rychlicki, 1993; Grunewald and Drago, 1990).

In this study, we compare the effects of activated carbon and other carbon additions on thermal decomposition of n-dodecane, cyclohexane, and ethylbenzene, as three different types of hydrocarbons present in jet fuels, and investigate the influence of oxygen complexes present on the carbon surface on thermal decomposition of cyclohexane and ethylbenzene.

EXPERIMENTAL

Thermal stressing experiments were carried out on 10 ml n-dodecane, cyclohexane and ethylbenzene in 316 stainless steel batch reactors at 450°C for 1 to 23 hours in a nitrogen atmosphere (Gergova et al., 1996). The high surface area activated carbon (PX-21), the carbon black (FW200), and another activated carbon (Asbury 5562) were obtained from Amoco Oil company, Degussa company in Germany, and Asbury company, respectively. Approximately 200mg of each carbon was added to model compounds prior to thermal stressing. The N_2 -BET surface areas of the three carbons are given below.

	PX-21	FW200	Asbury5562
Surface area(m^2/g)	3000	500	1200

Gas chromatography (GC) of liquid samples was conducted using a Perkin-Elmer 8500 GC with fused silica capillary column. Gas products were also analyzed by Perkin-Elmer Auto System GC. Compounds in the liquid products were identified by capillary Gas Chromatography-Mass Spectrometry (GC-MS) using a Hewlett-Packard 5090 II GC coupled with 5971A mass selective detector.

Boehm titrations (Boehm,) were performed with the three carbons to determine the concentrations of surface functional groups. For titrations, two- or three-gram samples of carbons were added in 200ml of various acidic and basic solutions prepared previously; all the solutions were 0.1M except Na_2CO_3 which was 0.05M. The solutions with added carbons were agitated for 48 hours, and filtered prior to titration. A 10 ml sample of filtered solutions was titrated with either 0.1M HCl or 0.1M NaOH solution depending on whether the acidic or basic functional groups are determined. Phenolphthalein or methylorange was used as an indicator in titrations.

The Asbury 5562 AC was bathed in strong nitric solution to oxidize its surface. A 20 g of activated carbon was bathed with 4M nitric acidic solution at 75°C for 2 hours. After bathing with acidic solution, the activated carbon was rinsed with distilled water until the washing water is neutral. The washed sample was dried in a vacuum oven. Boehm titrations were carried out on the oxidized carbon also to determine the acidic and basic functional groups on the surface.

RESULTS AND DISCUSSION

Thermal Decomposition of n-Dodecane. Despite the large differences in their BET surface areas the activated carbon PX-21 and the carbon black FW200 showed the same effect on thermal decomposition of hydrocarbons. Therefore, no results will be presented on the behavior of FW200 in thermal stressing experiments. Figure 1 shows the total concentrations of cycloalkanes and aromatics in the products obtained from stressing of n-dodecane at 450°C for 1 and 3 h with and without added PX-21. When PX-21 is added, higher concentrations of aromatic compounds are obtained in the products, indicating that the carbon surface promotes dehydrogenation reactions, possibly through hydrogen shuttling activity, as proposed before (Gergova et al., 1996) and discussed below.

In gaseous products, hydrogen and ethane concentrations were higher, whereas ethylene concentration was lower with PX-21 compared to those obtained without PX-21. Higher ethane and lower ethylene concentrations with PX-21 can be attributed to the stabilization of ethyl radicals (formed by ß-scission reactions) on the carbon surface. Combined with the data on the concentrations of cycloalkanes and aromatics in the liquid products, the gas analysis suggests

that the carbon surface shuttles hydrogen from cycloalkanes to stabilize the free radicals produced by thermolysis of n-dodecane. In other words, the carbon surface appears to be active in both dehydrogenation (e.g., of cycloalkanes) and hydrogenation (e.g., of ethyl radicals) reactions. One possible mechanism for the proposed hydrogen shuttling activity is the sequential hydrogenation and dehydrogenation of aromatic ring systems on the carbon surface. The stabilization of free radicals on carbon surface can explain why thermal decomposition of n-dodecane is suppressed with inhibition of solid deposition on metal surfaces (Gergova et al., 1996).

Thermal Decomposition of Cyclohexane. Thermal stressing of cyclohexane with/without PX-21 gave similar results to those obtained from stressing n-dodecane. The addition of PX-21 inhibited the thermal cracking of cyclohexane and gave much higher concentrations of benzene in the liquid products. The data shown in Figure 2 clearly demonstrates the dehydrogenation activity of PX-21 which produced in long duration experiments almost 30 times higher benzene concentrations compared to that obtained without PX-21. Similar to the results obtained with n-dodecane, the analysis of gaseous products showed that the presence of PX-21 gave higher concentrations of hydrogen and ethane, and lower concentrations of ethylene compared to those obtained without PX-21.

Thermal Decomposition of Ethylbenzene. In contrast to the results obtained from stressing n-dodecane and cyclohexane, the additions of PX-21 promoted cracking reactions and increased the amount of carbonaceous deposit on the reactor wall. The liquid products obtained with PX-21 was much darker. Figure 3 shows that much higher concentrations of benzene, methylbenzene, dimethylbenzene, styrene and methylethylbenzene were obtained when PX-21 was added to ethylbenzene. The major product was dimethylbenzene.

The gas analyses showed the same trends as those observed with n-dodecane and cyclohexane, that is, higher concentrations of hydrogen, ethane (and methane), and lower concentrations of ethylene were obtained when PX-21 was present. There was almost no ethylene present in the gases obtained with PX-21. These results suggest that the carbon surface still acts as a hydrogen shuttler to methyl and ethyl radicals, but compared to n-dodecane and cyclohexane reactions, there is much less amount of hydrogen to shuttle. It appears that demethylation of the ethyl group (producing a resonance stabilized benzyl radical) and methylation of subsequently formed methylbenzene (to produce dimethylbenzene) are the major reactions. The higher extents of cracking observed with PX-21 can be attributed to the abstraction of hydrogen by the carbon surface which, in this case, appears to destabilize the pyrolysis system.

Surface Characterization of Carbons using Boehm Titration. Based on the Boehm titration results, the equivalent numbers of each basic and acidic solution neutralization were calculated. As shown in Table 1, small concentrations of basic groups are present on the surface of PX21 and 5562AC, but no basic groups are detected on the FW200. There are large concentrations of acidic groups present on both PX21 and FW200 surfaces, but relatively small concentrations of acidic groups are detected on 5562AC surface. If the acidic groups are divided into four individual groups, large concentrations of carboxyl and lactone groups are found on the surface of both PX-21 and FW200, but none is present on 5562AC. Compared to carboxyl and lactone groups, phenolic and carbonyl groups are less abundant on PX21 and FW200 surfaces than those on 5562AC.

It appears that PX21 and FW200 with high concentrations of surface acid groups, especially carboxyl and lactone groups, are very active during thermal decomposition of hydrocarbons. In contrast, 5562AC with low concentrations of acidic groups, but relatively high concentrations of phenolic and carbonyl groups did not show much activity during thermal stressing of hydrocarbons. These results suggest that oxygen functional groups are important for the activity of carbon surfaces during thermal decomposition of hydrocarbons.

Effects of Oxidation of 5562 Asbury Activated Carbon on Thermal Degradation of Ethylbenzene and Cyclohexane. Upon oxidation of 5562 Asbury activated carbon with nitric acid solution, all basic groups are decreased from 0.48 meq/g to 0.3 meq/g, and all acidic groups are increased from 0.65 meq/g to 2.1 meq/g (see Table 1). The oxidation treatment increased the concentrations of all major acidic groups except the phenolic group.

Untreated and oxidized Asbury 5562 activated carbon were used in thermal stressing experiments with ethylbenzene and cyclohexane. The thermal stressing of ethylbenzene and cyclohexane(10ml) was done with 300mg of as-received and oxidized 5562AC. Liquid product analysis shows that oxidized 5562AC shows the same effect during ethylbenzene pyrolysis as that observed with PX-21 and FW200, that is, more extensive cracking of alkyl side-chain was obtained with oxidized 5562AC than that observed with as-received 5562AC present. The addition of oxidized 5562AC promotes cracking reactions and increases the amount of carbonaceous deposit on the reactor wall. The liquid products obtained with the oxidized 5562AC was much darker in color.. Figure 4 shows that the addition of the oxidized carbon gave much higher concentrations of benzene, methylbenzene, dimethylbenzene, styrene and methylethylbenzene compared to those obtained with the untreated 5562AC. The major product was dimethylbenzene. The amount of ethylbenzene remaining was drastically reduced when the oxidized 5562AC was added during pyrolysis experiments (see Fig. 5). These results are the same as those obtained from the pyrolysis of ethylbenzene with PX21 or FW200.

In contrast to ethylbenzene pyrolysis, the addition of oxidized 5562AC inhibited the thermal cracking of cyclohexane and gave much higher concentrations of benzene in the liquid products

(see Fig. 6,7). The data shown in Figure 3 clearly demonstrates the dehydrogenation activity of oxidized 5562AC indicated by the increase in benzene concentration, however the isomerization activity (i.e., cyclohexane to methylcyclopentane) was reduced with the oxidized 5562AC . These results suggest that oxidized 5562AC behaves like PX- 21 and FW200 in promoting hydrogen transfer reactions.

It is important to note that even a very inactive carbon like Asbury 5562AC became active upon simple oxidation with nitric acid. These results confirm that oxygen functional groups, in particular acidic groups, on carbon surfaces play an important role during pyrolysis of hydrocarbons in the presence of added carbons. Some important reactions which appear to be catalyzed by active carbon surfaces include dehydrogenation of hydrocarbons, stabilization of free radicals at early stage of pyrolysis, and cracking of side chains on alkylaromatics.

CONCLUSIONS

Thermal decomposition behavior of hydrocarbons is strongly influenced by the presence of an activated carbon PX-21 and a carbon black FW200. The addition of PX-21 and FW200 inhibits thermal decomposition of n-dodecane and cyclohexane and solid formation on reactor walls, but promotes the decomposition of, and solid formation, from ethylbenzene. The increased stability of n-dodecane and cyclohexane systems is explained by effective hydrogen shuttling on the carbon surface. Increased extents of cracking and solid formation from ethylbenzene can be attributed to the hydrogen deficiency of the aromatic compound compared to the two alkanes.

Boehm titrations showed the most active carbons such as PX-21 and FW200 contain large concentrations of acidic, but low concentrations of basic surface groups. Especially carboxyl and lactone type groups are present in high concentrations on the surfaces of PX-21 and FW200, whereas no carboxyl and lactone groups are found on the surface of Asbury 5562AC. The nitric acid oxidation process effectively produced oxygen functional groups on Asbury 5562AC and increased its activity during thermal stressing of hydrocarbons. Oxygen functional groups appear to play a key role in determining the activity of carbon surfaces during thermal stressing of hydrocarbons.

ACKNOWLEDGMENT

Funding was provided by the US DOE under contract DE-FG22-92PC92104. We thank Mr. W. E. Harrison III of Wright Laboratory/Aero Propulsion and Power Directorate, Wright-Patterson AFB and Dr. S. Rogers of U.S. DOE for many helpful discussions.

REFERENCES

Heneghan, S. P., Zabarnick, S., Ballal, D. R., Harrison III, W. E., in *Proceedings 34th Aerospace Sciences Meeting & Exhibit,* Nevada, USA, **1996**, AIAA Paper No 96-0403.

Boehm, H. P., *Carbon*, **1994**, 32, 759.
Eser, S., *Carbon*, **1996**, 34, 539.

Eser, S., Gergova, K., Arumugam, R., and Schobert, H. H., in *Proceedings Carbon'92,* Essen, Germany, Paper E11, **1992**, p. 519.

Gergova, K., Eser, S., Arumugam, R. and Schobert, H. H., in *Proceedings of the 5th International Conference on Stability and Handling of Liquid Fuels,* Rotterdam, the Netherlands, **1994**, p.227.

Gergova, K., Arumugam, R., Chang, P. and Eser, S., *Preprints ACS Div. Pet Chem.*, New Orleans, USA, **1996**, 41(2), p.513.

Szymanski, G. S. and Rychlicki, G., *Carbon*, **1993**, 31, 247.

Grunewald, G. C. and Drago, R. S., *J. Mol. Catal.*, **1990**, 58, 227.

Table 1. Surface functional groups of different carbons.

	PX21, meq/g	FW200, meq/g	5562AC, meq/g	Acid treated 5562AC, meq/g
All Basic Groups	0.40	0	0.48	0.3
All Acidic Groups	3.3	3.3	0.65	2.1
Carboxyl	1.1	1.3	0	0.52
Lactone	1.9	1.6	0	0.86
Phenolic	0.1	0.1	0.2	0.12
Carbonyl	0.2	0.3	0.45	0.60

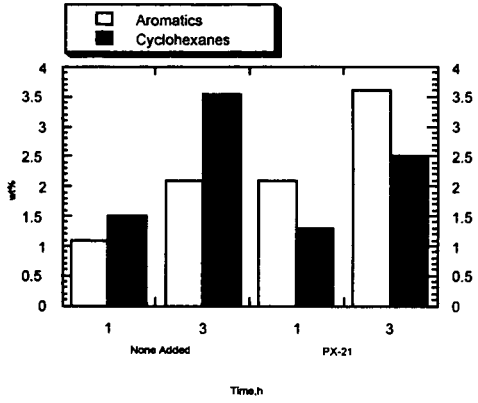

Figure 1. The concentrations of aromatics and cycloalkanes in the liquid products from the thermal decomposition of n-dodecane with/without PX-21.

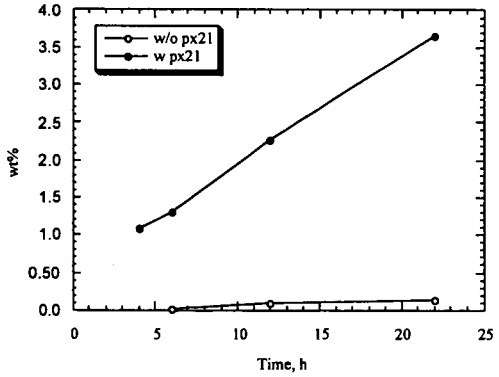

Figure 2. Benzene concentration in the liquid products from the thermal decomposition on cyclohexane with/without PX-21.

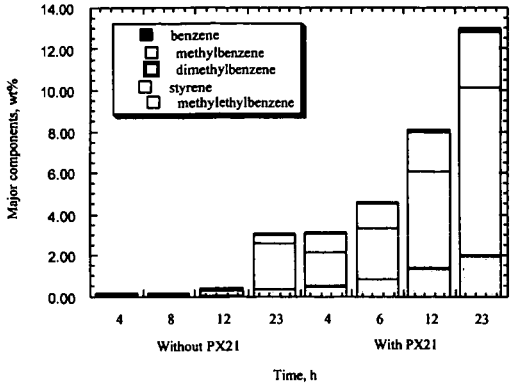

Figure 3. Concentrations of major components in the liquid products from the thermal decomposition of ethylbenzene with/without PX-21.

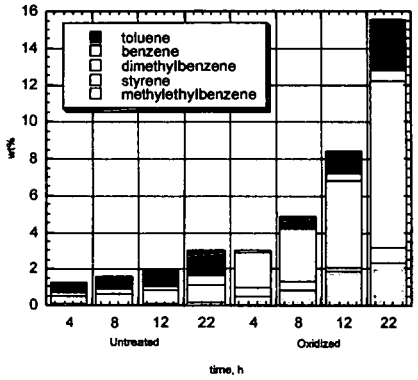

Figure 4. Major components from ethylbenzene pyrolysis with untreated/oxidized 5562AC.

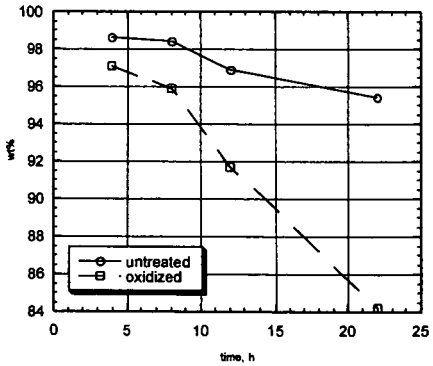

Figure 5. Ethylbenzene concentration from ethylbenzene pyrolysis with untreated/oxidized 5562AC.

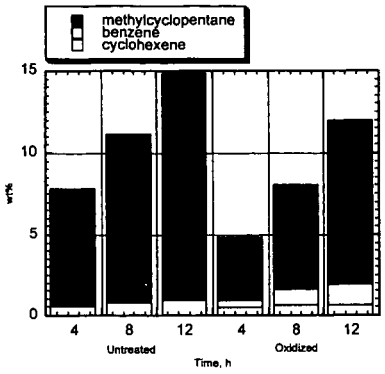

Figure 6. Major components from cyclohexane pyrolysis with untreated/oxidized 5562AC

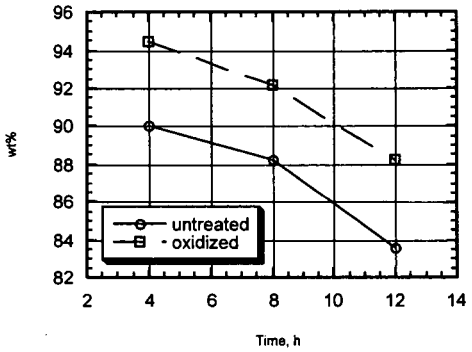

Figure 7. Ethylbenzene concentration from ethylbenzene pyrolysis with untreated/oxidized 5562AC.

USE OF MATHEMATICAL EXPRESSIONS FOR THE ESTIMATION OF SELECTED DIESEL FUEL PROPERTIES

D. Karonis, E. Lois, S. Stournas, F. Zannikos
National Technical University of Athens
Laboratory of Fuels and Lubricants Technology
Iroon Polytechniou 9, Athens 157 80, Greece

ABSTRACT

Mathematical expressions are presented, which predict some of the most important properties of diesel fuels. The experiments were performed using a fuel matrix of 128 gas oils, which covered the cetane index range 23-62. Although other parameters were also considered, the majority of the predictions were based on the distillation curve and the density of the fuels. Very good predictions were obtained for the aniline point, the kinematic viscosity at 40 °C, and for the fuels' aromatic content. The adjusted correlation coefficients in all cases is over 0.96.

LIST OF SYMBOLS

a,b,c,d,e,f,g,h,i	constants
ANIL	aniline point (°C)
AROM	aromatic content of the fuel (vol %.)
DENS	fuel density (g/mL at 15 °C)
D_{10}	distillation temperature for the 10% vol. of the fuel (°C)
D_{50}	distillation temperature for the 50% vol. of the fuel (°C)
D_{90}	distillation temperature for the 90% vol. of the fuel (°C)
FBP	final boiling point of the fuel (°C)
p	probability, the t-test to give a number equal or higher than t-ratio
R^2	correlation coefficient
R^2_{adj}	adjusted correlation coefficient
S	sulphur content of the fuel (wt %)
s	standard deviation

Greek Letters

ν_{40} kinematic viscosity (cSt at 40 °C)

INTRODUCTION

The properties of the gas oil streams in a modern refinery, vary widely, depending on the nature of the feedstock and the operating conditions. Straight atmospheric or cracking processes produce gasoils with properties that usually do not meet commercial specifications. Critical properties, such as the ignition quality, expressed with the cetane number increasingly become more severe, mainly for environmental reasons. Following production, the quality of the final gas oil products (diesel fuel) is adjusted by blending various gas oil streams in adequate quantities.

Modern blending processes need mathematical expressions that can predict accurately the amounts of each component to be blended, in order to meet the specifications of the market. The traditional use of tables and nomograms from the refineries for the estimation of the fuel blend properties, cannot satisfy the needs of the automated processes used in modern blending facilities[1-3]. Therefore, it would be desirable to find mathematical expressions for the most important specifications, using such parameters as the fuel distillation curve and density.

In the past, several investigators tried to identify the impact of the various fuel properties, either on the engine operating conditions or on emissions. The cetane number, as measured in a standard CFR engine, is the most significant property of diesel fuels, and for calculation purposes it can be approximated by the calculated cetane index [4-6]. The diesel fuel aromatic content, a property usually determined using chromatographic methods was found to correlate well with emissions from diesel engines [7-12]. The aniline point is related to the ignition quality of diesel

fuels through the diesel index [13, 14]. The kinematic viscosity is related to particulate emissions and performance of diesel engines, because of its impact on the droplet size distribution of the fuel at the injection system [15,16].
This work is an effort to present reliable mathematical expressions for the fuel's aromatic content, aniline point, and kinematic viscosity mainly using data from the distillation curve and the density.

EXPERIMENTAL SECTION

Sixteen gasoils with different properties were used as base fuels in this course of experiments, with their cetane index in the range of 23-62. They included straight run fuels from atmospheric distillation and cracking processes, i.e. light cycle oil from a fluid catalytic cracking unit and gasoils from visbreaker and hydrocracker. From these base fuels, 120 blends were prepared, covering a large spectrum of specifications that reflect both current and future trends. The properties of the total 126 fuels (base fuels and their mixtures), are listed in Table 1. All measurements were done according to the appropriate ASTM procedures.

STATISTICAL ANALYSIS

The data of the various fuel properties were analysed using standard statistical techniques. For each property, the parameters considered were the standard deviation s, the correlation coefficient R^2, and the adjusted correlation coefficient R^2_{adj}, which gives a more accurate behaviour of the model used. Each expression was tested through the t-test and probability number p, to ensure that only significant terms are used in the mathematical expressions [17]. All statistical parameters of the fuel properties considered in this paper, are listed in Table 2.

ESTIMATION OF THE KINEMATIC VISCOSITY

The kinematic viscosity of the fuel ν, was determined at 40 °C. The best results were obtained from the following equation:

$$v_{40} = a\cdot DENS + b\cdot DENS^2 + c\cdot D_{10}^2 + \frac{d}{D_{10}} + e\cdot D_{50}^2 + \frac{f}{D_{50}^2} + g\cdot D_{90}^2 + \frac{h}{D_{90}} + i \qquad (1)$$

Statistical parameters are given in Table 2. The results are depicted in Figure 1, where it can be seen that most of the points are close to the diagonal.

ESTIMATION OF THE ANILINE POINT

Aniline point is a simple procedure that gives an indication of the aromatic content of the fuel. The proposed equation for the aniline point is given below:

$$ANIL = a\cdot DENS + b\cdot(e^{-3.5\cdot(DENS-0.85)}-1) + c\cdot(D_{10}-215) + d\cdot(D_{10}-215)^2 + e\cdot(D_{50}-260) + f\cdot(D_{90}-310) + g\cdot(D_{90}-310)^2 + h\cdot S^2 + i \qquad (2)$$

In this case all variables have very high t-ratios and p-values equal to zero. The statistical parameters are given in Table 2. This means that all the predictor variables are significant. The results are given graphically in Figure 2.

ESTIMATION OF THE AROMATIC CONTENT

The aromatic content for diesel fuels is an important property since it affects both the density and the resulting emissions. The experimental determination of this specification requires special columns and it takes several hours to complete, ASTM D1319. Chromatographic techniques such as HPLC and SFC are also employed, but their instrumentation is very expensive. Modern techniques as FTIR give fast and good results. A mathematical expression for the calculation of aromatic content would be attractive. The following equation was found to give very good results:

$$AROM = a\cdot DENS^2 + b\cdot D_{10}^2 + \frac{c}{D_{10}} + \frac{d}{D_{50}} + e\cdot D_{90}^2 + \frac{f}{D_{90}} + g\cdot ANIL^2 + h\cdot S^2 + i \qquad (3)$$

In Table 2 are given the statistical parameters of the above equation. Graphical representation of the results shows that practically all the points are very well behaved, Figure 3.

CONCLUSIONS

Mathematical expressions which predict some important properties of diesel fuels have been experimentally determined, using a fuel matrix of 128 base fuels and blends. Very good predictions were obtained for the kinematic viscosity at 40 °C, the aniline point and the aromatic content. In all cases the adjusted correlation coefficients were just less than unity. These expressions can be used for a very accurate prediction of the actual values of these properties, when they cannot be measured directly.

ACKNOWLEDGEMENTS

The authors would like to thank Hellenic Aspropyrgos Refineries, Athens, Greece and Motor Oil Hellas Refineries, Athens, Greece, for supplying the gasoils that were used in this study.

REFERENCES

[1] Lois, E.; Stournas, S.; Karonis, D. Mathematical Expressions of Some Nonadditive Properties of Gas Oil-Residual Fuel Blends. *Energy and Fuels*. **1991**, *5*, 855.

[2] Obert, E. F. *Internal Combustion Engines and Air Pollution*; 3rd Edition, Intext Educational Publishers: New York, 1973.

[3] Diesel Fuels - SAE J313, SAE Handbook, 1992, Jun 89, *3*.

[4] Standard Method for Ignition Quality of Diesel Fuels by the Cetane Method; ASTM D-613, 1996.

[5] Standard Method for Calculated Cetane Index of Distillate Fuels; ASTM D-976, 1993.

[6] Standard Test Method for Calculated Cetane Index by Four Variables Equation; ASTM D-4737, 1996.

[7] Aromatic Hydrocarbon Types in Diesel Fuels and Petroleum Distillates by High Performance Liquid Chromatography with Refraction Index Detection; IP 391/90, 1996.

[8] Standard Method for Hydrocarbon Type Analysis in Liquid Petroleum Products by Fluorescent Indicator Adsorption; ASTM D-1319, 1996.

[9] Standard Test Method for Determination of Aromatic Content of Diesel Fuels by Supercritical Fluid Chromatography; ASTM D-5186, 1996.

[10] Li, X.; Chippior, W. L.; Gülder, Ö, L. Effects of Cetane Enhancing Additices and Ignition Quality on Diesel Engine Emissions. SAE Paper 972968, 1997.

[11] Lange, W. W.; Cooke, J. A.; Gadd, P.; Zürner, H. J.; Schlögl, H.; Richter, K. Influence of Fuel Properties on Exhaust Emmisions from Advanced Heavy-Duty Engines Consi-dering the Effect of Natural and Additive Enhanced Cetane Number. SAE Paper 972894, 1997.

[12] Ryan III; T. W., Erwin, J. Effects of Fuel Properties and Composition on the Temperature Dependent Autoignition of Diesel Fuel Fractions. SAE Paper 922229, 1992.

[13] Standard Test Method for Aniline Point and Mixed Aniline Point of Petroleum Products and Hydrocarbon Solvents; ASTM D-611, 1996.

[14] Diesel Index; IP 21, 1991.

[15] Standard Test Method of Kinematic Viscosity of Transparent and Opaque Liquids; ASTM D-445, 1996.

[16] Owen, K.; Colley T. *Automotive Fuels Handbook*; SAE, Warrendale, PA, 1991.

[17] Ryan, B.; Joiner, B.; Ryan, T. *Minitab Handbook*; 2nd Edition, PWS-KENT Publishing Company: Boston, 1992.

Table 1. Fuel Properties

Cetane Index	IBP (°C)	D_{10} (°C)	D_{50} (°C)	D_{90} (°C)	FBP (°C)	Density (g/ml, 15 °C)	v_{40} (cSt)	Aniline Point (°C)	Aromatic Content (% vol.)	Total Sulfur (% wt)
23.5	188	250	288	346	372	0.9550	3.85	20.9	73.0	1.82
24.3	154	242	276	341	369	0.9510	3.21	1.4	77.4	0.33
26.0	166	238	275	344	368	0.9420	3.16	7.0	74.3	0.30
27.0	185	235	274	340	366	0.9330	3.11	12.4	71.1	0.27
27.2	191	239	285	347	369	0.9330	3.62	19.8	69.4	0.28
27.3	190	249	290	355	372	0.9403	3.79	27.9	67.5	1.64
28.4	188	233	272	337	364	0.9240	3.06	17.5	67.9	0.24
28.6	188	252	288	347	373	0.9326	3.75	32.0	61.3	1.53
29.0	180	242	293	370	380	0.9346	3.85	20.4	65.8	0.34
30.2	193	233	270	334	360	0.9150	3.01	22.6	64.8	0.21
32.1	196	232	269	333	357	0.9060	2.96	27.6	61.6	0.18
32.4	194	247	296	354	369	0.9154	4.20	36.5	61.1	0.24
32.7	195	251	287	334	363	0.9100	3.64	43.0	51.9	1.22
34.0	205	252	290	356	382	0.9136	3.99	44.2	52.2	1.29
34.2	198	232	268	331	355	0.8970	2.92	32.1	58.5	0.15
35.8	185	228	254	332	361	0.8889	2.59	43.2	43.8	1.05
36.0	198	231	267	326	351	0.8880	2.87	36.8	55.4	0.12
36.8	189	247	287	328	361	0.8930	3.57	50.4	45.0	0.97
36.9	201	250	304	358	373	0.9012	4.78	46.8	54.2	0.19
37.5	185	225	257	337	369	0.8827	2.84	48.4	41.1	1.11
37.6	206	254	292	357	385	0.9012	4.07	50.6	46.3	1.12
38.3	200	230	267	323	348	0.8790	2.83	41.3	52.2	0.09
39.2	190	249	307	359	379	0.8941	4.91	55.1	52.2	0.18
40.2	185	223	262	353	369	0.8757	3.08	52.8	38.2	1.18
40.6	200	229	265	319	348	0.8700	2.78	45.9	49.0	0.05
40.8	206	255	294	357	383	0.8905	4.25	56.6	41.1	0.95
41.6	186	220	265	357	379	0.8706	3.16	55.0	35.1	1.25
42.9	198	227	265	313	344	0.8610	2.77	50.2	45.9	0.02
43.7	183	214	272	368	373	0.8642	3.42	58.5	32.2	1.32
43.8	185	218	272	363	376	0.8642	3.42	58.5	32.1	1.32
44.0	188	243	284	321	347	0.8691	3.48	60.3	33.8	0.64
44.1	206	256	295	359	386	0.8810	4.35	61.2	36.3	1.23
44.2	183	209	275	368	379	0.8618	3.50	60.8	30.7	1.35
44.5	185	215	275	368	379	0.8618	3.50	60.8	30.9	1.35
44.5	165	251	296	351	369	0.8771	4.01	59.1	38.1	0.12
44.7	196	229	268	323	353	0.8595	2.97	53.4	43.1	0.02
44.8	198	229	268	314	341	0.8578	2.85	53.8	42.3	0.05

Table 1. Fuel Properties (Continued)

Cetane Index	IBP (°C)	D_{10} (°C)	D_{50} (°C)	D_{90} (°C)	FBP (°C)	Density (g/ml, 15 °C)	v_{40} (cSt)	Aniline Point (°C)	Aromatic Content (% vol.)	Total Sulfur (% wt)
45.7	202	230	266	320	345	0.8561	2.80	55.1	41.2	0.03
45.8	182	210	284	365	375	0.8511	3.14	62.7	26.5	1.15
46.2	194	231	272	329	360	0.8580	3.11	56.4	40.0	0.02
46.5	185	215	284	372	385	0.8592	3.72	62.4	29.3	1.39
46.5	197	231	272	314	340	0.8550	2.93	56.9	39.1	0.07
46.7	219	257	316	362	381	0.8772	5.65	60.5	44.2	0.13
47.1	199	247	297	352	373	0.8691	4.11	63.8	32.8	0.18
47.5	208	257	297	340	386	0.8720	4.43	65.4	31.9	0.69
47.5	188	219	251	346	369	0.8439	2.8	63.2	23.5	0.91
47.5	206	231	265	321	347	0.8511	2.83	59.7	36.6	0.03
47.7	158	254	299	352	371	0.8701	4.13	65.4	33.9	0.10
47.8	225	268	327	371	384	0.8752	6.35	66.0	38.3	0.20
48.1	210	259	314	362	381	0.8742	5.29	61.9	42.1	0.12
48.1	194	235	278	338	363	0.8565	3.32	60.0	37.2	0.02
48.5	196	234	276	314	338	0.8518	3.02	60.6	35.5	0.10
48.5	188	225	261	355	388	0.8472	2.98	63.7	24.8	0.56
48.9	194	220	244	324	367	0.8355	2.45	64.5	20.5	0.66
48.9	182	210	284	365	375	0.8511	3.14	62.7	26.4	1.15
49.0	189	225	257	351	394	0.8435	2.80	64.1	23.4	0.92
49.0	214	261	302	360	386	0.8704	4.48	67.2	30.6	0.63
49.2	191	220	238	256	322	0.8247	2.06	65.6	16.2	0.28
49.4	195	220	240	270	354	0.8274	2.23	65.2	17.7	0.41
49.4	192	237	282	340	366	0.8550	3.56	63.0	34.2	0.02
49.4	203	232	264	323	347	0.8462	2.87	64.3	32.3	0.04
49.6	202	252	305	360	375	0.8638	4.67	68.7	29.2	0.27
49.6	191	225	252	346	391	0.8396	2.62	64.4	22.0	0.79
49.7	195	235	278	314	336	0.8500	3.08	62.7	33.1	0.11
49.8	195	226	246	333	395	0.8357	2.46	64.7	20.5	0.69
49.8	197	222	238	256	322	0.8239	2.06	65.6	16.2	0.28
50.2	191	224	246	359	381	0.8336	2.92	69.6	16.8	0.16
50.5	205	231	269	369	385	0.8462	2.58	73.8	18.9	0.17
50.5	170	257	300	354	373	0.8641	4.25	65.5	31.6	0.08
50.7	206	259	301	360	386	0.8650	4.55	69.8	28.1	0.56
50.9	190	239	287	342	368	0.8535	3.76	66.2	31.4	0.03
50.9	197	224	237	248	265	0.8200	1.94	66.4	14.7	0.15
50.9	209	258	299	361	388	0.8638	4.51	68.6	27.8	0.58
51.1	180	221	272	342	368	0.8430	3.16	68.6	28.0	0.28

Table 1. Fuel Properties (Continued)

Cetane Index	IBP (°C)	D_{10} (°C)	D_{50} (°C)	D_{90} (°C)	FBP (°C)	Density (g/ml, 15 °C)	v_{40} (cSt)	Aniline Point (°C)	Aromatic Content (% vol.)	Total Sulfur (% wt)
51.4	195	236	281	314	334	0.8475	3.15	65.3	30.5	0.13
51.6	205	227	241	257	301	0.8225	2.03	67.4	14.9	0.19
51.6	208	235	263	327	350	0.8412	2.90	68.9	27.6	0.05
51.6	198	222	240	270	354	0.8226	2.23	65.2	17.6	0.41
51.9	205	229	242	278	377	0.8282	2.18	67.8	15.2	0.18
52.0	165	214	279	349	372	0.8420	3.28	70.2	22.5	-
52.1	204	238	263	372	391	0.8404	3.23	72.4	16.7	0.26
52.1	228	274	333	375	388	0.8732	7.20	71.3	32.0	0.26
52.2	201	236	275	375	392	0.8452	3.77	73.8	17.2	0.3.0
52.4	214	237	254	368	390	0.8349	2.83	71.8	16.2	0.23
52.4	196	234	246	352	385	0.8302	2.49	68.2	15.7	0.22
52.4	187	219	268	333	359	0.8374	2.88	68.0	27.8	0.12
52.9	207	235	282	343	364	0.8460	3.57	70.1	24.1	0.28
53.0	203	239	273	337	358	0.8432	3.22	70.2	26.4	0.04
53.1	193	239	283	314	332	0.8451	3.23	67.9	27.7	0.16
53.2	188	247	292	348	370	0.8520	3.98	69.0	28.5	0.03
53.3	207	241	285	377	395	0.8475	4.07	75.2	17.4	0.32
53.8	193	230	267	290	302	0.8335	2.62	66.8	24.6	0.78
54.0	202	234	256	301	327	0.8303	2.57	69.0	18.5	0.18
54.1	210	259	299	365	390	0.8561	4.61	77.6	18.2	0.24
54.1	198	248	301	354	373	0.8530	4.52	72.2	23.2	0.15
54.2	195	243	282	345	361	0.8451	3.59	71.8	25.1	0.04
54.5	161	259	301	355	374	0.8554	4.41	71.0	26.0	0.05
54.7	191	244	284	314	331	0.8431	3.29	70.2	25.4	0.25
54.8	186	251	296	349	370	0.8505	4.26	71.6	25.6	0.03
54.8	210	244	334	370	385	0.8589	4.02	76.8	21.0	0.17
55.0	204	241	302	378	392	0.8492	4.43	75.4	17.7	0.32
55.1	186	238	270	311	330	0.8355	2.27	70.6	20.6	0.19
55.4	202	235	270	297	309	0.8330	2.71	70.3	19.2	0.62
55.6	186	248	293	351	367	0.8471	4.23	73.1	23.9	0.03
55.6	198	225	253	273	282	0.8213	2.24	66.5	20.3	0.68
55.9	195	238	279	309	328	0.8370	3.06	70.6	22.5	0.09
56.0	232	290	340	380	390	0.8712	8.16	76.7	25.7	0.33
56.0	212	254	303	353	380	0.8510	4.60	72.8	25.3	1.07
56.1	218	252	297	353	379	0.8483	4.16	74.3	20.5	0.89
56.3	225	270	320	364	385	0.8597	5.81	77.2	21.2	1.01
56.5	210	254	305	367	390	0.8505	4.57	73.8	23.1	0.15

Table 1. Fuel Properties (Continued)

Cetane Index	IBP (°C)	D_{10} (°C)	D_{50} (°C)	D_{90} (°C)	FBP (°C)	Density (g/ml, 15 °C)	v_{40} (cSt)	Aniline Point (°C)	Aromatic Content (% vol.)	Total Sulfur (% wt)
56.9	185	252	290	324	350	0.8431	3.60	72.8	23.0	0.15
57.1	184	255	293	335	356	0.8451	3.87	73.3	22.9	0.11
57.1	211	250	291	341	366	0.8432	3.69	71.2	22.1	1.00
57.2	180	260	300	353	369	0.8490	4.55	-	22.6	0.03
57.2	183	258	289	346	364	0.8470	4.19	73.9	22.7	0.07
57.6	188	249	285	313	329	0.8411	3.36	72.2	23.1	0.19
57.6	214	263	304	346	368	0.8500	4.51	72.8	22.6	1.23
57.8	194	260	305	360	386	0.8493	4.44	74.8	22.0	0.25
58.5	231	286	338	383	405	0.8642	7.85	77.2	23.4	0.20
58.8	221	281	324	363	385	0.8586	5.96	75.2	26.4	1.18
59.2	195	235	270	295	306	0.8252	2.81	74.6	17.5	0.03
59.9	216	285	335	380	397	0.8603	6.35	78.6	20.8	0.34
60.6	207	254	304	362	392	0.8410	4.53	81.0	18.6	0.08
61.5	239	312	351	382	390	0.8692	9.33	81.9	19.6	0.40
62.8	222	276	325	375	398	0.8489	6.12	83.4	19.2	0.09

Table 2. Statistical Parameters of Estimating Equations

Parameter	Equation (1)	Equation (2)	Equation (3)
a	124.080E+0	-12.248E+2	83.020E+0
b	-69.740E+0	-20.747E+1	24.970E-4
c	18.222E-5	38.215E-2	70.080E+2
d	38.601E+2	-24.400E-4	-11.009E+3
e	6.260E-5	12.106E-2	-32.528E-5
f	152.261E+3	55.730E-3	-19.659E+3
g	2.580E-5	87.490E-5	-71.388E-4
h	10.611E+2	34.537E-1	42.522E-1
i	-91.250E+0	10.945E+2	93.290E+0
s	2.472E-1	2.481E+0	1.654E+0
R^2	9.620E-1	9.780E-1	9.890E-1
R^2_{adj}	9.590E-1	9.770E-1	9.880E-1

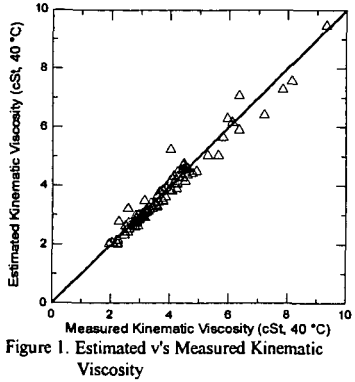

Figure 1. Estimated v's Measured Kinematic Viscosity

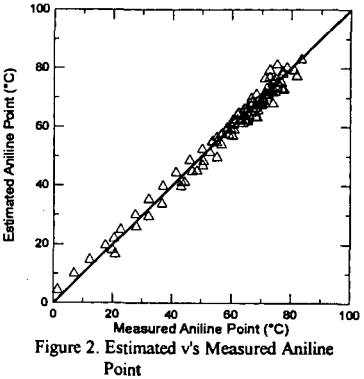

Figure 2. Estimated v's Measured Aniline Point

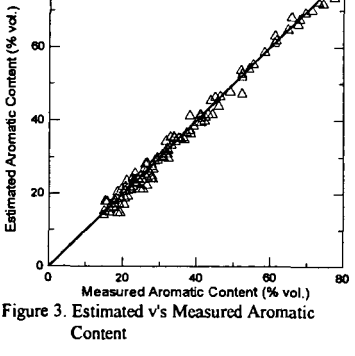

Figure 3. Estimated v's Measured Aromatic Content

CHARACTERIZATION OF AUTO-OXIDATION PRODUCTS OF AVIATION JET FUELS BY GAS CHROMATOGRAPHY COUPLED WITH MASS SPECTROMETRY

Jouni Enqvist (1), Esko Ranta (2) and Maarit Enqvist (3)

(1) VTT Chemical Technology, P.O.Box 1402, SF-33101 Tampere, Finland, (2) Laboratory of Organic Chemistry, P.O.Box 55, FIN-00014 University of Helsinki, (3) J&M Group Ky, P.O.Box 61, FIN 33961 Pirkkala, Finland

ABSTRACT

Hydroperoxides are important products in the liquid phase oxidation reactions of jet fuel hydrocarbons. For better understanding of the reasons for the differences in oxidative stability between different jet fuels, it would be useful to monitor the formation of oxidation products, especially hydroperoxides, from individual hydrocarbons. In this work, hydroperoxides were analyzed from fresh, long-time stored and high temperature oxidized jet fuel samples. The analytical procedure includes extraction of the hydroperoxides into deionized water, re-extraction into diethyl ether, subsequent trimethyl silylation and GCMS analysis. Tentative identification of two isomeric cymene hydroperoxides, the tetralin 1-hydroperoxide, isomeric methylindan hydroperoxides, and higher molecular weight substituted tetralin and indan hydroperoxide trimethylsilyl derivatives was obtained. Assignment of individual hydroperoxide isomers was not possible by mass spectra.

INTRODUCTION

Development of the aircraft and particularly of the jet engines seems to place more and more demands on the heat-sink efficiency of the jet fuel. The hydrocarbon mixture should resist higher fuel system component temperatures without thermal oxidative degradation or pyrolysis. Strategic long-term storing, also, places high demands for auto-oxidative and microbial degradation resistance of fuels.

Hydroperoxides are the principal primary auto-oxidation products of most hydrocarbons.[1] Oxidative degradation of jet fuel, which may appear as development of gums and insoluble deposits, unpredictable changes in lubricity, increased corrosiveness, poor water separation properties etc., correlates strongly with the formation of hydroperoxides, at least as intermediates. Soluble oxygen containing products may have useful effects on formation of boundary lubrication films chemically bonded on fuel system surfaces like the friction surfaces of fuel pumps but small amount of insoluble small molecular weight or polymeric secondary products may be harmful by causing fouling of critical engine components like fuel nozzles, augmentors etc. If the role of each oxidation-susceptible molecule in the degradation of the jet fuel could be understood, modifications of the refinery processes or design of more specific antioxidants could be possible, which in turn would result in better thermal and long term stability for the fuel.

Standard jet fuel oxidation tests do not give information about which individual chemical compounds are oxidized most rapidly. A jet fuel is comprised of at least hundreds of saturated paraffin, alisyclic (naphtenic) and aromatic hydrocarbons and may also contain some unsaturated olephinic hydrocarbons and trace amounts of sulfur, oxygen and nitrogen compounds. It is known that olephinic and several aromatic hydrocarbons oxidize much more rapidly than the saturated hydrocarbons. However, there is deficiency of even qualitative information about the individual products formed in oxidative degradation of jet fuels.

Direct detection of individual hydroperoxides and other oxidation products in a jet fuel is very difficult due to the complexity of the product mixtures and low concentration of each product. On the other hand, hydroperoxides are labile compounds and often decompose rapidly at optimal temperatures for GCMS analysis[2] or when treated with acids or bases.[3] Analysis of hydroperoxides by GCMS generally requires derivatization or other conversion into more thermally stable compounds.[4]

The objectives of this investigation were 1) to develop a practical method for the enrichment of hydroperoxides from oxidized jet fuels, and 2) to characterize the molecular structures of the enriched hydroperoxides by conversion into thermally stable derivatives followed by GCMS analysis. The aim of this article is to describe an analytical procedure for hydroperoxides based on water extraction of oxidized fuel samples followed by trimethyl silylation

of the hydroperoxide -OOH groups to the more stable -$OOSi(CH_3)_3$ groups[4] and application of GCMS technique for characterization of molecular structures of the most abundant hydroperoxides found in differently oxidized Jet A-1 samples.

EXPERIMENTAL

Materials. A fresh and differently oxidized Jet A-1 fuel samples were treated by procedures described below to obtain samples for GCMS analysis of hydroperoxides as their corresponding peroxytrimethylsilanes. One Jet A-1 sample (obtained from Sabena Airlines Depot, Brussels Airport, Belgium) was allowed to stand 2.5 years at room temperature in a sealed glass flask which was occasionally opened to air (to take samples for NMR). A 10 ml sample of this was extracted once with 50 ml of deionized water. The extract was then allowed to evaporate into dryness at room temperature. The evaporation residue was trimethylsilylated as described below to obtain Sample 1.

Other samples were a 100 ml fresh Jet A-1 (obtained from Finnish Air Force, Satakunnan lennosto, Tampere, Finland), a 50ml Jet A-1 sample oxidized 24 hours at reflux under oxygen atmosphere and a similarly oxidized 50 ml sample of a Jet A-1 sample that had been extracted three times with identical volume of deionized water. The corresponding GCMS samples (Sample 2, Sample 3 and Sample 4) were obtained as described below.

Jet A-1 samples (except the aged one) was extracted three times with identical volume of deionized water, the water phases were combined, saturated with sodium chloride (p.a., Riedel-De Haen, Seelze, Germany) and extracted three times with one third volume of diethyl ether (glass distilled grade, Rathburn, Walkerburn, UK). Ether phases were combined and ether was evaporated with rotatory evaporator. 50 ml acetone (nanograde, Mallinckrodt, Paris, Kentucky, USA) was then added and evaporated with rotatory evaporator to dry the residue.

Derivatization and GCMS analysis. Trimethylsilylation: a 100 µl sample (for Sample3 and Sample 4) or the whole evaporation residue (for Sample 1 and Sample 2) was mixed with 100 µl of BSTFA (Merck, Darmstadt, Germany) and 1 ml of toluene (nanograde, Mallinckrodt, USA) or diethyl ether (for Sample 1) was then added. At least two hours of reaction was allowed prior to analysis by GCMS. Analyses were conducted with a GC (HP 5890) equipped with a quadrupole mass selective detector (HP 5970A series). For all analyses the EI electron energy was 70 ev and the ion source temperature 280 ^{o}C. All samples were introduced as 1.0 µl aliquots by autosampler. Sample 1 was analyzed with a 25 m x 0.2 mm capillary column (HP-1, polydimethylsiloxane, 0.11 µm film thickness), 90 ^{o}C injector temperature, split injection at 1:8.4 split ratio, and scan range from 30 to 300 amu. The temperature program for Sample 1 was 4 min at 60 ^{o}C, then to 200 ^{o}C at 5 ^{o}C/min, then to 280 ^{o}C at 20 ^{o}C/min, and 3 min hold at 280 ^{o}C. Sample 2, Sample 3 and Sample 4 were analyzed with a 30 m x 0.2 mm capillary column (Rtx-200, trifluoropropylmethyl polysiloxane, 0.10 µm film thickness), 200 ^{o}C injector temperature in splitless injection mode. For these samples the temperature program was 1.0 min at 70 ^{o}C, then to 120 ^{o}C at 2 ^{o}C/min, then to 200 ^{o}C at 4 ^{o}C/min and then to 280 ^{o}C at 8 ^{o}C/min, and the mass analyzer was scanned from 33 to 300 amu the first 10 min and from 33 to 500 amu the rest of the analysis time.

RESULTS AND DISCUSSION

Extraction into water was found to be a useful method for the isolation of hydroperoxides from hydrocarbons of the jet fuel. Many other oxidation products were also water extractable, and the extracts from the oxidized samples were actually quite complicated mixtures, especially those that were oxidized at high temperature (Sample 3 and Sample 4). On the other hand, the yield of the extraction from the fresh Jet A-1 sample (Sample 2) was so low that individual components could not be identified due to low signal to noise ratio (data not shown). Analysis of Sample 2 thus confirmed that the water extractables of the oxidized Jet fuel samples were essentially oxidation products. The water extraction for Sample 4 differed from the other samples in that considerable amount of insoluble gum was formed when water was added into oxidized mixture.

There may have been decomposition of hydroperoxides in the water extracts due to presence of carboxylic acids that were detected among the oxidation products. Partially because of this possibility, Sample 2, Sample 3 and Sample 4 were immediately re-extracted into diethyl ether. The other reason for the re-extraction was that azeotropic evaporation with water of some extracted components was detected in early experiments. Evaporation of diethyl ether can also be

done rapidly at a low temperature. Removal of the residual moisture by azeotropic distillation with acetone has the same benefits.

The effectiveness of the silylation reagent BSTFA was tested with cumene hydroperoxide (data not shown). MSTFA has been successfully used for trimethylsilylation of cumene hydroperoxide[4] and the product obtained by using BSTFA was confirmed to be the same by comparing the mass spectra. No side products were detected and the reaction appeared to be complete within an hour.

The trimethylsilyl derivatives of hydroperoxides, or more shortly, peroxytrimethylsilanes seem to usually yield, at best, weak molecular ions by 70 eV EI ionization. Loss of the trimethylsilylperoxy radical from molecular ion usually produces abundant $[M - 105]^+$ ion.[4] Important lower mass fragments often appear at m/z values 89 $[C_3H_9SiO]^+$, 75 $[C_2H_7SiO]^+$, 73 $[C_3H_9Si]^+$, 59 $[C_2H_7Si]^+$ and/or $[CH_3SiO]^+$, and 45 $[CH_5Si]^+$ and/or $[HSiO]^+$. Peak m/z 91 which appears in EI mass spectra of cumylperoxytrimethysilane and 1-tetralylperoxytrimethylsilane may have contribution from ion $[C_2H_7SiO_2]^+$.

TIC chromatogram of Sample 1 is represented in Figure 1. The most abundant analyte peaks in the chromatogram of Sample 1 correspond silylated products that have the fragmentation characteristics of peroxytrimethylsilanes. Examples of the mass spectra are represented in Figures 2 and 3. In Figure 3 there is also a reference spectrum of 1-tetralylperoxytrimethylsilane obtained by trimethylsilylation of tetralin hydroperoxide in an auto-oxidized tetralin sample. Mass spectrum in Figure 2 (RT 10.93 min) is interpreted to correspond a TMS derivative of an unknown isomer of cymene hydroperoxide. Peak assignments: M^+ at m/z 238, m/z 133 (-105 amu, loss of trimethylsilylperoxy radical), m/z 119 ($[CH_3C_6H_4CO]^+$ and/or $[C_3H_9SiOOCH_2]^+$ and/or $[CH_3C_6H_4CHCH_3]^+$), low mass ions as described in the previous paragraph. A TMS derivative of another isomer of cymene hydroperoxide at RT 11.78 min yielded almost identical mass spectrum (not shown). There are other significant analyte peaks in the TIC chromatogram of Sample 1 that are due to products that produce mass spectra consistent with peroxytrimethylsilanes with indan and tetralin ring structures up to molecular weight 264 which corresponds compounds with trimethylindan/dimethyltetralin moieties (data not shown).

Figure 1. TIC chromatogram of Sample 1

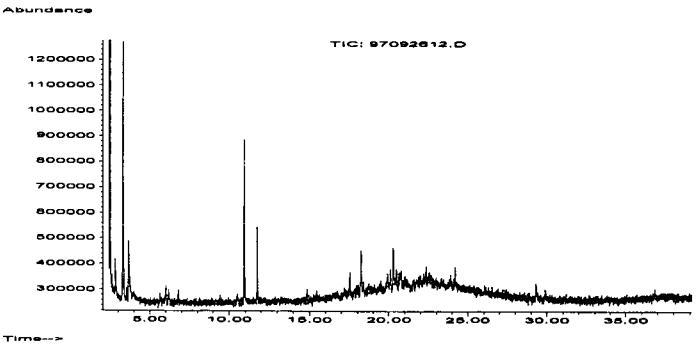

Figure 2. Mass spectrum of a compound (RT 10.93min) tentatively identified as a TMS derivative of an unknown isomer of cymene hydroperoxide.

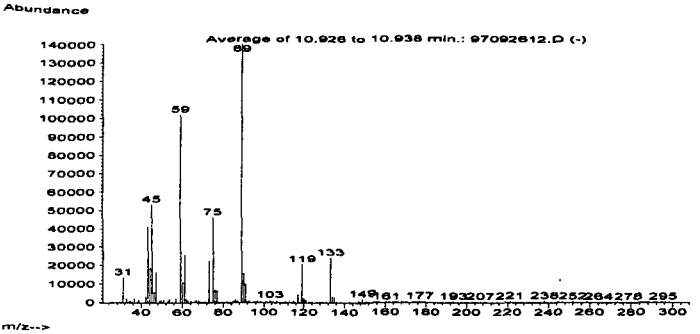

Figure 3. Mass spectra of a compound tentatively identified as tetralin hydroperoxide from Sample 1 and from an auto-oxidized tetralin sample.

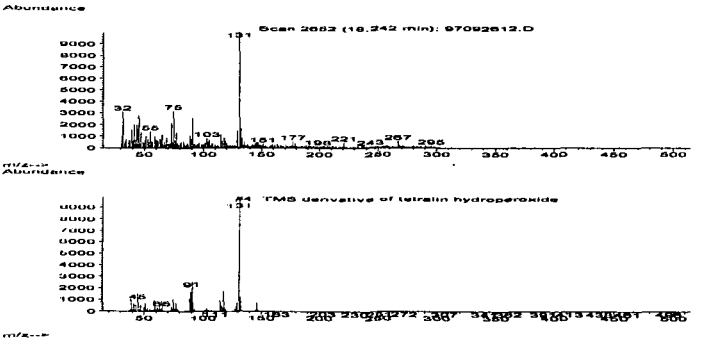

TIC chromatogram of Sample 3 is represented in Figure 4. In this sample only one distinct peroxytrimethylsilane peak was detected (Figure 5), and it appeared to be a cymene hydroperoxide derivative. Many types of silylated and nonsilylated oxidation products were found in Sample 3. Among the most abundant peaks were those of TMS ethers of phenols (Figure 6) indicating that phenols are important oxidation products. The phenols are probably formed by decomposition of benzylic alkylbenzene hydroperoxides via hydrolytic mechanism catalyzed by carboxylic acids which were also detected among the oxidation products in Sample 3.

Figure 4. TIC chromatogram of Sample 3.

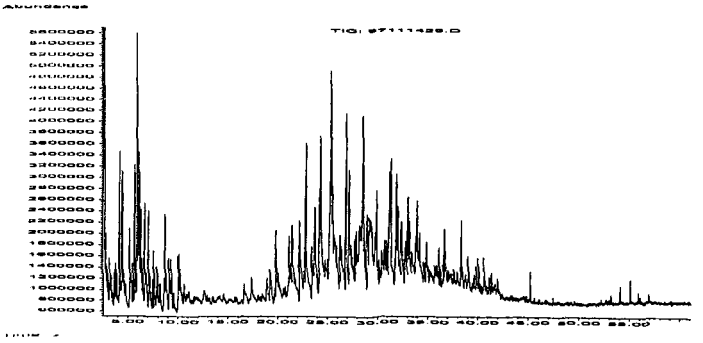

Figure 5. A partial TIC chromatogram of Sample 3. The peak at 5.5min is tentatively identified as a TMS derivative of an isomer of cymene hydroperoxide.

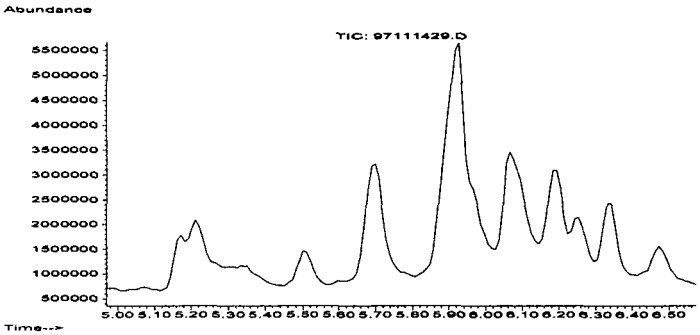

Figure 6. Reconstructed ion chromatograms showing the TMS derivatives of phenol (at 3.2 min), cresols (4.2-4.6 min), dimethyl- (or ethyl-) phenols (5.6-7.2 min), and trimethyl- (or isomeric) phenols in Sample 3.

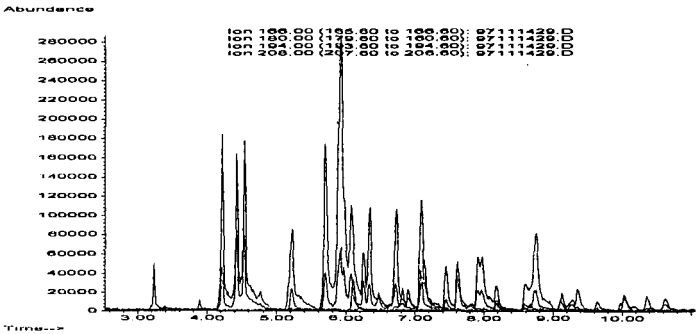

TIC chromatogram of Sample 4 is represented in Figure 7. This sample consisted of larger variety of oxidation products than Sample 3. The water extracted fuel was clearly more severely degraded during the oxidation than the normal fuel and yielded more of water extract and insoluble products. The darkening of the water extracted jet fuel was also much stronger. The TMS derivative of the suggested cymene hydroperoxide peak present in Sample 3, was also present in Sample 4.

Figure 7. TIC mass chromatogram of Sample 4.

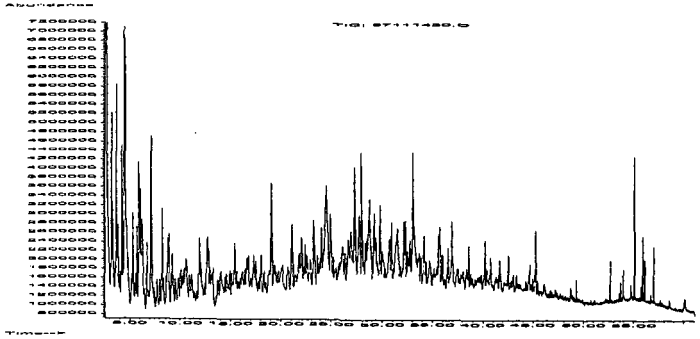

Table 1. Summary of the Experiments.

Samples	Oxidation Conditions	Results
Sample 1: Brussels Jet A-1 Oxidized as such	Two and a half years under air at ambient temperature	Several cymene, tetralin and indan hydroperoxides
Sample 2: Tampere Jet A-1 fresh	Not oxidized	No oxidation products could be identified due to low yield of extraction
Sample 3: Tampere Jet A-1 Oxidized as such	Refluxed 24 h under oxygen atmosphere.	Low on hydroperoxides, various other oxidation products, small amount of insolubles formed
Sample 4: Tampere Jet A-1 water extracted	Oxidized like sample 3	Dark brown product with deposits, oxidation products in the extract similar to as in Sample 3

The water extract of the fresh jet fuel served as the zero sample. The oxidation of the water extracted fuel produced a sample with the characteristics of heavily oxidized fuel, and indicated that separation of water may reduce the antioxidative resistency of Jet A-1 fuel and that presence of water may increase the amount of insolubles formed. The hydroperoxides formed during long-time storing are accumulated since they decompose slowly at low temperatures. In the water extract of the aged sample hydroperoxides were thus the main products. At fuel reflux temperatures the hydroperoxides were no more stable but mostly decomposed producing large variety of secondary products.

Jet fuel samples and oxidation procedures of this investigation are just examples of sample materials where analysis of individual hydroperoxides and other oxidation products could produce useful information about the chemical and tribological condition of the fuel in the molecular level. The four samples described in Table 1 represent examples of different crude oils, different refinery processes and different auto-oxidation conditions (oxidation time and temperature, presence and absence of antioxidant) that may be found in practical applications where determination of individual hydroperoxides would give useful information.

The present work by us is aimed for refinement of the GCMS method for quantitative determination of individual hydroperoxides with the emphasis of elucidation of molecular structures of the isomeric compounds by different spectroscopic techniques as well as characterization of secondary products.

Although all oxidation products cannot be analyzed by the method described, we believe that application of this method can result in better understanding of oxidative degradation and chemical change in long-term storing of middle distillate fuels in general. The method can be routinely applied to monitor of certain key hydroperoxides and other important oxidation products like phenols in the fuels. Effects of fuel additives into oxidation stability of the fuel can be now monitored in molecular level.

REFERENCES

1. Nonhebel, D. C., and Walton, J. C. in *Free-radical chemistry*, University Printing House, Cambridge, 1974, p 393
2. Foglia, T. A., Silbert, L. S., and Vail, P.D., *Journal of Chromatography*, 637 (1993), p 157
3. Mageli, L. O., and Sheppard, C. S., in Swern D., (Editor), *Organic Peroxides*, Vol. 1, Wiley-Interscience, New York, 1970, Ch. 1, pp 19-20
4. Turnipseed, S. B., Allentoff ,A. J., and Thompson, J. A., *Analytical Biochemistry*, 213 (1993) 218

ACKNOWLEDGEMENTS

Jet fuel specialists at Finnish Air Force and Sabena Airlines Depot are acknowledged for the samples and useful discussions, and Neste Oy Foundation for the financial support.

AUTOXIDATION OF DILUTED AVIATION FUELS

E. Grant Jones and Lori M. Balster
Innovative Scientific Solutions, Inc.
2786 Indian Ripple Road
Dayton, OH 45440-3638

Keywords: Autoxidation, Fuel Blend

INTRODUCTION

In addition to its role in combustion, aviation fuel serves as the primary heat sink for cooling component systems in military aircraft.[1] The efficiency of heat exchangers and the operation of many other critical fuel-line components can be compromised by fouling of surfaces caused by the accumulation of intractable gums. Products from autoxidation are the major source of surface fouling at temperatures below 400°C.[2] Although pure paraffins and hydrotreated fuels have high thermal stability, i.e., a low propensity for fouling surfaces, they can oxidize very rapidly in the absence of antioxidant protection. Species containing heteroatoms (present in low concentrations in most fuels) tend to inhibit or retard oxidation by acting as antioxidants. However, on the basis of the high relative abundance of O, S, and N in insoluble products, these same types of species have been implicated in surface fouling.

The thermal stability of lesser quality aviation fuels can be improved through hydrotreatment processes at the refinery which reduce the concentration of many heteroatomic species as well as dissolved metals and alkenes.[3] More severe hydrotreatment can also lower the concentration of aromatics. Thermal stability can be improved at a lower cost by the introduction of additives or additive packages.[4]

Our laboratory has been investigating the effect of fuel blending upon autoxidation.[5,6] Adding a small amount of a straight-run fuel that contains naturally occurring antioxidants to a hydrotreated fuel whose natural antioxidants have been removed during refining is equivalent to adding a small amount of antioxidant.[5-7] Conversely, the addition of a severely hydrotreated fuel to a straight-run fuel can be viewed as a means of diluting the concentration of many deleterious fuel components including antioxidants as well as aromatics. Such dilution causes compositional changes analogous to those achieved during hydrotreatment. In the present study this concept was explored by investigating the autoxidation of neat and diluted fuels and the changes in autoxidation arising from the introduction of some simple additives.

EXPERIMENTAL

Blends (1:10) are prepared by stirring together 10% aviation fuel and 90% Exxsol D-110, the latter being a mixture of paraffins and cycloparaffins containing no antioxidants and less than 1% aromatics. The methodology has been described in detail previously.[5] Liquid-phase oxidation occurs as air-saturated fuel passes through a single-pass heat exchanger operated isothermally at 185°C. A system pressure of 2.3 MPa ensures a single reaction phase with no headspace. It is assumed that the amount of dissolved O_2 is approximately the same for each fuel and blend.[8] Fuel reaction time (residence time) in the 0.81-m tube (i.d. 0.216 cm) is varied by changing the flowrate. Dissolved O_2 in the stressed fuel is measured by the GC method developed by Rubey and co-workers.[9] For the oxidation experiments, tubing treated with the Silcosteel process[10] was used to minimize catalysis that occurs on the surfaces of stainless-steel tubing. Additives employed in this study include the DuPont metal deactivator N,N'-disalicylidene-1,2-propanediamine [designated MDA (2 mg/L)], the hindered phenol antioxidant BHT (25 mg/L), and the Betz proprietary dispersant 8Q405 (100 mg/L).

RESULTS AND DISCUSSION

Oxidation of neat and diluted fuel: effect of additives on POSF-3084. POSF-3084 is a Jet-A fuel of low thermal stability containing 35 ppb of Cu. The oxidation behavior of neat and diluted fuel at 185°C is shown in Figure 1. In each case oxidation is autocatalytic as a result of formation and subsequent thermal and Cu-catalyzed[11] dissociation of hydroperoxides, which increases the source of free radicals. The impact of autocatalysis is reduced somewhat in the neat fuel because of the abundance of naturally occurring antioxidants which act either as primary antioxidants in a radical chain-breaking mechanism or as secondary antioxidants by destroying hydroperoxides. Diluted fuel contains fewer secondary antioxidants, resulting in higher hydroperoxide concentrations and more rapid oxidation at high conversion.

Dilution also reduces the concentration of dissolved Cu to ~ 4 ppb. Thus, Cu-catalyzed initiation is expected to be less important in diluted fuel than in neat fuel. By chelating the dissolved Cu with MDA, most of the effects of metal-catalyzed initiation can be eliminated. The results of introducing 2 mg/L of MDA into neat and diluted fuel are

shown in Figures 2a and 2b, respectively. With regard to slowing oxidation, MDA has a significant effect on the neat fuel and a minimal effect on the diluted fuel. This observation illustrates that ten-fold dilution of POSF-3084 almost totally removes any contribution from dissolved metals.

Hydrotreated fuels usually require the addition of a hindered-phenol antioxidant, such as BHT, for improved storage stability to offset the removal of natural antioxidants. Such fuels are sensitive to the introduction of additional BHT. For example, concentrations of BHT up to 70 mg/L have been shown to have an approximately linear effect in extending the delay in autoxidation of the severely hydrotreated JPTS fuel POSF-2976.[12] Figures 3a and 3b show the effect of introducing BHT into neat and diluted fuel, respectively. Both fuels exhibit delays in autoxidation, but the response to BHT is greater in the diluted fuel.

Dispersants are not expected to alter autoxidation. However, in some metal-containing fuels (POSF-3084, -3119) autoxidation has been reported to be slowed by the introduction of 8Q405.[4] It has been suggested that this behavior is due to metal deactivation rather than a radical chain-breaking mechanism.[4,13] Response to the addition of dispersant 8Q405 is shown in Figures 4a and 4b. The reduced sensitivity following dilution is not consistent with 8Q405 acting as a primary antioxidant; rather it supports another role, possibly related to metal deactivation.

Finally, is the oxidation behavior of diluted POSF-3084 similar to that of hydrotreated fuels? Figure 5 shows the similarity between diluted POSF-3084 and three severely hydrotreated fuels.

Oxidation of a series of diluted fuels. The oxidation behavior of twelve diluted aviation fuels is shown in Figure 6. This series includes fuels covering a broad range of thermal stability. Three points can be made. First, the fuel discussed in detail above is a representative example of this series. Second, with one significant exception (namely, POSF-2985), the curves are very similar in shape but rapid reaction is delayed in the same manner as we observed previously at this temperature with the addition of a primary antioxidant such as BHT to JPTS.[12] Since dilution has removed most of the impact of species such as metals and secondary antioxidants which require interaction with hydroperoxides, the observed delays may provide an indirect measure of the efficiency of naturally occurring primary antioxidants in slowing oxidation of the diluent.

CONCLUSIONS

Results presented here show that fuels diluted ten-fold with paraffins exhibit behavior more characteristic of hydrotreated fuels than of the original undiluted fuel with regard to autoxidation and response to additives. This is attributed to a reduction in the impact of dissolved metals and heteroatomic species that is analogous to compositional changes achieved during hydrotreatment.

ACKNOWLEDGMENTS

This work was supported by the Air Force Research Laboratory, Propulsion Directorate, Wright-Patterson Air Force Base, Ohio, under USAF Contract No. F33615-95-C-2507. The authors would like to thank Mr. Walter Balster for valuable discussions and Mrs. Marian Whitaker for editorial assistance.

REFERENCES

1. Edwards, T.; Anderson, S. D.; Pearce, J. A.; Harrison, W. E., III, High-Temperature JP Fuels--An Overview, AIAA Paper No. 92-0683, Presented at the 30th Aerospace Sciences Meeting and Exhibit, Reno, NV, 6-9 January 1992.
2. Hazlett, R. N. *Thermal Oxidation Stability of Aviation Turbine Fuels*, ASTM Monograph 1; American Society for Testing and Materials: Philadelphia, 1991, p 111.
3. Gary, J. H.; Handwerk, G. E. *Petroleum Refining*; Marcel Dekker: New York, 1994, p 187.
4. Jones, E. G.; Balster, W. J.; Balster, L. M. *ASME J. Eng. Gas Turb. Power* 1997, *119*, 830-835.
5. Jones, E. G.; Balster, L. M.; Balster, W. J. *Energy Fuels* 1996, *10*, 509-515.
6. Balster, L. M.; Balster, W. J.; Jones, E. G. *Energy Fuels* 1996, *10*, 1176-1180.
7. Zabarnick, S.; Zelesnik, P.; Grinstead, R. R. *ASME J. Eng. Gas Turb. Power* 1996, *118*, 271-277.
8. Striebich, R. C.; Rubey, W. A. *Prepr.-Am. Chem. Soc., Div. Pet. Chem.* 1994, *39*(1), 47-50.
9. Rubey, W. A.; Striebich, R. C.; Tissandier, M. D.; Tirey, D. A.; Anderson, S. D. *J. Chromat. Sci.* 1995, *33*, 433-437.
10. Restek Corporation, Bellfonte, PA.
11. Pedersen, C. J. *Ind. Eng. Chem.* 1956, *48*, 1881-1884.
12. Jones, E. G.; Balster, L. M., *Energy Fuels* 1997, *11*, 610-614.

13. Balster, W. J.; Balster, L. M.; Jones, E. G. *Prepr.-Am. Chem. Soc., Div. Pet. Chem.* 1996, *41*(2), 446-451.

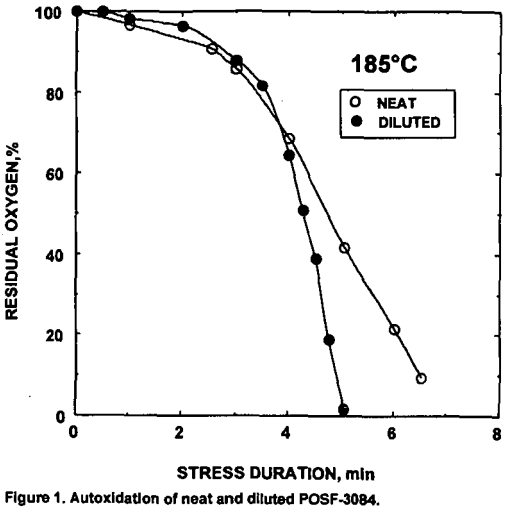

Figure 1. Autoxidation of neat and diluted POSF-3084.

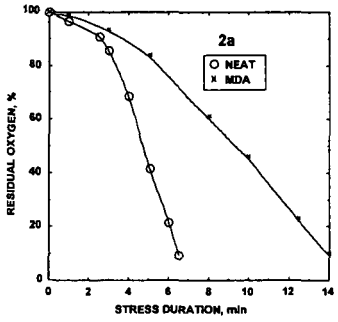

Figure 2a. Effect of MDA (2 mg/L) on neat fuel

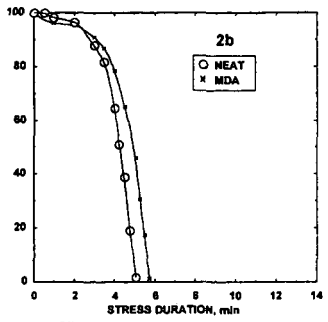

Figure 2b. Effect of MDA (2 mg/L) on diluted fuel.

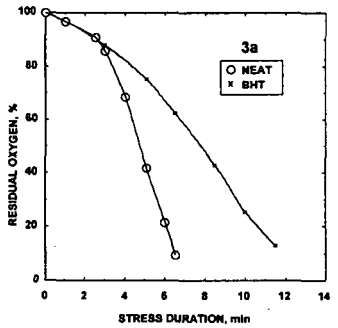

Figure 3a. Effect of BHT (26 mg/L) on neat fuel.

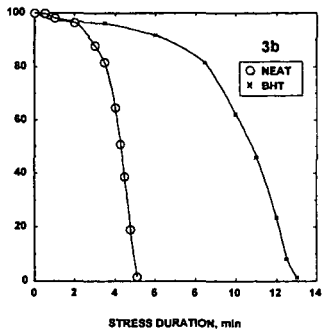

Figure 3b. Effect of BHT (26 mg/L) on diluted fuel.

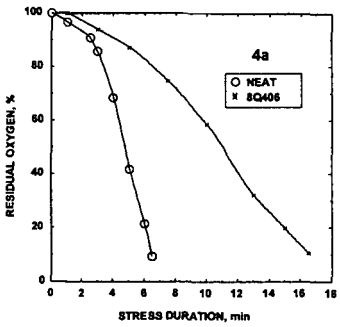

Figure 4a. Effect of 8Q405 (100 mg/L) on neat fuel.

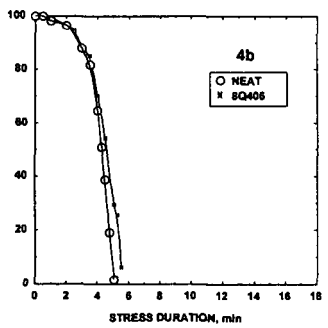

Figure 4b. Effect of 8Q405 (100 mg/L) on diluted fuel.

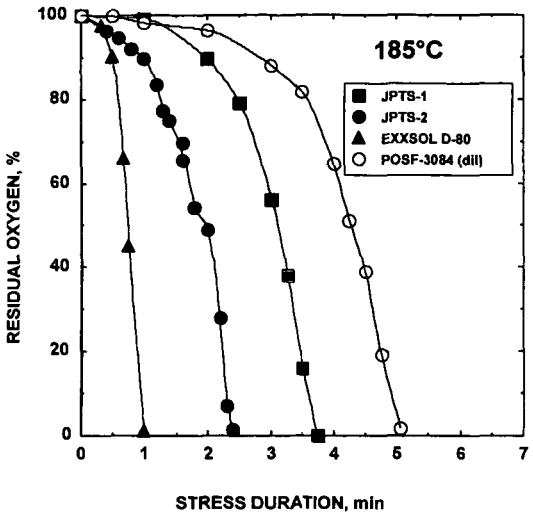

Figure 5. Comparison of diluted POSF-3084 with severely hydrotreated fuels.

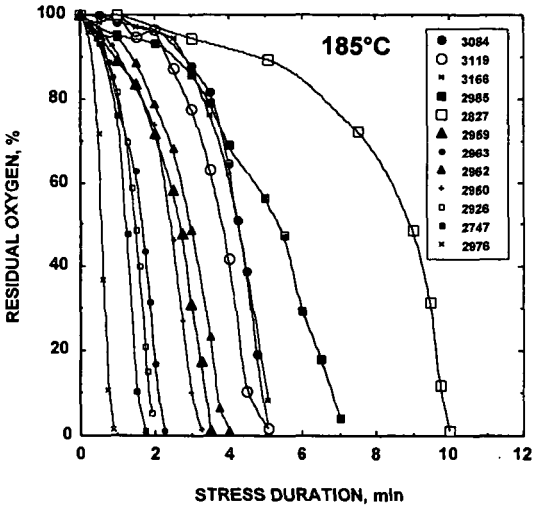

Figure 6. Oxidation of a series of diluted fuels.

AUTOXIDATION OF AVIATION FUEL BLENDS

Lori M. Balster and E. Grant Jones
Innovative Scientific Solutions, Inc.
2786 Indian Ripple Road
Dayton, OH 45440-3638

Keywords: Autoxidation, Fuel Blend, Surface Fouling

INTRODUCTION

The use of aviation fuel to cool component systems in military aircraft creates conditions under which fuel containing dissolved O_2 is exposed to hot surfaces. Liquid-phase oxidation from fuel heating during this application can lead to fouling of critical fuel-line surfaces; problems associated with surface fouling are predicted to become more severe in future aircraft where additional heat dissipation will be required.[1] Low-cost additives including antioxidants have been successful in reducing such fouling in both automotive[2] and aviation[3] fuels. A variation on the introduction of additives is the blending of two fuels. For example, adding a small amount of straight-run fuel which contains many natural antioxidants to a second fuel whose antioxidants have been reduced by refining techniques is equivalent to adding a small amount of antioxi-dant.[4-6] In an effort to better understand autoxidation and changes resulting from antioxidants and blending, the depletion of dissolved O_2 has been monitored in aviation fuels and fuel blends under high-pressure and elevated-temperature conditions that simulate, to some extent, the thermal oxidative stress experienced in aviation fuel lines.

In the present study we tracked depletion of dissolved O_2 at 185°C in a series of eight aviation fuels and many of their 1:1 blends. The selected fuels, summarized in Table 1, include JPTS, JP-7, JP-8, and Jet-A examples covering a broad range of thermal stability. The fuels are numbered approximately in order of decreasing thermal stability, and a blend of Fuels 1 and 8 is designated (1/8). The total quantity of surface insolubles measured for these fuels under the current test conditions ranges from 0.1 to 5 µg/mL. In general, after 22 min of stressing under these reaction conditions, fuels with high thermal stability deposit < 1 µg/mL of insolubles and fuels with low thermal stability deposit > 3 µg/mL.[7] The complex oxidation behavior of each fuel and fuel blend was tracked; the time, t, required to deplete dissolved O_2 by 50% was interpolated from the data and used as a simple measure of oxidation time.

The overall goal of these efforts is the reduction of surface fouling. The specific goal of this study was twofold: first, to investigate whether knowledge of the oxidation behavior of two neat component fuels would be sufficient to predict the oxidation behavior of their 1:1 blend and, second, to identify cases in which blending causes significant delays in autoxidation and search for corresponding delays or reduction in surface fouling. Any method of slowing autoxidation has potential for reducing the extent of surface fouling.

EXPERIMENTAL

Blends are prepared by stirring together equal volumes of the component fuels. The amount of dissolved O_2 is assumed to be approximately the same for each fuel.[8] The methodology used in this study has been described in detail previously.[5] Oxidation and deposition reactions occur as fuel that is saturated with respect to air at room temperature passes through single-pass heat exchangers (NIFTR's) operated isothermally at 185°C. A system pressure of 2.3 MPa ensures a single reaction phase with no headspace. Fuel reaction time (residence time) in the 0.81-m tube (i.d. 0.216 cm) is varied by changing the flowrate. Dissolved O_2 in the stressed fuel is measured by the GC method developed by Rubey and co-workers.[9]

Deposition experiments are performed separately using 1.6-m tubes at a fixed flow of 0.25 mL/min. Surface deposits are quantified using conventional surface-carbon burnoff of 5.1-cm sections cut from the tube at the completion of a 72-hr test.

RESULTS AND DISCUSSION

Oxidation behavior at 185°C for three representative fuels is shown in Figure 1. For the JP-7 Fuel 1--a paraffin/cycloparaffin mix--oxidation is very rapid (< 1 min) and cannot be followed accurately with current methods, whereas for Fuel 6 oxidation is quite slow (> 14 min). All of the remaining fuels oxidize at rates between these two limits. The dependence of Fuel 2 is representative of the behavior of a hydrotreated fuel with added hindered phenol as a synthetic antioxidant. The values of t for Fuels 1, 2, and 6 are ~ 0.6, 3.4, and 6.3 min, respectively. The main constituents of fuels are paraffins, cycloparaffins, aromatics, and alkenes. Many constituents of lesser abundance that contain hetero-atoms such as O, S, and N are very important as natural primary anti-

oxidants that serve to terminate free-radical chains or as natural secondary antioxidants that act to reduce self-initiation by destroying hydroperoxides. Hydroperoxides and dissolved metals in trace amounts can act as pro-oxidants by increasing the free-radical pool. The overall distribution of the major constituents, including antioxidants and pro-oxidants, determines the oxidation behavior. Fuels behave differently under conditions of thermal oxidative stress because each has a unique distribution of components.

Assuming that linear combinations of fuel constituents are achieved in the blends, exactly one-half of the antioxidants and pro-oxidants from each neat fuel is present in a 1:1 blend. In a simplistic view with the blend containing an average of the antioxidants and pro-oxidants from each fuel, the oxidation time may be the average of the times for the component fuels. This model can be checked by comparing the measured times and average calculated times, as shown in Figure 2. Only one-half of the blends approach the simple prediction indicated by the dashed line. The other blends oxidize more slowly than predicted and, in fact, usually oxidize more slowly than either component fuel. The origin of this effect that was originally reported[6] for fuel system (1/6) is not well understood. However, constituents of the slower oxidizing component seem to be more important in determining the oxidation of the blend. This effect occurs in blending two fuels with large differences in oxidation times, one being a severely hydrotreated fuel with reduced aromatic concentration and the other a slower oxidizing fuel of lower thermal stability containing naturally occurring pro-oxidants (dissolved metals) and antioxidants.

The results for many of the blends can be rationalized. For example, the pro-oxidant effect of dissolved metals in Fuel 8 is expected to be reduced by dilution with Fuel 1, and oxidation in that blend will be additionally slowed. An alternative explanation is based on the fact that phenolic antioxidants operate best at an optimum concentration. It can be argued that because lesser quality fuels contain a large excess of phenolic antioxidants, dilution may optimize their antioxidant effect. Both explanations can qualitatively account for the observations, but reliable prediction of the oxidation time for blends cannot be made at this time simply from knowledge of the oxidation behavior of the individual component fuels. The very complicated composition of aviation fuels plays an important role in determining the oxidation time not only for each fuel but also for blends. The presence of naturally occurring antioxidants and dissolved metals as well as the frequent addition to fuels of synthetic antioxidants and metal deactivators preclude simple predictions for blends.

The time dependence of surface fouling was studied in three blends (1/6, 1/7, 1/8) exhibiting unusually slow oxidation. Figure 3 shows the relative difference in surface fouling that resulted from mixing the paraffin Fuel 1 with Fuels 6, 7, and 8. Negative and positive values indicate decrease and increase, respectively, in the extent of surface fouling. Under conditions of 8 - 12 min of stressing, reductions are observed on the order of 0.8 - 1.6 µg/mL, reflecting the observed delays in oxidation. Dilution of Fuels 6, 7, and 8 of lower thermal stability with the severely hydrotreated Fuel 1 creates blends with improved thermal stability.

CONCLUSIONS

The oxidation behavior of 18 blends made from 1:1 mixing of eight component fuels has been studied. Knowledge of the oxidation behavior of the component fuels is not sufficient to permit prediction of the oxidation behavior of blends on the basis of averaging antioxidant and pro-oxidant effects. This is attributed to the complex interaction of fuel constituents including aromatics, naturally occurring antioxidants, and dissolved metals as well as synthetic antioxidants and metal deactivators. Many instances of unusually slow oxidation of blends involving straight-run and severely hydrotreated fuels have been observed. In several of these cases, surface fouling was found to be reduced at shorter stress times in agreement with observed slowing of autoxidation.

ACKNOWLEDGMENTS

This work was supported by the Air Force Research Laboratory, Propulsion Directorate, Wright-Patterson Air Force Base, Ohio, under USAF Contract No. F33615-95-C-2507. The authors would like to thank Mrs. Marian Whitaker for editorial assistance.

REFERENCES

1. Edwards, T.; Anderson, S. D.; Pearce, J. A.; Harrison, W. E., III, High-Temperature JP Fuels--An Overview, AIAA Paper No. 92-0683, Presented at the 30th Aerospace Sciences Meeting and Exhibit, Reno, NV, 6-9 January 1992.
2. Kalghatgi, G. T. Combustion Chamber Deposits in Spark-Ignition Engines: A Literature Review, SAE Paper No. 952443, 1995.
3. Hazlett, R. N. *Thermal Oxidation Stability of Aviation Turbine Fuels*, ASTM Monograph 1; American Society for Testing and Materials: Philadelphia, 1991, p 111.

4. Zabarnick, S.; Zelesnik, P.; Grinstead, R. R. *ASME J. Eng. Gas Turb. Power* 1996, *118*, 271-277.
5. Jones, E. G.; Balster, L. M.; Balster, W. J. *Energy Fuels* 1996, *10*, 509-515.
6. Balster, L. M.; Balster, W. J.; Jones, E. G. *Energy Fuels* 1996, *10*, 1176-1180.
7. Balster, W. J.; Jones, E. G.; Balster, L. M. Manuscript in preparation.
8. Striebich, R. C.; Rubey, W. A. *Prepr.-Am. Chem. Soc., Div. Pet. Chem.* 1994, *39*(1), 47-50.
9. Rubey, W. A.; Striebich, R. C.; Tissandier, M. D.; Tirey, D. A.; Anderson, S. D. *J. Chromat. Sci.* 1995, *33*, 433-437.

Table 1. Fuels studied.

NO	FUEL	TYPE	TREATMENT	AROMATICS (%,vol)	TOTAL SURFACE INSOLUBLES FORMED AT 185°C (µg/mL)	TOTAL SULFUR (ppm)	METALS (ppb)
1	Exxsol D-80	JP-7	hydrotreated	<1	0.5	3	
2	POSF-2976	JPTS	hydrotreated	8	0.1	0	
3	POSF-2747	Jet-A-1	hydrotreated	19	0.1	37	Cu, <5
4	POSF-2980	Jet-A	Merox-treated	17	1.6	614	Cu,<5;Fe, <5
5	POSF-2934	JP-8	straight-run	18	1.9	755	Cu, 44*
6	POSF-2827	Jet-A	straight-run	19	2.6	790	Cu, <5;Fe, 8
7	POSF-3119	Jet-A	straight-run	~20	4.5	1000	Cu, 7;Fe, 26
8	POSF-3084	Jet-A	straight-run	18	4.8	527	Cu, 35;Fe, <5

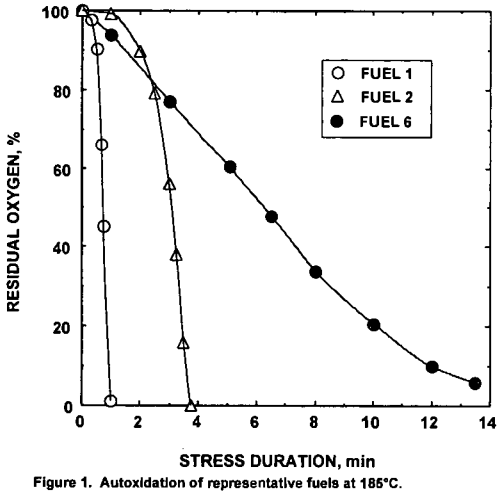

Figure 1. Autoxidation of representative fuels at 185°C.

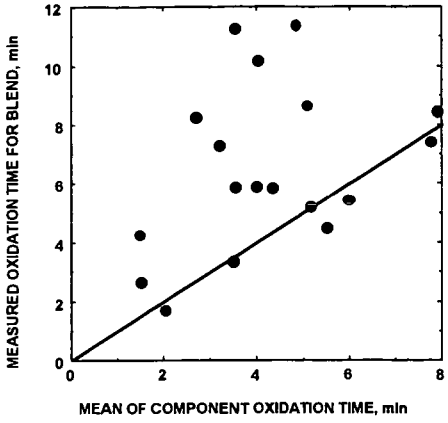

Figure 2. Comparison of measured and calculated oxidation times

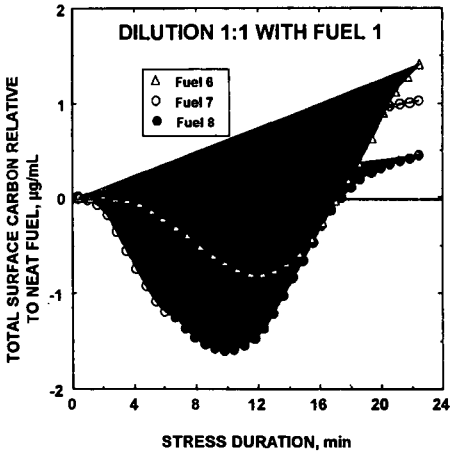

Figure 3. The effect of blending on total surface carbon.

LIQUID-PHASE OXIDATION KINETICS OF AVIATION FUELS

E. Grant Jones
Innovative Scientific Solutions, Inc.
2786 Indian Ripple Road
Dayton, OH 45440-3638

James M. Pickard
Kinetica, Inc.
Mound Advanced Technology center
720 Mound Avenue
Miamisburg, OH 45343

Keywords: Autoxidation, Fuels, Oxidation Kinetics

INTRODUCTION

Liquid-phase oxidation occurs when fuel that contains dissolved O_2 is used as the primary heat sink for cooling aircraft subsystems.[1] Insoluble products of oxidation reactions can foul heated surfaces, resulting in expensive downtime for cleaning and replacement of heat exchangers, fuel-control valves, and injectors. Computational fluid dynamics (CFD) models[2] have been successful in calculating the extent of surface fouling in selected fuel systems. The general application of such models depends on calibration using experimental fouling data and is limited by simple representations of very complicated oxidation chemistry. Furthermore, the fact that each fuel is unique in its distribution and abundance of components adds to the complexity of the oxidation processes. More detailed knowledge of oxidation kinetics of several representative aviation fuels is needed to assist in improving CFD calculations and the understanding of the fundamentals of fuel autoxidation.

Over the past several years, our laboratory has been measuring the depletion of dissolved O_2 under elevated-temperature (150-225 °C), elevated-pressure, and isothermal conditions to simulate the thermal oxidative stress conditions existing in aircraft fuel lines. An important factor in these studies has been the reduction of surface catalysis. Stainless-steel surfaces were found to catalyze autoxidation; however, the use of passivated tubing (Silcosteel process)[3] enabled the study of autoxidation with minimal effects from surface catalysis.[4]

This paper summarizes recent kinetic studies of the oxidation of several representative aviation fuels. Results are reviewed for a Jet-A fuel, POSF-2827, that has been studied both as a neat fuel[5] and as a mixture catalyzed by Fe_2O_3.[6] New data are presented which extend the range of studied fuels to include both a rapidly oxidizing paraffin blend, Exxsol D-80, which is analogous to a JP-7 fuel, and a hydrotreated Jet-A fuel, POSF-3428.

EXPERIMENTAL

The methodology used in NIFTR (Near-Isothermal-Flowing-Test-Rig) studies of oxidation and deposition has been described in detail previously[7]. Liquid-phase oxidation occurs as air-saturated fuel passes through a single-pass heat exchanger operated isothermally at 185 °C. A system pressure of 2.3 Mpa ensures a single reaction phase with no head space. Fuel reaction time (residence time) in the 0.81-m tube (i.d. 0.216 cm) was changed by varying the flowrate. Dissolved O_2 in the stressed fuel was measured by the GC method developed by Rubey and co-workers.[8] In experiments where the initial O_2 concentration was varied, fuel was sparged with different gas blends of O_2 and N_2 using a Porter CM 4 interface module and F200 thermal mass flow controllers.

RESULTS AND DISCUSSION

POSF-2827. POSF-2827 is a Jet-A fuel with a thermal stability ranging from average to below average. Reduced thermal stability coupled with very slow oxidation, as shown at 458 K in Figure 1, has been attributed to a large excess of natural antioxidants.[5] The overall effect of these antioxidants is a low steady-state concentration of hydroperoxide, ROOH, and the absence of autocatalysis at higher O_2 conversion. Such a system with an approximately constant rate of initiation provided an excellent test for application of the NIFTR technique in collecting data for evaluating Arrhenius kinetic parameters. Since the reaction is 0.5 order in O_2, it is explained according to the following simplified autoxidation mechanism:

$$RH + O_2 \rightarrow R\bullet + \bullet O_2H \qquad \text{(i)}$$

$$RO_2H \rightarrow RO\bullet + \bullet OH \qquad \text{(i')}$$

$$R\bullet + O_2 \rightarrow RO\bullet_2 \qquad \text{(ii)}$$

$$RO\bullet_2 + RH \rightarrow RO_2H + R\bullet \qquad \text{(iii)}$$

$$2RO\bullet_2 \rightarrow \text{Neutral products} \qquad \text{(iv)}$$

where R• is a radical, $RO•_2$ is a peroxy radical, and RO_2H is the hydroperoxide. Reactions (i) and (i') represent initiation, (ii) and (iii) are propagation, and (iv) termination. Reaction (i') is the major initiation reaction in hydrotreated fuels; it is of minor importance in fuels containing large concentrations of heteraromatic species and natural antioxidants. Data analysis over the temperature range 438-478 K yielded $\log(k_{ap}/M^{-1/2}s^{-1}) = (12.9 \pm 0.4) - (36.9 \pm 0.8)/\theta$, where k_{ap} is the apparent rate coefficient and θ is 2.303 RT kcal mol^{-1} (R is the ideal gas law constant and T is absolute temperature). At lower temperature, the self-initiation of the autoxidation is negligible. The addition of an external initiator (2,2'-azobis[2-methylpropionitrile], AIBN) over the temperature range 393-414 K resulted in $\log(k_{iii}/(2k_{iv})^{1/2}/M^{-1/2}s^{-1/2}) = (7.08 \pm 0.3) - (18.6 \pm 0.5)/\theta$.[5]

POSF-2827 (4 ppm Fe_2O_3). Figure 1 shows changes arising from the introduction of 4 ppm of Fe_2O_3 into POSF-2827. Fe_2O_3 acts as a heterogeneous catalyst in accelerating autoxidation. The kinetic data for oxidation in the presence of Fe_2O_3 are consistent with reaction acceleration from dissociation of an Fe_2O_3-ROOH adduct formed by the adsorption of ROOH on the Fe_2O_3 surface; and subsequent H-atom abstraction by surface adsorbed radicals. Data analysis yielded $\log(k_{ap}/M^{-1/2}s^{-1}) = (11.7 \pm 0.5) - (27.7 \pm 0.9)/\theta$ for the catalytic oxidation. The average value of $E_{iii} - E_{iv}/2 = 18.6$ kcal mol^{-1} determined from AIBN initiation coupled with $E_{ap} = 27.7$ kcal mol^{-1} implies $E_i \approx 18$ kcal mol^{-1} for initiation by Fe_2O_3.[6]

Paraffin/cycloparaffin blend (Exxsol D-80). This blend is representative of the highly thermally stable JP-7 fuel (in the absence of a lubricity additive) as used in high performance military aircraft such as the SR-71. With very low concentrations of aromatics (< 1%) and no natural or synthetic antioxidants, Exxsol D-80 oxidizes rapidly. Depletion of O_2 over the low-temperature range 408-438 K is given in Figure 2. Unlike POSF-2827 oxidation, this system is dominated by thermal dissociation of ROOH, as evidenced by acceleration at higher conversion. The kinetic data are described by $\log(k_{ap}/M^{-1/2}s^{-1}) = (9.5 \pm 0.2) - (26.3 \pm 0.4)/\theta$; the solid lines illustrate fits from these parameters. Oxidation has been studied at 413 K for different initial concentrations varying from 10 to 100% O_2-saturation at room temperature. The results, shown in Figure 3, are also fitted with the same kinetic parameters. Initial rates are independent of O_2 concentration, consistent with initiation by trace quantities of ROOH. Analysis of the ROOH data led to $\log(k_{iii}/(2k_{iv})^{1/2}/M^{-1/2}s^{-1/2}) = (3.3 \pm 1.3) - (12.5 \pm 2.6)/\theta$.

POSF-3428. The fuels discussed above represent two extremes both in thermal stability and oxidation behavior. POSF-3428 is more representative of a broad spectrum of aviation fuels having intermediate stability and reaction rates controlled by hydroperoxides. The oxidation behavior shown in Figure 4 is autocatalytic and the solid lines were calculated using the same mechanism as that for Exxsol D-80, with thermal decomposition of ROOH as the dominant source of initiation. The kinetic data are summarized by $\log(k_{ap}/M^{-1/2}s^{-1/2}) = (12.3 \pm 0.9) - (34.7 \pm 1.8)/\theta$

CONCLUSIONS

The apparent rate coefficients describing liquid-phase oxidation have been measured in four fuel systems using the NIFTR apparatus. The fuel reactivities may be ranked inversely according to the magnitudes of the apparent activation energies for autoxidation. Apparent activation energies follow the trend: POSF-2827 > POSF-3428 > POSF-2827 (4 ppm Fe_2O_3) > Exxsol D-80. The most unreactive fuel with respect to autoxidation is POSF-2827; the reason being that the fuel the fuel contains heteroaromatic speices(sulfur componds) that scavenge ROOH. The most reactive fuel is Exxsol-D80 which contains less than 1% aromatics and is devoid of natural ROOH scavengers. The extremes in reactivity are also reflected by the rates of initiation. Since appreciable ROOH does not accumulate in neat POSF-2827, initiation is controlled by reaction (i). This results in $E_i \approx 37$ kcal mol^{-1} for the spontaneous initiation of POSF-2827. For Exxsol D-80, initiation is dominated by ROOH dissociation with $\log(k_i'/ s^{-1}) \approx 16 - 33/\theta$.

ACKNOWLEDGMENTS

This work was sponsored by the Air Force Research Laboratory, Propulsion Directorate, Wright-Patterson Air Force Base, Ohio, under Contract No. F33615-95-C-2507. The authors would like to thank Ms. Lori Balster for conducting the dissolved O_2 measurements and Mrs. Marian Whitaker for editorial assistance.

REFERENCES

1. Edward, T.; Anderson, S. D.; Pearce, J. A., Harrison; W. E., III, High-Temperature JPFuels–An Overview, AIAA Pasper No. 92-0683, Presented at the 30th Aerospace Sciences Meeting and Exhibit, Reno, NV, 6-9 January 1992.

2. Katta, V. R.; Jones, E. G.; Roquemore, W. M. "Development of Global-Chemistry Models for Jet-Fuel Thermal Stability Based on Observations from Static and Flowing Experiments," AGARD-CP-536, Paper No. 19., 1993.
3. Restek Corporation, Bellfonte, PA.
4. Jones, E. G.; Balster, L. M.; Balster, W. J. *Energy Fuels*, **1996**, *10*, 831-836.
5. Pickard, J. M.; Jones, E. G. *Energy Fuels*, **1996**, *10*, 1074-1077.
6. Pickard, J. M.; Jones, E. G. *Energy Fuels*, **1997**, *11*, 1232-1236.
7. Jones, E. G.; Balster, L. M.; Balster, W. J. *Energy Fuels*, **1996**, *10*, 509-515.
8. Rubey, W. A.; Striebich, R. C.; Tissandier, M. D.; Tirey, D. A.; Anderson, S. D. *J. Chromat. Sci.* **1995**, *33*, 433-437.

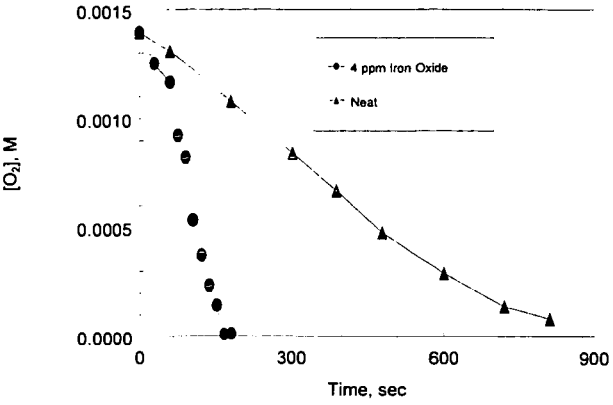

Figure 1. Oxygen depletion vs time for neat and iron-oxide (4 ppm)-treated fuel.

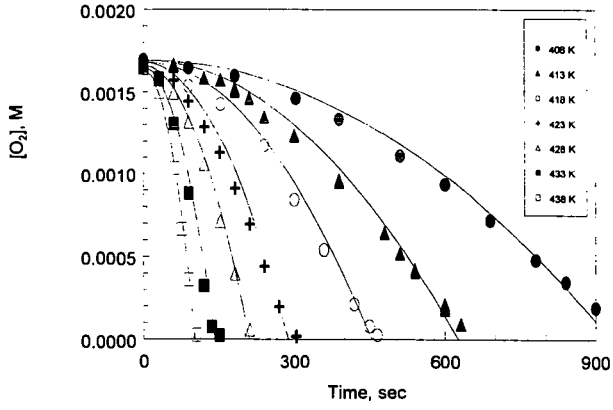

Figure 2. Influence of temperature on oxygen depletion : air-saturated Exxsol D-80 from 408 to 438 K.

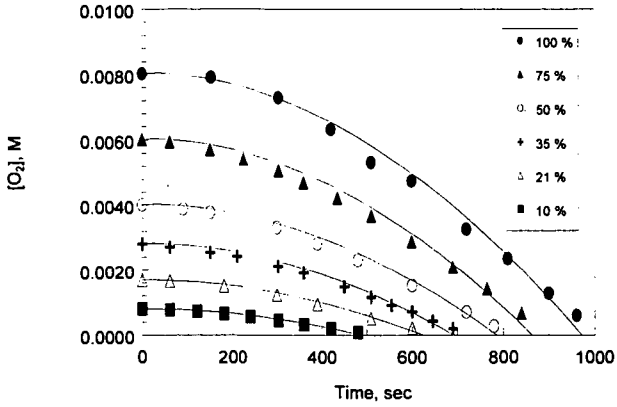

Figure 3. Influence of oxygen concentration on oxygen depletion: air-saturated Exxsol D-80 at 413 K.

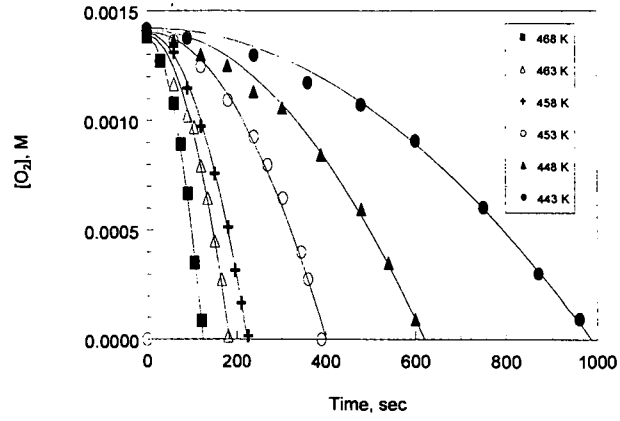

Figure 4. Influence of temperature on oxygen depletion: air-saturated POSF-3428 from 408 to 438 K.

JET FUEL SYSTEM ICING INHIBITORS: SYNTHESIS AND STABILITY

[a,b]George W. Mushrush, [b]Erna J. Beal, [b]Dennis R. Hardy, [a]Wayne M. Stalick, [a]Subhash Basu, [c]Dennis Grosjean, and [d]John Cummings

[a]George Mason University, Fairfax, VA 22030, [b]Navy Technology Center for Safety and Survivability, Washington, DC 20375, [c]Innovative Scientific Solutions Inc., 2786 Indian Ripple Road, Dayton, OH 45440, and [d]Naval Air-Warfare Center, Trenton, NJ 08628

ABSTRACT

The current fuel system icing inhibitor additives, used both by the military and commercial aviation, are ethylene glycol monomethyl ether (EGME) and diethylene glycol monomethyl ether (DiEGME). These deicing compounds are toxic at the concentrations that are required for effective deicing. This observation points to an immediate need for non-toxic, inexpensive, and biodegradable deicing compounds. The synthesis of polar sugar derivatives represents viable alternatives to glycol based additives. The synthesis and characterization of acetals, ketals, ethers, and esters of oxoacids will be discussed. These alternative deicing compounds are cheap, fuel stable, and exhibit similar icing inhibitor characteristics to EGME and DiEGME.

INTRODUCTION

The literature of deicing additives for jet fuels is rather sparse. Those articles that have appeared are related to concentration determination, stability in fuels, and health implications of these additives(1, 2). Currently the fuel icing inhibitor additives, ethylene glycol monomethyl ether (EGME) and diethylene glycol monomethyl ether (DiEGME), are mandatory in all military aircraft fuels and are optional in world-wide commercial aviation fuels depending on route, flight length, and season. Unfortunately, ethylene glycol based deicing compounds are toxic at the concentrations that are required for effective deicing (2). These additives are leached out of the fuel and into water bottoms and when this water is drained from fuel system sumps, filters and storage tanks it contains EGME and/or DiEGME thus creating a personnel health hazard. Also, glycols exert high oxygen demand for decomposition and when they get into the environment they cause the death of aquatic organisms as dissolved oxygen is depleted. These observations all point to an immediate need for non-toxic, inexpensive, and biodegradable deicing compounds. The approach of our laboratory is to utilize the large U.S. surplus of sugars as the basis for the synthesis of biodegradable deicing compounds. These potential deicing candidates must satisfy many constraints. They must be soluble in jet fuel, soluble in water, fuel stable during storage, and exhibit similar or enhanced ice inhibiting characteristics to currently used deicing compounds.

The latter of these constraints, concerning the behavior of deicing compounds in fuels, is being investigated in our laboratory since there are no readily available software programs to estimate either the physical or colligative properties of middle distillate fuels. A large number of physicochemical and toxicological properties are prerequisite to a reasonable hazard assessment of a chemical (1). However, environmental fate, and toxicity of chemicals can be estimated using computer models. These predicted values provide the guidance towards synthesizing safer icing inhibitors for this project.

EXPERIMENTAL

The general synthesis procedure followed for the synthesis of the glycerol acetals and ketals was that reported for the synthesis of the 2,2-dimethyl-1,3-dioxolane-4-methanol, compound **I** (3). The procedure was modified for the synthesis of the formaldehyde (compound **II**), and acetaldehyde (compound **III**), adducts. Acetone (232g, 4.5moles), or acetaldehyde (197g, 4.5 moles), or formaldehyde (135g, 4.5 moles), was added to glycerol (100 g, 1.1 moles) in a toluene solvent (300 mL), containing 3.0 g *p*-toluene sulfonic acid and 255 g of 5A molecular sieves all in a 2,000 mL two-necked, round-bottomed flask fitted with a mechanical stirrer and a condenser. A freezing mixture of ethylene glycol and water at -25.0 °C was circulated through the condenser. The stirred reaction mixture was heated under gentle reflux for 33 hrs using a heating mantle. After reflux, the condenser was disconnected and excess acetaldehyde was allowed to evaporate. The acidic reaction mixture was neutralized with 3.0 g sodium acetate. The molecular sieves were separated by vacuum filtration using a Büchner funnel. The resulting liquid was distilled under vacuum. The colorless organic product distilling at 80-82?C/10 mm was collected for the acetone derivative to give a yield of 88%; for the acetaldehyde derivative the

product distilling at 85-90 ?C/10mm was collected to give a yield of 80 %; and for the formaldehyde derivative the product distilling at 95-96?C/10 mm was collected (4).

Computational Methods. In order to estimate environmental fate and certain physical properties, a suite of programs developed by Syracuse Research Corporation was used (5). Well established computational methods are used in these programs.

DISCUSSION

The reaction products of aldehydes and ketones with glycerol have been known for more than 100 years. These compounds were usually regarded as intermediates in synthetic procedures and little interest was expressed in them. The compounds in this study are simpler than the. carbohydrates and carbohydrate derivatives so they were the subject of this initial investigation Acetal and ketal formation is catalyzed by either mineral acids or Lewis acids. The intermediate hemi-acetal or hemi-ketal is not usually isolated. The compounds were subjected to testing for deicing characteristics and compared to EGME, DiEGME, and dipropylene glycol. Dipropylene glycol was included because industries and the Federal Aviation Administration have recommended it as a replacement for the ethylene based deicers. The freezing point tests were conducted in a one gallon simulator rig. The data showed that both compounds **II** and **III** were effective deicers and closely paralleled the behavior of EGME and DiEGME(6). Compounds **II** and **III** show similar time vs temperature dependence The compounds were also tested for fuel instability and incompatibility reactions. They were tested for storage stability by ASTM method D5304-92 in JP-8 (7).

Additives in this Study

These compounds, along with their estimated physical properties and environmental toxicity profile, are presented in Table 1. Compound **I** appears to have excellent potential properties as a deicing agent. This compound has been well characterized in the literature and is considered to be relatively non-toxic (8). It is used commercially as a solvent, plasticizer, and solubilizing and suspending agent in pharmaceuticals. Additionally, it is miscible in hydrocarbons, gasolines, turpentine, oils, and water; making it an ideal candidate as an icing inhibitor. Although Compound **I** has a higher dermal dose per event than current deicers this is countered by its lower toxicity and dermal permeability; due, perhaps in part, to its higher lipophilicity. Compound **I** is decomposed in the atmosphere at a rate comparable to current deicers. Like current deicers, it is not rapidly volatilized from aquatic systems. Upon ingestion, possibly at mouth pH but certainly at stomach pH, this compound is readily broken down into acetone and glycerol. Both of these compounds have relatively low toxicity and environmental concerns. The second of the compounds synthesized, compound **III**, exhibits a lower dermal permeability and dermal dose per event than any of the other compounds in this study. The decomposition products upon ingestion, which are glycerol and acetaldehyde, are also relatively non-toxic; acetaldehyde is even less toxic than acetone. Acetaldehyde is one of the metabolized products of ethanol.

Compound **II** was dismissed due to the formation of formaldehyde upon decomposition under mildly acidic conditions. Formaldehyde is a known toxic and carcinogenic agent and the use of formaldehyde adducts in this study was ceased for this reason. This concern aside, compound **II** exhibits similar properties to the other compounds in this study, with a lower dermal dose per event.

All three compounds were found to be soluble in jet fuel at the levels necessary for inhibiting the formation of ice; and closely paralleled the behavior of EGME and DiEGME(4). Accelerated fuel instability and incompatibility studies using ASTM method D5304-92 in JP-8 (7) showed negligible formation of solids (<0.01 mg) and no increased peroxidation.

CONCLUSION

Testing and evaluation of these new deicing compounds derived from sugars showed that they exhibited properties that make them ideal candidates for the next generation of deicing compounds. Both Compounds **I** and **III** are predicted to be environmentally benign and relatively nontoxic at the concentrations necessary for inhibiting ice formation. Compound **I** has been well characterized due to its current commercial applications, and the need for further investigation into the toxicity of Compound **II** is indicated. Other analogs from reduced sugars have been synthesized and evaluated and will be reported on in subsequent papers. The substituted forms of reduced sugars have the potential for the ideal combination of lipophilic and hydrophilic character necessary for deicing applications.

ACKNOWLEDGMENT

The authors would like to express appreciation to Syracuse Research Corporation, the Air Force Office of Scientific Research (AFOSR) under grant number 5-25016, and the Office of Naval Research for research support.

REFERENCES

(1) Basak, S. C., Niemi, G. J. , Veith, G. D. J. of Mathematical Chemistry. 4,.185 (1990).

(2) U.S. Department of Health & Human Services, Agency for Toxic Substances and Disease Registry, Tech. Rpt for Ethylene Glycol/Propylene Glycol Rprt 205-88-0608, May 1993.

(3) Organic Synthesis Collective Volume 3, ed. E.C. Horning, pp 502-504, Wiley:New York, 1965.

(4) Mushrush, G.W., Stalick, W.M., Beal, E.J., Basu, S.C., Slone, J.E., Cummings, Petroleum Science & Technology. 15(3,4), 237 (1997).

(5) Meylan, W., Syracuse Research Corporation.DERMAL *for Windows*, Version 1.23, (1996).(a). MPBP *for Windows*, Version 2.51, (1996); (b). WSKOW *for Windows*, Version 1.20, (1996); (c). HENRY *for Windows*, Version 2.51, (1995); (d) AOP *for Windows*, Version 1.80, (1996); (e).KOC *for Windows*, Version 1.57, (1995); (f) *Estimation Program Interface for Windows*, Version 2.00, (1995).

(6) Stirling, K. Q., Ripley, D. L. Partition Coefficients of Icing Inhibitors in JP-4 and JP-5 Jet Fuel, U. S. Department of Energy and Naval Air Propulsion Center, Final Report DE-FC22-83FE60149, October 1990.

(7) ASTM ?Standard Test Method for Assessing Distillate Fuel Storage Stability by Oxygen Over pressure,? Annual Book of ASTM Standards; ASTM:Philadelphia, Part 0.05.01, ASTM D5304-92, (1992).

(8) Sanderson, M. D. J. Pharm. Pharmacol. 11, 150 (1959) and 11, 446 (1959).

	Compound I	Compound II	Compound III
Dermal permeability K_p cm/hr	5.00×10^{-3}	6.94×10^{-4}	1.17×10^{-3}
Dermal dose per event (at concentration of 100 mg/cm^3 for 0.25 hr) in mg/cm^2	0.0430	0.0048	0.0079
log K_{ow} (lipophilicity)	1.07	-0.50	-0.09
Vapor pressure in mmHg	0.0647	0.2700	0.1140
Water solubility in mg/L	3.459×10^4	9.918×10^5	3.914×10^5
Henry's Law Constant in atm x m^3/mol	1.91×10^{-9}	1.08×10^{-9}	1.44×10^{-9}
OH rate constant in cm^3/molecules x sec	2.50420×10^{-11}	2.68248×10^{-11}	$2.99376 \times 10^{-}$
Atmospheric half-life in hrs.	5.125	4.785	4.287
Soil adsorption coefficient K_{oc}	1.00	1.00	1.00
Volatilization from model river in years (half-life)	60.30	94.712	75.62
Volatilization from model lake in years (half-life)	38.60	688.76	550.00
Biological Oxygen Demand in days (half-life)	2-15	2-15	2-15
LC_{50} in ug/L for *Pimephales Promelas*	1.67×10^7	2.36×10^7	------
Bioconcentration factor for *Pimephales promelas*	1	1	1

Table 1. Compounds based upon the reduced sugar mannose

	Ethylene glycol mono-methyl ether (EGME)	**Di(ethylene glycol) mono-methyl ether (DiEGME)**
Dermal permeability K_p in cm/hr	4.98×10^{-4}	2.97×10^{-4}
Dermal dose per event (concentration of 100 mg/cm^3 for 0.25 hr) in mg/cm^2	4.66×10^{-3}	1.3×10^{-3}
log K_{ow} (lipophilicity)	-0.77	-1.18
Vapor pressure in mmHg	9.2200	0.2160
Water solubility in mg/L	1.000×10^{6}	1.000×10^{6}
Henry?s Law Constant in atm x m^3/mol	4.19×10^{-8}	6.50×10^{-10}
OH rate constant in cm^3/ molecule x sec	1.19983×10^{-11}	2.60139×10^{-11}
Atmospheric half-life in hours	10.698	4.934
Soil adsorption coefficient K_{oc}	1.00	1.00
Volatilization from model river in years (half-life)	11.32	6660.27
Volatilization from model lake in years (half-life)	82.30	4.4844×10^{5}
Biological Oxygen Demand (BOD) in days (half-life)	2-16	2-16
LC_{50} in ug/L for *Pimephales promelas*	2.15×10^{7}	2.96×10^{7}
Bioconcentration factor (BCF) for *Pimephales promelas*	1	1

Table 2. Estimated values for current FSII additives

STUDIES OF SILYLATION AGENTS AS THERMAL-OXIDATIVE JET FUEL ADDITIVES

S. Zabarnick, M.S. Mick, R.C. Striebich, R.R. Grinstead, and S.P. Heneghan
University of Dayton Research InstituteAerospace Mechanics Division,
300 College Park, Dayton OH 45469-0140

INTRODUCTION

Derivatization techniques are well known methods to alter species structures to make them more amenable to chemical analysis. Silylation is one type of derivatization process, in which species which contain reactive hydrogen atoms are reacted with an appropriate agent resulting in the conversion of these reactive hydrogen sites to relatively unreactive trimethyl silyl sites (1). Silylation is widely practiced in chromatographic analysis to improve analytical quantitation and transport, increase detectability, increase volatility, and decrease surface interactions. In general, silylating agents are able to react with the active hydrogens in the following species: acids, alcohols, thiols, amines, amides, and enolizable ketones and aldehydes. A variety of agents are known, which vary in their reactivity, selectivity, side reactions, and character of reaction by-products.

Jet fuel is used as a coolant in advanced military aircraft; the hot fuel reacts with dissolved oxygen forming oxidized products. These oxidized products include gums and solid deposits which can coat fuel system surfaces resulting in filter plugging, fouling of close tolerance valves, valve hysteresis, and other problems. Various chemical additives and additive combinations have been utilized to inhibit oxidation and/or reduce deposition. For example the U.S. Air Force JP-8+100 additive package contains a dispersant, an antioxidant, and a metal deactivator. It is generally agreed that the advanced military aircraft being presently conceived will have significantly higher heat loads which will be dumped into the fuel. This higher fuel temperature will result in substantially increased oxygen consumption and subsequent increased deposition.

The substantially higher fuel system temperatures of advanced aircraft will result in complete or near complete oxygen consumption. Additives which delay oxidation, such as antioxidants, metal deactivators, and hydroperoxide decomposers, will be unable to provide significant benefits in reducing deposition under time/temperature conditions where dissolved oxygen consumption is assured. Thus alternative additive techniques need to be explored. Dispersant additives can still be useful under these conditions.

In this study we explore the use of silylation agents as jet fuel additives for reducing oxidative deposition. Silylation agents have the ability to react with the heteroatomic species, such as phenols, which have been implicated in deposit producing mechanisms. Thus they have the potential to chemically transform these species into relatively innocuous silylated products. In this work we study the effect that silylation agents have on jet fuel oxidation and deposition. We show that these additives result in an increased oxidation rate and substantially reduced deposition. These results show that silylation agents may be useful as jet fuel additives for preventing oxidative deposition in advanced aircraft fuel systems including endothermic fuel systems. Silylation agents may also prove to be useful in easing identification of fuel components, particularly those detrimental to fuel thermal stability.

EXPERIMENTAL

Fuel oxidation and deposition characteristics were evaluated in the quartz crystal microbalance/Parr bomb system (QCM) which has been described in detail previously (2,3). All fuel oxidation tests were run at 140C and one atmosphere of air initial pressure. It is heated with a clamp-on band heater and its temperature is controlled by a PID controller through a thermocouple immersed in the fuel. The reactor contains an rf feedthrough, through which the connection for the quartz crystal resonator is attached. The crystals are 2.54 cm in diameter, 0.33 mm thick and have a nominal resonant frequency of 5 MHz. The crystals were acquired from Maxtek Inc. and are available in crystal electrode surfaces of gold, silver, platinum, and aluminum. For the studies reported here gold crystal electrodes were used. The QCM measures deposition (i.e., an increase in mass) which occurs on overlapping sections of the two sided electrodes. Thus, the device responds to deposition which occurs on the metal surface and does not respond to deposition on the exposed quartz.

The device is also equipped with a pressure transducer (Sensotec) to measure the absolute headspace pressure and a polarographic oxygen sensor (Ingold) to measure the headspace oxygen concentration. Previous studies have demonstrated the value of determining the oxidation characteristics of fuels and fuels with additives. A personal computer is used to acquire data at one minute intervals during the experimental run. The following data are recorded during a run: temperature, crystal frequency, headspace pressure, headspace oxygen concentration, and crystal damping voltage.

The reactor is charged with 60 mL of fuel, which is sparged with the appropriate gas for one hour before each test. The reactor is then sealed and the heater is started. All runs in this study were performed at 140C; heat-up time to this temperature is 40±5 minutes. Most runs are conducted for 15 hours, after which the heater is turned off and the reactor allowed to cool. Surface mass measurements can only be determined during the constant temperature (±0.2C) portion of an experimental run. The crystal frequency is converted to a surface mass measurement using the process described below.

The theory that relates the measured frequency changes to surface mass has been presented in detail elsewhere (4). The frequency change of a crystal immersed in a liquid fuel can be due to two effects: the first results from changes in the surface mass density, the second is due to changes in the liquid density and viscosity. At constant temperature and relatively small extents of chemical conversion the liquid properties remain constant and the frequency change can be related to surface deposition via the equation

$$\rho_s = -\left(2.21 \times 10^5 \text{ g}/(\text{cm}^2 s)\right)\frac{\Delta f}{f_0^2} \qquad (1)$$

where f_0 is the unperturbed resonant frequency, Δf is the change in resonant frequency, and ρ_s is the surface mass density (mass/area). The reproducibility of the mass deposition measurements on fuels is limited to ±20% for the QCM technique. The fuels studied and some of their properties are listed in Table 1. The fuels were acquired from the Fuels and Lubricants Division of Wright Laboratory, Wright-Patterson AFB, OH, and are referred to by the Wright Lab assigned accession number. Silylation agents were acquired from Pierce Chemical.

The fuels were tested at 140C for 15 hours in a static reactor which utilizes a quartz crystal microbalance (QCM) for measuring deposition, and a polarographic oxygen sensor which monitors the oxygen concentration in the reactor headspace, for monitoring the oxidation process. The experimental apparatus has been described in detail previously (2).

RESULTS AND DISCUSSION

Jet fuel is a complex mixture which is primarily composed of branched and straight chain alkanes, cycloalkanes, and alkyl-substituted aromatics. In addition, various heteroatomic species may be present at relatively small concentrations, including but not limited to: phenols, peroxides, alcohols, organic acids, sulfides, thiols, thiophenes, and amines. In the absence of these heteroatomic species, this hydrocarbon mixture oxidizes readily at elevated temperature via the classic hydrocarbon autoxidation mechanism. For example, a pure alkane, such as dodecane, or a highly treated petroleum fraction, such as Exxsol D-110, will completely consume all available oxygen in the QCM system on the order of minutes at 140C. But, real jet fuels oxidize much more slowly. Even severely hydrotreated fuels require two to five hours to consume the available oxygen at this temperature. Less severely processed fuels can require 5 to 60 hours to consume the available oxygen. These real fuels oxidize more slowly than pure hydrocarbons, due to the presence of these heteroatomic species. These species slow oxidation by intercepting alkyl peroxy radicals and/or by decomposing alkyl hydroperoxides to non-radical products (3,4). Thus the removal of such species should result in a significant increase in the oxidation of the fuel. This effect is illustrated in the hydrotreatment process, which removes heteroatomic species and results in highly oxidizable fuel. These same species which slow oxidation of fuel, also play important roles in forming surface and bulk deposits upon fuel oxidation. Thus, a fuel which is treated to remove such heteroatomic species will oxidize rapidly and display reduced deposition formation.

Treating jet fuel with silylating agents results in the reaction of species with active hydrogens to form trimethylsilyl derivatives. For the case of an alkyl phenol, the following reaction occurs:

We are converting a phenol with a reactive hydrogen to its trimethylsilyl derivative, which is much less reactive and does not contain an active hydrogen. The resulting compound is not reactive towards alkylperoxy radicals (relative to the original phenol) and thus does not interfere with the fuel autoxidation chain. Analogous reactions to the above are also possible for other compounds with active hydrogens.

To explore the effect that silylation has on jet fuel we added one mL of hexamethyldisilazane (HMDS) to 60 mL of fuel F-3119 and stressed this additized fuel in the QCM at 140C for 15 hours. The resulting oxygen sensor and QCM deposition plots for the neat and additized fuel are shown in Figure 1 and 2. The headspace oxygen plot shows that HMDS causes a substantial increase in the oxidation rate of the fuel. The resulting oxygen decay is nearly as fast as a pure hydrocarbon solvent (oxidation complete in 2 to 2.5 hours). The deposition plot shows that HMDS causes a >90% decrease in deposition during the run. It is apparent that treatment of this fuel with HMDS results in significant removal of species which delay oxidation. In addition, removal of these species results in reduced deposition.

It is interesting to compare these results with another technique which removes heteroatomic species, solid-phase extraction (SPE). Of the heteroatomic species present, silica gel SPE removes only those that have significant polarity. Previously, we have demonstrated that SPE treatment reduces deposition significantly, but does not increase oxidation as substantially (2).

To investigate the chemical changes that occur in the fuel upon silylation treatment we used gas chromatography–mass spectrometry (GC-MS) after preconcentration of the polar fuel species via SPE with subsequent methanol back extraction. This technique is particularly useful for identification of phenol species in the fuel. The results of these analyses (not shown) demonstrate substantial conversion of fuel phenols to their silylated derivatives.

There exist a variety of silylation reagents which display varying silylation selectivity, reactivity, side reactions, and character of reaction by-products. For example, while HMDS requires elevated temperatures for reaction, silylation with N,O-bis[trimethyl]acetamide (BSA) can be performed at room temperature. We therefore have the ability to control the time and/or temperature at which the silylation reaction occurs. The ability to remove phenols within aircraft fuel lines during the heating of the fuel in its transport through the fuel system is highly desirable. The presence of phenols can be desirable during fuel storage as they inhibit oxidation, but their presence is undesirable in fuel systems due to their contribution to fouling. By proper choice of a silylation additive, we may be able to design a fuel where the silylation reaction occurs at a location of choice in the fuel system with subsequent rapid consumption of oxygen.

The promise of silylation additives does not come without potential disadvantages. These include cost, water sensitivity, and problems due to product formation in combustors. Presently, silylation additives are relatively expensive, when compared to common jet fuel additives, as they are produced in relatively small quantities for derivatization in chemical analysis. Silylation reagents react rapidly with water and humid air forming undesirable silanols. It is expected that silylating reagents and silylated products will be rapidly oxidized to silicon dioxide within the combustion chamber. This may have a negative effect on combustor and turbine materials depending on the physical form of the silicon dioxide product.

CONCLUSIONS

In this study we explore the use of silylation agents as jet fuel additives for reducing oxidative deposition. Silylation agents have the ability to react with the heteroatomic species, such as phenols, which have been implicated in deposit producing mechanisms. Thus they have the potential to chemically transform these species into relatively innocuous silylated products. In this work we study the effect that silylation agents have on jet fuel oxidation and deposition. We show

that these additives result in an increased oxidation rate and substantially reduced deposition. These results show that silylation agents may be useful as jet fuel additives for preventing oxidative deposition in advanced aircraft fuel systems including endothermic fuel systems. Silylation agents may also prove to be useful in easing identification of fuel components, particularly those detrimental to fuel thermal stability.

ACKNOWLEDGMENTS

This work was supported by the US Air Force, Fuels and Lubrication Division, Air Force Research Laboratory, Wright-Patterson AFB, OH under contract Nos. F33615-92-C-2207 and F33613-97-C-2719 with Mr. Charles Frayne as technical monitor.

REFERENCES

1. Pierce, A.E. *Silylation of Organic Compounds*; Pierce Chemical Co., Rockford, IL 1968
2. Zabarnick, S. *Ind. Eng. Chem. Res.* **1994**, 33, 1348-1354
3. Heneghan, S.P., Zabarnick, S. *Fuel* **1994**, 73, 35-43
4. Zabarnick, S. *Energ. Fuels.* **1997**, submitted.

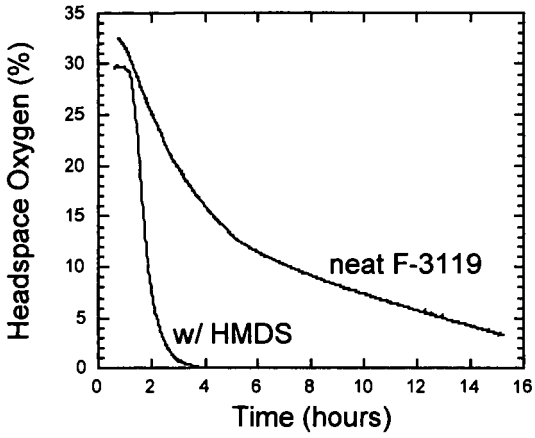

Figure 1. Plots of Headspace Oxygen for Fuel F-3119 with and without HMDS.

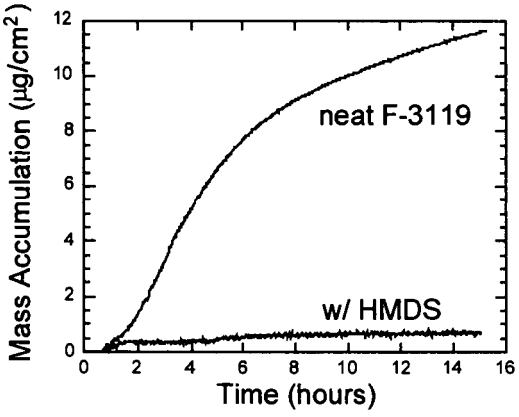

Figure 2. Plots of Mass Accumulation for Fuel F-3119 with and without HMDS.

REACTION KINETICS IN SUPERCRITICAL FLUIDS

Robert E. Morris[a] and Robert F. Brady, Jr[b].

[a]Navy Technology Center for Safety & Survivability, Code 6181
and [b]Materials Synthesis and Processing Branch, Code 6123,
Naval Research Laboratory, Washington, DC 20375

KEYWORDS: supercritical fluids, kinetics, AIBN, jet fuel oxidation

INTRODUCTION

Supercritical fluids constitute a unique medium for synthesis and processing, particularly near the critical point of the solvent where large changes in solvent properties can be obtained with relatively small changes in pressure. There is relatively little information available concerning the impact of pressure on reaction rates in the vicinity of the solvent critical point, particularly in free-radical processes. In studies of spin-exchange reactions between nitroxide free radicals near the critical point of ethane, Randolph and Carlier (1) found that rate constants were independent of radical concentrations. However, extreme effects of local radical density augmentation were observed due to solvent clustering near the critical point. Cluster lifetimes compared to solute-solute collision probabilities were a determining factor in the ten-fold increase in reaction rates at the critical point. The nature of the transition state will determine how solvent clustering and reactant mobilities will impact reaction rates as the solvent moves from sub- to supercritical conditions. First-order rate constants for the thermal decomposition of α–chlorobenzyl methyl ether in supercritical 1,1-difluoroethane demonstrated (2) that the greatest impact of small changes in pressure on the rate constants were in those regions where the solvent compressibility was high, i.e., near the critical point. This was explained in terms of changes in dielectric strength of the supercritical solvent, which can influence the solvatochromic transition energy. Partial molar volumes of solutes can reach negative thousands of cm^2/mol in highly compressible near-critical fluids in contrast to very small values in liquid solvents. Such large negative activation volumes and entropies suggest that solvent clusters are more ordered around the transition state than the reactants. Such solvent clustering will exert a significant impact on the reactivity of free radicals in a supercritical fluid.

As fuel temperatures approach approximately 350° - 375°C, many researchers have observed a decline in the amounts of thermal deposits. This has been explained in terms of chemical and physical effects. Since hydroperoxides thermally decompose at approximately 280 - 300°C, this was taken as evidence that deposition is linked to the presence of hydroperoxides. Another explanation proposed for this behavior is that, at these temperatures, components of the fuel can reach a supercritical state. Thus, the increased solvency of the supercritical fuel components was thought to be responsible for redissolving the insoluble products. The critical point of JP-5 fuel has been calculated(3) to occur in the range of 382° - 415°C at 300 - 380 psi (21 - 26 bar). In a series of single tube heat exchanger experiments, Edwards and Zabarnick (4) demonstrated that fuel oxidation chemistry was the determining factor in the amounts of insoluble products formed under those conditions and not simple supercritical solvency effects. However, this work did not address the impact of supercritical conditions on the free radical chemistry. Fuels subjected to conditions where components can reach their critical point may undergo chemical changes that would not necessarily form insoluble products at that time. Electron transfer reactions between metals and fuel constituents would also be mediated by solvent cluster lifetimes, which may play a role in the influence of catalytic metals on fuel properties.

In an effort to bridge the gap between gas phase and liquid phase chemistry, this work has been directed towards elucidating the impact of temperature and pressure on the free radical autoxidation mechanism of hydrocarbons near the critical point. This paper describes the apparatus and methods developed to obtain *in-situ* measurements of reaction kinetics in sub- and supercritical solvents. Some preliminary results of kinetic

measurements of the thermal decomposition of a free-radical initiator, 2,2'-azobis(isobutyronitrile) (AIBN) in supercritical CO_2 are presented.

EXPERIMENTAL

Materials. Carbon dioxide (SCF grade 99.99%, Matheson) was passed through a Chromtech high pressure oxygen and moisture trap and a Chromtech high pressure activated carbon trap to remove hydrocarbons. 2,2'-azobis(isobutyronitrile) (AIBN, Aldrich, 98%) was recrystallized from methanol.

Apparatus. The apparatus used to perform *in-situ* optical kinetic measurements is shown in Figure 1. Two ISCO type 100DX 100 mL syringe pumps were coupled via a check valve assembly to allow operation in dual pump mode, to facilitate rapid filling and pressure equilibration of the reactor. The pump cylinders were cooled to facilitate rapid filling. A Rheodyne injection valve was incorporated in a sampling loop to allow for the introduction of liquid modifiers or reactants into the gas stream. A Parr high pressure stirred mini-reactor was fitted with two 2.5 cm dia. x 1.3 cm thick fused silica windows located near the bottom, 180° apart. Reactor vessels with internal volumes of 25 and 450 mL were used in the kinetic experiments. The reactor was fitted with a pressure transducer and a variable restrictor for provide a means for sampling during an experiment for analysis.

Kinetic measurements were obtained optically over the range of 180 to 650 nm. A xenon arc lamp was coupled to a fused silica fiber optic bundle which was focused through the reactor window onto another fiber optic bundle interfaced to an Oriel Multispec 1/8 meter spectrograph. A grating was used that provided a bandpass of 164 nm at a resolution of 0.4 nm with a 50 μ slit. An Oriel Instaspec II 1024 channel photodiode array (PDA) was operated with a personal computer, which allowed for data acquisition at a maximum rate of 62 kHz. Software routines were written to acquire background corrected PDA counts and absorbance measurements at predefined intervals.

Characterization of AIBN decomposition at sub-critical conditions was performed with a HP 6890 gas chromatograph equipped with a nitrogen specific detector. Product characterization was performed using an HP 5890 gas chromatograph with a Finnigan ion trap mass spectrometer detector.

Kinetic Procedure. The reactant was placed in the reactor and purged with argon for 5 - 10 minutes then with SFC grade CO_2 for one minute. The reactor was then pressurized to approximately 75.8 bar (1100 psi). After the reactor reached thermal equilibrium, the pressure was adjusted to the desired final pressure by addition of CO_2. Optical measurements, in background corrected PDA counts, were obtained every 15 min for up to 8 hours. First-order rates were determined from photometric absorbance calculated from the acquired optical measurements.

RESULTS AND DISCUSSION

In order to study the impact of supercritical solvents on the mechanism of hydrocarbon autoxidation, a model compound that constitutes a convenient source of free-radicals was first examined. The compound, 2,2'-azobis(isobutyronitrile) (AIBN) is commonly used as a free-radical polymerization initiator. The thermal decomposition of AIBN is well known and has been studied in supercritical CO_2 by DeSimone, et al (5). In the initial phase of this study, the kinetics of the thermal decomposition of AIBN were examined in the kinetic reactor described above in supercritical CO_2 at a pressure of 172 bar (2500 psi) and compared with their earlier work (5) performed at 276 bar (4000 psi).

As shown in Figure 2, thermolysis of AIBN generates free-radicals which have been proposed (6) to form in solvent cages. These radicals can either diffuse out of these cages or dimerize to form a transient keteaimine adduct (II) that can, in turn dissociate

to regenerate the radicals. Solvent-solute interactions would exert an effect on the relative rates of diffusion out of the solvent cage and combination within the cage to form the adduct shown. Lower AIBN decomposition rates reported (5) in carbon dioxide compared with benzene illustrate the polar nature of the transition state and the impact of local changes in solvent dielectric properties. GC-MS analysis of AIBN in thermally stressed sub-critical benzene in the gas phase shows evidence of concurrent formation of compound II with a decrease in the abundance of the free radicals.

From absorbance measurements obtained during a typical kinetic experiment in supercritical CO_2 at 60°C and 172 bar, AIBN absorbance is shown (Figure 4) at 354.8nm and compound II at 290.1. The corresponding first-order plots of AIBN decomposition and the intermediate formation are shown in Figure 5. From the slopes of these plots, the rate constants (k_1) were calculated at 172 bar to be 7.4×10^{-5} s^{-1}, 1.5×10^{-5} s^{-1} and 4.8×10^{-5} s^{-1} at 40, 50 and 60°C, respectively. The Arrhenius treatment of these data indicated the activation energy for thermal decomposition of AIBN in these experiments to be 80.9 kJ-mol^{-1}.

The activation volume of species (x) is often expressed as $\Delta v^{\ddagger} = -RT\ (d\ln k_x / dp)_T$. To examine the effect of pressure on the formation rate of II, kinetic measurements were obtained as a function of pressure at 50°C from 76 to 172 bar. The effect of pressure is clearly shown in Figure 6, where the first-order formation constants (k_2) are plotted against pressure. While dielectric changes in carbon dioxide would be small at high pressures, in this region near the critical pressure of CO_2 (73.8 bar), the compressibility is high and local changes in dielectric properties can change by large amounts with small pressure changes. From a plot of the logarithm of k_2 vs pressure, the activation volume for the intermediate product was estimated to be -143 cc/mole.

SUMMARY

Real-time measurements of reaction kinetics in supercritical solvents has been demonstrated by examination of a model free radical source. However, while the kinetic rates measured in these experiments were self-consistent, they are higher by from 3 to 9 times than the values reported (5) for k_1 at 276 bar. Moreover, the activation energy determined from these measurements was also lower than expected. Current efforts are underway to resolve these discrepancies before the work is extended to include radical trapping compounds and hydroperoxides.

ACKNOWLEDGEMENTS

Funding for this work was provided by the Office of Naval Research.

LITERATURE CITED

(1) Randolph, T. W. and Carlier, C. *J. Phys. Chem.* **1992**, *96*, 5146.

(2) Johnston, K. P. and Haynes, C. *AIChE J.* **1987**, *33* (12), 2017.

(3) Martel, C. R. Air Force Aviation Fuel Thermal Oxidation Stability R&D. In *Jet Fuel Thermal Stability*; NASA TM 79231; Taylor, W. F., Ed.; NASA Lewis Research Center: Cleveland, OH, November 1978; pp 41-52.

(4) Edwards, T and Zabarnick, S. Ind. Eng. Chem. Res. **1993**, *32* (12) 3117.

(5) Guan, Z.; Combes, J. R.; Menceloglu, Y. Z. and DeSimone, J. M. *Macromolecules*, **1993**, *26*, 2663.

(6) Wu, Chin-Hua S.; Hammond, G. S.; Wright, J. M. *J. Am. Chem. Soc.* **1960**, 82, 5386.

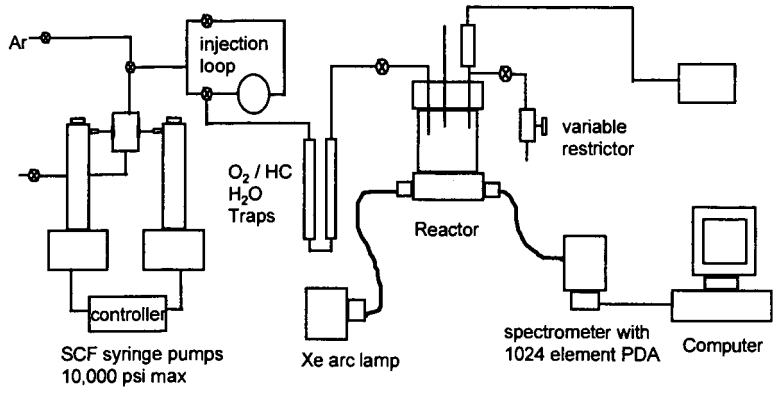

Figure 1. Schematic representation of apparatus for performing kinetic measurements in supercritical media.

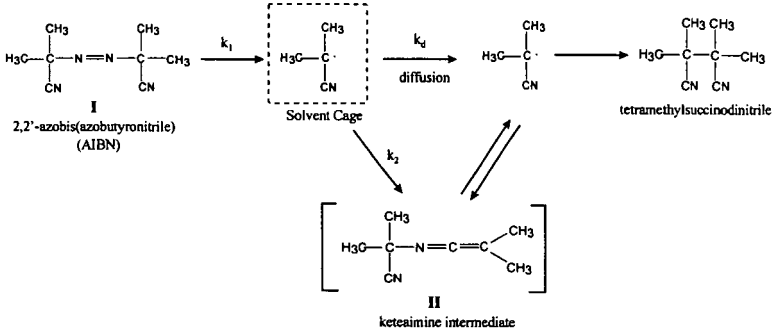

Figure 2. Thermal decomposition mechanism of AIBN (DeSimone, 1993)

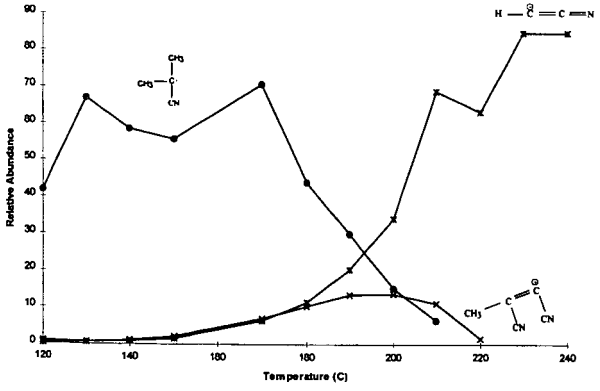

Figure 3. Major thermal decomposition products of AIBN in benzene at sub-critical conditions.

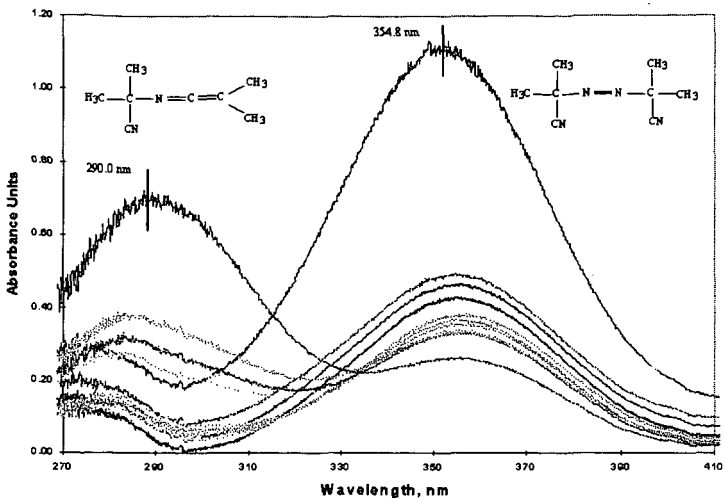

Figure 4. Absorption characteristics of AIBN thermal decomposition of AIBN in supercritical CO_2 at 60°C and 172 bar (not all scans shown).

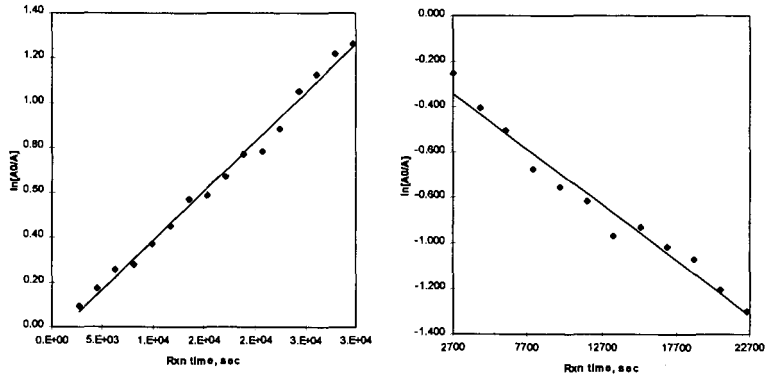

Figure 5. First order plots of AIBN thermal decomposition (left chart) and intermediate formation (right chart).

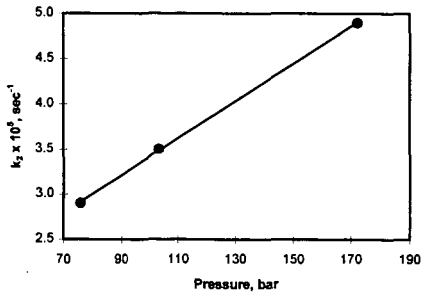

Figure 6. Variation of first order formation rate of ketamine intermediate with pressure.

SUPERCRITICAL-PHASE THERMAL DECOMPOSITION OF JET FUEL COMPONENTS: MODEL COMPOUND STUDIES

Jian Yu and Semih Eser
Fuel Science Program
Department of Materials Science and Engineering
209 Academic Projects Building
The Pennsylvania State University
University Park, PA 16802

INTRODUCTION

In an advanced aircraft, the fuel is the primary sink for the heat generated on board. With the development of high-speed aircraft, it is expected that the future fuel system will be operating at high-temperature supercritical conditions because of the increased thermal load (Edwards and Zabarnick, 1993). At high-temperature supercritical conditions, the fuel may decompose to form solid deposits. Solid deposition in various fuel system components, such as valves, filters, and fuel lines, could create serious problems in the operation and maintenance of aircraft. It is important to study supercritical fuel decomposition process in order to develop thermally stable jet fuels.

In this work, the thermal decomposition of n-decane (n-C_{10}), n-dodecane (n-C_{12}), n-tetradecane (n-C_{14}), n-butylbenzene (BBZ), n-butylcyclohexane (BCH), decalin (DHN), and tetralin (THN) was studied under supercritical conditions. The results from thermal decomposition of C_{10}–C_{14} normal alkanes have been reported previously (Yu and Eser, 1997a, 1997b) and were presented here for completeness. These model compounds were selected because they are typical components found in jet fuels. It has been shown that both petroleum-derived and coal-derived fuels contain significant amounts of long-chain alkanes, alkylbenzenes, and alkylcycloalkanes (Lai and Song, 1995a, 1995b). The coal-derived fuels also contain significant amounts of decalins and tetralins.

EXPERIMENTAL

Most of the model compounds used in this study were obtained from Aldrich. The n-butylbenzene and n-butylcyclohexane were obtained from TCI America. The purities of all compounds were higher than 99%. Decalin consisted of 47.90% of cis-decalin and 51.88% of trans-decalin as well as a small amount of tetralin and other impurities. All model compounds were used as received. Table 1 shows the critical properties of the model compounds.

Thermal reaction experiments were carried out at 400–475 °C and 10–100 atm (initial pressure) in a Pyrex glass tube reactor and, in some cases, in a 316 stainless steel tubing bomb reactor. A fluidized sand bath was used to heat the reactor. Before an experiment was started, the sand bath was preheated to the desired temperature. The reactor was then plunged into the bath. The heat-up period for the glass tube to reach 450 °C was less than two minutes and the corresponding value for the tubing bomb was about four to five minutes. It was found that the temperature of the sand bath was very uniform and was always within ±1 °C of the desired temperature after the heat-up period. After a given reaction time the reactor was removed from the bath and was cooled down using pressurized air (the glass tube) or quenched in cool water (the tubing bomb).). The reaction products from the tubing bomb experiments were separated into gases and liquids for analysis. The gaseous products from glass tube experiments were not collected because of the extremely low gas yields.

The liquid products were analyzed quantitatively by a Perkin Elmer 8500 GC equipped with a DB-17 capillary column and a flame ionization detector (FID). The compounds in the liquid products were identified by gas chromatography-mass spectrometry (GC-MS) using a Hewlett Packard (HP) 5890 II GC connected with an HP 5971A mass selective detector. The identifications of the major compounds were also made by running standard mixtures. The gaseous products from the tubing bomb experiments were analyzed quantitatively using a Perkin Elmer AutoSystem gas chromatograph (GC) equipped with two different columns and detectors. One stainless steel column packed with 80/100 Chemipack C18 was used to determine the yields of C_1–C_6 gases with an FID. The other stainless steel column packed with 60/80 Carboxen-1000 was used to determine the yields of H_2, CO, CO_2, CH_4, C_2H_2, C_2H_4, and C_2H_6 with a thermal conductivity detector (TCD). The gaseous products were identified and quantified by using standard gas mixtures.

RESULTS AND DISCUSSION

Kinetics. Previous studies show that thermal decomposition of hydrocarbons usually follows a first-order rate law (Steacie, 1946; Fabuss et al., 1964). Therefore, the rate constants were determined by the following first-order expression:

$$k = \frac{1}{t} \ln \frac{1}{1 - x} \tag{1}$$

where x is the fraction of the reactant converted (conversion), k is the rate constant (h^{-1}), and t is the reaction time (h). The conversions were obtained from the thermal decomposition experiments in the glass tube reactor at different temperatures for different times. A fixed loading ratio, defined as the ratio of the initial sample volume to the reactor volume, of 0.36 was used in the experiments.

Figure 1 shows the relationship between $\ln[1/(1 - x)]$ and time for the thermal decomposition of n-butylbenzene. Similar linear relationships between $\ln[1/(1 - x)]$ and time were obtained for the decomposition of other model compounds. From the slopes of the lines in Figure 1, the first-order rate constants at different temperatures can be obtained. Table 2 shows the calculated first-order rate constants for the thermal decomposition of seven model compounds. From Table 2 one can see that for the three n-alkanes, the first-order rate constant increases with the increasing carbon number (at the same temperature). Among C_{10} hydrocarbons, the rate constant decreases in the order of BBZ > n-C_{10} > BCH > DHN > THN.

According to the first-order rate constants shown in Table 2, the apparent activation energies (E_a, kcal/mol) and preexponential factors (A, h^{-1}) can be determined using the following Arrhenius law:

$$k = A \exp(-E_a / RT) \tag{2}$$

Figure 2 shows the Arrhenius plots from the thermal decomposition of model compounds. The apparent activation energies and preexponential factors obtained from the Arrhenius plots are also shown in Table 2. The slight differences between the apparent activation energies for the three n-alkanes may arise from the experimental uncertainty.

Product Distributions. The reaction products from the thermal decomposition of C_{10}–C_{14} n-alkanes under supercritical conditions can be divided into two categories: those from the primary reactions and those from the secondary reactions of the primary products. The primary products include n-alkanes from C_1 to C_{m-2} (m = number of carbon atoms in the reactant) and 1-alkenes from C_2 to C_{m-1}. The secondary products include cis- and trans-2-alkenes, n-C_{m-1}, n-C_{m+1}, and C_{m+2} to C_{2m-2} normal and branched alkanes. There are also small amounts of cyclopentanes and cyclohexanes. The yields of branched alkanes lighter than the reactant are not significant until high conversions are reached.

The liquid products from thermal decomposition of n-butylbenzene can also be divided into the primary products and the secondary products. The primary products include toluene, styrene, ethylbenzene, benzene, allylbenzene, and tetralin. The secondary products include n-pentane, 2-methylbutane, n-propylbenzene, isopropylbenzene, sec-butylbenzene, isobutylbenzene, n-pentylbenzene, 1-propylbutylbenzene, 1,3-diphenylpropane, 1,4-diphenylbutane, 1,3-diphenylhexane, and three other C_6-diphenyls. At higher conversions (> 30%), more than 150 liquid compounds were found. The gaseous products from thermal decomposition of n-butylbenzene include hydrogen, methane, ethane, ethylene, propane, and propylene.

The liquid products from n-butylcyclohexane thermal decomposition include the primary products cyclohexane, methylenecyclohexane, cyclohexene, methylcyclohexane, vinylcyclohexane, allylcyclohexane, ethylcyclohexane, some C_{10} alkenes and butylcyclohexenes, and the secondary products 1-methylcyclohexene, 3-methylcyclohexene, methylcyclopentane, 1-ethylcyclohexene, and n-propylcyclohexane. Some high-molecular-weight compounds, including n-pentylcyclohexane, n-hexylcyclohexane, several C_7 and C_8-cyclohexanes, dicyclohexylmethane, dicyclohexylethane, C_5-dicyclohexyl, and C_6-dicyclohexyl, were also found. At the highest conversion obtained in this study (39%, 475 °C, 20 min), about 130 peaks were observed from the chromatogram of the liquid products. The gaseous products from thermal decomposition of n-butylcyclohexane include hydrogen, methane, ethane, ethylene, propane, propylene, butane, and butene.

The major liquid products from the thermal decomposition of decalin include spiro[4,5]decane, 1-methylcyclohexene, 1-butylcyclohexene, and 1-methylperhydroindan. Also appearing, but in slightly lower yields, are toluene, some C_4-cyclohexenes, n-butylbenzene, and three unidentified compounds which eluted between trans-decalin and tetralin from the GC column. Some minor products include cyclohexane, cyclohexene, methylcyclopentane, methylcyclohexane, 3-methylcyclohexene, methylenecyclohexane, benzene, ethylbenzene, n-butylcyclohexane, tetralin, naphthalene, and some high molecular weight compounds. At 450 °C for 60 min, about 80 compounds were found in the liquid products. The gaseous products include hydrogen, methane, ethane, ethylene, propane, propylene, butane, and butene.

The most abundant liquid product from thermal decomposition of tetralin under supercritical conditions is 1-methylindan, followed by naphthalene, n-butylbenzene, and 2-methylindan. Also appearing, but in lower yields, are n-propylbenzene, ethylbenzene, and toluene. Hydrogen is dominant gaseous product. Other gases include methane, ethane, ethylene, propane, propylene, butane, and butene.

Effects of Supercritical Conditions on Product Distributions. Figure 3 shows the changes in overall molar yields of C_6–C_{13} n-alkanes, C_6–C_{13} 1-alkenes, C_6–C_{12} 2-alkenes, and C_{14+} normal and branched alkanes with the initial reduced pressure from the thermal decomposition of n-C_{14} at 425 °C for 15 min. The initial reduced pressure ($P_r = P/P_c$) was calculated at the given temperature and loading ratio using the Soave-Redlich-Kwong equation of state (Soave, 1972). It can be seen that the overall yield of C_6–C_{13} n-alkanes increases and that of C_6–C_{13} 1-alkenes decreases as pressure increases. The large changes in product distributions with pressure occur in the near-critical region. While the overall yields of C_6–C_{12} 2-alkenes and C_{14+} alkanes are low at low-pressure sub-critical conditions, their yields become significant at high-pressure supercritical conditions.

Figure 4 shows the effects of pressure on product distributions from the thermal decomposition of n-butylbenzene at 425 °C for 15 min. The major primary products are toluene and styrene. It can be seen that as pressure increases, the styrene yield decreases and the toluene yield increases. In contrast to a higher yield of styrene in the sub-critical region, a higher toluene yield is obtained in the far supercritical region. It is clear that high-pressure supercritical conditions suppress the formation of styrene. On the other hand, the yields of the high-molecular-weight products increase with the increasing pressure. Although not shown in Figure 4 because of low yields, the yields of some other high-molecular-weight products, such as 1-propylbutylbenzene and three other C_6-diphenyls, also increase with the increasing pressure.

CONCLUSIONS

Supercritical-phase thermal decomposition of jet fuel model compounds follows a first-order kinetics. Among the compounds studied, n-butylbenzene exhibited the highest reactivity, followed by n-C_{14}, n-C_{12}, n-C_{10}, n-butylcyclohexane, decalin, and tetralin.

Thermal decomposition of C_{10}–C_{14} n-alkanes under supercritical conditions gave high yields of C_{3+} n-alkanes and significant amounts of heavy alkanes which are usually not observed under low-pressure sub-critical conditions. The pyrolyses of n-butylbenzene and n-butylcyclohexane were dominated by side-chain cracking. The formation of significant amounts of diphenylalkanes from pyrolysis of n-butylbenzene under supercritical conditions indicates that the reaction mechanism under these conditions is different from that under lower-pressure sub-critical conditions. The thermal decomposition of decalin and tetralin under high-pressure supercritical conditions was dominated by isomerization reactions. This is different from the results obtained under low-pressure and high-temperature conditions where cracking reactions (for decalin) or dehydrogenation reactions (for tetralin) dominate.

ACKNOWLEDGMENT

This work was supported by the U.S. Department of Energy, Pittsburgh Energy Technology Center, and the Air Force Wright Laboratory/Aero Propulsion and Power Directorate, Wright-Patterson AFB. Funding was provided by the U.S. DOE under Contract DE-FG22-92PC92104. We would like to express our gratitude to Prof. Harold H. Schobert of Penn State for his support. We thank Mr. W. E. Harrison III and Dr. T. Edwards of AFWL/APPD and Dr. S. Rogers of PETC for many helpful discussions.

REFERENCES

1. Daubert, T. E.; Danner, R. P. *Physical and Thermodynamic Properties of Pure Chemicals; Design Institute for* Physical Property Data, AIChE: Washington, DC, 1992.
2. Edwards, T.; Zabarnick, S. *Ind. Eng. Chem. Res.* **1993**, *32*, 3117.
3. Fabuss, B. M.; Smith; J. O.; Satterfield, C. N. *Adv. Petro. Chem. Refin.* **1964**, *9*, 157-201.
4. Lai, W.-C.; Song, C. *Fuel*, **1995a**, *74*, 1436.
5. Lai, W.-C.; Song, C. In *Advanced Thermally Stable Jet Fuels*, Technical Progress Report, April 1995 – June 1995, The Pennsylvania State University, August 1995b.
6. Soave, G. *Chem. Eng. Sci.* **1972**, *27*, 1197.
7. Steacie, E. W. R. *Atomic and Free Radical Reactions*; Reinhold: New York, 1946.
8. Teja, A. S.; Lee, R. J.; Rosenthal, D. J.; Anselme, M. *Fluid Phase Equil.* **1990**, *56*, 153.
9. Yu, J.; Eser, S. *Ind. Eng. Chem. Res.* **1997a**, *36*, 574.
10. Yu, J.; Eser, S. *Ind. Eng. Chem. Res.* **1997b**, *36*, 585.

Table 1. Critical Properties of Model Compounds

	T_c, °F	T_c, °C	P_c, psia	P_c, atm
n-C_{10}[a]	652	345	304	20.7
n-C_{12}[a]	725	385	262	17.9
n-C_{14}[a]	786	419	228	15.5
n-butylbenzene[b]	729	387	419	28.5
n-butylcyclohexane[b]	741	394	373	25.4
cis-decalin[b]	804	429	470	32.0
trans-decalin[b]	777	414	411	28.0
tetralin[b]	837	447	525	35.7

[a] Teja et al. (1990). [b] Daubert and Danner (1992).

Table 2. Kinetic Parameters for Thermal Decomposition of Model Compounds

	rate constant, h^{-1}					
reactant	400 °C	425 °C	450 °C	475 °C	E_a[a]	log$A$[b]
n-C_{10}	0.0341	0.174	0.758		60	18.0
n-C_{12}	0.0453	0.231	1.13		62	18.8
n-C_{14}	0.0640	0.364	1.67		63	19.3
BBZ	0.0891	0.422	1.72		57	17.6
BCH		0.0613	0.313	1.40	65	19.1
DHN		0.0238	0.132	0.669	69	20.1
THN		0.0090	0.0370	0.139	58	16.1

[a] E_a, apparent activation energy in kcal/mol. [b] A, preexponential factor in h^{-1}.

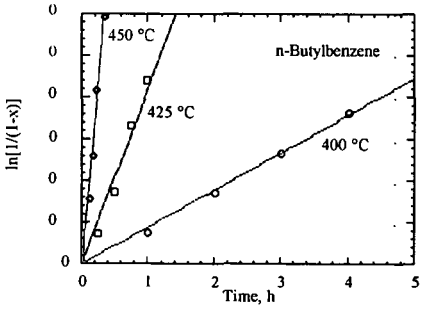

Figure 1. ln[1/(1-x)] versus time from thermal decomposition of n-butylbenzene.

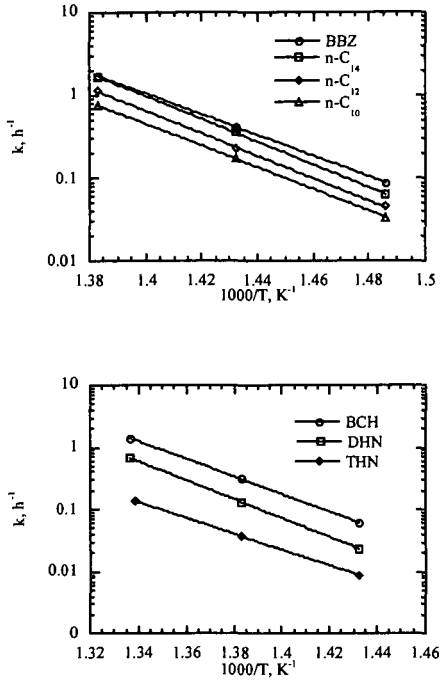

Figure 2. Arrhenius plots from thermal decomposition of jet fuel model compounds

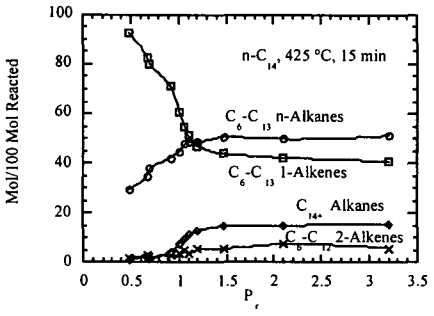

Figure 3. Product yields versus P_r from n-C_{14} at 425 °C for 15 min.

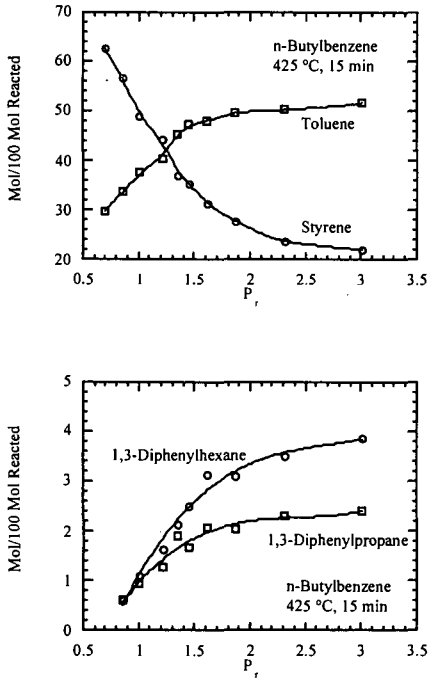

Figure 4. Product yields versus P_r from n-butylbenzene at 425 °C for 15 min.

SUPERCRITICAL-PHASE THERMAL DECOMPOSITION OF JET FUEL COMPONENTS: MIXTURE STUDIES

Jian Yu and Semih Eser
Fuel Science Program
Department of Materials Science and Engineering
209 Academic Projects Building
The Pennsylvania State University
University Park, PA 16802

INTRODUCTION

Jet fuels consist of hundreds of compounds, including long-chain alkanes, alkylbenzenes, and alkylcyclohexanes (Lai and Song, 1995). Coal-derived fuels also contain significant amounts of decalins and tetralins. In a previous paper (Yu and Eser, 1998), we have presented the results from the thermal decomposition of some typical jet fuel model compounds, including C_{10}–C_{14} n-alkanes, n-butylbenzene (BBZ), n-butylcyclohexane (BCH), decalin, and tetralin, under supercritical conditions. The studies on pure model compounds have provided valuable information on jet fuel thermal decomposition. However, these studies can not answer the question on how individual compounds interact with each other during the thermal reactions of jet fuels.

In this work, the thermal decomposition of some binary mixtures of jet fuel model compounds was studied under supercritical conditions. Five binary mixtures were used in this study, including n-C_{12}/n-C_{10}, n-C_{12}/n-C_{14}, n-C_{12}/BBZ, n-C_{12}/BCH, and BBZ/BCH. Every mixture consists roughly of 50 wt% of each component.

EXPERIMENTAL

The n-C_{10}, n-C_{12}, and n-C_{14} were obtained from Aldrich while BBZ and BCH were obtained from TCI America. All model compounds have 99+% purity and were used as received. Thermal reaction experiments were carried out in a Pyrex glass tube reactor with a strain point of 520 °C. In a typical experiment, the reactor was loaded, sealed, and then plunged into a fluidized sand bath preheated to the desired temperature. After a given reaction time, the reactor was removed from the bath and then was cooled down using pressurized air.

A Perkin Elmer 8500 gas chromatograph (GC) equipped with a DB-17 column and a flame ionization detector (FID) was used for the quantitative analysis of liquid products. The compounds in liquid products were identified by gas chromatography–mass spectrometry (GC–MS) using a Hewlett Packard (HP) 5890 II GC connected with an HP 5971A mass selective detector. The identifications of major compounds were also made by running standard mixtures. The gaseous products were not analyzed because of the extremely low yields.

RESULTS AND DISCUSSION

Reaction Rates. The changes in conversions of individual model compounds with reaction time were obtained from the thermal decomposition of the mixture at 425 °C for 15–60 min with a loading ratio of 0.36. The loading ratio was defined as the ratio of the initial sample volume at room temperature to the reactor volume. Figure 1 shows the conversion of n-C_{12} as a function of reaction time for the thermal decomposition of the pure compound, in n-C_{12}/n-C_{10} mixture, and in n-C_{12}/n-C_{14} mixture. One can see that the conversion of n-C_{12} is affected by the presence of the second compound. While the conversions for the decomposition of n-C_{12} in n-C_{12}/n-C_{14} mixture are higher than those for the decomposition of pure n-C_{12}, the conversions of n-C_{12} in n-C_{12}/n-C_{10} mixture are slightly lower than those for the decomposition of pure n-C_{12}. These results suggest that the lighter alkane inhibits the decomposition of the heavier one while the heavier alkane accelerates the decomposition of the lighter one.

Figure 2 shows the conversion of n-C_{12} as a function of reaction time for the thermal decomposition of the pure compound, in n-C_{12}/BBZ mixture, and in n-C_{12}/BCH mixture. It can be seen that the presence of BBZ accelerates the decomposition of n-C_{12} and the presence of BCH inhibits the decomposition of n-C_{12}. The increased decomposition rate of n-C_{12} in the presence of BBZ can be explained by the increased radical concentration, resulting from the much faster initiation reaction of BBZ. The increase in radical concentration leads to an increase in the rates of hydrogen abstraction from n-C_{12} and thus an increase in n-C_{12} decomposition rates. On the other hand, the addition of BCH to n-C_{12} reduces the radical concentration for the

decomposition of n-C_{12} because some of the radicals produced from n-C_{12} decomposition abstract hydrogen atoms from BCH instead of n-C_{12}.

Figure 3 shows a comparison of BBZ conversions from the thermal decomposition of pure BBZ, in BBZ/n-C_{12} mixture, and in BBZ/BCH mixture, under similar conditions. It seems that n-C_{12} and BCH exhibit very similar inhibiting effect on the decomposition of BBZ. This is probably due to very comparable hydrogen abstraction rates from C_{12} and BCH by free radicals. The decomposition of BBZ is inhibited by the addition of n-C_{12} or BCH because some of the radicals, which would abstract hydrogen atoms from BBZ in the absence of n-C_{12} or BCH, abstract hydrogen atoms from n-C_{12} or BCH. Since the rates of hydrogen abstraction from n-C_{12} and BCH are comparable, both compounds exhibit similar inhibiting effect on the decomposition of BBZ.

Product Distributions. The major components in liquid products from supercritical-phase thermal decomposition of n-C_{12}/BBZ mixture were identified. Figure 4 shows the GC chromatogram of the liquid products from n-C_{12}/BBZ mixture at 425 °C for 60 min with an initial reduced pressure ($P_r = P/P_c$) of 2.04. The initial reduced pressure was calculated at the given temperature and loading ratio using the Soave-Redlich-Kwong equation of state (Soave, 1972). The products produced from the thermal decomposition of the binary mixture include those found in the decomposition of the pure compounds and those found only in the mixture reactions. The products formed from the decomposition of n-C_{12} component include series of n-alkanes and 1-alkenes lighter than n-C_{12} and some heavy normal and branched alkanes. The products produced from the decomposition of BBZ component include toluene, styrene, ethylbenzene, benzene, allylbenzene, tetralin, and some secondary products, including n-propylbenzene, isopropylbenzene, sec-butylbenzene, isobutylbenzene, n-pentylbenzene, 1-propylbutylbenzene, 1,3-diphenylpropane, 1,4-diphenylbutane, and four C_6-diphenyls. Some products unique to the reaction of the mixture are also formed, including six C_{14}-benzenes, a series of high n-alkylbenzenes up to n-dodecylbenzene, a series of 1-propylalkylbenzenes up to 1-propylundecylbenzene, and some other alkylbenzenes with branched side chains.

Figure 5 shows a comparison in product distributions between supercritical and sub-critical conditions. The reactions were carried out at 425 °C for 60 min. Two loading ratios were used: 0.36 (supercritical, $P_r = 2.04$) and 0.08 (sub-critical, $P_r = 0.77$). It can be seen that supercritical conditions favor the formation of n-alkanes, toluene, and high-molecular-weight compounds, and suppress the formation of 1-alkenes and styrene.

CONCLUSIONS

Individual compounds interact with each other in the thermal reactions of binary mixtures. The compound with low reactivity inhibits the decomposition of the compound with high reactivity while the latter accelerates the decomposition of the former. Supercritical-phase thermal decomposition of n-C_{12}/BBZ mixture produces not only the products found in the decomposition of pure compounds but also the products unique to the reaction of the mixture. High-pressure supercritical conditions result in the formation of significant amounts of high-molecular-weight compounds.

ACKNOWLEDGMENT

This work was supported by the U.S. Department of Energy, Pittsburgh Energy Technology Center, and the Air Force Wright Laboratory/Aero Propulsion and Power Directorate, Wright-Patterson AFB. Funding was provided by the U.S. DOE under Contract DE-FG22-92PC92104. We would like to express our gratitude to Prof. Harold H. Schobert of Penn State for his support. We thank Mr. W. E. Harrison III and Dr. T. Edwards of AFWL/APPD and Dr. S. Rogers of PETC for many helpful discussions.

REFERENCES

1. Lai, W.-C.; Song, C. *Fuel*, **1995**, *74*, 1436.
2. Soave, G. *Chem. Eng. Sci.* **1972**, *27*, 1197.
3. Yu, J.; Eser, S. This symposium.

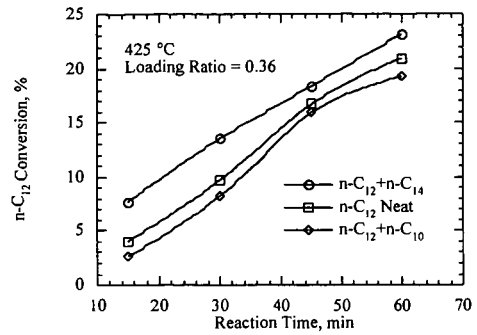

Figure 1. Conversion of n-C_{12} versus reaction time from thermal decomposition of pure compound, in n-C_{12}/n-C_{10} mixture, and in n-C_{12}/n-C_{14} mixture.

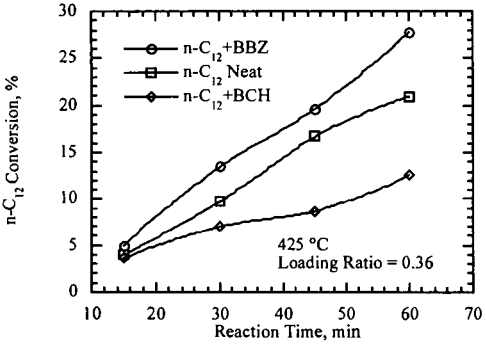

Figure 2. Conversion of n-C_{12} versus reaction time from thermal decomposition of pure compound, in n-C_{12}/BBZ mixture, and in n-C_{12}/BCH mixture.

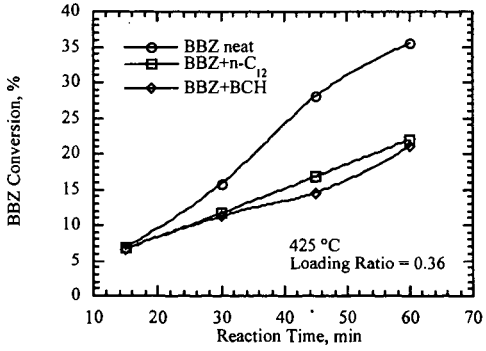

Figure 3. Conversion of BBZ versus reaction time from thermal decomposition of pure compound, in BBZ/n-C_{12} mixture, and in BBZ/BCH mixture.

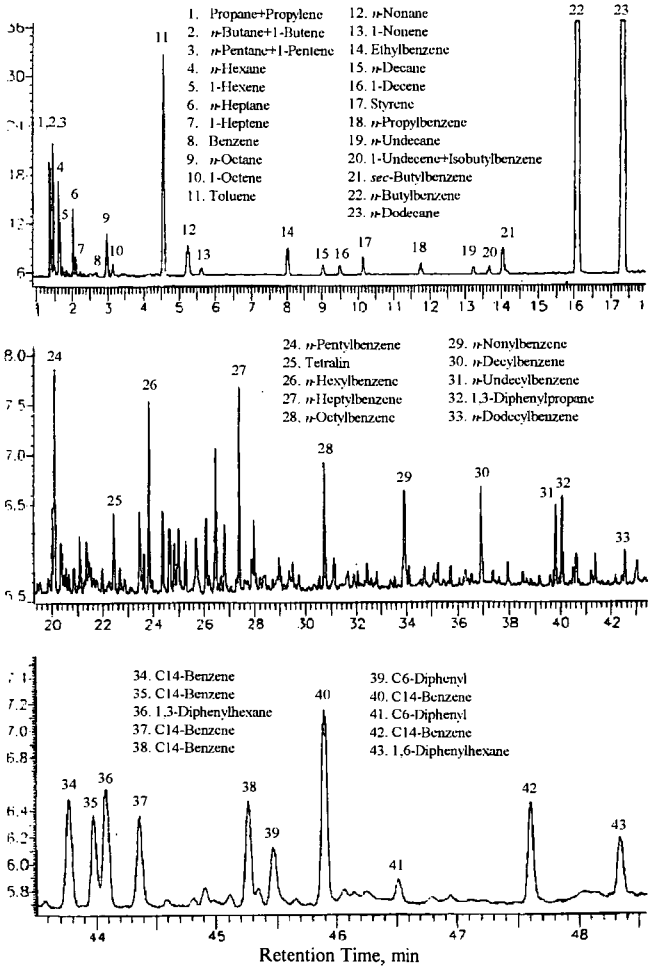

Figure 4. GC chromatogram of liquid products from thermal decomposition of n-C_{12}/BBZ mixture at 425 °C for 60 min with a loading ratio of 0.36.

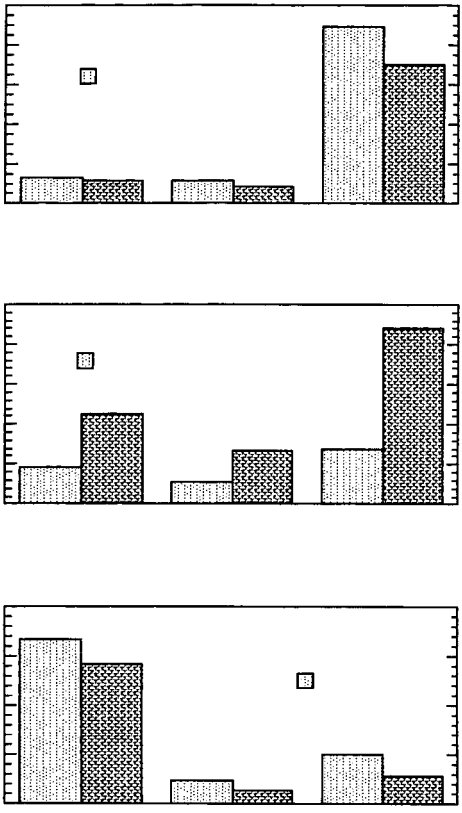

Figure 5. Comparison of product distributions between supercritical and sub-critical conditions.

THE CHANGING NATURE OF DEPOSITS FORMED DURING THERMAL STRESSING OF JET FUELS

R. Malhotra
SRI International, Menlo Park, CA 94025

and

M. A. Serio
Advanced Fuel Research, East Hartford, CT 06138

ABSTRACT

A JP-5 fuel was subjected to thermal stress at various temperatures in a flow tube with a wire stretched along its length. The deposits formed on the wire, as well as those collected on a filter were examined by field ionization mass spectrometry. Two distinct kinds of spectra were observed. The first had a picket-fence like appearance and the masses corresponded to long chain alkanes. The spectrum spanned a mass range from about 300 to 500 Da. The alkanes in the fuel have molecular weights ranging from about 130 to 240. These waxy deposits were formed possibly by the coupling of alkyl radicals. The second class of deposits is characterized with a very rich spectrum spanning a mass range from 200 to 800 Da. Evidently, this deposit is formed by the reaction of many different fuel components and not just the alkanes. FT-IR examination of this deposit showed a strong peak due to aromatic C-H stretch. Implications of these two kinds of deposits to the overall thermal instability of jet fuels will be discussed.

INTRODUCTION

The fuel in an aircraft is subjected to much thermal stress, and in advanced aircraft the degree of thermal stress is only expected to increase. This stress often results in the formation of insolubles that end up depositing on engine parts, fuel lines, and nozzles. In some instances, the deposits at critical points can completely block the flow of fuel to the engine with disastrous consequences. Not surprisingly, therefore, the thermal stability of jet fuels has been the subject of many studies, and jet fuels must pass the JFTOT test for thermal stability before they are deemed acceptable.

In pioneering work, Hazlett demonstrated the importance of autoxidation process in deposit formation during thermal stressing of fuels.[1] This process involves generation of radical species, which initiate a chain reaction with oxygen to give hydroperoxides, which are then considered to react with minor fuel components, that likely contain nitrogen and/or sulfur, to produce insoluble deposits. A substantial amount of work has been performed to elucidate the mechanisms of deposit formation, and many details have been added to this picture; however the essential aspects of this theory have been validated.[2]

A number of attempts have also been made to model the deposit formation. The models often treat all deposits as a lumped component, and proceed to describe the build up as a function of thermal stress (time, temperature).[3] Simple Arrhenius behavior is often assumed, although there is evidence that the observed activation energy in systems at low temperatures (long time) tends to be significantly lower than that observed at high temperatures (short time).[4] This behavior is clearly indicative of a change in the mechanism, and it should be reflected in the models, if they are to correctly describe the phenomena.

In this paper we show that the chemical nature of the deposits at lower and higher temperatures is markedly different. This finding is in concert with the varying activation energies, and might provide a basis for building a more accurate model.

EXPERIMENTAL

A JP 5 fuel was flowed through a heated, glass-lined, stainless tube (1/8" OD, 0.7" ID, 44" long) at 0.5 mL/min. A stainless steel wire (0.008" dia) was stretched along the center of the tube, and some of the deposits were collected on this wire. The effluent passed through a stainless steel filter (0.2 μm) where the insolubles were collected. The effluent fuel cools before reaching the filter, and so the deposits on the wire represent materials that are insoluble in the hot fuel, whereas those on the filter are of materials insoluble in the fuel at the lower temperature of the filter. The wire deposits and the filtered deposits were analyzed by an Fourier transform infrared (FTIR) spectrometer and a field ionization mass spectrometer (FIMS).

RESULTS AND DISCUSSION

FIMS analysis of the fuel showed the molecular weight of the component species ranged from about 120 to 230 Da, with an average value of about 170 Da. The spectrum also shows components with whole range of unsaturation indices, as would be expected of a typical fuel. The FIMS of the deposits collected on the wire and the filter at 150°C are shown in Figure 1. These spectra are characterized by a picket-fence like appearance. The prominent peaks are 14 Da apart and centered around 340 Da. The masses correspond to acyclic alkanes ($14n + 2$), although they could also be due to acyclic ketones. These components are expected to arise from the autoxidation of alkanes. The long-chain waxy products are dimers resulting from the coupling of the alkyl and alkoxy radicals are not likely to be very soluble in the fuel and therefore it is not surprising that they drop out of the solution most readily. The filter deposits collected at 150°C show a very similar spectrum. The amount of the filter deposit was considerably larger, and consequently, the spectrum is less noisy. The filter deposit also shows peaks corresponding to dimers formed by the coupling of species other than acyclic alkanes.

Figure 2 shows the analogous spectra collected at 450°C. Although the amount of the wire deposit collected was larger at the higher temperature, its spectrum—and hence its nature—is essentially the same as that collected at 150°C. In contrast, the spectrum of the filter deposit is very rich, and shows a broad distribution of masses ranging from about 180 to over 800 Da. The waxes seen in the wire deposit are also present, but they are overshadowed by the other components.

FIMS analysis of the deposits clearly shows that the thermal deposits fall into two classes. The first are the alkane-rich waxes, which tend to be more insoluble, plate out even when the fuel is hot. These deposits do not contain much heteroatoms, except for some oxygen. The other class consists of a wide range of compounds, possibly with a much higher heteroatom content. This class of compounds forms later in the sequence, it is more soluble, and precipitates out when the fuel is somewhat cooler. The waxy deposits could also absorb the other fuel components and in effect increase their residence time in the hot zone. If that case, we would expect the rate of deposit formation to increase with time. Indeed, that was observed by Kamin and coworkers[5] when they monitored the deposit formation in a JFTOT with a fiber optic monitor. A preliminary model that incorporates the two different classes of deposits was able to mimic this time dependent variation in the rate of deposit formation.

REFERENCES

1 Hazlett, R. N.; Hall, J. M.; Matson, M, *Ind. Eng. Chem., Prod. Res. Dev.* **1977**, *16*, 171.

2 Hazlett, R. N., "Thermal Oxidation Stability of Aviation Turbine Fuels," ASTM Monograph Series, ASTM, Philadelphia, 1991.

3 See for example, Heneghan, S. P.; Chin, L. P., *Proceedings of the 5th Intl. Conference on Stability and Handling of Liquid Fuels* **1994**, p. 91.

4 Private communication from V. Reddy, cited by Heneghan, S. P., *Am. Chem. Soc., Div. Petr. Chem. Prepriints* **1991**, *39(1)*, 14.

5 Kamin, R. A.; Nowack, C. J.; Darrah, S. ., *Proceedings of the 3rd Intl. Conference on Stability and Handling of Liquid Fuels* **1988**, p. 240.

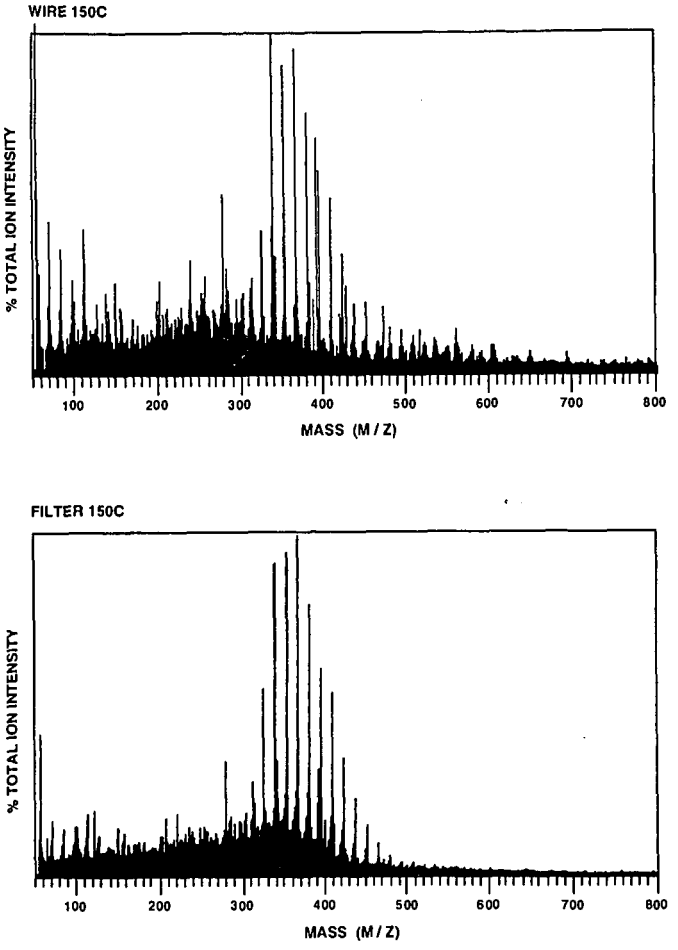

Figure 1. Field ionization mass spectrum of deposits collected on (a) wire and (b) filter from thermal stressing of aerated JP5 at 150°C.

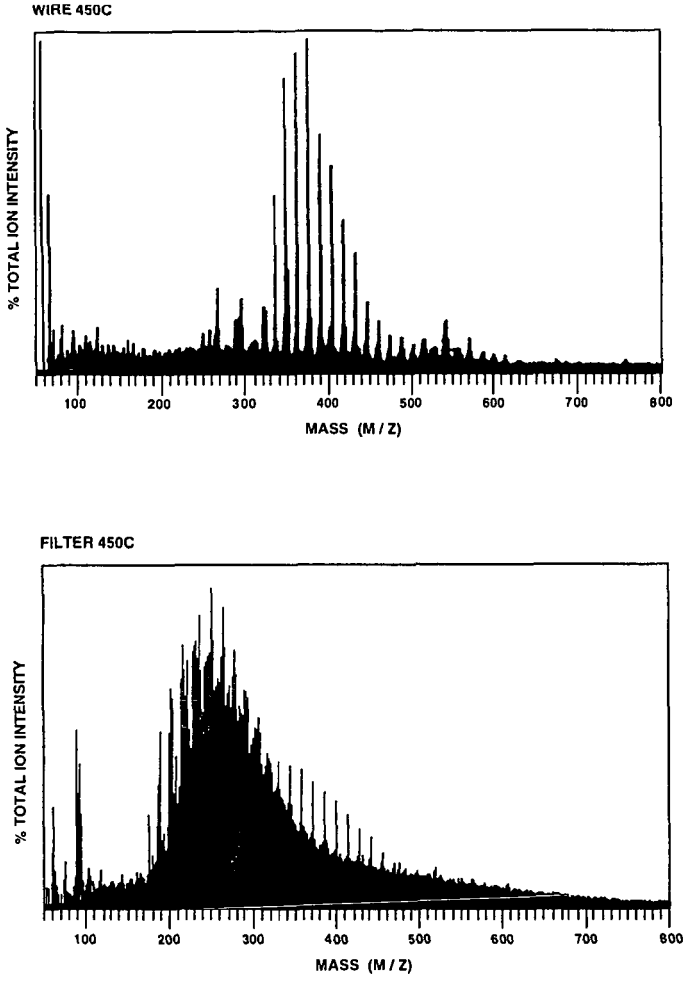

Figure 2. Field ionization mass spectrum of deposits collected on (a) wire and (b) filter from thermal stressing of aerated JP5 at 450°C.

THERMAL STABILITY MEASUREMENT DEVICES REVISITED: GRAVIMETRIC JFTOT VERSUS SIMULATED TEST RIG

S.G. Pande[1] and D.R. Hardy

Code 6181, Naval Research Laboratory
Washington, D.C. 20375.
[1]Geo-Centers, Inc. Lanham, MD 20706

KEYWORDS: jet fuel thermal stability, temperature, fuel velocity, MDA

INTRODUCTION

Fuel thermal stability is one of the most critical fuel properties,[1] consequently, a reliable method for its measurement is desirable. The Jet Fuel Thermal Oxidation Tester (JFTOT: ASTM D3241) has been designated as the specification test method for measuring the aviation turbine thermal stabilities of commercial fuels (ASTM D1655), and military fuels (MIL-T-5624). However, JFTOT data have been reported to correlate poorly[2-5] with the thermal deposit results from test rigs that were designed to simulate the aircraft engine fuel system. Two examples of many such simulated test rigs include: (a) the injector feed arm rig (IFAR),[2] which measures burner stem fouling; and (b), the single tube heat transfer rig (STHTR),[3,4] which measures fuel degradation within an oil cooler. Reported disparities between the JFTOT and the IFAR/STHTR have been ascribed to:

(1) The short test duration of the JFTOT (2.5 hr).[2,4] This was the explanation given to account for the beneficial effect of MDA (the commonly used metal deactivator, N,N'-disalicyclidene-1,2-propane diamine), observed in the JFTOT, and the innocuous effect of MDA on extended testing in the IFAR.[2]

(2) The differences in flow velocities. For example, in the JFTOT, the fuel flow is laminar (3 mL/min) whereas in aircraft operating systems, the flow is turbulent.[3,5]

To explore these differences, we used the gravimetric JFTOT (grav-JFTOT) since its operating conditions are not only similar to the JFTOT, but it has the added advantage of quantifying both the surface and bulk fuel deposits, based on weight.[6] Furthermore, the grav-JFTOT offers a more sensitive measure of the bulk fuel deposits than the JFTOT because the pore size of its effluent filter is considerably smaller, viz., 0.8 micron versus 17 microns for the JFTOT.

The effect of test duration was examined in a recent study, the results of which do not support the explanation that test duration is a factor. Specifically, we found[7] MDA to be beneficial in a non-copper doped Jet A and JP-5 type (Jet A + antioxidant) fuel, on extended duration testings which were conducted in the grav-JFTOT for approximately 150 hours.

Regarding the effect of fuel velocity on fuel thermal deposition, compared to laminar flow, turbulent flow has been suggested to increase thermal deposition by increasing both the mass transfer of oxygen to the heated surface and the quantity of reactants.[3,8] Nevertheless, on increasing test duration in the IFAR,[2] an underlying variable appears to be a temperature effect. In this paper we report the results of a grav-JFTOT study that was designed to investigate the effects of increasing temperature on thermal deposits, with and without the presence of MDA.

EXPERIMENTAL

Materials. All materials were used as received. The test fuel was a typical, though aged, JP-5. The metal deactivator, N,N'-disalicyclidene-1,2-propane diamine, commonly known as MDA, was obtained from Pfaltz and Bauer and used at 5.8 mg/L concentration.

Procedure. Thermal stability was determined using the grav-JFTOT. This laminar flow, bench test method gives the weight of total thermal deposits formed when the filtered fuel flowing at 3mL/min, under a back pressure of 500 psi, passes over a stainless strip (grade 302 and approximately 7 cm long, 0.5 cm wide, and 0.025 mm thick), contained in a strip

holder that is heated to 260°C, for 2.5 hours. These are the standard operating conditions of the grav-JFTOT.

However, for the studies conducted, the test temperatures ranged from 165° to 350°C for the neat fuel, and 220 to 350°C for the MDA additized fuel. The overall temperature range of 165° to 350°C was selected to mimic temperature increases in the IFAR, which include: the 165°C inlet fuel temperature and subsequent increases in the inner wall temperature. Specifically, in the IFAR, over a 70-h test duration and at a flow rate of 72 kg/h (approximately 1500 mL/min), the inner wall temperature increased from an initial 300°C to approximately 440°C.

The test duration per test temperature in the grav-JFTOT was 5 hours, and to simulate continuity, the same strip was used in the series of temperature-testings conducted per test fuel. The total deposit is the sum of the deposits formed on the stainless steel strip and the filterables contained in the effluent. The effluent was filtered using two Magna nylon membranes of 0.8 micron pore size. Further details of the method are described elsewhere.[6,9]

RESULTS AND DISCUSSION

Neat Fuel. The effects of increasing wall temperature on thermal deposition in the grav-JFTOT, for the strip and filterable deposits are depicted in Figures 1 and 2, respectively. The overall results indicate a typical deposit distribution pattern for the grav-JFTOT, viz., higher deposition in the filterables than on the strip. Nevertheless, for both types of deposit, similar deposition profiles were observed with an increase in temperature. For example, in the case of the filterables, at 165° to 200°C, thermal deposition is apparently constant and likely simulates the "induction period" observed in the IFAR;[2] as the temperature is increased from approximately 200° to 300°C, deposition increases, but on further increase in temperature, i.e., from approximately 320°-350°C, deposition decreases.

For the temperature range, 200°-300°C, the rate of increase of the *total* thermal deposit with temperature is in accordance ($R^2 = 0.99$) with the well known Arrhenius rate equation (rate = constant x $e^{-E/RT}$), where E is the activation energy, R, the gas constant, and T, the temperature in kelvin (see Figure 3). Moreover, calculation of the activation energy gives a value of approximately 83 kJ/mol. The corresponding value (65 kJ/mol) for the same fuel, obtained using a turbulent flow test rig, viz., the Naval Aviation Fuel Thermal Stability device (NAFTS), may be regarded as somewhat similar.

Comparison with the IFAR. The thermal deposition profile described above for the grav-JFTOT - wherein thermal deposition was plotted versus temperature - is similar to the IFAR's thermal deposition profile, wherein thermal deposition was plotted versus test duration. Specifically, in the case of the IFAR, with increasing test duration, an initial low rate of deposition, which was interpreted[2] to be an "induction period" is followed by an increase, then a decrease in thermal deposition.[2]

Furthermore, in the IFAR, the increase in deposition with test duration is concomitant with an increase in the inner wall temperature (ΔTIW), since ΔTIW was the parameter used to measure thermal deposition. Use of the ΔTIW parameter is based on the relationship[2] that the weight of carbon $\propto [\Delta TIW]^2$. Consequently, based on the above analyses, the operative variable between the two test devices is likely related to a temperature effect and *not* to a difference in flow velocity. In addition, the "induction period" that is reported to occur[2] can also be ascribed to a temperature effect as demonstrated in the profiles of the plots in Figures 1 and 2.

MDA Additized Fuel. For the MDA additized fuel, the strip and filterable thermal deposition profiles versus temperature show similar trends to that of the neat fuel, but the rate of deposition differed significantly with the type of deposit measured (Figures 1 and 2). For example, relative to the neat fuel, the rate of increase of the *strip* deposit was significantly lower in the MDA additized fuel. In contrast, the rate of increase of the *filterable* deposits of the MDA additized fuel was fairly similar to that of the neat fuel. These differences may well explain the beneficial effect of MDA observed in the JFTOT, where mainly the surface tube deposits are measured, versus the innocuous effect observed in the IFAR, on increasing test duration.[2] The diminished performance of MDA on increasing test duration in the IFAR,[2] may

well be due to a temperature effect, specifically, to the relative stability of MDA as the IFAR's initial inner wall temperature increases (see below). Possible breakdown of the MDA molecule at high temperatures (no numerical values given) has been suggested by Clark *et al.*[10]

Realistic operating conditions/temperature effect. Temperature is considered to be the most important physical factor in fuel thermal deposition.[11] The initial operating conditions in the IFAR (e.g., inner wall temperature of 300°C) were selected to represent a severe condition.[2] However, this severity is further exacerbated by subsequent temperature increases with increasing test duration. Such temperature increases likely exceed realistic operating conditions. Consequently, at inner wall temperatures above 300°C, the results obtained in the IFAR are flawed. Thus, the innocuous effect observed with MDA, on increasing test duration, is also likely flawed.

CONCLUSIONS

The overall results suggest that the underlying variable between laminar and turbulent flow test devices for measuring thermal stabilities is a temperature effect and not their differences in flow velocities. Thus, the initial low rate of deposition observed in the turbulent flow test rigs, which was interpreted as an "induction period" is likewise a function of temperature.

At increasing test temperatures, the beneficial effect of MDA observed in the JFTOT (ASTM D3241) may well be related to the type of deposit measured, viz., surface deposit. In contrast, thermal deposition based on the corresponding filterable deposits, which comprise the bulk of the total deposits in the grav-JFTOT, is in agreement with the findings observed in turbulent test rigs for neat and MDA-doped jet fuels.

Consequently, the diminished performance of MDA/innocuous effect observed on increasing test duration in the IFAR, may be related to an increase in temperature effect. However, in the IFAR, the MDA results are likely flawed since its operating conditions, on increasing test duration, are not only severe but unrealistic. In conclusion, on the basis of test conditions, particularly, the very important parameter, temperature, the gravimetric JFTOT offers a more realistic measurement of fuel thermal stability than the IFAR.

ACKNOWLEDGMENTS. The authors thank the Office of Naval Research (Dr. M. Soto) for funding support.

LITERATURE CITED

(1) Lyon, T.F., Fuel Thermal Stability Outlook for GE Aircraft Engines in 1991; In Aviation Fuel Thermal Stability Requirements, ed Kirklin, P.W. and David, P., ASTM STP 1138, American Society for Testing and Materials: Philadelphia, PA., May 1992, p. 73.

(2) Kendall, D.R.; Houlbrook, G.; Clark, R.H.; Bullock, S.P.; Lewis, C. The Thermal Degradation of Aviation Fuels in Jet Engine Injector Feed Arms. Part I. - Results from a Full Scale Rig. Presented at the Tokyo International Gas Turbine Congress, October, 26-31, Tokyo, Japan, 1987, Paper 87-IGTC-49.

(3) Kendall, D.R. and Mills, J.S. , SAE Technical Paper Series, 851871, Society of Automotive Engineers: Warrendale, PA, 1985.

(4) Clark, R.H. The Role of a Metal Deactivator in Improving the Thermal Stability of Aviation Kerosines. Presented at the *3rd International Conference on the Stability and Handling of Liquid Fuels*: London, September 1988, Paper No. 47, p.283, Institute of Petroleum, 1989.

(5) Clark, R.H.; Stevenson, P.A. *Prepr.-Am. Chem. Soc., Div. of Fuel Chem.* **1990**, *35*, 1302.

(6) Beal, E.J.; Hardy, D.R.; Burnett, J.C. In (a) *Proceedings of the 4th International Conference on Stability and Handling of Liquid Fuels:* Orlando, FL, Nov. 1991, pp. 245-259. (b) *Aviation Fuels Thermal Stability Requirements*, ASTM STP 1138; Kirklin, P.W.; David, P., Eds; American Society for Testing and Materials: Philadelphia, PA, 1992, pp. 138-150.

(7) Pande, S.G. and Hardy, D.R. accepted for publication in *Energy and Fuels*, **1998**.

(8) Clark, R.H. and Thomas, L. SAE Technical Paper Series, 881533, Society of Automotive Engineers: Warrendale, PA, 1988.

(9) Pande, S.G.; Hardy, D.R. *Energy and Fuels* **1995**, *9*, 177-182.

(10) Clark, R.H.; Delargy, K.M.; Heins, R.J. *Prepr.-Am.Chem. Soc., Div. Fuel Chem.* **1990**, *35*, (4), 1223.

(11) Hazlett, R.N. *Thermal Oxidation Stability of Aviation Turbine Fuels*; ASTM Mongraph 1, American Society of Testing and Materials: Philadelphia, 1991, page 51.

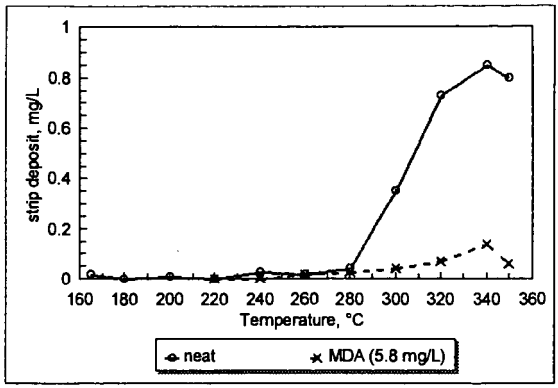

Figure 1. Effect of temperature on strip thermal deposit for a JP-5 fuel: with and without MDA.

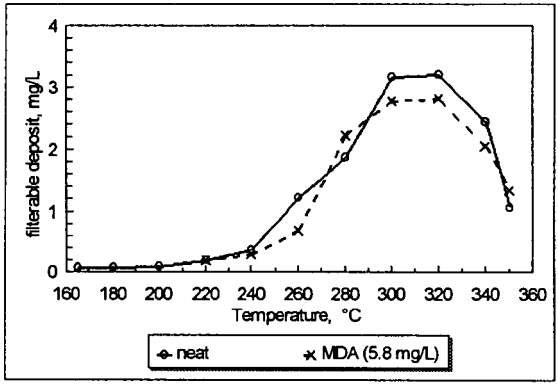

Figure 2. Effect of temperature on filterable thermal deposits for a JP-5 fuel: with and without MDA.

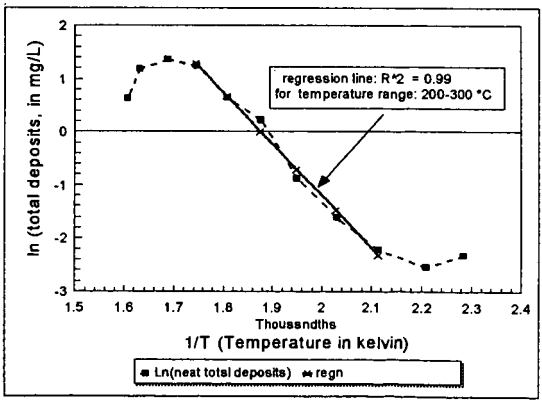

Figure 3. Arrhenius plot of total gravimetric JFTOT deposits formed at test temperatures, 165-350°C for a JP-5 fuel.

ANALYTICAL SEPARATION AND QUANTITATION OF SPECIFICATION LEVELS OF MDA IN AVIATION FUELS

R.C. Striebich, R. R. Grinstead and S. Zabarnick
Aerospace Mechanics Division, KL-463
University of Dayton Research Institute
300 College Park
Dayton, Ohio 45469-0140

INTRODUCTION

Metal deactivator additive (MDA) has been used for the past fifty years to chelate metals which accelerate oxidation reactions in distillate materials (1). Presently, MDA is added to aviation fuel in the concentration range of 0 - 5.8 mg/L. Because of its surface activity and adsorptive properties, MDA may be reduced in concentration as the fuel is handled. Also, as fuels are used to cool hotter aircraft engine components, metal concentrations may increase due to degradation of fuel system materials. Consequently, reduced concentrations of MDA may be insufficient to prevent accelerated autoxidation reactions. The ability to measure the concentration of MDA in storage stability tests, thermal stressing studies and additive addition in the field is important to the success of new thermal stability additives such as JP-8+100 (2).

This work describes a new technique for the determination of metal deactivator additive in aviation fuels and provides some examples of how this measurement can be used to understand the role and fate of MDA in thermally-stressed fuel systems. Several techniques are available in the literature which were not satisfactory for use with distillate fuels having high polars content , low levels of MDA, or for thermally stressed fuels (3,4,5). The technique described herein may be used for specification level analysis of small amounts of sample (200 μL) without analyte concentration or significant sample preparation.

Direct Analysis of MDA

Previous work has been performed in which gas chromatography - mass spectrometry (GC-MS) and similar chromatographic techniques were used to measure MDA concentration directly. However, the polarity and surface activity of MDA made direct detection impossible without specially deactivated chromatographic columns, split liners, and glass wool. Unfortunately, detection limits, detector linearity, and repeatability continued to be poor, even after the activities of these surfaces were reduced. Calibration curves for MDA in toluene indicated detection limits of 10 - 20 mg/L typically, with even higher detection limits for more complex solvent matrices. In order to lower the detection limits, silica gel solid-phase extraction (50:1 concentration) was performed for most aviation fuel samples, concentrating the polar fuel components and improving detectability. Although this technique was used to track MDA disappearance in thermally stressed systems, sample preparation time and reproducibility/repeatability were unacceptable.

Chemical Derivatization

The analysis of MDA was performed by reacting this highly adsorptive polar compound with the silylating agent N,O-bis[trimethylsilyl]acetamide (BSA) to form the derivatized product as shown:

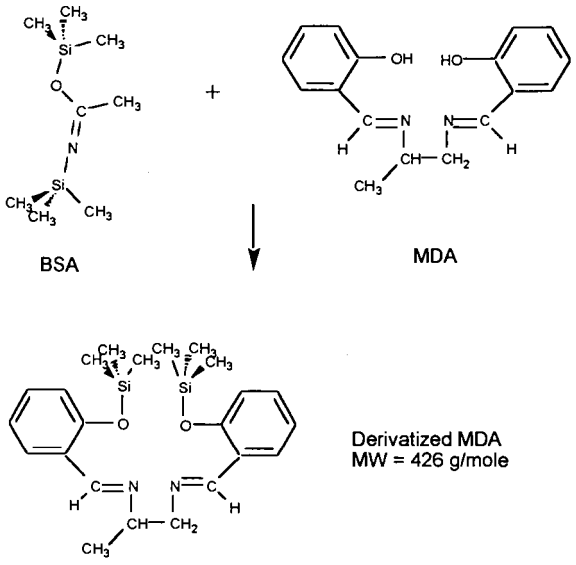

Figure 1. Derivatization reaction of N,O-bis [trimethylsilyl] acetamide (BSA) with MDA.

BSA is a common trimethylsilyl donor which reacts to replace active hydrogens from phenols, acids, thiols and amines with the trimethylsilyl functionality (7). These reactions typically occur in nearly 100% yields; in this case, no MDA or partially silylated compounds were detectable after reaction. The reaction occurs at room temperature and although the resultant derivatized compound has a molecular weight of 426 g/mole, its non-polar nature allows it to be eluted from typical non-polar chromatographic columns at temperatures similar to MDA elution.

EXPERIMENTAL

MDA from a 75% mixture in aromatic solvents (Octel America) was used to make standard mixtures in a reference kerosene (Aldrich Chemical) at concentrations between 0 and 10 mg/L. Two hundred microliters of each solution were pipetted into glass micro-inserts and sealed in a GC vial (Hewlett Packard). A 10 µL full scale syringe (Hamilton) was used to add 5 µL of BSA (Pierce) to each sample. Care was taken to minimize exposure of the BSA to atmospheric moisture since BSA is highly reactive with water. Finally, each solution was mixed for approximately 10 seconds on a vortex mixer.

The GC-MS (Hewlett Packard 5890/5971) was operated in the selected ion monitoring mode (220, 235 amu) for the majority of the analyses. The gas chromatograph was programmed linearly from 150 (1 minute hold) to 280°C (5 minute hold) at 10°C per minute. The chromatographic column was a 30 meter, 0.25 mm ID, 0.25 micron film thickness HP-5 capillary column (Hewlett Packard), although almost any non-polar column having a thermal stability greater than 300°C would be suitable. Preliminary analyses indicated that a thin film (0.1 micron film thickness) column may be desirable for both resolution and analysis time. Interferences (from fuel or stressed fuel components) were separated from the derivatized MDA signal by knowledge of the correct retention time as well as the specificity of the selected ions and the ion ratios. The 220 and 235 ions were used for MS quantitation; these ions were the strongest ions in the mass spectrum for the MDA derivative.

RESULTS AND DISCUSSION

Calibration work indicated that this technique could be used to measure specification levels of MDA in hydrocarbon matrices. Figure 2 shows typical calibration curves between 0 and 10 mg/L MDA, demonstrating the linearity of the detector and the quantitative yields from the addition of BSA to each calibration solution. One should note that the intercept for the curve is

non-zero, indicating a lower detection limit of approximately 0.5 mg/L, possibly due to adsorption of the MDA on the glass vial before the BSA is added.

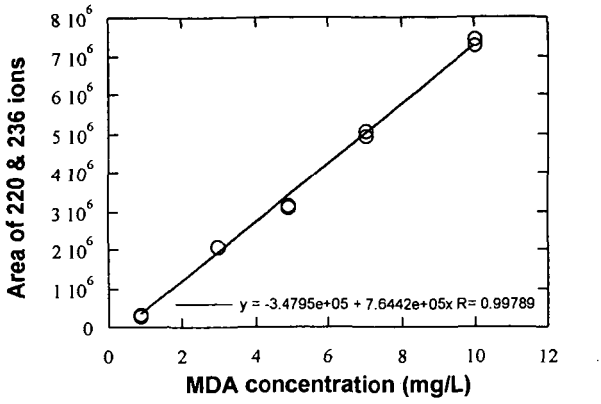

Figure 2. Typical calibration for derivatized MDA in a reference kerosene.

The lower detection limit (approximately 0.5 mg/L) of MDA as shown in figure 2 was affected by the adsorption of MDA to the glass insert and other surfaces to which the MDA is exposed. If BSA is added to a 10 mg/L MDA solution and the derivatized MDA serially diluted with kerosene to produce analytes between 0 and 1 mg/L, the minimum detectable level of MDA derivative is greatly decreased and linearity of detection greatly improved. This observation is consistent with MDA being adsorbed to active sites in the glass vial which have high surface to volume ratios, affecting the lower level standards more than higher level standards. The use of plastic inserts did not improve the amount of MDA adsorbed before it could be derivatized. Further studies may be conducted to see if surface deactivation (using an MDA wash solution) would enhance lower level detection of the additive.

Effect of Fuel Matrix on Measurement

A series of Jet A and JP-5 aviation fuels were spiked with a known amount of MDA. These samples were treated with BSA and duplicate measurements of each were used to quantitate the level of MDA (see Table 1). No history of the origin of the fuel was available; levels of MDA which may have already existed in the fuel were not available and could not be traced.

Table 1
Results of Analysis of Samples Spiked with MDA

Sample ID	Fuel type	MDA added (mg/L)	MDA measured (mg/L)
POSF-2985	Jet A	2.0	2.0
POSF-2963	JP-5	2.0	2.2
POSF-2963	JP-5	6.0	5.0
POSF-3119	Jet A	2.0	2.7
POSF-3084	Jet A	2.0	2.8
POSF-2926	Jet A	2.0	2.4
POSF-2827	Jet A	2.0	2.8
POSF-3059	Jet A	2.0	2.5
POSF-2962	JP-5	6.0	6.0
POSF-2962	JP-5	2.0	2.5

All of the measurements obtained (POSF-2963 as an exception) were greater than or equal to the amount added to the original fuel. We suspect that these fuels may have been doped with MDA at the refinery (up to 5.8 mg/L is allowable). As the history of each fuel was unknown, all samples were reanalyzed with BSA alone to detect low levels of MDA. With the exception of POSF-2962, all samples showed small amounts of uncomplexed MDA present (less than 0.5 mg/L). Attempts were made to quantify the MDA, but the calibration curve was non-linear

between 0 and 1 mg/L due to adsorption of the small amounts of MDA on surfaces. Further work needs to be conducted to improve the low level accuracy (and precision) of this technique.

Samples POSF-2962 and POSF-2963 were of considerable interest because it is not known whether MDA that is chelated with a metal in solution can also be silylated. To examine this question, POSF-2962 was spiked with copper naphthenate (to 100 ppb copper) and renamed POSF-2963. This fuel (POSF-2963) was measured by ICP-AES to have a copper content of 98 parts-per-billion (ppb), with iron and zinc levels measured at 60 and 14 ppb, respectively. Because the mass spectrometer was used to detect a specific mass at a specific retention time, MDA complexed with copper and silylated should not be detected at the same retention time as MDA not complexed with copper. Therefore, POSF-2962 should have higher levels of MDA measured than its counterpart, POSF-2963, which was subjected to copper. This was indeed the case as shown in Table 1 for fuel spiked at the 2.0 and 6.0 mg/L levels of MDA: in each case, MDA concentration was higher in the POSF-2962 sample than the POSF-2963 sample. Further studies (using fuels with known processing histories) will be conducted to determine the chemistry of derivatization reactions for copper-containing MDA.

Measurement of Field Samples for Additive Content

An additive package currently being investigated for Air Force fuels, JP-8+100, is comprised of several additives including a detergent/dispersant, antioxidant and the metal deactivator additive, MDA. Because the additive is introduced in the field at the user level, measurements of the level of MDA could provide an important check on the techniques used to deliver and mix the additive package. Four samples were obtained from active air bases currently using the JP8+100 additive and were received in undeactivated one gallon cans. Results from the four samples indicated that MDA concentrations were below the desired level of 2.0 mg/L with most measurements indicating less than 1 mg/L. Because field sampling cans have a low surface to volume ratio, one would probably suspect the glass containers used in the laboratory for the poor recovery of MDA. Additional work will address the possible deactivation of these surfaces so that field sampling of the additive package will predict or indicate problems in the field.

Tracking Additive Concentration During Stressing Tests

Thermal stressing may decrease additive concentration in some fuels, so the ability to track additive concentration is of interest. Figure 3 shows that the MDA concentration decreases as a function of time with oxidative stressing at 180°C. MDA concentration decreases as a function of time due to its reaction with other species. As MDA reacts it may become less effective as a chelation additive, and therefore unable to complex metals which may increase in concentration during stressing due to materials degradation (7).

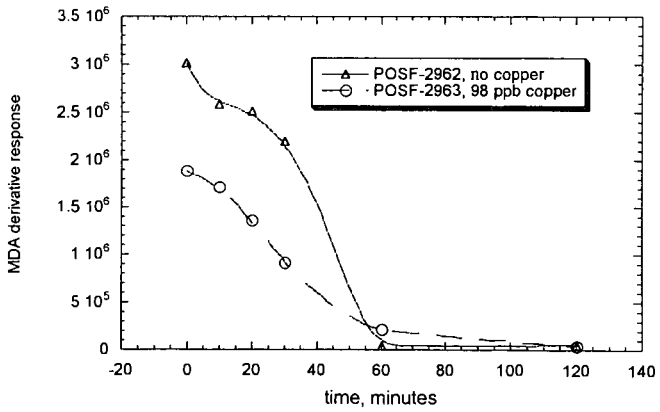

Figure 3. MDA reaction during thermal stressing of neat and copper-doped fuel in the Isothermal Corrosion Oxidation Tester.

CONCLUSIONS

Metal deactivator additive (and potentially, other phenolic additives) can be successfully analyzed using chemical derivatization followed by GC-MS detection. Because of the surface active nature of MDA, conventional chromatographic techniques are prone to poor accuracy and precision, as well as high detection limits. Derivatization with BSA can be conducted at room temperature using extremely small samples (200 μL) with sensitivity sufficient to cover the specification range of the additive. Analysis time due to selected ion monitoring on the GC-MS can be as short as 13 minutes. Consequently, this technique can be used to evaluate additive concentrations in the field, track additive usage in stressing studies and to understand the relationship between metal deactivator additive and surfaces or metals in the fuel.

ACKNOWLEDGMENTS

This work was sponsored by the US Air Force, AFRL/PRSF, at Wright-Patterson AFB, Ohio under contract number F33615-97-C-2719. Mr. Charles Frayne was the technical monitor.

REFERENCES

1. Pederson, C. J., *Ind. Eng. Chem. Res.*, 48, pp. 1881-1884, 1936.
2. Heneghan, S.P., Zabarnick S., Ballal, D. R., Harrison III, W. E., J. Energy Res. Tech., 118 , pp. 170-179, September 1996.
3. Kauffman, R.E., ASME Publication 97-GT-77, ASME: Orlando, FL, June 1997.
4. Henry, C., Octel America analytical method , November 1995.
5. Schulz, W.D., ACS Petroleum Preprints, 37, 2, San Francisco, CA, March 1992.
6. Zabarnick, S., ASME Paper No.: 97-GT-219, ASME: Orlando, FL, June 1997.
7. Pierce, A.E., Silylation of Organic Compounds, Pierce Chemical Co., Rockford, IL, 1968.

What is a Flame?
A Review of 50 Years of Research

Robert H. Essenhigh; E.G. Bailey Professor of Energy Conversion
Department of Mechanical Engineering
The Ohio State University; Columbus, Ohio: 43210

"The great issues of science are more often qualitative than quantitative"

Introduction. Research on the structure and characteristics of flames has been in progress now for nearly two centuries, but in spite of being able to list well-known flame properties (Table 1), a unique definition of a flame would seem to be still elusive. The question this raises is whether flame properties are so diverse that such definition is impossible, or whether there may be aspects of flame behavior that are yet to be discovered. What evidently is missing is an axiomatic framework for organizing flame properties; and to create such a framework, first, requires answer to the Title question: "What is a flame?"

The answer to this question, as will be shown, is ambiguous; but it provides a direction to pursue. This leads to a conceptual division of flames into three broad categories, as set out in Table 2. The two major Categories, I and II, in this Table broadly represent Combustion Science and Combustion Engineering which, itself, identifies something of a previous disconnect in combustion analysis where engineering systems – notably industrial furnaces – are commonly sidelined in combustion texts. This Table 2 formulation places them more centrally in the general scheme of combustion analysis; it also has significant impact on concepts of flame properties, as will be seen.

There is also a starting thread of axiomatization in this Table 2 Classification, and this is substantially expanded by amplification of Category II, as set out in Table 3. The matter of definitions, nevertheless, is central; and to examine this, we first require some historical context. This also raises the issue implied by the paper sub-title: What period of time was the most active and productive in combustion research? and the pass-out question this also raises is: What might we expect in the next half century?

Historical. ***Origins.*** Combustion research can reasonably be regarded as having an ancestry and prologue in the oxidation studies of the last half of the 18th century which *inter alia* demolished the Phlogiston theory and set the basis for modern chemistry. The defining moment for the start of combustion science is generally accepted as the studies by Sir Humphrey Davy in 1813-1815 – in connection with very-practical problems of gas explosions in coal mines – with his two-property demonstration (simultaneously with his invention of the safety lamp) of: low combustion limits in fuel/air mixtures; and variation of flame speed with fuel concentration. In the most general terms, these two properties are central to the two principal characteristics of most flames as set by the questions: "Is ignition maintained, and is the flame stationary or moving?" In that sense, the field of combustion science was largely defined by Davy's discoveries.

Development. Historically, subsequent research was substantially guided by one or both of two needs: first, the need for information -- a data base -- essentially the measurements of flame speeds and combustion limits, and spin-off's from those; and, second, the need for data interpretations, or theoretical development of flame propagation and combustion mechanisms. Significant also were the drivers for the research that shifted with time but were very much dominated through much of the 19th century by considerations of fire and safety, notably in coal mines. On that account, much of the resulting emphasis was on ignition, low limits, and flame suppression; and propagation was investigated more as a consequence of behavior in large scale experiments, with large-scale explosion-gallery tests on gas and coal mixtures dating from the 1870's. In the current (20th) century, the drivers for fundamental investigations moved more to practical problems, notably, after WWII related to gas turbines and rockets, but then later to air pollution and other environmental problems.

It was also implicitly recognized even in the early studies that a data base by itself can have empirical engineering value but, scientifically, it is essentially worthless without (correct) interpretation. The emphasis in the safety-dominated investigations, consequently, was very much on fundamental studies, to be able to understand and control the practical problems of explosion; at the same time, surprisingly, there was evidently a notable disconnect from the practical problems of industrial combustion, for example, in furnaces (Table 2, Category II flames) which in consequence were developed on a substantially *ad-hoc* or empirical basis. The significant injection of science into combustion engineering appears to have been largely a consequence of World War II.

In the two centuries following Davy, pursuit of the data base development expanded the determination of combustion limits and flame speeds into measurements on fuels other than gases: vapors, solid particles, and liquid drops; and expanded the range of measurements into supportive and supplementary determinations of ignition properties, ignition temperatures, temperature profiles, flame temperatures, reaction times, and ultimately of reaction rates. The results, in general, showed variations in numerical properties from fuel to fuel but substantially, otherwise, showed the same qualitative patterns of behavior: there were upper and lower combustion limits; minimum ignition energy requirements; and flame speeds and temperatures that varied with

concentration in substantially the same pattern of: lower values at the limits; and peaking near the stoichiometric.

Quantification. Quantitatively, the pattern of results for different fuels was both different and the same. In the "base-line" laminar flames (Category I of Table 2) for different hydrocarbon fuels – gases, liquids, and dispersions of particulate solids – reaction times or flame thicknesses are very fuel-type dependent: thicknesses of laminar flames range from 1 mm for gases to 1 m for pulverized coal, a range of three orders of magnitude. Likewise, propagation mechanisms range from conduction to radiation. Peak temperatures, however, are very similar, with energy-densities for stoichiometric fuel-air mixtures averaging close to 100 Btu/ft^3 for hydrocarbon gases, liquids, or dispersions of particulate solids, and generating T_{ad} values of about 2000°C (3600°F). More surprising, laminar flame speeds and low limits, also, are essentially fuel-type independent, being roughly the same or of the same order, with most laminar speeds (Su values) in the range half to one meter per second, and low limits at about 100% excess air, corresponding to mixture energy-density values averaging 50 Btu/ft^3 or half that of the stoichiometric.

In fixed beds of particulate solids (e.g., lump coal), values (of flame speeds and reaction intensities) were different again, but historically such systems were generally treated or implicitly regarded as outside the "main" stream of combustion theory and development, although latest developments in "Filtration" combustion (Table 3, Class II.2), as set out below, may change this perception. Flame spread, ignition and extinction behavior, and batch combustion (Category III of Table 2), likewise, were typically treated substantially on a stand-alone basis, and this is seen in the ordering and emphasis in today's standard combustion texts. Much of this reflected the disconnect between combustion science and combustion engineering noted earlier.

Associated with all this was the complementary development of steadily improving instrumentation, with increasing ability to make measurements of local temperatures, concentrations, and velocities, and fluctuations of those parameters, together with fast data recording and analysis. The development of optical methods, particularly by lasers, allowing non-intrusive measurement was particularly valuable. Such measurements are critically important, but less as part of fundamental combustion studies than as supporting techniques for accurate development of phenomenological descriptions, and for testing analytical predictions. Analysis, nevertheless, remains hostage to correct interpretation, preferably mechanistic, of the observed phenomena, and this remains the central issue even at this time.

Combustion Engineering. In parallel with this history, but with long pre-cedents, there were major but largely-independent developments in combustion engineering. Combustion science and engineering have now almost merged, but the historical account shows their effective independence until relatively recently. Even apart from use of flames in heating caves (with a "million" year history), the use of furnaces – and concomitant control of fire – for pottery, brick, and metals production has origins 10,000 and more years back. Additionally, in the last half of the 18th century there were three significant advances: first, James Watt's development of the steam engine, of which the invention of the condenser – a (recuperative) heat exchanger – was a crucial part; second, in the 1790's, the invention of the hot blast – another (regenerative) heat exchanger application – for blast furnaces (a form of Filtration Combustion) which transformed iron manufacture; and third, in the same decade, the start of coal gasification in coke ovens that subsequently, with pipelined distribution (already significant by the 1820's), ultimately transformed street lighting, home heating, cooking appliances, and industrial furnace operations. For the coal gas from coking ovens, with a typical content of 50% H_2 and 35% CH_4, the world was half way to a hydrogen economy two centuries ago. These industrial operations are presented in Table 2 as Category II and in Table 3 as Class I applications.

These developments all represented major commercial use of combustion in engineering systems, albeit developed largely empirically, but with considerable sophistication even in the early 1800's when combustion science studies had barely started. Through the following 19th century, these applications were extended by development of more advanced, high-temperature regenerative furnace systems, notably, in addition to bricks and refractories, for glass melting, and for steel making using the Bessemer and the Open Hearth (the BOF is a 1940's development, a century later). The significance of the (regenerative) preheat was the, generally unrecognized potential, jointly, for super-adiabatic flame temperatures, and for stabilization of high velocity flames. This meant that some major technological problems, notably the fast flame stabilization, had already been solved, by empirical development, long before they were even recognized and defined in scientific terms.

Scientific Elements. The scientific aspects starting in the early 1800's could not, in fact, be addressed until key theoretical concepts had been developed. The two key theoretical elements required in analysis of even the simplest 1-D (Table 2: Category I) laminar flames are heat transfer and kinetics; and first applications of these elements to flames, in the Mallard and le Chatelier (MLC) model, were in the last half of the 19th century with prediction of flame speed and of the temperature profile through a flame. This became the prototype for subsequent flame models involving other modes of heat transfer (radiation and convective exchange), with extension then to analysis of other flame types, notably turbulent and 3-D flames. In that first laminar flame model, (conductive) heat transfer dominates the initial temperature rise up to "ignition", but some form of kinetics assumption is required from ignition through the reaction zone.

Separately, this model also re-raised the question of definition of ignition, in this case, in mid-flame; this problem was the practical driver both in Davy's original studies of gas combustion

and in Faraday's studies in 1844 of coal ignition, also in connection with coal mine explosions. It was not until the mid-1930's that the Semenov Thermal Explosion Theory (TET) provided a (thermal-based) theoretical model for batch ignition. The definition of ignition in a continuous (Category I) flame is still open, however, although the gap was potentially closed by Vulis' (late 1940's) treatment of the continuous flame as a PSR sequence with a definable TET ignition cell in the middle of the flame. This was updated in 1974 but is still incomplete.

The theoretical background needed for these flame model developments in the preceding century required two fundamental insights. The first was elimination of the Caloric theory, in the first half of last century, which played the same blocking role in thermal sciences that the Phlogiston theory had played in the chemical sciences half a century earlier. The second was formulation of kinetics, in the second half of the century, initially specified as a phenomenological statement in the Guldberg and Waage *Law of Mass Action* (LMA), and then importantly extended by the introduction of the Arrhenius statement for the velocity constants. This phenomenological model itself then opened up enquiry into the mechanism behind the LMA statement, and the answer that emerged, in the first half of the current century was the Bodenstein dissociation model leading critically into understanding of chain reactions and consequences of that behavior that, for gases particularly, could result in escalation to explosion and detonation.

In its turn, the "mechanism" of dissociation was identified as being, simultaneously, a phenomenological behavior in its own right, implying thereby a more detailed underlying mechanism, and this led to the postulates of the activated complexes and then, in more detail, the study of molecular orbital trajectories as the basis for *ab initio* calculations of reaction rates. Both these further approaches are major stand-alone developments in chemical physics; for purposes of combustion studies in flames, however, phenomenological kinetics mostly suffices.

Even so, only by the middle of this (20th.) century was the dissociative kinetic basis sufficiently established that attention could be turned to extensive measurement, and development of a kinetics data base. This first required identification of governing elemental reactions with debates continuing, for example, as late as the 1950's on whether H or OH was the dominant radical for hydrogen combustion. Even in the 1960's, for lack of adequate information on elementary reactions, and/or inability (for lack of computing power) to handle the equations sets involved, there was still continuing use of rates measured in global or quasi-global terms for fuel reacting, one-step, to end products (CO_2 and H_2O), or slightly more elaborately, reacting first to CO and H_2 with a selected suite of the hydrogen reactions to complete the model.

The developments since then, largely in the last 30 years, with the almost explosive growth of data on elementary reaction velocity constants, requires no further comment. This has been further supplemented by development of model codes, first for calculating equilibrium properties and then, in the last decade or so, kinetics codes, combined in many cases with flow codes to be able to calculate complete flame behavior in a flowing stream. This, however, may in some instances be a double-edged problem, if the codes – particularly the flow elements – are extrapolated outside the window of verification.

These developments represent major understanding of and potential for applications of combustion theory to engineering problems and (with some reservations) this procedure is now largely standard practice. Nevertheless, a potential for unification existed half a century ago, and it still deserves examination. This combines the Vulis PSR-sequence model for a 1-D flame already mentioned (in connection with in-flame ignition) with the Bragg Criterion for (gas-turbine) combustion chamber design.

A Unifying Factor: The Vulis Model and the Bragg Criterion. The Bragg Criterion (1953) for combustion chamber design resulted from generalization of a detailed analysis of the Rolls Royce Trent jet engine, with the conclusion that: the ideal (design target) mixing configuration should be: a Perfectly-Stirred Reactor (PSR) inlet segment for fastest ignition, followed by a Plug-Flow Reactor (PFR) segment for optimum burn-out. The *engineering* problem of creating the PSR/PFR fluids mixing configuration is a major one, but separate. Importantly, however, it provides a clear target for the design intent; it also provides a link to the Vulis model.

The relation this has to the Vulis model then derives from the question: In the Vulis PSR-sequence model, what is the effect of changing the size of the PSR cells? This was explored in a separate publication (1974) obtaining the general result that: in the flame region *before* the point of inflection (ignition point) in the T-t curve, increasing the PSR size results in faster combustion or reduced time to ignition; and, after the POI, for fastest burn-out, requires the reverse, namely, reduced cell size. In the limit of a single cell for ignition and multiple cells for burn-out, this corresponds exactly to the Bragg Criterion.

Review of actual engineering (industrial) furnaces and burners, very largely developed empirically, typically show an approximation to this PSR/PFR mixing configuration. This will be more evident in what follows.

This provides the summary background to consider the definition of a flame.

What is a Flame? A flame is something that can always be identified as such after the fact, but an *a priori* definition that is *necessary and sufficient* does not seem to exist. Common flame properties often incorporated in "definitions" are listed in Table 1. None, however, is unique.

Property 1 is denied by pyrophoric and hypergolic materials; an example is pyrophoric ignition of very fine iron particles blown into air. *Property 2* is common to many reactions that are not combustion. *Properties 3 and 4* are denied in the limiting case of the Perfectly Stirred

Reactor (PSR) when a flame front and thus a flame speed can not be defined, as discussed in more detail below. *Property 5* is denied when there is thermal backmix, the Category II of Table 2. *Property 6* is reversed when there is thermal backmix, and the statement inverts to become: "When the flame is stable, the (local) flame speed and mixture speeds are in balance" (essentially, then, a trivial consequence). *Property 7* is denied with preheat: combustion limits are extended -- the requirement is for maintaining the sensible plus chemical energy above a minimum energy density of about 50 Btu/ft^3. *Property 8* is denied under a range of thermal feedback conditions (*see* Category II of Table 2; *also* Table 3). *Property 9* is not unique to flames: hot materials, in general, radiate in the visible; moreover, radiation from hydrogen flames is not in the visible.

Flame Categories. This failure in finding a unique property for definition of a flame suggests that the factors governing in flames may be incompletely identified. An alternative approach suggested by examination of the Table 1 listings, and the comments above, led to the first two (primary) alternative Categories of flame types identified in the classification of Table 2. The key distinction between these two Categories is whether the flame speed is an *independent* or a *dependent* property of the fuel mixture and of the combustion system. However, study of Filtration Combustion (Class II.2 in Table 3) suggests that even this may turn out to be either simplistic or limited. To put these in perspective requires separate evaluation. Flame stabilization is examined first.

Flame Stabilization. Classical concepts of flame stabilization are formulated in terms of velocity balancing. The concept originates with 1-D laminar flames and has been translated, in turbulent flames, to local behavior. For the standard one-dimensional (1-D, MLC) flow system, the flame speed depends only on the mixture composition. The argument is that, if flame is propagating down a tube, against no flow or low velocity flow, then the flame will be stabilized if the mixture-approach flow-velocity is increased until the velocities balance. This is a valid representation in plug-flow systems, and in similar systems where there is no back-mix such as the Bunsen burner; but – possibly excepting the Filtration Combustion (FC) systems, as already identified – the velocity-balancing argument can fail if there is any degree of thermal preheat by backmix or other method.

In flow-backmix and heat recovery or Thermally Assisted Flame (TAF) systems (Table 3), which thus includes nearly all practical (engineering) flame systems in furnaces or engines, the incoming mixture is preheated in one way or another, and the flame speed is increased. The flame speed, however, is then a dependent property of the system. In the case, for example, of a standard unswirled jet burner firing into a furnace in an SE (Sudden Expansion) configuration (a Table 3 Class II.1 device), the jet velocity is commonly of the order of 10 m/s, but the fundamental flame speed for the incoming mixture, whether gas, or oil, or pulverized coal, is usually about 1 m/s. The flame, nevertheless, is stable on account of the backmix flow of hot combustion products generated by the momentum of the incoming jet. The aerodynamics of this mixing behavior is key, and is a pattern studied intensively through the late 1940's to early 1960's, notably by the IFRF but also by many others.

The standard interpretation of that behavior is that the flame is then stabilized on account of the *increase in flame speed* due to the backmix-governed preheat. The conclusion is arguable, however, even for this single unswirled jet configuration since the degree of backmix-preheat – and thus the increase in flame speed – depends on the primary jet momentum so that the flame speed is now a *dependent* not an independent property of the system. In other words, "Which is the cart and which is the horse?" The flame "speed" can be changed for the same mass flow of incoming mixture solely by increasing the jet velocity (for example, by reducing a pipe diameter). Indeed, with increased jet velocity, the flame generally moves *up*stream (up to a final blow-off or blow-out limit).

That argument becomes even less supportable if the degree of backmix is proportionately increased, for example, by introducing swirl or double swirl or additional down-stream jets, to the point that the primary flame region converges to an approximation of a Perfectly Stirred or zero-dimensional (0-D) Reactor. At that limit, ignition is then distributed throughout the combustion volume; thus, there is no formally definable "flame front" where ignition starts; a flame speed can not therefore be defined; flame stabilization no longer depends on velocity balancing, and interpretation in those terms thus becomes meaningless. Separately, this also has consequences for burn-out and combustion efficiency; this is considered later.

The clearest practical demonstration of this 0-D structure is the Putnam "Octopus" burner, consisting of 8 raw gas jets at the corners of a cube, directed at the cube center. The flame produced is substantially spherical, inside a flame envelope, but there is no flame "front" in the conventional sense of the word so, supporting the statements above, no flame speed can be defined, and there is therefore no potential for defining velocity balancing. Likewise, there is no "flame holder", nor flame "attachment" to a holder (behavior commonly identified in burner studies and assumed to be significant). Since velocity-balancing is evidently invalid as explanation for the flame stabilization, some other criterion is required.

Intuitively, there would appear to be two criteria for stabilization of such a flame, one thermal and one mechanical. The evident thermal stability condition is that the reacting mixture in the flame zone satisfies the standard PSR or WSR thermal extinction (TET) conditions (based on balance between thermal generation by reaction and thermal loss by convection/radiation). The mechanical stability condition is thought to be a zero momentum integral over the surface of

a Control Volume enclosing the flame. For other standard jet flame systems (straight jet, or swirled, or other) the same conditions could apply: it requires definition of a relevant CV inside the combustion chamber, to which the two criteria proposed may then apply. This needs to be examined further; first steps have been taken resulting in definition of an "information flow path" as part of the required CV definition, but the results at this time are essentially open-ended.

Thus, in support of the earlier assessment, this view of flame stabilization clearly incorporates all the thermally-assisted systems listed as Class I and Class II.1 in Table 3. The essential characteristic of the thermal assist in these two classes is that it is provided either externally, through heat exchangers, or internally but by a (fluid) backmix flow process. The focus of flame stabilization in practical terms is being able to design engineering devices in which flame stability is reasonably assured over the expected operating conditions, such as no *flame-out* in a jet engine at 35,000 ft, for example.

As also previously noted, however, this approach does not address the further class, Class II.2, of Filtration Combustion. This is also one that also operates with thermal assist; the thermal assist in this case, however, is in the form of a direct "counterflow" to the mixture flow. Consequently, it presents ambiguities, and may in fact be a stand-alone case.

Filtration Combustion (FC). This is defined as combustion of a reactive gas in a porous bed and, as listed in Table 3 (Class II.2) has two sub-sets: (1) systems in which the gas reacts with the porous medium, such as oxygen in air reacting with coke or coal; and (2) a fuel mixture such as methane-air reacting in the bed pores. Filtration Combustion has been proposed as a new category of flame types but, in fact, it has a long though largely unrecognized history. The second sub-set [Class II.2(2)] has at least a two-decade history of study, but the history of the first sub-set – study of coal combustion and sinter beds – is over a century. Recognition of the commonality of the two sub-sets is also very recent, certainly within the last decade; likewise, essentially complete solution of the governing equations (for combustion of anthracite in a fixed bed) with experimental verification is also as recent (*1984*). As mentioned earlier, such combustion systems have commonly been regarded as stand-alone or non-mainstream. What is important in this new recognition is the degree to which this flame Class can evidently co-ordinate a range of apparently disparate reaction systems, unexpectedly *including*, as a *limiting* condition, the 1-D, Category I flames, as will now be shown.

The physical system consists of a porous bed of particles or porous sintered block with reactive gas or gas mixture flowing through. The reaction is in the gas phase and/or at the surface of the particles. Heat released by reaction raises the temperature of both the gas mixture and the porous solid, and generates different temperature profiles that will also cross. Heat transfer required for ignition of incoming material is by conduction through the gas (as in the Category I flames) but also by radiative-conduction through the porous solid which provides the thermal assist. At any local point in the bed a key element is the (conductive/convective) heat exchange between the gas and the solid, governed by a heat exchange coefficient, h. The complete system is then described by two DE's of substantially identical form, namely that of the MLC equation, but with an additional interchange term involving h, and with different parameter values for the gas and the solid phases.

The outcome of the process, predicted theoretically and supported experimentally, is that 1-D flames can behave in the classic manner of the MLC (Table 2, Category I) model, showing blow-off and flash back. Unlike the basic MLC model, however, the flames show "unusual" characteristics, notably: flame stabilization at very much higher fluid flow speeds than for the mixture without the porous body support – as in the other TAF systems; also, superadiabatic flame temperatures; very low limiting blow-off velocities, as low as 1 mm/s; and extended combustion limits.

As already noted above, however, with the exception of the very slow blow-off velocity, these "unusual" properties are shared by all the other Thermally Assisted Flame (TAF) systems although this is not commonly identified. In addition, however, a different property also exists that depends on the heat exchange coefficient, h, between the gas and solid. If this is progressively reduced, the reduction is effectively equivalent to progressive reduction of the solid density. In the limit, corresponding to no solid bed, the thermal interchange term in the equations vanishes, and the effect is to reduce the two governing equations to one, namely the MLC equation for the combustion of a free gas mixture; thus, the system converges to a Category I flame system. The outcome is a possible change of focus. We might reasonably regard the twin DE's of the Filtration Combustion (FC) set as the base DE's for propagating laminar 1-D flames; and the original classic MLC system then defines a limiting or special-case boundary behavior for zero porous body density. In this sense, it is the original MLC flame rather than the FC flame that might then be seen as "anomalous".

This alone suggests a need for a re-evaluation of the Category I flame properties. It sets the "peripheral" engineering systems of fixed beds (coal, coke, MSW, etc:) in a central role. Most particularly, however, it challenges even the classic 1-D (MLC) system as defining a "fundamental" flame speed. The same gas/air mixture composition can have different stationary flow velocities, i.e., flame speeds for different porous configurations and materials. What then is so special or "fundamental" in the case of propagation in gas phase combustion governed only by conductive heat transfer as in the MLC flame?

Review and Evaluation. This representation of 1-D flame systems as members of a general Filtration Combustion set, with the MLC flame as a special case for an infinitely porous solid, can now be contrasted with the PSR or zero dimensional (0-D) limit of the Category II (thermal backmix) flames. What are commoniy regarded as 2-D or 3-D flame systems are definable as incompletely 0-D with 1-D components (i.e., Well Stirred as contrasted with Perfectly Stirred). The initial emphasis for nearly all flames of *practical* interest is then on their 0-D or near 0-D characteristics at the burner: notably, the mechanical and thermal stability of a relevant CV, if such can be defined. This focus transfers attention away from flame speed as a unique governing property, and one that has been a major focus of many past flame studies. This transfer of attention gains particular significance when examining practical flame systems which by default are nearly all turbulent. It is in turbulent flames that the idea of flame front and flame speed need particular examination.

Adequate discussion of turbulent flames is not possible here for space limitations. Nevertheless, to identify key elements, studies of turbulent flames commonly show dispersed regions of reaction, and a common view of the development of the reaction through the flame zone is that it can be represented in many cases by contorted surfaces propagating into unignited fuel mixture. The detailed modeling of the behavior is then addressed by such means as strained wrinkled laminar flamelet analysis, assuming the flamelet is "thin", or by distributed reaction zone theory for thick flamelet or reacting regions. The pre-supposition here is that the unignited region requires transfer of heat and/or dissociated species for extension of the reaction (flame propagation) into the fresh mixture, as in the standard laminar flame model. For a turbulent jet flame in an open cold environment this has substantial relevance. For a jet in an enclosure such as a furnace, however, where measurements typically show substantial temperature fields adjacent to the jet, the question may be less to do with what it takes for ignition and more to do with why flames extinguish: in particular, with distributed reaction zones found in turbulent flames, there can be local extinction of identifiable volumes.

In the form of the existence of low limits, the problem of flame extinction is, in fact, one of the two critical characteristics first addressed by Davy in 1813, and still essentially unresolved in spite of many studies. A major common factor, identified by Burgess and Wheeler in 1912, is that the low combustion limit, calculated as an energy density, is approximately constant at about 50 Btu/ft^3 for all hydrocarbon fuels, solid, liquid, or gas. This has never been elaborated except to the demonstration that the (50 Btu/ft^3) critical energy density can also be satisfied by the sum of chemical (reaction) energy and sensible energy from preheat. It is this that allows reduction of the low limit by preheat. The reason for this is still unidentified but it could be key both to a solution to that problem and to a final interpretation of flame behavior.

Summary and Conclusions. The conclusion that emerges from this review is that, if a common organizing principle exists, that can be used to create combustion studies in an axiomatic framework, that organizing principle does not yet appear to have been identified or formulated. However, this evaluation also provides a framework to define the direction of continued research, starting with a review of combustion knowledge with the objective, if possible, of creating an appropriate axiomatic framework. A starting point and current example is the Filtration Combustion concept, as discussed above. More generally, there is the potential identified by the classification into Categories I, II, and III. The direction taken to develop such a framework could then start to set the general agenda for the next phase of work into next century. This can be addressed at two levels: the "tactical" level, and the "strategic" level.

At the tactical level, this concerns possible theoretical/analytical procedures (but appropriately including advanced experimental methods for more detailed and accurate determination of reaction processes). Of possible analytical procedures, there are four in particular that would seem to justify particular attention. The first is the use of integral formulations of the governing equations of different reacting systems. The oldest and best known of these procedures is the Rankine-Hugoniot analysis. These well-known formulations are generally limited to 1-D systems, however, and it is a question to consider whether similar analysis of more complex geometries might not be rewarding. It has been successful, for example, in application to diffusion flames, and also to flame spread, leading in this latter case to the inverse fuel-density relation governing flame spread rate. The potential for other configurations needs to be explored.

Less well known is the Furnace and Engine Analysis procedure that provides an equation (of common form) for the Firing Curve for any furnace or engine. This provides an immediate and common integral analytical framework for engineering devices that also defines many of the first-level combustion problems that are found inside the devices. This is substantially developed. Wider use essentially needs only appropriate attention.

A third procedure that is now being pursued aggressively, that is mentioned here for note, is analysis by Deterministic Chaos. Current application to fluid beds and to i.c. engines shows the versatility of the approach. This procedure, in particular, is showing value jointly in practical engineering application and, at the scientific level, in improving precision of knowledge. To a degree, this is also an integral approach. Significantly, this is removing the past constraint of linearization of non-linear behavior that has disguised much real behavior of both practical and intrinsic interest.

A fourth procedure that beyond statement about a decade ago is not known to have been used, is the Species Stream Function (SSF). What this is potentially capable of doing, as shown in the original SSF paper by re-analysis of the classic Burke-Schuhmann diffusion flame, is to

determine the trajectories of the reacting molecules (and thus their temperature and, potentially, their reaction histories), and simultaneously determine the fuel flux density arriving at any location on the flame or reacting surface. Intuitively, this would seem to be relevant to analysis of turbulent flames.

At the strategic level, this concerns the possible axiomatization of combustion concepts, particularly incorporating and merging both combustion science and combustion engineering. One example is provided as already discussed by the new developments in Filtration Combustion where this can be seen as an organizing principle that merges propagating 1-D gas flames, either free or in porous bodies, and combustion in solid fuel beds. A second example is the potential of the Vulis PSR-sequence flame model combined with the Bragg Criterion. Similar critical examination of the reality of the other entries in the Thermally Assisted Flames category is also needed. All these approaches would seem to have a useful degree of organizing principle even though, as already noted, this still excludes the major areas of, for example, fires and flame spread. Further study is clearly needed.

Finally, this overall evaluation also provides a framework for answering the implied question of the sub-title. The 19th century developments were critical in first formulating the combustion problem and developing the initial concepts, mostly in phenomenological terms, but also initiating mechanistic descriptions. The first half of the present century mostly saw transformation of those concepts into mathematical formulations with a degree of intial testing. The second half has been more focused on developments of data bases and applications with, also, more detailed and sophisticated (largely computerized) analytical treatments. In spite of all these results, however, there is still no clear answer to the question: "What is a flame?" It would appear that to answer this question, new concepts or insights are required. It would seem reasonable to expect, in response to the pass-out question, that this will be the contribution of the 21st century.

Table 1: Flame Phenomena and Characteristics

1. Minimum ignition energy requirement: potential for bifurcation characteristics
2. Reaction zone: region of exothermic reaction
3. Bounded reaction zone: flame front division between non-reacting and reacting region
4. Propagation: translation of flame front into unburned mixture
5. Flame speed: fundamental property of the mixture composition
6. Flame stabilization: obtained when flame speed is matched by mixture speed.
7. Combustion limits: flame propagation fails below and above lower and upper limits
8. Flame Temperatures: limited at adiabatic
9. Visible radiation characteristics of reaction zone

Table 2: A Classification of Flames

Category I: Fundamental Flame Systems
Primary Property: Flame speed is a fundamental *independent* property of the fuel mixture
Secondary Property: Flame stabilizes when the mixture and burning velocity are matched
Primary Characteristic: Non-recirculating flow, nor thermal assist
Defined by: Rankine-Hugoniot equations
Interpreted by: Mallard and le Chatelier (MLC) model

Category II: Thermally-Assisted Flame Systems (*see also* Table 3)
Primary Property: Flame stabilization is possible in high speed flows
Secondary Property: Flame speed is a variable, *dependent* property of the combustion system
Primary Characteristic: Thermally assisted (backmix flow and *other*)
Defined and Interpreted by: 3-D conservation and kinetics equations

Category III: Miscellaneous
Surface flames (flame spread); fires, intermittent/batch combustion, ignition . . .

Table 3: Thermally-Assisted Flame Systems

Class I: External Heat Recovery by downstream heat exchanger(s):
Exs: Blast furnace; Open Hearth; glass tank; brick kiln; boiler . . .

Class II: Internal Heat Recovery

II.1 *Flow driven*: standard burners; non-swirling/swirling jets; FB's; etc; applications in standard [3-D] industrial furnaces and engines

II.2 *"Filtration" Porous Body Systems*

(1) Reacting porous body (solid fuel bed, sinter bed, blast furnace . . .)

(2) Reactive gas mixture in Porous Body

COMBUSTION CHARACTERISTICS OF HYDROGEN-PROPANE MIXTURES

A. Choudhuri and S.R.Gollahalli
School of Aerospace and Mechanical Engineering

R. Mallinson
School of Chemical Engineering

Institute of Gas Utilization Technology
University of Oklahoma, Norman, OK, 73019

Key words: Combustion, Hydrogen, Hydrocarbons, Mixed Fuels

ABSTRACT

An experimental study of the combustion and pollution characteristics of a diffusion flame of hydrogen-propane fuel mixtures is described. Flame appearance, visible length, radiative fraction of heat release, the emission indices of NO, NOx, and CO, and the inflame profiles of temperature and composition are presented. Results are compared for the flames of pure hydrogen, and the hydrogen-propane mixtures with 20% and 35% (volume) of propane.

INTRODUCTION

Because of their increased availability, relatively superior burning characteristics, and low pollutant emission potential, gaseous fuels such as compressed natural gas (CNG) and liquid petroleum gas (LPG) have recently received increased attention as potential fuels for transportation applications. A major problem that is hindering the wide-spread application of these fuels is their storage at a reasonable energy density. The Institute of Gas Utilization Technology (IGUT) at the University of Oklahoma is studying various methods, including dissolving natural gas in heavier hydrocarbons as a means of increasing the energy-density [1]. On another front, hydrogen has been advocated and studied for use in internal combustion engines [2]. The high reactivity and flame velocity of hydrogen offer additional benefits, particularly for the so-called lean-burning engines. Because of the highly nonlinear nature, the combustion characteristics of fuel mixtures cannot be predicted from those of the constituent fuels. Hence, a program to study the application of the fuel mixtures in laboratory flames, in engines on dynamometer test stands, and in actual automobile vehicles is in progress at the IGUT. This paper, one of a series of papers [3, 4] on mixed fuel characteristics, deals with the combustion of hydrogen-propane mixtures in a diffusion flame.

EXPERIMENTAL DETAILS

Experiments were conducted in a vertical steel combustion chamber of 76 cm × 76 cm cross section and 163 cm height. The chamber was fitted with rectangular windows of dimensions 20 cm × 20 cm ×145 cm on all of its four side walls. Three of the windows were fitted with Pyrex plate glass and the fourth was fitted with a slotted metal sheet for introducing probes. Air was induced by natural convection into the test chamber through a 20 cm diameter circular opening in the base plate. Three layers of fine-wire-mesh screens were used to provide a uniform flow. The circular fuel burner used in these experiments consisted of a stainless steel tube of 2 mm ID, which injected fuel into an atmosphere of air. The burner projected 14.5 cm above the chamber floor.

Propane and hydrogen were supplied from cylinders, through pressure regulators, rotameters, a mixing chamber, and in-line filters. The two fuels were mixed inside an annular mixing device in which secondary fuel was injected into the stream of primary fuel through a concentrically located injector. The length of the mixing device was sufficiently large (>150 hydraulic dia.) to ensure the homogenous mixture of fuels. For a fixed jet exit Reynolds number, the volume flow rate of the hybrid fuel was calculated for different mixture conditions. The volume flow rates of the primary and secondary fuels were then regulated with calibrated rotameters. The fuels used were of commercial grade with 98% purity.

The instrumentation included a computer-controlled-thermocouple based data acquisition system, a computer-aided precision two-dimensional positioning mechanism, various gas analyzers, a radiometer, a low-energy He-Ne laser for soot concentration, and a high speed camcorder (with strobe and back-illuminating option). For measuring exhaust emissions, a quartz flue gas collector was mounted over the visible flame, and axially aligned with the burner . A sample profile across the collector diameter showed a variation of less than 1.5% in species concentration, and hence, the center point data were treated as the average representative values. Gas samples were collected from combustion products through an uncooled-quartz probe of tip diameter 1 mm and treated to remove particulate and moisture with a series of filters and an ice-chilled moisture trap. The sampling flow rate was adjusted such that the suction and local free stream velocities in the flow-

field were close enough to ensure *quasi-isokinetic* sampling [5]. Chemiluminescence was used to measure the concentration of NO and NO_x. Two non-dispersive infrared (NDIR) analyzers were used to measure the concentration of CO and CO_2.

The species concentrations inside the flames were measured with another uncooled quartz probe. The inside diameter of this sampling probe was increased from 0.5 mm at the probe inlet to 6 mm over a short distance of 20 mm which allowed a sudden expansion of the gas sample, thus freezing its composition. The sample was analyzed using the same analyzers used in the exhaust emission measurements. Neglecting the gradient broadening effect and lack of quenching, the uncertainties in the species concentration measurements are estimated to be less than 9% of the mean value. Temperature profiles in the mixed fuel flame were measured with a Platinum-Platinum 13% Rhodium (Type R) in-house-made L-shaped thermocouple probe with the wire diameter 127μm and bead diameter 280 μm. To measure the temperature in 100% hydrogen flame, a Tungsten-5% Rhenium vs. Tungsten-26% Rhenium (Type C) thermocouple with wire diameter 127 μm and bead diameter 370 μm was used. Since this thermocouple rapidly deteriorates under oxidizing conditions, a coating of high temperature ceramic cement was used on all exposed parts of the thermocouple except the bead. The output was sampled at 1 kHz over a period of 20 seconds, and on-line averaged over 1 second using a computer-controlled high-speed data acquisition system hardware and a PC based data acquisition software. Flame radiation was measured with a wide-angle (150^0) highly sensitive pyrheliometer with absorptivity of 0.96.

The visible flame height was determined with a high-speed video camera. Strobe recording technique (1/6 second-interval progression, 1/2000 s.) along with back-light illuminating and DEIS (digital electronic image stabilization system) method were used to visualize the flame image in a dark background. A modified version of the technique proposed by Yagi and Iino [6] was used to measure the soot concentration. A He-Ne laser beam was passed through the flame and due to the presence of soot, the beam intensity was attenuated. The amount of attenuation was measured using a pyro-electric laser power meter placed on the other side of the beam. Table 1 shows the nominal experimental conditions and Table 2 shows the estimated uncertainties in measurements.

RESULTS AND DISCUSSION

Appearance and Flame Length

With the increase of propane concentration in the Hydrogen-Propane hybrid fuel, both flame luminosity and flame lengths increase [Fig. 1]. At Reynolds number =150, pure hydrogen produces a visible flame length of 30.5 mm which increases sharply as the propane concentration increases in the mixture. The Hydrogen-Propane fuel produces a visible flame which is approximately 10% taller than the corresponding Hydrogen-Natural gas flame [7]. The Hydrogen-Propane flames are much more luminous than the Hydrogen-Natural gas flame. Furthermore, the flame shapes are considerably different in both cases. At a Reynolds number = 150 and 80-20% mixture condition, in Hydrogen-Natural gas flame a dull yellow-orange zone appears from the mid-flame region to the far-burner region which is surrounded by a faint blue envelope, whereas in the Hydrogen-Propane flame, the whole far burner region is luminous yellow at that condition. This change in appearance is due to the increased soot formation in the Hydrogen-Propane flame. The chemical structure of propane is favorable to form PAH (polycyclic aromatic hydrocarbons) which is now believed to be the cause of soot inception. At Reynolds numbers of 1000, and 3000 the *soot wings* and the *soot breakthroughs* are more prominent than those in the Hydrogen-Natural gas flames. The trend of flame length increase with higher propane concentration in the fuel mixture is comparable to Roper's correlation [8].

Radiative Heat Loss Fraction

At the Reynolds Number of 150 the radiative heat loss fraction increases from 3.5% for 100% H_2 to 7.2% for 80-20% Hydrogen-Propane flame[Fig. 2]. After that, it does not change appreciably with the increase of propane concentration in the mixture. The increase of radiative heat loss factor is certainly due to the increased radiation from both molecular (CO_2) band and continuous sources (soot particles). However, the asymptotic behavior of flame radiation factor at concentrations more than 20% of propane in the mixture reveals that increased soot formation beyond a certain concentration increases self absorption of radiation between the soot particles [4]. At the Reynolds numbers of 1000 and 3000, this behavior is extremely significant. The flame radiation factor at these Reynolds numbers increases sharply below 20% propane concentration in the mixture. Beyond that concentration, although the flame radiation factor increases, it occurs at a slower rate than that at lower concentrations. At all Reynolds number and mixture conditions, Hydrogen-Propane flames have higher radiation factors than those of Hydrogen-Natural gas flames, as expected.

Emission Indices (EI)

Measurements of emission indices of NO, NO_x, and CO of Hydrogen-Propane flames at different Reynolds Number and mixture conditions are shown in Fig. 3. Only the results at a Reynolds

number =150 are shown here. The results at higher Reynolds numbers (1,000 and 3,000), which exhibit the same trends as those at Re =150 are available in Choudhuri's thesis [7].

NO Emission Index(EI_{NO}): With the increase of propane concentration in the mixture, at all Reynolds numbers, the NO emission index decreases sharply. At Reynolds number =150, the emission index of NO has a value of 0.8 g/kg at the baseline condition (95%-5% Hydrogen-Propane) which decreases to 0.45 g/kg at 80%-20% Hydrogen-Propane mixture. It continues to decrease and then attains a value of 0.28 g/kg for the 65%-35% Hydrogen-Propane mixture. It is notable that the Hydrogen-Propane flame has lower NO emission indices than those of the Hydrogen-Natural gas flame. As mentioned earlier in a high temperature diffusion flame the *Thermal-Zeldovich* mechanism is the primary route of NO formation. Since this mechanism is highly temperature dependent and the Hydrogen-Propane has lower effective flame temperature than the Hydrogen-Natural gas flame these results are expected.

NO_x Emission Index (EI_{NO_x}): The emission index of NO_x follows the same trend as the emission index of NO at all Reynolds numbers. It is also evident that a very small amount of NO_2 is formed in the Hydrogen-Propane hybrid fuel flame. This occurs because an increase of propane concentration in the mixture reduces the concentration of intermediate radicals, OH and O, which are essential to form NO_2. Furthermore, the increased propane concentration increases the radicals like CH and H which ultimately remove NO_2 from the flame. At a Reynolds number =150, the emission index of NO_x has a value of 0.9 g/kg at the baseline condition which decreases to 0.34 g/kg for the 65-35% Hydrogen-Propane mixture. This indicates that the emission index of NO_2 which has a value of 0.1 g/kg decreases up to 60% with the increase of 30% concentration of propane in the mixture.

Carbon monoxide Emission Index (EI_{co}): The carbon monoxide emission index increases with the increase of propane concentration in the mixture at all Reynolds numbers. This is expected, since adding more propane in the mixture means introducing more carbon atoms into the flames which results in an increase of CO. The carbon monoxide emission index (at Reynolds number =150) increases from a value of 0.3 g/kg at the baseline condition to a value of 0.9 g/kg for the 65%-35% Hydrogen-Propane mixture. However, for Hydrogen-Propane flames the carbon monoxide emission index has higher values compared to the Hydrogen-Natural gas flame. This is reasonable since propane has a higher carbon/hydrogen ratio than natural gas.

Volumetric Soot Concentration (w)

Volumetric soot concentrations measured at different axial locations and Reynolds numbers are shown in Fig. 4. Similar to the Hydrogen-NG flames, the Hydrogen-Propane flames have also high soot concentrations in the mid-flame region. As mentioned earlier, mid-flame region is the location of soot inception and growth. However, Hydrogen-Propane flames produce more soot than Hydrogen-Natural gas flame. Also, it is evident that soot formation increases sharply for the increase of propane concentration from 20% to 35%. This phenomenon is consistent with the earlier explanation given for the trend of the flame radiation factor. At a Reynolds number =150, 80%-20% Hydrogen flame has a peak soot concentration of 1×10^{-7} g/cc which jumps to 9.5×10^{-7}g/cc with the increase of 15% concentration in mixture. In fact, from the soot concentration point of view, 65-35% Hydrogen-Propane flame behaves almost like pure propane flames. This may be related to the complex soot inception and PAH formation in hydrocarbon flames.

Flame Structure

Temperature Profiles: Radial Temperature profiles at different axial locations for the different Hydrogen-Propane mixtures at a Reynolds number of 150 are presented in Fig. 5. In the near-burner region the dual hump nature of temperature profiles are prominent in all of the conditions. In the near-burner region, the peak temperature occurs at the flame sheet, and it is found to be 1980 K for the 80%-20% Hydrogen-Propane mixture and Reynolds number =150. The peak temperature in the near-burner region is in the range of 1980 K to 2000 K compared to 2250 K in the pure hydrogen flame. The addition of 20% propane in the hydrogen reduces the effective flame temperature by more than 250 K. The effective flame temperature drops again with the increase of an additional 15% propane concentration in the mixture. The 65%-35% Hydrogen-Propane mixture has approximately 100 K lower flame temperature than the 80%-20% Hydrogen-Propane mixture. Since close to the burner, soot concentration is not significant, the drop in the peak temperature in the Hydrogen-Propane flame with the increase of propane concentration in the mixture can be attributed to the banded radiation from molecular source (increased CO_2) and the lower energy input due to the higher propane concentration. Close to the mid-flame zone, both the 80%-20% and the 65%-35% Hydrogen-Propane flames show the dual hump temperature profile. Similar to the near-burner region, the temperature in the mid-flame also decreases with the increase of propane concentration in the mixture, again due to the increase of flame radiation and lower energy input. In the far-burner region, temperature profiles show a single peak close to the burner-axis. However, the peak effective flame temperature does not change appreciably with the increase of propane concentration for the mixture from 20% to 35% propane concentration. This is probably due to the higher amount of soot-oxidation which compensates radiation loss locally at higher propane concentrations in the mixture.

Concentration Profiles:

The full set of concentration profiles of CO_2, CO, NO, NO_x and O_2 are available in Choudhuri, 1997. As expected CO_2 concentration profiles were similar to the temperature profiles and oxygen concentration profiles follow the inverse trend of those of CO_2. Further NO and NOx profiles were similar. Hence, for brevity only CO and NOx profiles are shown here (Figs. 6 and 7).

Carbon monoxide(CO): Close to the burner, the CO concentration profiles show peaks in flame sheets for all three Reynolds number and mixture conditions of Hydrogen-Propane hybrid fuel. This reveals that close to the burner, reactions are mostly confined to the fuel-oxidizer interface. Further downstream, the CO concentration profiles show an axial peak which indicate that CO forming at the stochiometric contour at the flame edges start accumulating at the burner axis. At all conditions, in the far-burner region CO has lower concentration compared to mid-flame region. This is understandable since CO is rapidly oxidized between the mid-flame to far-burner region. As expected, Hydrogen-Propane flames have higher CO concentration compared to Hydrogen-Natural gas flames due to the higher carbon input rate.

Nitrogen Oxides (NO_x): As mentioned earlier, the Thermal-Zeldovich route is the dominant NO formation mechanism when flame temperatures are more than 1800 K. Since thermal NO is strongly temperature dependent, usually the NO temperature profiles follow the temperature profiles. Hydrogen-Propane flames for 80%-20% and 65%-35% mixtures have the peak flame temperature equal to/more than 1800 K. Hence, it can be expected that only thermal NO formation is active, and hence the concentration profiles follow the temperature profiles. Furthermore, Hydrogen-Propane flames have lower effective flame temperature which results in lower NO concentration than that of Hydrogen-Natural gas flames. The above mentioned trends are significant for all three Reynolds numbers and mixture conditions. Also, it is found that the Hydrogen-Propane mixture has a lower NO_2 concentration than that of hydrogen-natural gas flames. This is because, due to the high concentration of radicals CH, H, NO_2 removal rate is faster in hydrogen-propane flames compare to hydrogen-natural gas flames.

CONCLUSIONS

Flame luminosity and visible length of a diffusion flame of hydrogen-propane mixtures increase with the increase of propane concentration. The radiation fraction of heat release increases initially with the propane concentration and levels off above 30% (by volume). Soot production increases continuously with propane content of the fuel. The emission indices of NO and NOx decrease and the emission index of CO increases with the increase of propane fraction. The peak temperature in the flame decreases monotonically with the increase of propane content.

REFERENCES

1. Starling, K. E., Ding, E.R., Harwell, J.H., and Mallinson, R. G., "Method for Improving Natural Gas Energy Density at Ambient Temperature," *Energy and Fuels*, Vol. 9, 1995, pp. 1062-1065.

2. Shresta, S. O. B., and Karim, G. A., "Hydrogen as an Additive for Spark-Ignition Engine Applications," Proceedings of the 32nd Inter-Society Energy Conversion Engineering Conference, Honolulu, HI, July 1997, Vol. 4, pp. 910-915.

3. Choudhuri, A. R., and Gollahalli, S. R., "Structure of Laminar Jet Diffusion Flames of Fuel Gas Mixtures," International Joint Power Generation Conference & Exposition, Denver, CO, November 1997. Vol. FACT-1, pp. 309-318.

4. Choudhuri, A. R. and Gollahalli, S. R., "Comparison of the Structure of Diffusion Flames of the Mixtures of CNG with Hydrogen," AIAA Paper No. 98-0266, 1998

5. Fristrom, R. M., "Probe Measurement in Laminar combustion System. Workshop on Combustion," Measurements in Jet Propulsion Systems-1975, Purdue University, 1975 pp. 318-324.

6. Yagi, S. and Iino, H., "Radiation From Soot Particles in Luminous Flames," *Eighth Symposium (International) on Combustion*. The Combustion Institute. Pittsburgh, PA. 1960, pp. 288-293.

7 Choudhuri, A., R., "Experimental Studies on Hybrid Fuel Combustion,". M. S. Thesis, University of Oklahoma, Norman, OK, 1997.

8 Roper, F. G., The Prediction of Laminar Jet Diffusion Flame Sizes: Part I. Theoretical Model," *Combustion and Flame.*, Vol. 29. (1977). pp. 219-226.

Table 1. Nominal Experimental Conditions

Fuel:	Propane (94%+ methane) (0-35% vol.)
	Hydrogen (98%+) (100-65% vol.)
Jet diameter:	2 mm
Jet exit velocity	2.5-157.7 m/s
Jet exit Reynolds number	150-3000
Jet exit Froude number	420-1.2x10^6
Ambient Temperature	295 K
Ambient Pressure	104 kPa

Table 2. *Estimated Uncertainties*[*]

Measurements	% of Mean Value
Flame Height	15
Emission Index	1.7
Radiative Heat Loss	2
Concentration of NO	7.9
Concentration of NO_x	8.2
Concentration of CO_2	8.6
Concentration of CO	8.8
Concentration of O_2	4
Temperature	1.4
Soot Concentration	6.4

[*] Based on Student's t-test at 95% confidence

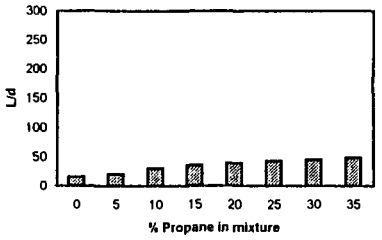

Fig 1: Effect of Propane Concentration (vol.%) on Flame Length (Re=150)

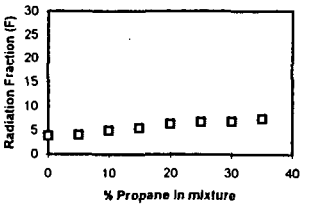

Fig. 2: Effect of Propane Concentration (vol.%) on Radiative Fraction (Re=150)

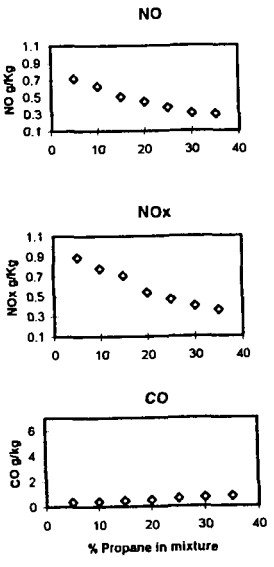

Fig. 3 Effect of Propane Concentration (vol.%) on Emission Indices (Re=150)

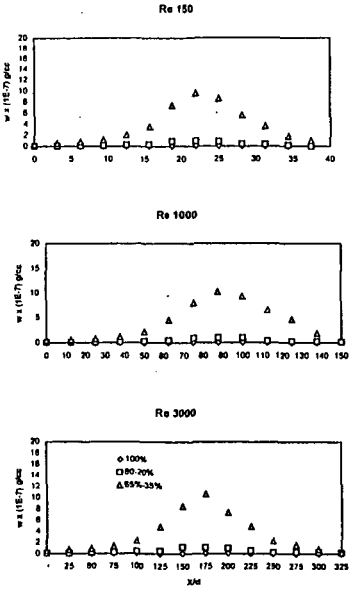

Fig. 4: Effect of Propane Concentration (vol.%) on Volumetric Soot Concentration

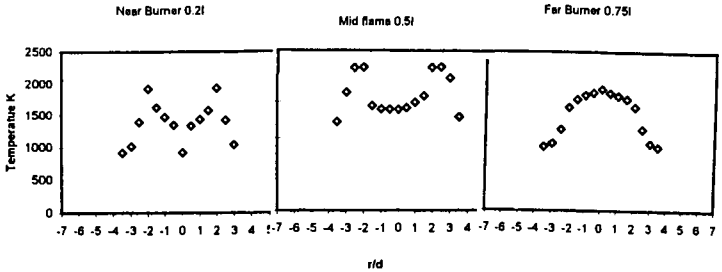

Fig. 5: Temperature Profiles in the Near-Burner (x/L=0.33), Mid-flame (x/L=0.5) and Far burner (x/L=0.67) Regions of the Flames (Re=150)

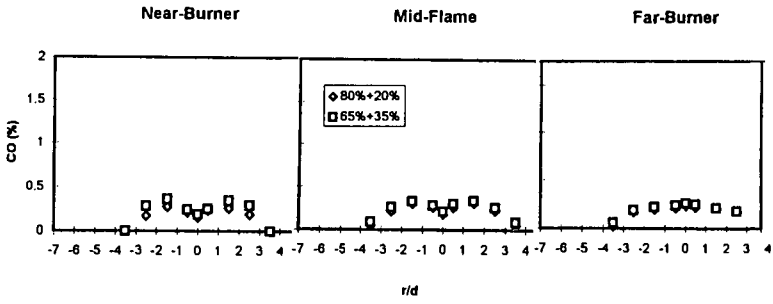

Fig. 6: Concentration Profiles of CO in the Near-Burner (x/L=0.33), Mid-flame (x/L=0.5) and Far burner (x/L=0.67) Regions of the Flames (Re=150)

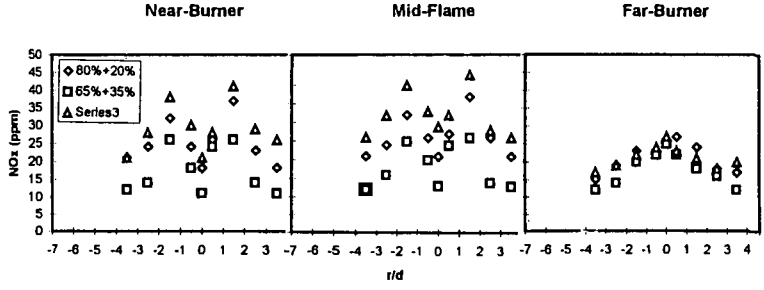

Fig. 7: Concentration Profiles of NOx in the Near-Burner (x/L=0.33), Mid-flame (x/L=0.5) and Far burner (x/L=0.67) Regions of the Flames (Re=150)

KINETIC MODELING OF GAS-PHASE AROMATICS OXIDATION AND GROWTH

Hai Wang

Department of Mechanical Engineering
University of Delaware
Newark, Delaware 19716

INTRODUCTION

The kinetics of aromatics oxidation and growth are studied using ab initio quantum chemistry methods, RRKM calculations, and detailed kinetic modeling. This work is motivated by both fundamental and practical considerations. While significant advance has been made in the understanding of the oxidation kinetics for aliphatic hydrocarbon combustion, comparatively fewer studies have been conducted on aromatics.[1,2] Such a disparity in emphasis is expected because of the significantly more complex nature of the aromatic kinetics. It is also obvious that since most practical fuel blends consist of large amounts of aromatics, satisfactory modeling and manipulation of the combustion processes would not be possible without a quantitative description of their oxidation kinetics. Such a concern is further substantiated by recognizing the role of aromatics kinetics in engine knock,[3] in soot production,[4-12] in the emission of polycyclic aromatic carcinogens,[13] in fullerene synthesis,[14] and in fuel-cell technology.[15,16]

Previously, a detailed kinetic model of benzene and toluene oxidation has been proposed by Emdee, Brezinsky, and Glassman,[2] on the basis of flow-reactor experiments at the temperatures between 1100 to 1200 K and at atmospheric pressure. Benzene oxidation at high temperatures was further examined through detailed kinetic modeling. Several kinetic models have been proposed and tested against experimental data, including the species profiles in the burner-stabilized low-pressure benzene flame[17–19] of Bittner and Howard,[20] and the laminar flame speeds of benzene-air and toluene-air mixtures.[19,21,22] It was shown that the proposed models predicted reasonably well each individual set of the experimental data, but a comprehensive and physically justifiable model, which is capable of closely predicting *all* the available experimental data, is still lacking.

The aim of this work is to develop a comprehensive kinetic model of aromatics oxidation and mass growth in combustion. In this article, we report a preliminary kinetic model, which describes the high-temperature oxidation of benzene and toluene. Numerical results are present and compared to experimental data from previous flow reactor,[2] flame[20,21] and shock-tube studies.[23]

METHODOLOGIES

Quantum Chemical Calculations

We employed Pople's G2 method[24] and its simplified versions[25-29] for the calculations of the thermochemical data, including enthalpy of formation, entropy and heat capacity for the relevant molecular and radical species, and the potential energy surface of chemical reactions. Isodesmic reactions[30] are used to determine the enthalpy of formation. The transition-state structures are initially optimized with the spin-unrestricted Hartree-Fock (UHF) method, employing the split-valence 3-21G basis set. The structures were further optimized at the HF/6-31G(*d*) level and refined at the UMP2(full)/6-31G(d) level. In all calculations, we employed the analytical gradient procedure and the combined Synchronous Transit and Quasi-Newton (STQN) method.[31] The vibrational frequencies were obtained from the geometries optimized at the UMP2(full)/6-31G(d) level of theory.

Rate Coefficient Calculations

Many elementary reactions of aromatics are chemically activated, involving the stabilization and isomerization of the hot adduct. The rate coefficients of these reactions are not known and are determined in the present study using the RRKM method.[32,33] The RRKM parameters, including the vibrational frequencies and rotational constants of the reactants and transition states, are obtained from the quantum chemical calculations. Details of the RRKM computer code are documented elsewhere.[34]

Detailed Kinetic Modeling

A detailed kinetic model of benzene and toluene oxidation at high-temperature is compiled. The model consists of 65 species and 340 elementary reactions. The reaction kinetics of C_1 and C_2 species are based on the GRI-Mech (version 1.2).[35] For large species, the reaction pathways and rate coefficients are obtained from literature data (e.g., ref 36). Many rate parameters are analyzed using the RRKM methods in our previous studies,[37,38] as well as in the present work.

Calculations of the laminar flames are carried out using the Sandia Chemkin-II[39] and Premix[40] codes. The reverse rate coefficients are computed via equilibrium constants. While the thermochemical data of cyclopentadiene and cyclopentadiene

derivatives are obtained through quantum chemical calculations, others are taken from ref 35, and from the compilation of Burcat and McBride.[41] .

RESULTS

The first step during the oxidation of the aromatics is the disintegration of the aromatic ring structure. This is followed by the oxidation of the resulting products to CO and finally to CO_2. Previous studies[2,21] show that the initial oxidation of benzene leads primarily to phenol and phenoxyl, followed by the formation of cyclopentadiene and the cyclopentadienyl radical. The disintegration of the cyclic structure occurs at the stage when the C_5 species are oxidized. It was found that the oxidation of the C_5 species is often the bottle neck during benzene oxidation. Here, we examined the reaction pathway and analyzed reaction rate coefficient for one of these bottleneck reactions, i.e., the thermal decomposition of cyclopentadienone

$$c\text{-}C_5H_4O \rightarrow \text{products} .$$

Figure 1 presents the energy diagram of the above reaction. The rate coefficients computed using the RRKM are shown in the inset. It is seen that unlike the previously proposed pathway, the minimum energy path leads to cyclobutadiene, which may subsequently isomerize to vinylacetylene, or it may dissociate to acetylene.

Figure 2 presents the comparison of the experimental[2] and computed concentration profiles of selected species during benzene oxidation in a flow reactor at 1100 K and with the equivalence ratio equal to 0.67. It is seen that the present kinetic model predicts very well the concentrations of benzene, CO, acetylene, and cyclopentadiene. The model tends to underpredict the concentration of phenol. Figure 3 presents the comparison of species profiles during toluene oxidation at 1190 K and with the equivalence ratio equal to 1.33. Again, the major species profiles, including toluene, CO, benzene, phenol, benzaldehyde, methane, and acetylene are predicted well.

Figure 4 shows the comparison of the experimental[21] and computed laminar flame speeds of benzene- and toluene-air mixtures at atmospheric pressure. It is seen that the kinetic model predicts slightly larger flame speeds than the experimental data for benzene. However, the variation of the flame speed on the equivalence ratio is nicely predicted.

The experimental and computed major and minor species profiles are presented in Figure 5 for a burner-stabilized benzene-oxygen-argon flame at 20 torr.[20] It is seen that the model predicts very well the variation of the major species profile as a function of distance from the burner. The model also predicts well the shape and magnitude of such minor species as the H atom and the OH radical.

In Figure 6, we plot the experimental[23] and computed ignition delay time of a benzene-oxygen-argon mixture at a pressure of 2.5 atm. The present kinetic model appears to overpredict the data slightly, but the variation of the ignition delay on temperature is well reproduced.

DISCUSSION

We have shown that a detailed kinetic model of benzene oxidation can account for the main features of benzene and toluene oxidation under a variety of combustion conditions. Recognizing, however, that many practical combustion devices operate at elevated pressures, it is essential to extend the predictive capability of the model to high pressures as well. Because of the variation of the reaction pathways and rate coefficients as a function of pressure, low-pressure models usually fail when they are used for prediction at high pressures. The inherent reason is that many reactions involving the aromatic species are chemically activated, involving the competition of collisional stabilization and dissociation/isomerization of the hot adduct. For example, the reaction between the cyclopentadienyl and the OH radical initially leads to a vibrationally excited cyclopentadienol, which may be stabilized by collision with other molecules, or it may dissociate to the singlet cyclopentadienylidene + H_2O or c-C_5H_4OH + H. Unlike the reaction pathways at low pressures, the stabilization process becomes favorable at elevated pressures. The change in the reaction product often means a change in the overall fuel destruction routes.

While it is often difficult to obtain reliable fundamental combustion data at elevated pressures, reliable extrapolation of the reaction rate coefficients is now possible with the recent advances in quantum mechanical methods and reaction rate theories. These methods can be and should be used for the further refinement and extrapolation of the base model developed in the present study.

CONCLUSION

A detailed kinetic model of benzene and toluene oxidation is developed. It is shown that the kinetic model predicts reasonably well the available experimental data of benzene and toluene oxidation in flow reactors, flames, and shock tubes.

Acknowledgment The work utilized the computer system Power Challenge Array at the National Center for Supercomputing Applications, University of Illinois at Urbana-Champaign.

REFERENCES

(1) Brezinsky, K. *Prog. Energy Combust. Sci.* **1986**, *3*, 1.
(2) Emdee, J. L.; Brezinsky, K.; Glassman, I. *J. Phys. Chem.* **1992**, *96*, 2151.
(3) Sawyer, R. F. *Twenty-Fourth Symposium (International) on Combustion*; The Combustion Institute: Pittsburgh, 1992, pp. 1423-1432.
(4) Haynes, B. S.; Wagner, H. Gg. *Prog. Energy Combust. Sci.* **1980**, *7*, 229.
(5) Calcote, H. F. *Combust. Flame* **1981**, *42*, 215.
(6) Homann, K. H. *Twentieth Symposium (International) on Combustion*; The Combustion Institute: Pittsburgh, 1984, pp. 857-870.
(7) Bittner, J. D.; Howard, J. B. in *Soot in Combustion Systems and its Toxic Properties*; Lahaye, J.; Prado, G. Eds.; Plenum: New York, 1983.
(8) Bockhorn, H.; Fetting, F.; Wenz, H. W. *Ber Bunsenges. Phys. Chem.* **1983**, *87*, 1067.
(9) Frenklach, M.; Warnatz, J. *Combust. Sci. Technol.* **1987**, *5*, 265.
(10) Frenklach, M.; Wang, H. *Twenty-Third Symposium (International) on Combustion*; The Combustion Institute: Pittsburgh, 1991, pp. 1559-1566.
(11) Howard, J. B. *Twenty-Third Symposium (International) on Combustion*; The Combustion Institute: Pittsburgh, 1991, p. 1107.
(12) McKinnon, J. T.; Howard, J. B. *Twenty-Fourth Symposium (International) on Combustion*; The Combustion Institute: Pittsburgh, 1992, pp. 965-971.
(13) Longwell, J. P. *Nineteenth Symposium (International) on Combustion*, The Combustion Institute, Pittsburgh, 1982, pp. 1339-1350.
(14) Howard, J. B., *Twenty-Fourth Symposium (International) on Combustion*; The Combustion Institute: Pittsburgh, 1992, pp. 933-946.
(15) Otsuka, K.; Yamanaka, I.; Hosokawa, K. *Nature*, **1990**, 697.
(16) Otsuka, K.; Furuya, K. *Electrochim. Acta* **1992**, *37*, 1135.
(17) Lindstedt, R. P.; Skevis, G., *Combust Flame* **1994**, *99*, 551.
(18) Zhang, H.-Y.; McKinnon, J. T. *Combust. Sci. Technol.* **1995**, *107*, 261.
(19) Tan, Y. W.; Frank, P. *Twenty-Sixth Symposium (International) on Combustion*; The Combustion Institute: Pittsburgh, in press.
(20) Bittner, J. D.; Howard, J. B. *Eighteenth Symposium (International) on Combustion*; The Combustion Institute: Pittsburgh, 1980, p. 1105.
(21) Davis, S. G.; Wang, H.; Brezinsky, I.; Law, C. K. *Twenty-Sixth Symposium (International) on Combustion*; The Combustion Institute: Pittsburgh, in press.
(22) Lindstedt, R. P.; Maurice, L. Q. *Combust. Sci. Technol.* **1996**, *120*, 119.
(23) Burcat, A.; Snyder, C.; Brabbs, T., NASA Technical Memorandum 87312, 1986.
(24) Curtiss, L. A.; Raghavachari, K.; Trucks, G. W.; Pople, J. A. *J. Chem Phys.* **1991**, *94*, 7221.
(25) Curtiss, L. A.; Raghavachari, K.; Pople, J. A. *J. Chem Phys.* **1993**, *98*, 1293.
(26) Smith, B. J.; Radom, L. *J. Phys. Chem.* **1995**, *99*, 6468.
(27) Mebel, A. M.; Morokuma; Lin, M. C. *J. Chem. Phys.* **1995**, *103*, 7414.
(28) Bauschlicher, C. W., Jr.; Partridge, H. *J. Chem. Phys.* **1995**, *103*, 1788.
(29) Wang, H; Brezinsky, K. *J. Phys. Chem.* in press.
(30) Hehre, W. J.; Ditchfield, R.; Radom, L.; Pople, J. A. *J. Am. Chem. Soc.* **1970**, *92*, 4796.
(31) Peng, C.; Schlegal, H. B. *Isr. J. Chem.* **1993**, *33*, 449.
(32) Robinson, P. J.; Holbrook, K. A. *Unimolecular Reactions*; Wiley: New York, 1972.
(33) Gilbert, R. G.; Smith, S. C. *Theory of Unimolecular and Recombination Reactions*; Blackwell Scientific: Oxford, 1990.
(34) Wang, H.; Frenklach, M. *J. Phys. Chem.* **1994**, *98*, 11465.
(35) Frenklach, M.; Wang, H.; Goldenberg, M.; Smith, G. P.; Golden, D. M.; Bowman, C. T.; Hanson, R. K.; Gardiner, W. C.; Lissianski, V. *GRI-Mech–An Optimized Detailed Chemical Reaction Mechanism for Methane Combustion*; GRI Technical Report No. GRI-95/0058, November 1, 1995.
(36) Baulch, D. L.; Cobos, C. J.; Cox, R. A.; Frank, P.; Hayman, G.; Just, TH.; Kerr, J. A.; Murrells, T.; Pilling, M. J.; Troe, J.; Walker, R. W.; Warnatz, J. *Combust. Flame*, **1994**, *98*, 59.
(37) Wang, H.; Frenklach, M., *J. Phys. Chem.* **1994**, *98*, 11465.
(38) Wang, H.; Frenklach, M., *Combust. Flame* **1997**, *110*, 173.
(39) Kee, R.J.; Rupley, F.M.; Miller, J.A., Sandia Report SAND 89-8009B; Sandia National Laboratories: Albuquerque, New Mexico, 1989.
(40) Kee, R. J.; Grcar, J. F.; Smooke, M. D.; Miller, J. A., Sandia Report SAND85-8240 UC4; Sandia National Laboratories: Albuquerque, New Mexico, 1985.
(41) Burcat, A.; McBride, B. *1997 Ideal Gas Thermodynamic Data for Combustion and Air-Pollution Use*; Technion Aerospace Engineering (TAE) Report # 804, 1997.

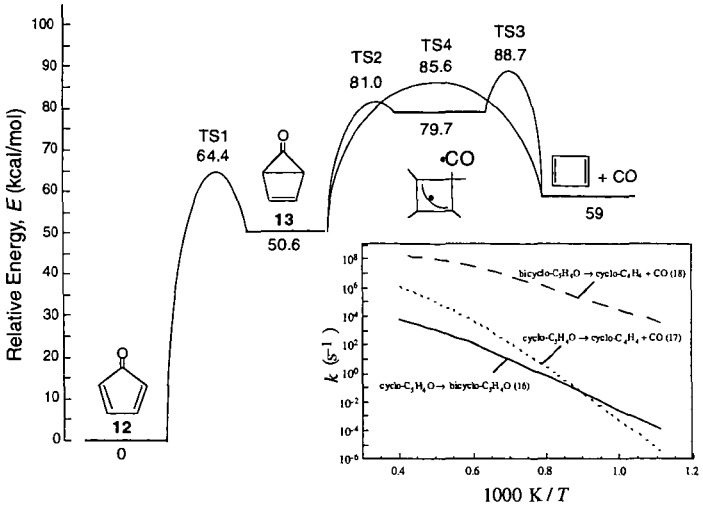

Figure 1. Energy diagram and the rate coefficients (p = 1 atm) computed for the thermal decomposition of cyclopentadienone.

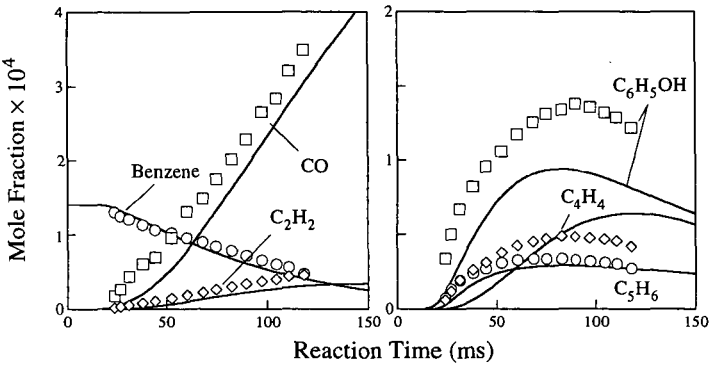

Figure 2. Experimental[2] and computed species profiles for benzene oxidation (0.14% C_6H_6-1.62% O_2-N_2, the equivalence ratio $\phi = 0.67$) in a flow reactor at 1100 K and 1 atm pressure.

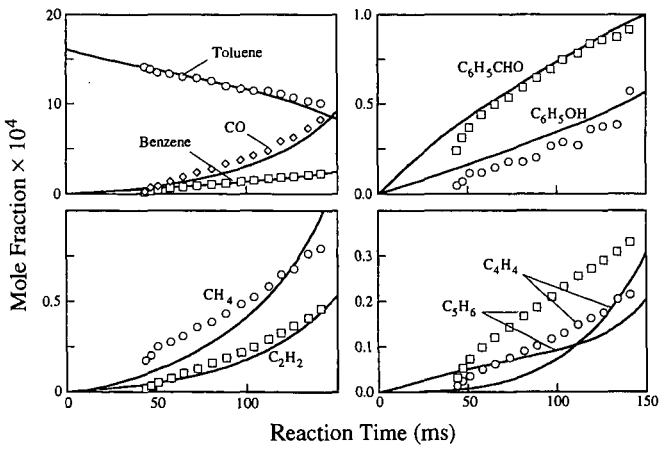

Figure 3. Experimental[2] and computed species profiles for toluene oxidation (0.162% C_7H_8-1.094% O_2-N_2, the equivalence ratio $\phi = 1.33$) in a flow reactor at 1190 K and 1 atm pressure.

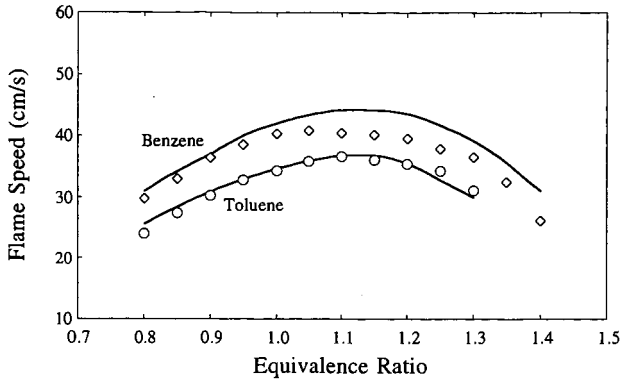

Figure 4. Experimental[21] and computed laminar flame speed of benzene- and toluene-air mixture at 1 atm pressure.

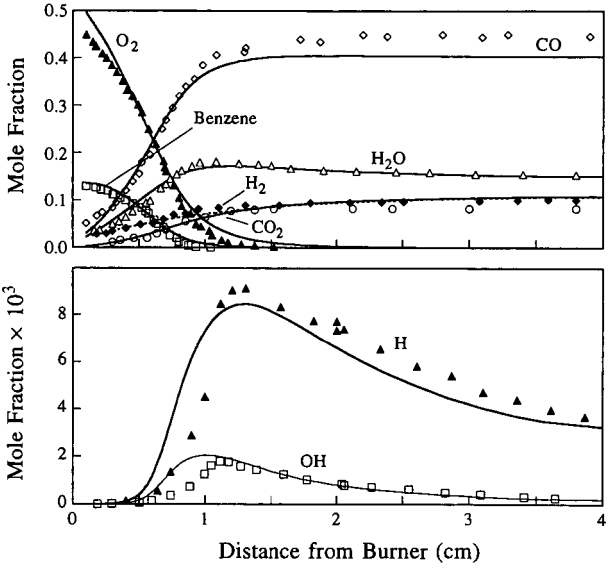

Figure 5. Experimental[20] and computed species profiles in a burner-stabilized laminar premixed flame, burning a 13.5% benzene-56.5 % O_2-Ar mixture at 20-torr pressure.

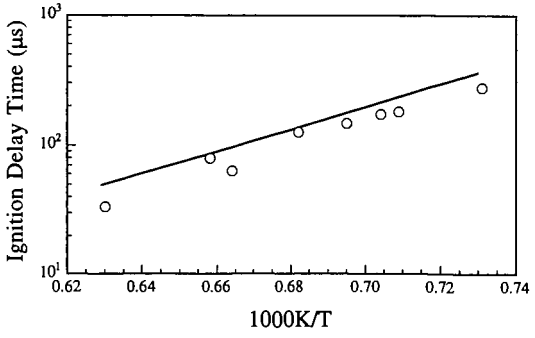

Figure 6. Experimental[23] and computed ignition delay time for a 1.69% benzene-12.675% O_2-Ar mixture at p_5 = ~2.5 atm.

SPECTRALLY AND TEMPORALLY RESOLVED LASER INDUCED FLUORESCENCE (LIF) PROVIDES INSIGHT INTO THE MECHANISM OF FLAME RETARDATION

Brian M. Cullum, Pramod K. Khulbe, Brian J. Marquardt
and S. Michael Angel*

Department of Chemistry and Biochemistry
University of South Carolina
Columbia, South Carolina 29208
Phone (803) 777-2779
Fax (803) 777-9521
E-mail : Angel@psc.sc.edu
**-Author to whom correspondence should be sent*

KEYWORDS: laser induced fluorescence, brominated flame retardants, and time resolved

ABSTRACT

Presently two major theories exist on how flame retardants work.[1,2] Temporally resolved LIF has been used to determine the extent to which the chemical kinetic theory of flame retardation applies to the effect of brominated flame retardants, such as decabromodiphenyl oxide (DECA) and hexabromocyclododecane (HBCD), on flame retardation. We have shown that the primary effect of these brominated flame retardants is chemical in nature as opposed to physical, lending credence to the radical trap theory of flame retardation.

INTRODUCTION

In the present work, we are measuring the effect of two brominated flame retardants (HBCD and DECA) on the concentration of OH radicals in a methane/air flame. This is done by monitoring both the laser induced fluorescence (LIF) intensity and the fluorescence lifetime of the $^{\bullet}$OH. In these experiments, we monitor the $^{\bullet}$OH fluorescence intensity and lifetime while aspirating various concentrations of the flame retardants dissolved in toluene into the flame. Monitoring the lifetime of the radical species provides insight into the flame inhibition process because $^{\bullet}$OH is a key species in the propagation of combustion in a flame. If the primary method of inhibition was based on the heat capacity of the brominated species, removing heat from the reaction, then the rate of molecular collisions and temperature in the flame would be reduced. This in turn would cause the fluorescence lifetime of the flame species, including $^{\bullet}$OH, to increase. However, if the primary mechanism of action of these brominated flame retardants is based on the radical trap theory, then the $^{\bullet}$OH radical, and other radical flame species that can be dynamically quenched, would show a reduction in lifetime proportional to the amount of bromine introduced into the flame. In this study we provide evidence that suggests that this is the case. From instantaneous intensity measurements, it can be shown that the concentration of ground state $^{\bullet}$OH is depleted upon addition of brominated flame retardants. In addition $^{\bullet}$OH lifetime measurements show that the $^{\bullet}$OH excited state is also being quenched upon addition of brominated flame retardants, suggesting that the reactivity of the excited state and ground state are similar and that the mechanism of quenching of the ground state is chemical.

EXPERIMENTAL

LIF setup

In these experiments, a frequency doubled fundamental of a Q-switched Nd:YAG laser (Quantel International Model 580-20) was used to pump a frequency doubled dye laser (Continuum Model Nd6000) using Rhodamine 6G and emitting approximately 3.5 mJ/10 ns pulse at 281.10 nm. The laser wavelength was tuned to the $A^2\Sigma^+ \rightarrow X^2\Pi$ transition of $^{\bullet}$OH. The laser beam was focused to a point on the front edge of a six inch slot burner using an f/8 plano convex lens. This supplied sufficient laser power to saturate the $^{\bullet}$OH radical in the flame. $^{\bullet}$OH fluorescence was collected by an f/4 lens and focused onto the slit of a 0.85 meter double monochromator (SPEX model 1404), with 0.012 nm resolution, to resolve the 314.58 nm emission. The fluorescence signal was monitored using a photomultiplier tube (Hammamatsu

Model R2949) that was 50 Ω - coupled to a 500 MHz digital sampling oscilloscope (Lecroy Model 9350L).

In addition to the setup described above, the temperature of the flame was monitored using thermally assisted laser induced fluorescence (TALIF) of $^{\bullet}$OH. This required the laser dye to be changed to *Rhodamine 101* and a wavelength of *306.80 nm* to be produced. This exitation scheme promotes electrons from the ground vibrational level of the $X^2\Pi$ state to the ground vibrational level of $A^2\Sigma^+$ state.

RESULTS AND DISCUSSION

$^{\bullet}$OH Concentration

By monitoring the change in intensity of the LIF signal at various concentrations of flame retardant it can be seen that increased flame retardant concentrations have a dramatic effect on the $^{\bullet}$OH radical concentration. This is in good agreement with results reported previously by several authors.[1-5] The decrease in LIF shows that the flame retardant is removing $^{\bullet}$OH radicals from the flame. The results show that PVC/HBCD mixtures cause a dramatic reduction in LIF signal with even small amounts of HBCD added. This is in agreement with the theory that one of the primary modes of flame retardation is by removing the highly energetic species of $^{\bullet}$OH, by either preventing formation of the $^{\bullet}$OH or by removing it from subsequent propagation steps. In addition, increased concentrations of DECA with and without 4% Sb_2O_3, were aspirated into the burner to determine their relativc affect on $^{\bullet}$OH in the flame. The first observation of this shows that the HIPS/DECA mixtures without Sb_2O_3 show little or no change in the relative amount of $^{\bullet}$OH present. Although not well not understood, it has been observed that DECA requires the addition of Sb_2O_3 as a synergist before it has any noticeable flame retardant properties.[6] In addition to this it can be seen that the relative amount of $^{\bullet}$OH present in the flame is very sensitive to the concentration of DECA added, with 4% Sb_2O_3, and begins to level off at approximately 7-8% (w/w) bromine. This corresponds to the 3:1 stoichiometric ratio of Br to Sb, which has been found to be optimal for this compound.[6] At any point beyond this ratio Sb becomes the limiting reagent in the system, and removal of $^{\bullet}$OH is expected to level off as observed.

$^{\bullet}$OH Lifetimes

Time resolved LIF of $^{\bullet}$OH in the flame front of an atmospheric premixed methane/air flame has been reported to range between several hundred picoseconds up to 8 ns depending on the flame conditions that are used as well as the region of the flame that is probed.[7-19] If reduction of $^{\bullet}$OH concentration in the flame occurs by collisional quenching of the excited state, or dynamic quenching, a reduction in the fluorescence lifetime would occur. However, if the physical model were to be the primary mechanism of inhibition then the temperature of the flame would decrease causing fewer collisions, thereby increasing the lifetime of the $^{\bullet}$OH.

All fluorescence lifetimes are relative to the lifetime of $^{\bullet}$OH with the polymer dissolved in toluene and aspirated into the flame. From this work it is evident that the lifetime of $^{\bullet}$OH significantly decreases upon addition of HBCD, approximately 40% of the original lifetime. This provides evidence to support the idea of dynamic quenching of $^{\bullet}$OH, or the radical trap theory. While it does not prove that $^{\bullet}$Br is the species in the flame responsible for this trapping, it is strong evidence that $^{\bullet}$OH is being actively removed from the system by collisional reactions with some species produced from HBCD. The change in lifetime begins to level off at higher flame retardant concentrations, probably an artifact caused by the 2.0 ± 0.1 ns resolution of the LIF system. In the case of HBCD, the lifetime should continue to decrease up to the point that the probabilty between the two molecules colliding is virtually zero.

To determine whether this radical trap theory is the primary source of inhibition for the combination of DECA with HIPS, the same experiment was performed. Interestingly, when the relative change in $^{\bullet}$OH lifetime is plotted for the mixture of HIPS with various concentrations of DECA, there is no significant change. However, when those same concentrations of DECA in HIPS are blended with 4% Sb_2O_3 and aspirated into the burner, a dramatic decrease in the $^{\bullet}$OH lifetime was observed. At the maximum DECA concentration this lifetime decreases to approximately 55% of the lifetime without flame retardant and synergist. This leads to the idea that the mixture of DECA, HIPS and 4% Sb_2O_3 also generates radical traps as did the

HBCD/PVC combination. In addition, it shows that without the synergist this collisional inhibition does not occur. This suggests that the Sb_2O_3 is responsible for the dynamic quenching or is necessary for creating species such as $SbBr_3$ that may be responsible.[6]

In an attempt to try to model the data from these flame retardants, structurally similar compounds for HBCD and DECA were chosen. These compounds were cyclohexyl bromide and bromobenzene respectively. Each of these compounds were diluted in toluene to concentrations covering the same range as the flame retardants concentrations used. These compounds show an unexpected trend in the $^{\bullet}OH$ lifetime. In both cases, the lifetimes increased slightly. In the case of cyclohexyl bromide, the highest concentration yielded a lifetime approximately 116% of the toluene/PVC solution aspirated into the flame. While for bromobenzene this increase in lifetime was approximately 112% of the toluene/HIPS blank. These results lead to the conclusion that these compounds do not dynamically quench $^{\bullet}OH$ in the flame. However, the relative $^{\bullet}OH$ concentration in the flame does decrease slightly with increasing concentrations of the brominated species. Therefore it would seem that there is a reduction in the combustion due to the presence of these compounds. However, it appears to be physical in nature. Following the heat capacity theory of Larsen one would expect the lifetime of the $^{\bullet}OH$ to increase in this case.[2] The addition of heat absorbing species into the flame reduces the temperature and thus the $^{\bullet}OH$ concentration. In addition, by removing heat, or energy, from the flame, there will be fewer collisions and the lifetime of flame species such as $^{\bullet}OH$ is expected to increase slightly.

Temperature Measurements

Flame temperature measurements were made on the flame itself; with polymer added; with polymer and 30% flame retardant; and with polymer, and 30% flame retardant with 4% synergist added. The temperature of the methane/air flame with no added sample was determined to be 1962 K with a standard deviation of 6 K (based on five replicate measurements). The temperature decreased to aproximately 1610 K when the polymer alone was aspirated into the flame. This is because the flame was fuel rich to begin with and the addition of toluene as the polymer solvent increased the amount of fuel in the flame without increasing the oxidizer. There was no further change in the flame temperature upon addition of the flame retardants. This lends credence to the thought that the primary mechanism of action of these flame retardants is not physical, or the temperature would have decreased with the addition of flame retardant and synergist.

CONCLUSIONS

In the work presented here, we show that the addition of the halogenated flame retardants, HBCD and DECA with 4% Sb_2O_3, to a methane/air flame reduces the amount of $^{\bullet}OH$ present thereby inhibiting combustion. More importantly however, is the fact that the chemical kinetic theory of flame retardation by halogenated flame retardants is supported by time resolved LIF. While the physical theory proposed by Larsen[2], is shown not to be the primary source of inhibition. The results using the compounds cyclohexyl bromide and bromobenzene which were chosen to model HBCD and DECA respectively seem to support the fact that there is a physical flame suppression component, while the overall decrease in $^{\bullet}OH$ lifetime for the flame retardants shows that the primary inhibition comes from a chemical quenching mechanism. In addition, this technique appears to be a good means of quantitating the efficiency various brominated flame retardants, and possibly non-brominated flame retardants.

ACKNOWLEDGMENTS

We would like to gratefully acknowledge Dr. Rich Lyon of the Federal Aviation Administration (FAA) for support of this work under, grant # 95-G-030. Also, we would like to thank Albemarle Corp. for samples of the flame retardants that were used in this work, and for helpful conversations with Dr. Sam Thomas and Dr. Govind Kumar.

REFERENCES

1. Butlin, R. N., and Simmons, R. F., *Combust. Flame* 12:447 (1968).
2. Larsen, E. R., *JFF / Fire Retardant Chemistry* 2:5 (1975).
3. Coward, H. F., and Hartwell, F. J., *J. Chem. Soc.* 1522 (1926).
4. Coward, H. F., and Gleadll, J. J., *J. Chem. Soc.* 243 (1930).
5. Coward, H. F., and Jones, G. W., *Bull. Bur. Mines* 503 (1965).
6. Pettigrew, A. *Encyclopedia of Chemical Technology*. Kirk - Othmer, New York, NY, 1993; p. 954.
7. Köllner, M., and Monkhouse P., *Appl. Phys. B* 61:499 (1995).
8. Schwarzwald, R., Monkhouse, P., and Wolfram, J., *Chem. Phys. Lett.* 158:65 (1989).

9. Alfano, A., *Appl. Opt.* 28:5010 (1989).
10. Kohse-Höinghaus, K., Jefferies, J. B., Copeland, R. A., Smith, G. P., and Crosley, D. R., *Twenty-Second Symposium (International) on Combustion*, The Combustion Institute, Pittsburgh, 1986, p. 857.
11. Stepowski, D., and Cottereau, M. J., *Combust. Flame* 40:65 (1981).
12. Cattolica, R. J., and Mataga, T. G., *Chem. Phys. Lett.* 182:623 (1991).
13. Heard, D. E., Jeffries, J. B., and Crosley, D. R. *Chem Phys. Lett.* 178:533 (1991).
14. Fiechtner, G. J., King, G. B., Laurendeau, N. M., and Lytle, F. E. *Appl. Opt.* 31:2849 (1992).
15. Garland, N. L., and Crosley, D. R. *Twenty-Second Symposium (International) on Combustion*, The Combustion Institute, Pittsburgh, 1986, p.1693.
16. Smith, G.P., and Crosley, D. R. *J. Chem. Phys.* 85:3896 (1986).
17. Fairchild, P.W., Smith, G. P., and Crosley, D. R. *J. Chem Phys.* 79:1795 (1983).
18. Smyth, K. C., Tjossem, P. J. H., Hamins, A., Hamins, J. H., and Miller, J. H. *Combust. Flame* 79:366 (1988).
19. Andresen, P., Bath, A., Gröger, W., Lülf, H. W., Meijer, J. J., and Meulen, T. *Appl. Opt.* 27:365 (1988).

FIGURES

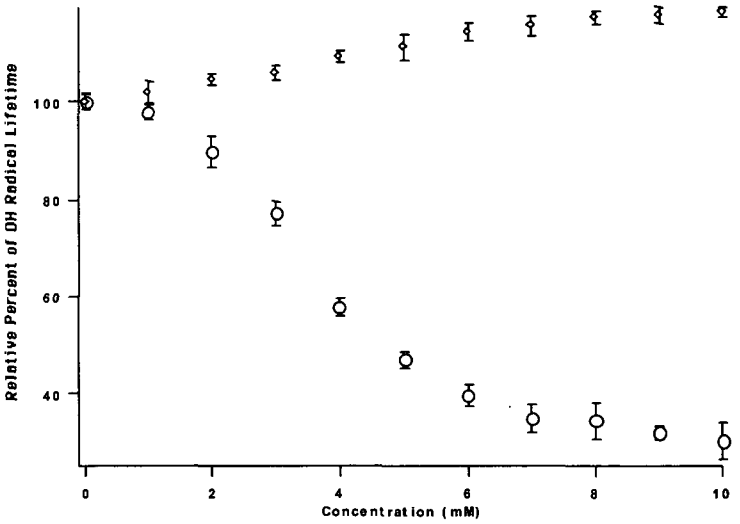

Figure 1: Relative effect of HBCD (shown by hollow circles) and cyclohexyl bromide (shown by hollow diamonds) on the fluorescence lifetime of $^{\bullet}$OH radical. The concentrations of these compounds in a toluene solution is shown on the x-axis, and the relative effect of $^{\bullet}$OH radical lifetime is shown on the y-axis. The $^{\bullet}$OH radical lifetime is shown with respect to the lifetime of $^{\bullet}$OH radical when polymer and solvent are aspirated into the burner.

IGNITION QUALITY OF RESIDUAL FUELS IN DIESEL ENGINES

C.P.G. Lewis, C. Schenk and W.J.M. Stassen
Shell Research and Technology Centre Amsterdam
Badhuisweg 3, 1031 CM Amsterdam, The Netherlands

Keywords: Residual fuel oil, Ignition performance in diesel engines, Calculated Carbon Aromaticity Index.

SUMMARY AND INTRODUCTION.

The key to efficient operation of a diesel engine is in the controlled ignition and combustion of the fuel. One factor which has a significant impact on these processes is the ease with which the fuel will ignite in the engine. In particular, the time delay period between the commencement of fuel injection into the engine, and fuel ignition occurring, is critical. The duration of this period, called the ignition delay, can impact on power output, combustion efficiency (and hence fuel efficiency and exhaust emissions), and engine maintenance. Ignition delay is influenced primarily by engine design and operation, and to a lesser extent by the characteristics of the fuel.

Research in the eighties has demonstrated that, in addition to engine and operational parameters, the aromaticity of the fuel has a pronounced effect on ignition performance. A good correlation was established between the carbon aromaticity and the readily available physical properties density and viscosity of residual fuel oil. This correlation, designated as the Calculated Carbon Aromaticity Index (CCAI), makes it possible to obtain an indication of the ignitability of the fuel and to rank fuels on ignition quality, similar to the cetane index for distillate fuel. From later experience it is recognised that the CCAI is only a first estimation of ignition performance and that also other fuel parameters must play a role. A laboratory test rig has been developed to measure ignition performance on small scale, which confirms the correlation between ignition delay and CCAI. In addition the possible relationship between CCAI and the stability of residual fuel is being discussed.

WHAT IS A RESIDUAL FUEL?

Diesel engines, in particular low speed low speed marine propulsion engines, are often using residual fuel oils. These fuels are distinguished by differences in viscosity, boiling range, combustion characteristics, chemical composition and many other properties. They consist for the major part of residues from crude oil processing. A residual fuel is a mixture of several refinery streams like short residues, long residues, gasoil, cracked residues etc. Blends of these components are made to a specifications like viscosity, density sulphur content and stability. A viscosity specification is related to pumpability of the fuel in the customers plant and atomisation in the engine. A density specification is to assure the effectiveness of separators that are used to remove (traces of) water and other impurities from the fuel. A specification on sulphur content keeps the SO_2 emissions within limits. The stability specification prevents the flocculation of asphaltenes in the fuel, thus preventing blockage of filter systems and problems with injection pumps and injectors.

Residual fuels are extremely complex mixtures which can roughly be divided into paraffinic and naphtenic/aromatic (asphaltenic) types according to crude oil origin. They can be considered as a dispersion of asphaltenes in an oily medium (the continuous phase) which is known as the 'maltenes'. The definition of the asphaltenes and the maltenes relates to the fact that when a fuel is diluted with low molecular weight paraffinic solvent such as heptane, a brown or black precipitate is produced. The toluene soluble part of the precipitate is defined as asphaltenes, the remainder being impurities like sand, rust etc. The heptane soluble part of the fuel oil is defined as the maltenes. Thus the asphaltenes together with the maltenes comprise the residual fuel; the proportion of each will depend on the nature of the fuel oil.

DIESEL ENGINE COMBUSTION

The principle behind the operation of a diesel engine is the compression-ignition cycle. Downward movement of the piston causes air to be drawn into the engine cylinder where it is compressed on the upward stroke of the piston. This compression heats the contents of the cylinder to around 550°C, which is about the same as a red hot element in an electric oven. Fuel is injected as the piston approaches the end of the compression stroke (also called Top Dead Centre -TDC) and ignites spontaneously. The increase in pressure generated by the fuel burning provides the power of the engine.

In order to more fully understand the meaning of the term ignition delay, and the influence that this can have on diesel engine performance, it is necessary to look more closely at the combustion process of the fuel in the engine. This process occurs in three distinct phases.

Firstly, the fuel is injected into the engine under high pressure as a stream of very fine liquid droplets. As these droplets meet the hot air in the cylinder they begin to vaporise and mix with the surrounding air.

Secondly, after a short delay, the heat of compression causes spontaneous ignition to occur, and a period of rapid uncontrolled combustion follows as the accumulated vapour formed during the initial injection phase is vigorously burned. This delay, between the commencement of injection of the fuel droplets and the moment of spontaneous ignition of the fuel vapour, is known as the ignition delay period, and occurs in all diesel engines.

The third phase is a period of controlled combustion which maintains pressure on the piston, and is characterised initially by the steady and even combustion of the fuel as it continues to be injected into the engine, and ends with the complete burn out of the fuel after injection has terminated.

During phases two and three, the pressure in the engine cylinder rises rapidly and considerable stresses are imposed on the piston. It is desirable to keep the *rate* of pressure rise as low as possible, and this is achieved by ensuring that the minimum quantity of fuel is present in the cylinder prior to ignition. This means that the ignition delay period should be as short as possible. Power output of the engine is optimised if ignition takes place at piston TDC and is followed by smooth and rapid combustion. To satisfy these requirements it is necessary in practice to begin the injection of fuel just before TDC to allow for the effect of the ignition delay.

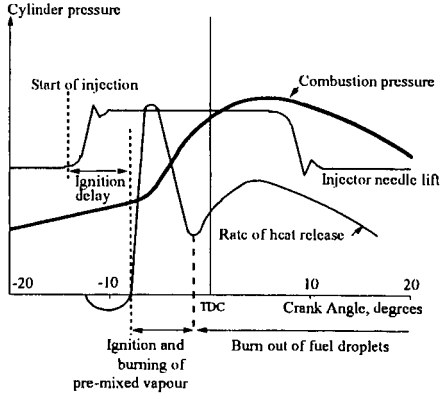

Figure 1a. Fuel combustion - good ignition characteristics

Figure 1a. is a diagram illustration showing the relationship between the fuel injection into the engine, and the pressure variation which occurs in the engine cylinder as the fuel ignites and combusts. In normal operation, given good ignition and combustion characteristics, the pressure variation will follow the smooth profile indicated by the "*Combustion pressure*" curve in the diagram, well within the design parameters of the engine.

IGNITION DELAY

Too short an ignition delay period does not normally create operational problems, but there is likely to be a loss of fuel efficiency. An extended ignition delay however can lead to poor running of the engine and, in the extreme, to damage of engine components. This is because with long ignition delay a relatively large amount of fuel droplets will have been injected and vaporised in the cylinder by the time ignition occurs. On igniting, this large amount of accumulated vapour will combust almost explosively leading to a sudden and abnormally high *rate* of pressure rise and a high cylinder pressure, beyond that for which the engine was designed or perhaps can tolerate in the longer term.

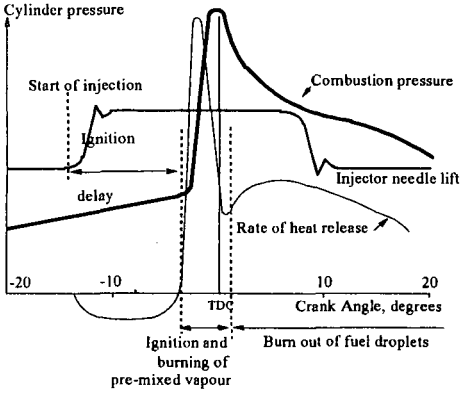

Figure 1b. Fuel combustion - "poor" ignition characteristics

Figure 1b. illustrates the type of effect which can be expected with a fuel having "poor" ignition quality. The effect manifests itself as the characteristic and audible "knock" of a poorly running diesel engine. It causes shock loading on the engine, and possible damage to cylinder heads, pistons, piston rings, liners, crankshafts etc.; a significant drop in power may also occur.

The delay between fuel injection and ignition is, therefore, a most important part of the combustion cycle, and is a function of not only the properties of the fuel, but non-fuel factors like engine design and operating conditions have a much greater effect. In engine operation, ignition delay can be significantly reduced by ncreasing charge air pressure and temperature, the load on the engine and the speed of the engine. The advice to the engine operator is to make every effort to maintain as close as possible to full load thermal conditions at all loads and speeds. Many engine manufacturers promote the use of charge air preheaters at part load operation in order to achieve this ideal, and minimise the potential for fuel ignition problems.

RESIDUAL FUEL IGNITION QUALITY - THE SHELL CCAI CONCEPT [1,2]

Ignition difficulties when using distillate fuels are almost unheard of. For many years the ignition quality of these fuels, such as gas oil, has been characterised primarily by a parameter known as Cetane Number, although to a lesser extent other methods such as Cetane Index or Diesel Index have been used. Current international specifications for marine distillate fuels, such as the ISO 8217: 1996 and BS MA100: 1996, include a minimum specification limit for Cetane Number.

Regrettably there is no similar widely recognised procedure for characterising the ignition quality of residual fuel oil. For a number of reasons the methods used for determining ignition quality of distillate fuels are not relevant, and cannot be applied to residual fuel oils. Therefore in the early eighties Shell Research embarked upon a programme with the objective of gaining an understanding of the factors controlling the ignition performance of residual fuel oils, and to identify means of characterising ignition quality.

Both the physical and chemical properties of residual bunker fuel oil were found to have an influence on ignition performance, physical properties of significance being viscosity and temperature. Atomisation quality is greatly affected by fuel viscosity. Too high a viscosity at injection increases fuel particle size, which reduces spray dispersion, hinders fuel/air mixing in the cylinder, and extends ignition delay. Many engine designs now incorporate fuel management systems capable of operating at temperatures which allow a wide range of residual fuels to be burned without difficulty.

The relevance of the chemical composition of residual fuel oil on ignition was demonstrated in work carried out by Shell Research, which lead directly to the recognition that ignition performance relates to fuel aromaticity. Since aromaticity is a difficult parameter to measure in the absence of specialist laboratory equipment, Shell derived the concept of calculating residual fuel aromaticity. The resulting Calculated Carbon Aromaticity Index (CCAI) can be calculated on the basis of known specification properties of viscosity and density, and it is this parameter which has gained favour as currently the most practical and meaningful method for characterising ignition quality of residual fuel oils.

CCAI can be calculated from the following formula:

$$CCAI = D - 81 - 141 LogLog(Vk + 0.85) - 483 Log(\frac{T + 273}{273})$$

Where: **D** = density at 15°C, kg/m³
Vk = kinematic viscosity (mm²/s) at temperature **T**°C

It must be stressed that CCAI is a unit-less number and gives the means of **ranking** the ignition qualities of different residual fuel oils; the lower the number, the better the ignition characteristics. CCAI does **not** give an absolute measure of ignition performance since this is much more dependent upon engine design and operating conditions. **For this reason no attempt has been made to include limiting values in international standards, since a value which may be problematical to one engine operated under adverse conditions may perform quite satisfactory in many other instances. Modern medium speed engines will tolerate CCAI values up to 870 to 875, and values up to 890 and beyond are acceptable to some engine types.** Medium speed diesel engines are more sensitive to fuels having poor ignition characteristics than are low speed cross head engines, which in general are much more tolerant of higher CCAI values.

The limits for viscosity and density currently in place in international marine fuel specifications in themselves provide a control of ignition quality for the main residual fuel oil grades. For example, a 380 mm²/s (@ 50°C) fuel oil at maximum specification density of 991 kg/m³ will give a CCAI value of 852, whilst a 180 mm²/s (@ 50°C) fuel oil having the same density has a CCAI of 861. Ignition characteristics improve with increasing viscosity, or decreasing density.

Ignition difficulties can become more acute at lower fuel viscosity (e.g. below ISO RMD15) if there is not a significant corresponding reduction in density. This is one reason for the lower density limits applying to the lower viscosity grades in the international specifications.

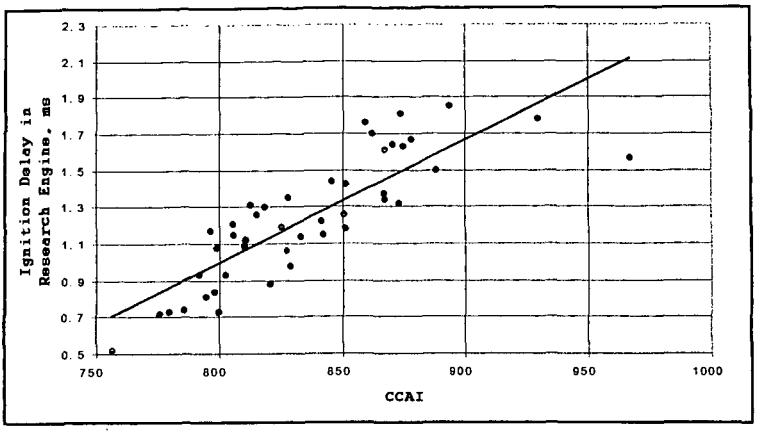

Figure 2: Correlation Ignition delay - CCAI

The correlation between ignition delay and CCAI is not ideal (Figure 2). The scatter of data points around the regression line is rather large. At lower engine outputs the scatter even is larger. This is not only due to experimental errors since cases have been reported where from 2 fuels with comparable analyses one fuel gave ignition problems at low engine output but the second fuel ran as normal. Recent research seems to indicate that there is a correlation with the nature of blending components in addition to CCAI. Combining the ignition delays as a function of CCAI for fuels of the same nature, the scatter around the regression line dramatically reduces. In our research engine at low output differences up to 1 millisecond can be found for fuels with the same CCAI but blended from different components. Obviously this millisecond can be the difference between a running or a stalling engine. More study into the background of this phenomenon is needed.

SMALL SCALE IGNITION DELAY TEST-RIG

Occasionally heavy fuels appear on the market that give engine performance not entirely predicted by their CCAI, while certain fuels can also have an abnormal combustion performance. To assist customers in these cases and for background studies the ignition delay test-rig developed by Shell Research may be used for quick performance testing, giving information on both the ignition and the combustion process. The test-rig consists of an electrically heated cylindrical combustion chamber in which compressed air at a pressure of 50 Bar is allowed to reach a temperature up to 550°C. Using a commercially available injection pump and injector a single quantity of fuel is injected into the combustion chamber. Ignition delay is measured as the time elapsed between the start of injection and the moment the pressure inside the test-rig starts to rise. The combustion process is monitored from the light emission from the 'explosion' in the combustion chamber.

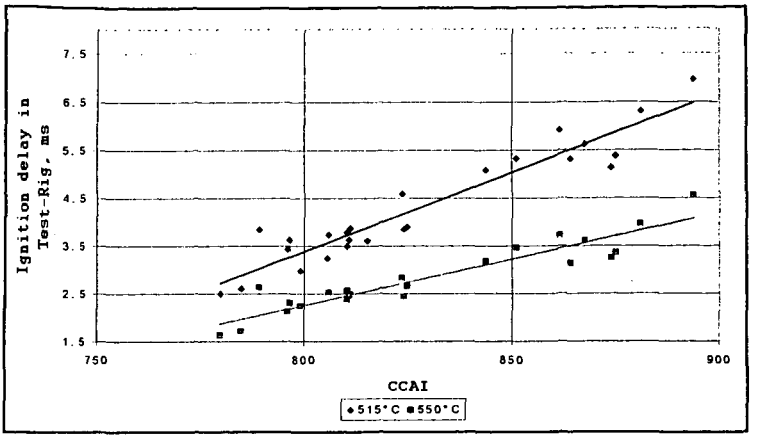

Figure 3: Ignition delay in the Test-Rig as a function of CCAI

A very good correlation between CCAI and ignition delay is found in this test-rig (Figure 3). The correlation is even better than found in the research engine. This may be caused by the fact that in the test-rig there is much more control of the relevant parameters like air pressure and temperature. Because the thick steel walls of the rig are heated from the outside and kept clean from the inside there will be no hot spots or glowing deposits present that can influence the ignition of the fuel. On the other hand in contrast to an engine there is no swirl and twirl in the combustion space. In the Test-Rig usually longer ignition delays are observed than in an engine. One of the reasons is the much higher air to fuel ratio which is being used in the Test-Rig in order to limit the pressure rise due to the combustion of the fuel.

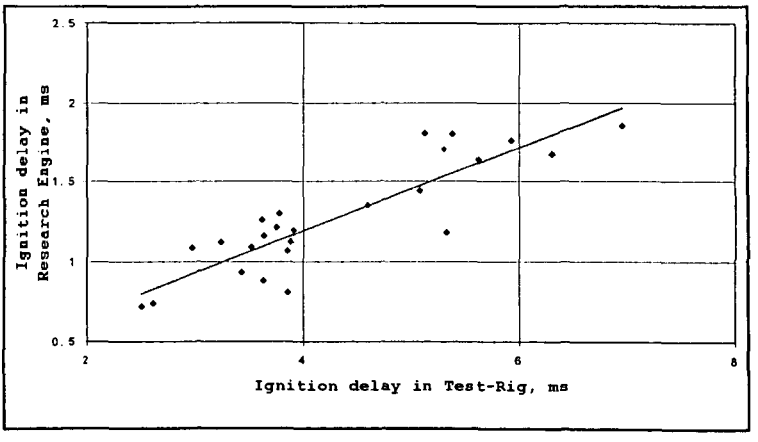

Figure 4: Ignition in the research engine compared to those in the Test-Rig

A satisfactory correlation has been established between ignition test-data obtained in a single cylinder research engine and in the test-rig (Figure 4), particularly at medium to high engine power outputs. It should be emphasised, however, that ignition delay and combustion are very much dependent on engine design and settings, and therefore it will not be possible to translate

a result into the ignition delay in a specific engine. The results can, like CCAI, only be used for a relative ranking of fuel quality. The advantages of the test-rig compared to engine testing are the small amount of fuel sample required (≈1 litre) and the short testing time (1 hour).

FUEL STABILITY [2,3]

An unstable fuel will form a sludge which consists of flocculated asphaltenes. In a stable fuel the asphaltenes are 'peptised' (i.e. colloidally dispersed), but if the equilibrium is disturbed part of the asphaltenes will agglomerate and precipitate as 'sludge'. Such a disturbance of the equilibrium between the asphaltene micelles and the maltenes is brought about by a reduction in the aromaticity i.e. the C/H ratio of the maltenes.

It will be clear that in a stable fuel all the asphaltene micelles are completely peptised and in equilibrium with the maltene phase. In the case of stable fuels the concept of 'reserve of stability' is important. It relates to the latitude of the asphaltene micelle/maltene system allowed in dilution or heat treatment without any sludge precipitation. In the case of fuels without stability reserve the equilibrium is so delicately balanced that the slightest change in external conditions will bring about instability. Such fuels of the latter types, although stable immediately after production, will probably commence to throw down sludge as a result of instability development during normal storage and handling. Hence, every effort is made by the refinery to blend fuels having sufficient 'reserve of stability'. This means that, in blending a residual fuel, a distillate stock of sufficiently high aromaticity (high C/H ratio) must be used.

For many years Shell companies have used the Shell Hot Filtration Test as a refinery control for stability. It has been shown that a relation exists between the Shell Hot Filtration Test and the Aromaticity Ratio of the fuel [3]. This is the ratio between the aromaticity of the maltene phase and the aromaticity required by the asphaltenes to remain in solution. For stable fuels the aromatic ratio should be larger than 1 and preferably be larger than 1.1. In an attempt to simplify stability control, we also looked at CCAI as a measure of stability.

Because CCAI represents both the aromaticity of the asphaltene and the maltene phase, it cannot be used to quantify the aromaticity ratio between these two phases. Nevertheless it can give a first indication of potential instability upon mixing of fuels. In a stable fuel the aromaticity of the maltene phase will be higher than the required aromaticity of the asphaltenes. In practice this means that the aromaticity of the maltene phase is higher than that of the entire fuel. When mixing fuels in a tank with about equal CCAI values no instability should therefore be expected. However, with a large difference in CCAI values the chance exists that the aromaticity of the maltene phase decreases to a level at which the asphaltenes with the highest aromaticity requirements become unstable and start flocculating. Because CCAI is not directly related to the required aromaticity of the asphaltenes nor with the stability reserve it is yet not possible to give an indication of how much CCAI difference between the several streams is allowable.

The CCAI apparently can only be used as 'rule of thumb' tool to indicate the compatibility of fuels mixed in a customer's tank. More research is needed to set up a simple way of predicting stability of fuels without performing the elaborate test methods which are now being used to determine the balance between the required and available aromaticity.

References:

1. The ignition performance of fuel oils in marine Diesel engines, A.P. Zeelenberg et al, 15th CIMAC Conference, Paris, June 1983
2. Lubricants and Fuels in Ships, Shell Marine Service World Wide.
3. The Stability of Residual Fuels- Theory and Practise of the Shell Concept, 16th CIMAC Conference, Oslo, June 1985

DETERMINATION OF TEMPERATURE AND CHEMICAL COMPOSITION PROFILES OF METHANOL OPPOSED FLOW DIFFUSION FLAMES.

A. Santiago , S. Malary - University of Bridgeport, Bridgeport, CT.

An opposed flow diffusion flame (OFDF) can arise in the stagnation boundary layer when an oxidizing jet impinges on a surface issuing a volatile fuel and an ignition source is introduced. Figure 1 illustrates the behavior of a typical OFDF. This configuration is frequently employed in experimental and numerical studies of laminar flames. The opposed flow or counterflow configuration is, according to Dixon-Lewis [1], the most appropriate configuration for the investigation of the composition and microstructure of laminar flames.

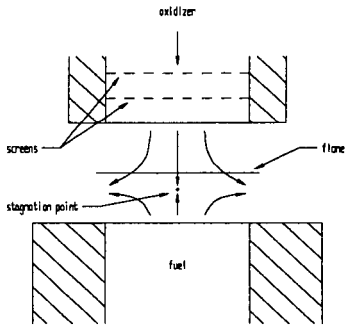

Figure 1

Chemical kinetic models are important tools for describing combustion systems. Measurements of combustion gases at temperatures higher than 1000K are complicated by the presence of fast reactions and the typically small size of the reaction zone. However, reaction mechanisms at higher temperatures are simpler and kinetic models can be validated for stable compounds with well-established measurement techniques. Reaction mechanisms for the oxidation of methanol, CH_3OH, were developed using data following from measurements involving shock tubes and turbulent flow reactors. These comprehensive mechanisms are discussed with some detail in [2, 3] and have been used to predict the oxidation of methanol for other flows. Extinction measurements for pure methanol OFDF's have been reported [4] and the influence of its presence in solutions with heptane and toluene on structure and flammability limits has also been examined [5]. However, measurements and models of structure for pure methanol OFDF's are not found reported in the published literature. Our measurements provide an opportunity to test the applicability of kinetic rate constants accompanying published comprehensive reaction mechanisms for methanol oxidation.

Measurements of temperature and stable species of CH_3OH opposed flow diffusion flames (OFDF's) are compared with profiles obtained by numerical methods, i.e. kinetic models. Combustion measurements are carefully undertaken with quartz microprobes and gas chromatography. An OFDF burner is used to generate stable axially-symmetric laminar diffusion flames. A mixture of oxygen (O_2) and nitrogen (N_2) is directed vertically downward and impinges on the flat, horizontal surface of a pool of liquid CH_3OH. Ignition of the CH_3OH vapor is used to initiate burning. See Figure 2. Continuous sampling using a gas sampling valve with a 250 µl sampling loop is employed. Low back pressures in the lines conveying the sampled gas to the gas chromatograph ensure reaction quench in the wake of the recovery shock in the probe, downstream of the sonic probe tip opening. These lines are heated in order to prevent the condensation of water and any other low boiling point liquids. Analysis is accomplished with single packed column separation employing HayeSep polymers. Temperature profiles are measured using Pt/Pt-10% Rh thermocouples and a precision x-y positioner. Measured temperature profiles are subsequently corrected for radiative losses.

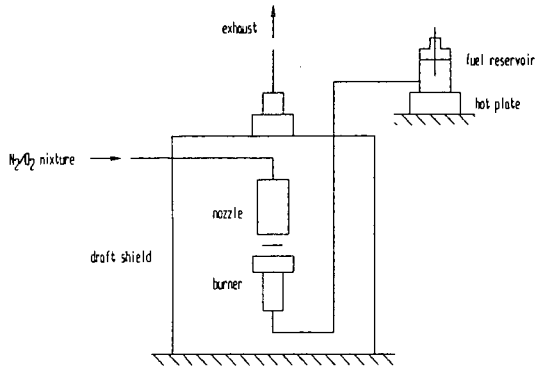

Figure 2

References

1. Dixon-Lewis, G. and Missaghi, M., "structure and Extinction Limits of Counterflow Diffusion Flames of Hydrogen-Nitrogen Mixtures in Air," *Twenty-Second Symposium (international) on Combustion*, pp. 1461-1470 (1988).
2. Westbrook, C.K. and Dryer, F.L., "Chemical Kinetic Modeling of Hydrocarbon Combustion," *Prog. Energy Combust. Sci.*, v. 10, pp. 1-57 (1984).
3. Westbrook, C.K., "Chemical Kinetics of Hydrocarbon Oxidation in Gaseous Detonations," *Combust. Flame*, v. 46, pp. 191-210 (1982).
4. Hamins, A. and Seshadri, K., "Prediction of Overall Chemical Kinetic Rate Parameters Near Extinction for Diffusion Flames Burning Multicomponent Fuels," *Combust. Sci. Tech.*, v. 38, pp. 89-103 (1984).
5. Hamins, A. and Seshadri, K., "The Structure of Diffusion Flames Burning Pure, Binary and Ternary Solutions of Methanol, Heptane, and Toluene," *Combust. Flame*, pp. 295-307 (1987).

ASSESSING COAL QUALITY IMPACT ON P.C. COMBUSTION BEHAVIOR

Stephen Niksa

Niksa Energy Associates
1745 Terrace Drive, Belmont, CA 94002

KEYWORDS: Coal pyrolysis, NOx, kinetics, modeling

ABSTRACT

This paper demonstrates a computational approach for assessing coal quality impacts that achieves the accuracy of laboratory testing for a fraction of the expense. It is based on FLASHCHAIN, the world's most extensively evaluated model for the thermal decomposition of coal. Two applications are considered here. First, the model is used to identify the parameter values in the simple devolatilization rate expressions used in coal combustor simulators that mimic the FLASHCHAIN predictions. In the second application, predicted yields for rapid heating conditions and coal-nitrogen release are used as regression variables in engineering correlations to relate coal quality to NO_x emissions and unburned carbon in ash (as LOI) from full-scale furnaces.

INTRODUCTION

With the advent of so-called coal network depolymerization models, it is now possible to predict how the different properties of various coals will affect the initial stages of pulverized coal combustion. Three phenomenological network models are available [1-3]. All represent devolatilizaiton as a depolymerization that disintegrates coal's macromolecular structure into smaller volatiles fragments with subsequent reintegration of larger intermediates into char. Whereas FLASHCHAIN and the CPD model are based on the same concise set of rate mechanisms, the FG-DVC model is all-encompassing. Each can generate predictions for yields, transient evolution rates, and various product characteristics based on coal-specific characterization data.

Although these models' underlying mechanisms share much in common, there are also tangible performance aspects to consider. To date, FLASHCHAIN has been used to predict the devolatilization behavior of more than 400 different coals from every geographical region worldwide. No other model comes close to this level of performance, simply because only FLASHCHAIN simulations can be performed without specialized and expensive laboratory tests. The only sample-specific information needed is the proximate and ultimate analyses of the coal. And full simulations require only a few seconds on modern personal microcomputers.

FLASHCHAIN predicts the yields, release rates, and compositions of all major products of coal devolatilization, including nitrogen species and all major gas species, from any coal at any operating conditions. Some 70 coals have been included in published performance evaluations [1]. Here we focus on applications.

One immediate application of FLASHCHAIN is to use it as a replacement for the rudimentary rate expressions currently used in coal combustor simulators. While conceptually straightforward, this option entails extensive re-coding, and provides more detailed information on product compositions than can be used within current limitations on modeling turbulence-chemistry interactions in large-scale systems. A more expedient strategy delivers the benefits of FLASHCHAIN without the development costs of modifying the large-scale combustor code. Instead of installing FLASHCHAIN as a new submodel, we use it to identify the parameter values that make the simpler rate expressions currently in use mimic the FLASHCHAIN predictions. For example, nominal devolatilization rates can always be defined from any model predictions according to the following rearrangement of a single first-order reaction rate law:

$$\langle k \rangle = (dV/dt)/(V_\infty - V(t))$$

where $\langle k \rangle$ is the nominal devolatilization rate constant, $A \exp(-E_a/RT)$, s^{-1}; V(t) is the instantaneous volatiles yield and V_∞ is the ultimate weight loss. The volatiles release rate, instantaneous yield and ultimate yield are assigned with the rates and yields for gas and tar release predicted by FLASHCHAIN.

Predicted ultimate weight loss and tar yields are compared to measured values in Fig. 1a. Although all samples in this evaluation are hv bituminous coals and the test conditions were directly comparable, weight loss ranges from 40 to 60 %, and tar yields range from 20 to 40 %. The FLASHCHAIN predictions depict these ranges, and also depict the sample-to-sample variability among individual coals. Yet the predictions are based only on the proximate and ultimate analyses.

In Fig. 1 b, predicted rates during uniform heating at different rates illustrate how the nominal rates change as heating rates are varied. Devolatilization rates increase in direct proportion to increases in heating rate; they increase by a factor of 6 for every order of magnitude increase in heating rate. The apparent activation energies are surprisingly uniform, becoming only slightly larger for faster heating rates

information to assign a particle heating rate, FLASHCHAIN can be used to assign parameters in simple global rate laws for any coal type. Whereas a single first order expression was analyzed here, the same approach can also be applied with competing 2-step or distributed activation energy rate laws. It can also be used to assign rates for the release rates of individual products, including nitrogen species.

Above and beyond applications as a devolatilization submodel in detailed simulations, FLASHCHAIN can also be used as a virtual coal laboratory. In this sense, it provides the same information that would normally be acquired in, for example, drop-tube tests, such as rapid heating volatiles yields, the partitioning between volatile- and char-nitrogen species, soot loadings, and gas compositions and heating values. In turn, these quantities can be used as regression variables in engineering correlations that relate coal properties to macroscopic boiler performance characteristics.

For example, FLASHCHAIN has been incorporated into a PC-Based software package developed by EPRI called the NO_XLOI Predictor that estimates NO_x emissions in the exhausts of full-scale utility boilers. As depicted in Fig. 2a, the structure of the calculation is straightforward. The user provides a few measured values of NO_x emissions and describes the major furnace operating conditions, such as the firing configuration, the type of NO_x control technology, the firing capacity, etc. The user also enters the proximate and ultimate analyses for the coal that was fired while the data was recorded, as well as those for any coals that he or she wants to screen. This computer program then predicts the NO_x emissions for the set of coals being screened when they are burned *under the same firing conditions* as were used when the data was collected.

In this program, FLASHCHAIN is used to predict two critical characteristics that relate coal properties to NO_x emissions: First, it predicts the total amount of volatiles driven off the coal while it is being heated under flame conditions, where heating rates approach 10^5 K/s and temperatures approach 3000 °F. The weight loss under flame conditions typically exceeds the proximate volatile matter contents by 20 to 100 %, which explains why NO_x emissions do not correlate very well with fuel ratios determined from typical ASTM proximate analyses. The second critical information from FLASHCHAIN is the partitioning of fuel-nitrogen species among gaseous pyrolysis products and char. This partitioning is important because only the chemistry involving gaseous nitrogen compounds can be affected by aerodynamic NO_x abatement strategies that regulate

An evaluation for full-scale coal-fired furnaces appears in Fig. 2b. These predictions are for situations that were not part of the database used to formulate the regressions. The software predict NO_x emissions for coal ranks from subbituminous through lv bituminous within 10 to 15 ppm of observed values. We also expect that the same basic approach would work as well in correlating coal quality impacts on plan area heat release rates, near-burner radiation loads, heat rates, furnace exhaust temperatures, and steam-side temperatures.

REFERENCES

1. Niksa, S., *Combust. Flame* 100:384 **(1995).**
2. Solomon, P. R., Hamblen, D. G., Serio, M. A., Yu, Z.-Z., and Charpenay, S., *Fuel* 72:469 **(1993)**.
3. Fletcher, T. H., Kerstein, A. R., Pugmire, R. J., Solum, M. S., and Grant, D. M., *Energy Fuels* 6:414 **(1992)**.

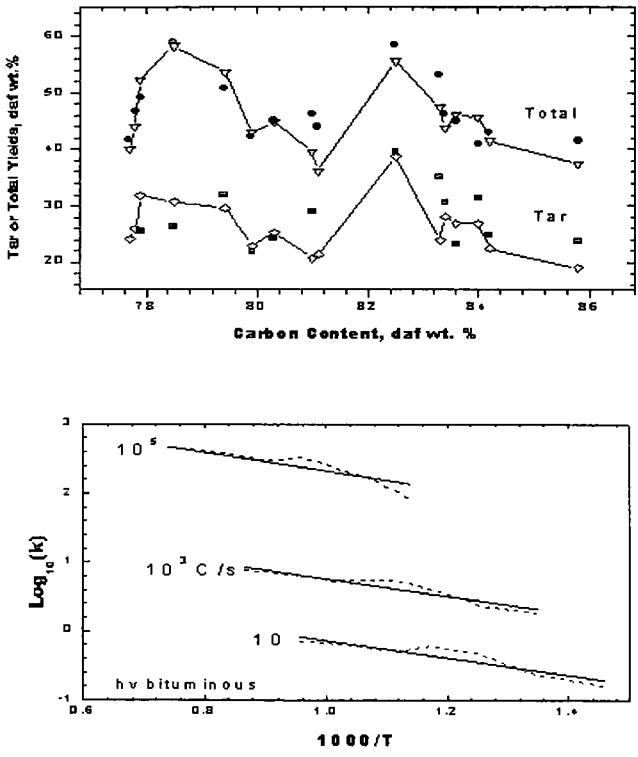

Figure 1. (a, top) Measured weight loss and tar yields from hv bituminous coals compared to FLASHCHAIN predictions (∇). (b, bottom) Nominal devolatilization rates based on the single first-order reaction (solid lines) and FLASHCHAIN (dashed curves) for devolatilization of a high volatile bituminous coal at three heating rates.

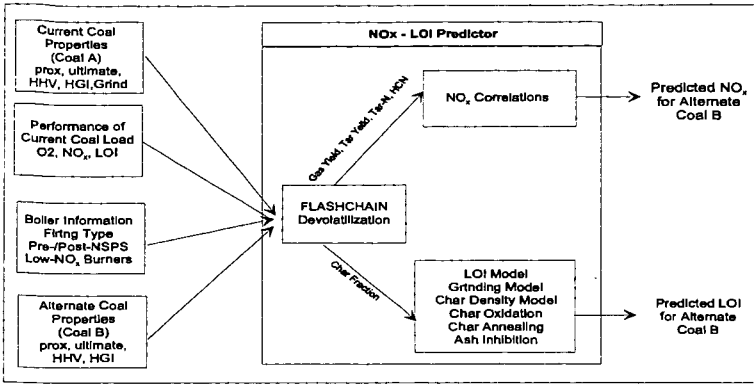

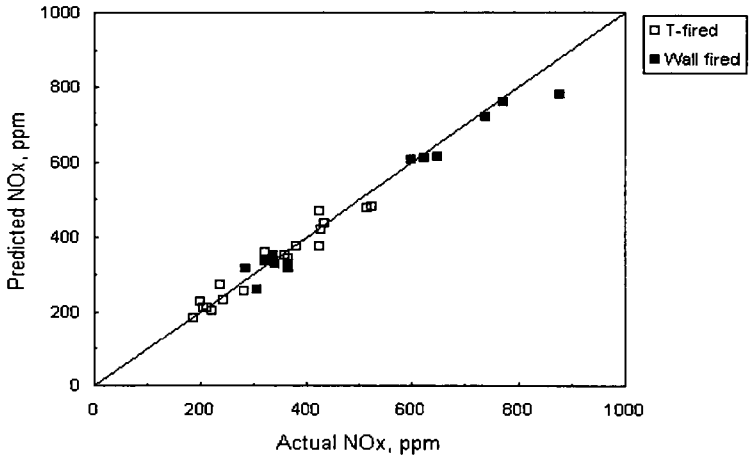

Figure 2. (a, top) Calculation structure for EPRI's NO_X LOI Predictor. (b, bottom) Evaluation of predicted exhaust NO_X levels from full-scale coal-fired utility boilers.

DEVOLATILIZATION, A MOLECULAR MODELING APPROACH

Jonathan P. Mathews, Patrick G. Hatcher, Alan W. Scaroni
Fuel Science Program, 211 CUL, The Pennsylvania State University,
University Park, PA 16802

Keywords: Vitrinite, devolatilization and char structure.

Abstract
Simulated devolatilization of in-house generated molecular models, which are representative of both the chemical and physical structures of bituminous coals, provides a unique insight into bond breaking and bond reforming mechanisms. A series of molecular models for rapidly heated bituminous vitrinites chars is presented. It was necessary to include bond formation in addition to bond breaking reactions to simulate the devolatilization process. Strong bond cleavage, sometimes prior to weak bond cleavage, was important for structural transitions. Structural units attached to the vitrinite/vitrinite-char matrix with two or fewer bonds contributed the bulk of the mass loss. However, bond-forming reactions also incorporate such structures into the char matrix, thereby reducing their probability of release. Internal hydrogen redistribution is responsible for the extent of molecular orientation in these bituminous vitrinite chars.

Introduction

There have been a number of different models proposed for the devolatilization (pyrolysis) process. Unfortunately, even with a relatively complete chemical structure, the pyrolysis behavior of coals can not be predicted a priori. Some of the devolatilization models rely on network models while others employ structural or functional group models (1-5). All the devolatilization models are simplistic with regard to coal structure and none incorporate physical properties. Realistic molecular models would be of considerable aid in following and understanding the devolatilization process. It is well recognized that the maceral groups found in coal are chemically and physically distinct over most of the rank range (6) and thus behave differently during devolatilization. A significant reduction in the complexity of devolatilization is achieved here by considering only the vitrinite maceral group, specifically telocollinite obtained from Sigillaria tree remains.

Experimental

Pure vitrinites (purity obtained from microscopic evaluations) were obtained from obvious tree remains in the roofs of the Upper Freeport and Lewiston-Stockton coal seams. Narrow size fractions were obtained by wet sieving. The 200x400 mesh (US Standard Sieve) cut was analyzed by a combination of chemical (^{13}C CPMAS, ^{1}H CRAMPS NMR, flash-pyrolysis gc-ms, proximate and ultimate analyses) and physical techniques (surface area, helium density, particle size, and shape). Molecular structures of the vitrinites were generated using the SIGNATURE program (7, 8) and their physical evaluation made using one of its components (9). Molecular structures of the chars were made by manipulation (devolatilization) of the vitrinite structures. The chemical and physical evaluation of the chars models being performed by the SIGNATURE program and its components.

Vitrinite-chars were produced by rapid heating (10^5 °s^{-1}) in a nitrogen atmosphere in a drop-tube reactor operating at a temperature of 1,400 °C. The chars were collected at different positions to represent the transition from vitrinite to devolatilized char. Tar was removed by THF solvent extraction, and NMR samples were treated with SmI_2 to remove free radicals and improve the quantitative nature of the NMR experiments. A portion of the samples were demineralized prior to certain characterizations. Otherwise the chars were analyzed in a manner similar to the vitrinites.

Results and Discussion

Structural characteristics of the vitrinites and vitrinite-chars are presented in Table 1. The vitrinites, although similar in bulk characteristics, differ in the fine structure and devolatilization behavior. The elemental compositions of the vitrinite and vitrinite-chars are presented in Table 2. Despite having different initial fine structures, the devolatilized char structures are chemically similar but physically different. Helium densities of dry, demineralized samples were 2.04 and 1.34 g/cm3 (ash-free basis), BET surface areas were 11.2 and 0.5 m^2/g, and particle swelling factors of 2.5 and 1.8 were obtained by laser light scattering for the UF and LS vitrinite-chars, respectively.

Devolatilization was performed manually on the vitrinite models, initially according to devolatilization "rules". Initially, this was a simple bond-breaking process based solely on bond strength. However, using this weakest-first approach resulted in a structure that was too aromatic, and did not yield the required mass loss. It was also evident that a large concentration of free radicals was present. Radical recombination of multiple radical pairs resulted in a very dense and strained char. This indicated that the pyrolysis process could not be considered solely as a bond breaking process, but rather as a combined bond breaking and bond forming process. Thus, the initial rationale for the computational devolatilization was found to be in considerable error.

The question that arises is "under what conditions will stronger bonds break before or around the same time as weaker bonds?". There are two extremes for bond breaking: infinite time with infinitesimal temperature rise, and rapid heating. Under infinite time with infinitesimal temperature rise the bonds will be broken in order of bond strengths. Where the temperature rise is rapid, there is energy available to break stronger bonds before all weaker bonds have had an opportunity to undergo homolytic bond cleavage. Assuming that at any point in time a structural unit (hydroaromatic or aromatic units) is more likely to have two bonds broken than three (or even

four), then those structures will contribute to the volatile fraction preferentially. However, this does not necessarily indicate that the vitrinite contains structures that are predetermined to be volatiles. Pyrolysis is a bond breaking and bond forming process, those structures initially bonded once or twice to the char matrix can be incorporated into the char matrix in such a manner as to inhibit release. Conversely, loss of a structural unit to the volatile fraction with proton radical capping of the bonding site can create structural units that can then be preferentially lost to the volatile fraction. This bond breaking, bond forming approach was used to generate the initial char structure from the 13 cm. sampling location (estimated particle temperature range of 650-950 °C, 0.06-0.15 s residence time and estimated mass loss of 20%). This mass loss approach appears to be valid in that, despite losing one fifth of the mass, the constitution of both vitrinites has changed little (Table 1). This was expected as it has been shown that the initial tar structure is chemically similar to the parent coal under rapid-heating pyrolysis conditions (10).

Preferential removal of units attached to the char matrix two or fewer times was used to generate the 23 cm. char models (1,090-1,400 °C particle temperature range and 0.15-0.33 s residence time). Again reasonable mass losses of 26 and 40 % were obtained for the UF and LS vitrinites, respectively. However, the atomic H/C ratios were too high and the carbon aromaticities of the chars too low. Thus, double bonds where introduced into the structure by hydrogen abstraction from aliphatic chains, creating two sp^2 hybridized carbons (which are included in the aromaticity values) or aromatization of hydroaromatic structures. Some of the hydrogen radicals formed were redistributed to terminate free radicals. This supply of hydrogen is instrumental in allowing thermoplasticity in the char with the resulting macroscopic flow and cenosphere formation. It has been suggested that a supply of hydroaromatic hydrogen is necessary for thermoplastic behavior (11). However, in addition to hydroaromatic hydrogen, for this coal structure a considerable quantity of hydrogen can be obtained from the sp^2 hybridization of short chain aliphatics (approximately C2-C3) that appear to be a component of the vitrinite structure, presumably from their presence in the parent lignin. This step also results in a structure where rapid and substantial loss of hydrogen with aromatic sheet growth can occur.

In the transition in the char structure from the 23 to the 33 cm. sampling location, the model mass loss was partially achieved by removing units attached to the char matrix two or fewer times. The remaining hydroaromatics underwent aromatization, and aliphatics were incorporated into the aromatic structures or were removed as methane or acetylene. The remaining oxygen in the char was assumed to be emitted only as CO, as it was well dispersed throughout the char model. Removal of a substantial quantity of hydrogen was necessary to achieve the appropriate H/C ratios (Table 2). This was achieved by hydrogen-carbon bond cleavage and subsequent radical-radical recombination or radical propagation with hydrogen radical expulsion. This hydrogen removal often increased the size of the aromatic units and because of the linear cantanation of the aromatic structures, generally resulted in preferential alignment of the aromatic units.

Pentagon ring formation from aromatic unit combination and from carbazole and fluorine structures resulted in curvature of the aromatic sheet. Seven membered ring structures are also created when chair and zig-zag configurations combine. This curvature prevents efficient stacking of the aromatic sheets and prevents graphitic formation. It may also be responsible for closed microporosity and hence a lower helium density. However, helium density values for the LS 33 cm. char model were considerably higher than the experimental value, 1.85 and 1.34 g/cc, respectively. Typical densities of chars generated by a slow heating rate (North American coals) are between 1.7 and 2.1 g/cc on an ash free basis. These values are consistent with the predicted char model density (1.85 g/cc). Given the constraints of the chemical evaluations, an experimental helium density value similar to that of a raw bituminous coal must be due to closed porosity.

A representation of the structural transitions for the LS vitrinite to char structures at the sampling locations of 13, 23 and 33 cm. is shown in Figure 1. The structures are in reasonable agreement with both mass loss and bulk composition and chemical structure.

Conclusions

Molecular models representative of telocollinte from the Upper Freeport and Lewiston-Stockton coal seams have been generated and subjected to simulated, rapid-heating devolatilization. Molecular models that are in reasonable agreement with the mass loss and chemical structural features of drop-tube reactor generated chars have been produced by following simple devolatilization rules. The bulk of the mass loss can be accounted for by structural units attached to the coal/char matrix by two or fewer bonds. However, the bond formation process may incorporate such structures into the char matrix in a manner that would preclude release, i.e. pyrolysis is a bond forming and bond breaking process. Strong bond rupture can occur at the same time as, or prior to, weak bond rupture. The changes in the carbon and proton aromaticities can be achieved by some hydroaromatization of hydroaromatic units but also by sp^2 hybridization of aliphatic carbons.

References

1. Gavalas, G. R., Cheong, P. H.-K. and Jain, R., *Ind. Eng. Chem. Fundam.*, 1981, **20**, 113.
2. Gavalas, G. R., Cheong, P. H.-K. and Jain, R., *Ind. Eng. Chem. Fundam.*, 1981, **20**, 122.
3. Niksa, S. and Kerstein, A. R., *Fuel*, 1987, **66**, (10), 1389.

4. Niksa, S. and Kerstein, A. R., *Energy & Fuels*, 1991, **5**, 647.
5. Solomon, P. R., Hamblen, D. G., M., C. R., Serio, M. A. and Deshpande, G. V., *Combustion and Flame*, 1988, **71**, 137.
6. Stach, E., Mackowsky, M.-T., Teichmuller, M., Taylor, G. H., Chandra, D. and Teichmuller, R., Coal Petrology, 1982, Berlin, Germany, Gebrueder Borntraeger.
7. Faulon, J.-L., Vandenbroucke, M., Drappier, J. M., Behar, F. and Romero, M., *Org. Geochem.*, 1990, **16**, 981.
8. Faulon, J.-L., Hatcher, P. G. and Wenzel, K. A., Am. Chem. Soc. Div. Fuel Chem. Prepr., 1992, **37**, 2, 900.
9. Faulon, J.-L., Mathews, J. P., Carlson, G. A. and Hatcher, P. G., *Energy & Fuels*, 1994, **8**, (2), 408.
10. Pugmire, R. J., Solum, M. S., Grant, D. M., Critchfield, S. and Fletcher, T. H., *Fuel*, 1991, **70**, 414.
11. Neavel, R. C., Coal Agglomeration and Conversion, West Virginia Geological and Economic Survey, 1975, Morgantown, WV. 120.

Table 1
Chemical Data for UF and LS Vitrinite and Chars

Sample	*fa*	Ha	CH3	H/C	H/Cali	H/Cali*
UF Vitrinite	0.79	0.45	0.08	0.76	1.9	1.2
13	0.83	0.51	0.06	0.73	2.1	1.6
23	0.87	0.44	0.07	0.64	2.1	1.5
33	1.00			0.24		
LS Vitrinite	0.82	0.45	0.05	0.78	2.4	2.2
13	0.86	0.47	0.05	0.75	2.4	2.2
23	0.87	0.58	0.04	0.68	1.7	1.2
33	0.99		0.00	0.21	0.0	0.0

fa is the aromaticity, Ha is the proton aromaticity, H/C is the atomic hydrogen to carbon ratio, H/Cali is the aliphatic atomic hydrogen to carbon ratio, H/Cali* is the non-methyl aliphatic atomic hydrogen to carbon ratio.

Table 2
Elemental Composition of UF and LS Vitrinite and Chars

Sample	No of C	No of H	No of N	No of O
UF Vitrinite	100	75.5	1.2	4.4
13	100	72.8	1.2	6.5
23	100	63.5	1.8	7.9
33	100	24.4	2.9	0.8
43	100	8.8	1.4	0.0
LS Vitrinite	100	77.9	1.4	6.3
13	100	75.3	1.4	4.2
23	100	68.0	1.4	6.2
33	100	20.7	1.6	0.2

Data presented are normalized to 100 carbon atoms, oxygen was calculated using the weight % obtained by difference.

Figure 1. Structural Transitions of the LS Vitrinite to Char. (The initial structure is the LS Vitrinite, followed by the 13 , 23 and 33 cm. char models)

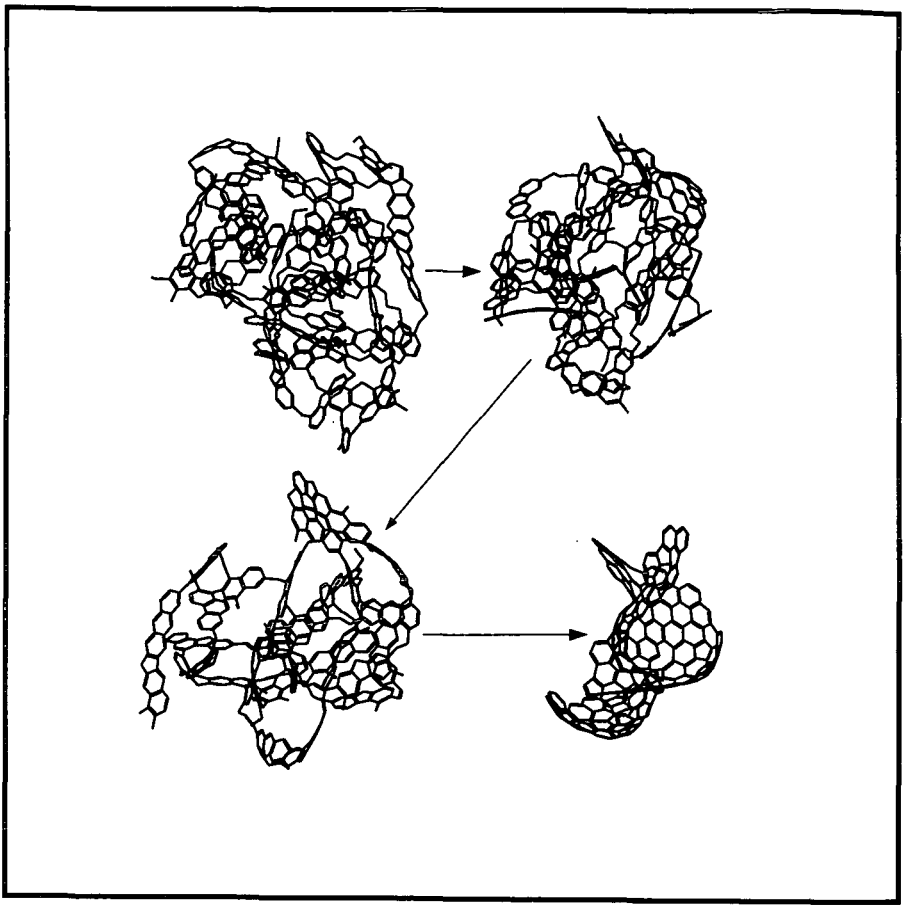

EVALUATION OF NITROGEN RELEASE CHEMISTRY USING DETAILED CHEMICAL STRUCTURAL CHAR DATA

S. T. Perry and T. H. Fletcher

Department of Chemical Engineering Brigham Young University, Provo, Utah 84602

Keywords: coal, pyrolysis, ^{13}C NMR, nitrogen

Introduction

Nitrogen release from coal during devolatilization is difficult to predict due to coal to coal variations. Two computer models for prediction of nitrogen release from coal during devolatilization have been proposed (Bassilakis et al., 1993; Niksa, 1995). Parameters in these models were tuned by matching predicted nitrogen release to light gas and tar nitrogen from various coals with experimentally measured values. Both models use a distributed activation energy first-order rate expression, with one or two coal-dependent parameters, which are then correlated to the ultimate analysis of the coal. The chemistry responsible for the variations in nitrogen release with coal type is not well understood, and therefore is only treated empirically in these models. These models are based on the following assumptions:

1. All fuel-bound nitrogen atoms are distributed randomly within the aromatic nuclei in the coal.
2. During tar release, tar aromatic nuclei "shuttle" nitrogen atoms contained therein to the tar product, in an amount proportional to the number of aromatic nuclei in the tar.
3. During primary devolatilization, the aromatic nuclei/aromatic rings are conserved within the pyrolysis products, that is, ring condensation and opening reactions are negligible, except for HCN production.
4. During devolatilization, the rate of release of nitrogen atoms from the aromatic nuclei can be described as a first order process with a distributed activation energy.

Based on these assumptions, the model proposed by Niksa (1995) predicts the nitrogen release as light gas based on changes in the ratio of moles of nitrogen to moles of aromatic nuclei (η_0). Alternatively, changes in the ratio of mass of nitrogen to mass of aromatic carbon ($R_{N\text{-}AC}$) can be used to predict light gas nitrogen release, the two variables differing only by a conversion factor:

$$R_{N-AC} = \left(\frac{MW_C}{MW_N} \cdot AC_{cl} \right) \eta_0 \qquad (1)$$

where MW_C and MW_N are the atomic weights carbon and nitrogen, respectively, and AC_{cl} is the number of moles of aromatic carbons per mole of aromatic clusters or nuclei. Alternatively, $R_{N\text{-}AC}$ can be calculated from measured ^{13}C NMR parameters and the ultimate analysis for a given coal, char, or tar sample, as follows:

$$R_{N-AC} = \frac{\%N}{\%C \cdot f_a'} \qquad (2)$$

where f_a' is the fraction of carbon atoms which are aromatic and %N and %C are the nitrogen and carbon weight percents on a dry ash-free (daf) basis in a coal or char sample. Since the value of AC_{cl} as calculated from ^{13}C NMR data typically contains a large degree of uncertainty, the variable $R_{N\text{-}AC}$ is used, since it is independent of the number of aromatic carbons per cluster.

In order to evaluate the adequacy of a first order rate expression with distributed activation energy in describing nitrogen release as light gas, a simple model was developed for comparison of actual changes in $R_{N\text{-}AC}$ during devolatilization for chars of various coals. This model is based on the same assumptions as the earlier models, but uses only three coal-independent parameters, which were adjusted to describe the average behavior of $R_{N\text{-}AC}$ in the chars of five coals during rapid devolatilization at 1250 K. In this model, the value of $R_{N\text{-}AC}$ is then assumed to decay as a first order process:

$$\frac{dR_{N-AC}}{dt} = -A_N \exp(-E_N / RT_p) \cdot R_{N-AC} \qquad (3)$$

where the activation energy (E_N) is distributed according to a normal probability distribution (with mean value of E_{0N} and a standard deviation of σ_N) as a function of the extent of $R_{N\text{-}AC}$ disappearance, in a manner similar to that used by Fletcher et al. (1992).

In order to correctly predict nitrogen release, devolatilization models must not only correctly predict tar and char yields, but must also correctly treat changes in the cluster molecular weight (MW_{cl}) and average cluster attachment molecular weight (MW_a) in the char. Since the nitrogen is contained only in the aromatic groups in the coal, a meaningful variable is the fraction of mass which is aromatic (f_a^{mass}). The %N in the char can then be calculated as follows:

$$\%N = R_{N-AC} \cdot R_{AC-AM} \cdot f_a^{mass} \tag{4}$$

where

$$f_a^{mass} = \frac{MW_{cl} - MW_a \cdot (\sigma + 1)}{MW_{cl}} \tag{5}$$

and

$$R_{AC-AM} = \frac{\%C \cdot f_a}{f_a^{mass}} \tag{6}$$

and $\sigma + 1$ is the average number of attachments per cluster. R_{AC-AM} is the ratio of aromatic carbon mass to the total aromatic mass in the char, which is assumed to remain constant during devolatilization. The nitrogen release is then calculated as follows:

$$NR = \frac{\%N_{coal} - f_{char} \cdot \%N_{char}}{\%N_{coal}} \tag{7}$$

where f_{char} is the daf char yield, as calculated by the devolatilization model. Thus, in order to correctly describe the chemistry of nitrogen release from char during devolatilization, a devolatilization model should correctly predict tar and char yields and f_a^{mass}, or an equivalent variable describing the char aromaticity.

Evaluation of Models

Devolatilization data reported by Fletcher and Hardesty (1992) were used for evaluation of the devolatilization model nitrogen release chemistry. They reported yields and ultimate analyses for the chars of five coals, entrained in nitrogen in an electrically-heated drop tube reactor for maximum gas temperatures of 1050 and 1250 K, and collected at various residence times. All of the coals and several of the chars for seven of the ten experimental conditions were also analyzed by ^{13}C NMR, giving quantitative details of the evolution of the chemical structure during rapid devolatilization for these coals. Particle temperature profiles were carefully measured, facilitating devolatilization model evaluation. Since yields and ultimate analyses of the tars were not reported for these data, evaluation of model predictions for nitrogen release to the tar were not possible.

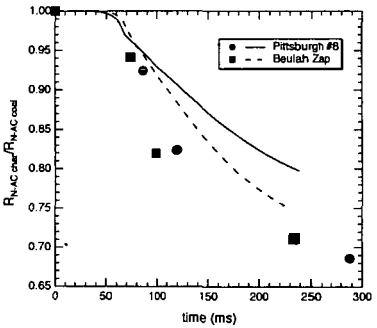

Figure 1. Comparison of predicted (lines) and measured (symbols) nitrogen to aromatic carbon ratios during rapid devolatilization at **1250 K** for the chars of three coals, normalized by the nitrogen per aromatic carbon ratio in the parent coal. R_{N-AC} decays more rapidly than average for these coals.

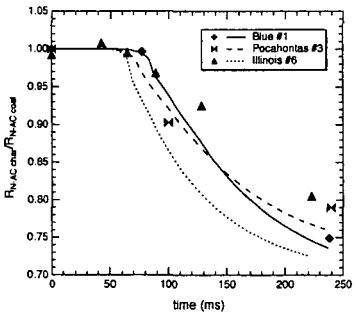

Figure 2. Comparison of predicted (lines) and measured (symbols) nitrogen to aromatic carbon ratios during rapid devolatilization at **1250 K** for the chars of two coals, normalized by the nitrogen per aromatic carbon ratio in the parent coal. R_{N-AC} decays more slowly than average for these coals.

To evaluate the use of a simple first order rate expression (Equation 3) to model nitrogen release to the light gas, three coal-independent constants were used. Values for the activation energy mean and deviation were taken to be 52 and 6 kcal/mol respectively for all coals (in a manner similar to Bassilakis et al., 1993) to describe HCN formation at both low and high heating rates. The pre-exponential factor was then varied to obtain the value which best modeled the changes in R_{N-AC} for the chars of all five coals during rapid devolatilization. A pre-exponential factor of $8.4 \times 10^8\ s^{-1}$ was found to adequately describe the decay of R_{N-AC} for all coals. In Figures 1-3, experimentally measured R_{N-AC} values in the char throughout devolatilization are compared with those predicted by the simple nitrogen release model, revealing an unmistakable bias by coal type. Since the particle temperature profiles were precisely measured for the devolatilization tests

discussed here, the biases in $R_{N\text{-}AC}$ behavior are not thought to be due to errors in the particle temperature profile. For some coals $R_{N\text{-}AC}$ decays consistently faster than the predicted values, and for other coals decaying consistently slower. What is more, the bias appears to change for some coals with changes in gas temperature.

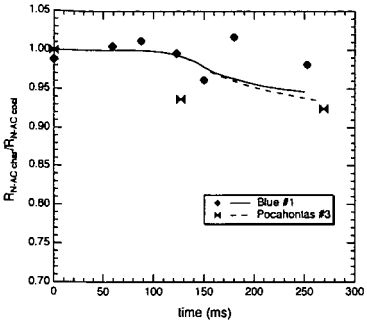

Figure 3. Comparison of predicted (lines)and measured (symbols) nitrogen to aromatic carbon ratios during rapid devolatilization at **1050** K for the chars of two coals, normalized by the nitrogen per aromatic carbon ratio in the parent coal.

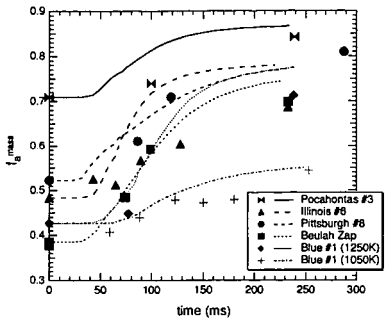

Figure 4. CPD predictions (lines) of f_a^{mass} compared with values as calculated from ^{13}C NMR analysis of coal chars produced during rapid devolatilization (symbols).

If reactivity is defined as the ease with which nitrogen is released as light gas during devolatilization, inspection of Figures 1 and 2 show that the order of HCN release reactivity for these five coals at 1250 K is Pittsburgh #8 > Beulah Zap > Blue #1 > Pocahontas #3 > Illinois #6. This order of reactivity does not correlate well with rank, nor does it seem to correlate with the O/N ratio. For the data available at 1050 K it appears that the order of reactivity is Pocahontas #3 > Blue #1. Thus Pocahontas #3 and Blue #1 appear to have different activation energies, the former releasing more rapidly than the latter at low temperature, and the latter releasing more rapidly than the former at high temperature .

Chemical Percolation Devolatilization (CPD) model predictions of f_a^{mass} during devolatilization are compared with the experimentally measured values in Figure 4. Except for Illinois #6, the predictions are quite good, generally deviating less than 4% (absolute) from the data.

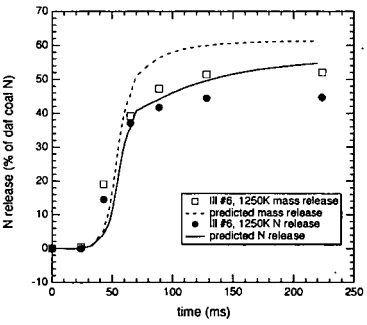

Figure 5. Predicted and measured mass and nitrogen release from 106-125μm PSOC 1493D Illinois #6 coal during rapid devolatilization at 1250 K in a drop tube reactor.

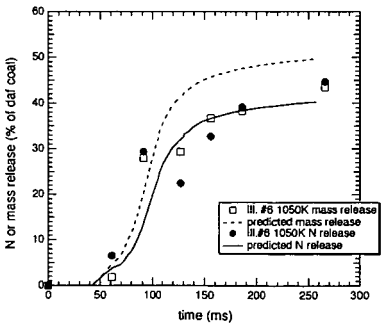

Figure 6. Predicted and measured mass and nitrogen release from 106-125μm PSOC 1493D Illinois #6 coal during rapid devolatilization at 1050 K in a drop tube reactor.

Using the CPD model for tar and total mass release predictions, the nitrogen release model (as described in the introduction) was evaluated against the data of Fletcher and Hardesty. Figures 5-12 compare the model predictions of nitrogen release as a fraction of daf coal nitrogen during rapid devolatilization against the experimentally measured nitrogen release for several coals. For the most part, the agreement is fairly good, except where mass release is incorrectly predicted. The mass release, as predicted by the CPD model, is also shown for reference, as the nitrogen release prediction depends directly on the predicted mass release according to Equation 6. In Figures 5 and 6, the nitrogen release is shown for devolatilization of Illinois #6 coal for two different gas

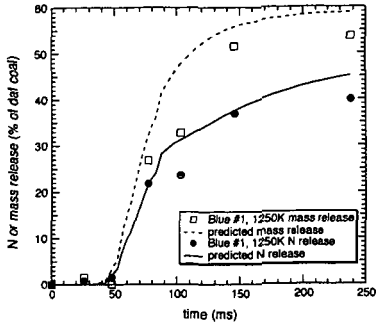

Figure 7. Predicted and measured mass and nitrogen release from 106-125μm PSOC 1445D Blue #1 coal during rapid devolatilization at 1250 K in a drop tube reactor.

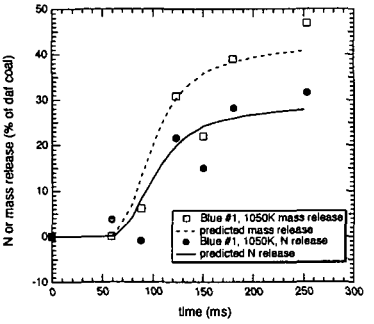

Figure 8. Predicted and measured mass and nitrogen release from 106-125μm PSOC 1445D Blue #1 coal during rapid devolatilization at 1050 K in a drop tube reactor.

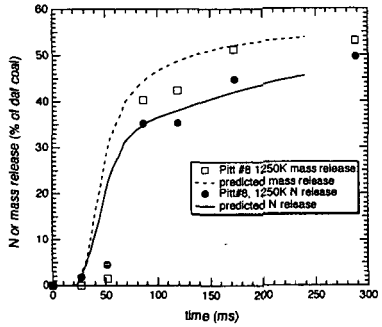

Figure 9. Predicted and measured mass and nitrogen release from 63-75μm PSOC 1451D Pittsburgh #8 coal during rapid devolatilization at 1250 K in a drop tube reactor.

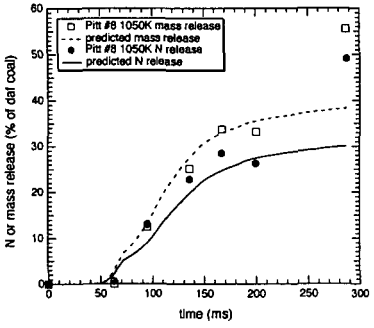

Figure 10. Predicted and measured mass and nitrogen release from 63-75μm PSOC 1451D Pittsburgh #8 coal during rapid devolatilization at 1050 K in a drop tube reactor.

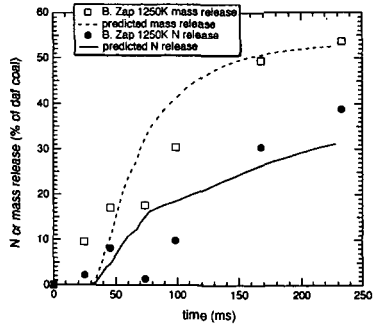

Figure 11. Predicted and measured mass and nitrogen release from 75-106μm PSOC 1507D Beulah Zap coal during rapid devolatilization at 1250 K in a drop tube reactor.

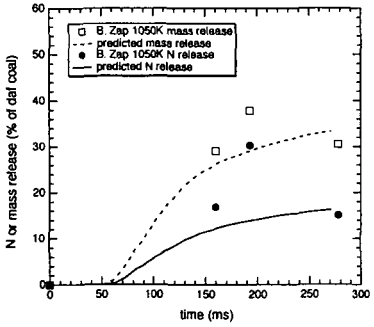

Figure 12. Predicted and measured mass and nitrogen release from 75-106μm PSOC 1507D Beulah Zap coal during rapid devolatilization at 1050 K in a drop tube reactor.

temperature profiles. The 1250 K chars for Illinois #6 seem to release very little nitrogen after 100 ms residence time. However, the experimentally measured nitrogen release at the 1050 K gas temperature condition continues to increase the entire 250 ms, eventually exceeding the level of mass release. This suggests that as much or more nitrogen was released as light gas at 1050 K than at 1250 K for Illinois #6 coal. On the other hand, Blue #1 (Figures 7 and 8) does not exhibit enhanced nitrogen release at the 1050 K condition, although the particle temperature is only 20 K cooler on average than that of the 1050 K Illinois #6 chars. This suggests a fundamental difference in the nitrogen release characteristics of the Blue #1 and Illinois #6 chars, which could possibly be due to differences in parent coal nitrogen functionality distribution. Such differences are not well modeled by a simple first-order rate expression with coal independent constants.

Conclusions

Nitrogen release models based on a dual mechanism of tar shuttling and nitrogen release from the char as light gas according to a first order rate expression with distributed activation energy can predict total nitrogen release fairly well. However, coal-dependent deviations from such a model are pronounced for the nitrogen release behavior during devolatilization. These deviations depend on coal type in a manner that seems to be independent of rank. Furthermore, the temperature dependence of the nitrogen release as light gas appears to vary from coal to coal. The reasons for these deviations are not well understood, but may be related to differences in char nitrogen functionality distribution.

Acknowledgemts

This work was funded in part by the New Energy and Industrial Technology Development Organization (NEDO) supervised by the Ministry of International Trade and Industry (MITI) of Japan, in collaboration with Professor Masakatsu Nomura at Osaka University. We also thank Dominic Genetti, Eric Hambly, and Todd Salisbury for many useful discussions.

References

Bassilakis, B., Y. Zhao, P. R. Solomon, and M. A. Serio "Sulfur and Nitrogen Evolution in the Argonne Coals: experiment and modeling," *Energy and Fuels*, **7**, 710-720 (1993).

Fletcher, T. H., A. R. Kerstein, R. J. Pugmire, M. S. Solum, and D. M. Grant, "Chemical Percolation Model for Devolatilization," *Energy and Fuels*, **6**, 414-431 (1992).

Fletcher, T. H. and Hardesty, D. R., "Compilation of Sandia Coal Devolatilization Data, Milestone Report, Milestone Report for DOE's Pittsburgh Energy Technology Center," contract FWP 0709, Sandia Report No. SAND92-8209, available NTIS (1992).

Niksa, S., "FLASHCHAIN Theory for rapid coal devolatilization kinetics. 6. Predicting the Evolution of Fuel Nitrogen from Various Coals," *Energy and Fuels*, **9**, 467-478, (1995).

Freeboard Combustion of High Ash Coals in Fluidised Bed

S V Srinivasan
S Rajaram
(Bharat Heavy Electricals Ltd., Tiruchirapalli, India)

Dr R Vasudevan
(School of Energy, Bharathidasan University, Tiruchirapalli, India)

1.0 Introduction :

Fluidised Bed Combustion (FBC) systems for firing high ash coals and low grade fuels are gaining wide acceptance in industrial and utility sectors in India due to abundance of such fuels. The resources of all types of coals in India is estimated to be 192 billion tonnes. As much as 40% of the resources contain more than 32% ash. Fluidised bed combustion is the only option to utilise these fuels in an economically viable and environmentally acceptable manner. Fluidised bed combustion has a number of attractions for steam generation. The major advantages include excellent combustion of wide variety of fuels, low pollutant emissions and increased heat transfer rates.

Commercial application of fluidised bed combustion for steam generation started in the late 70's in India. Present fluidised bed combustion boilers in India are of conservative design due to lack of information on the combustion characteristics of high ash coals in FBC. Further, since no sorbent is required with Indian coals due to their low sulphur content, the bed depths are much shallower compared to the deep beds adopted for high sulphur Western coals.

2.0 Role of Freeboard in Fluidised Bed Combustion Furnaces :

A critical grey area of FBC technology for boiler application is the design of the free board zone of the fluidised bed combustor. Free board zone is the region between the top of the fluidised bed and the first convective surface. Its primary function is to allow particles ejected from the bed to decelerate and fall back into the bed. It also provides additional gas to gas and gas to solid contact so that combustion of volatiles and char particles can take place. The phenomenon of free board combustion is a result of combustion of elutriated solids and the combustion of the unburnt volatiles. Proper estimation of the free board combustion is of vital importance in optimum design of fluidised bed combustion.

3.0 Free Board Combustion Phenomenon :

Bubble eruption at the bed surface is responsible for the solids release into the free board. Solids contained in the leading bulge portion of the bubble burst out as the bubble erupts at the free surface and are thrown up into the free board.

The possibility of incomplete combustion of volatiles in the bed and escaping to the free board also exists. Volatiles which are released during the time the coal particles are carried from the feed point to the top of the bed will be contained in an axially symmetric region centred on a vertical axis through the feed point. If sufficient oxygen is not supplied to this volatile release zone, the volatiles will escape the bed and burn in the free board.

The phenomenon of free board combustion is the net result of combustion of char in the elutriated solids and the combustion of unburnt volatiles escaping from the bed into the free board.

4.0 Free Board Combustion Model :

While individual models are available for estimating the elutriation rates and for volatile release in fluidised bed, stand-alone model to predict the free board combustion which can be directly applicable for boiler furnace design are very rare. With this purpose in mind, a model to prdict the free board combustion taking into account coal properties, coal size distribution, superficial fluidisation velocity & bed temperature has been evolved. This model has been developed for underbed fuel feeding system wherein the fuel is injected into the bed pneumatically through multiple feed points located in the air distributor. Considering the vigorous mixing and nature of combustion in fluidised bed, it is assumed that no carbon monoxide formed due to partial combustion of solid carbon in the bed escapes the bed. It is assumed that the volatile combustible portion escaping the fluidised bed, completely burns in the feee board zone which is a reasonable assumption.

Elutriation rate is determined by the following correlation :

$$\frac{E}{\rho_g U_o} = 2.19 \times 10^4 \left[\frac{\mu_g}{\rho_g U_o dp}\right]^{0.55} \left[\frac{U_o^2}{g\, di}\right]^{1.52} \left[\frac{\rho_g}{\rho_s - \rho_g}\right]^{2.6}$$

This correlation includes effects of viscous force, particle momentum & buoyancy force and hence more representative among the models for elutriation. The carbon in elutriated particle depends on the extent of combustion which has taken place in the fluidised bed. The specific burning rate is given by 1/ (1/hm + 1/Rc) , where hm is the mass transfer coefficient and Rc the reactivity. Mass transfer coefficient is determined based on Sherwood number and diffusivity. Reactivity is estimated based on rate constants for bituminous char. The same model is used for determining the carbon burn out in freeboard by suitably apportioning the rate controlling parameters.

For estimation of volatile combustion in the bed, a plume model based on instaneous release of volatiles and lateral diffusion is used. The cross-section over which the volatiles are released is determined by the solid diffusivity Dr which is estimated by using the correlation,

$$Dr = \frac{3}{10} \frac{\delta}{1-\delta} \frac{U_{mf} D_b}{\varepsilon_{mf}}$$

Extent of combustion of volatiles in the bed is dependent on the oxygen availability in this volatile release zone and the unburnt volatiles escape into the free board where the environment is conduckive for full combustion.

Enclosed figure shows the schematic of the model.

5.0 Experimental Facility & Test Details :

A test facility located in the R&D complex of BHEL, Tiruchi, was used for conducting the experiments. This facility consists of a 1m x 1m cross-section refractory lined combustor with a combustor height of 11m. Tube bundles are provided in the fluidised bed to extract heat and maintain the bed temperature. Under bed coal feeding system is provided. A shallow bed is adopted with an expanded bed height of 600 mm. The combustor is designed for balanced draft operation in the free board.

Tests were conducted with high ash sub-bituminous coals normally available for FBC boilers as fuel. The fuel rate was maintained constant in each test and the air flow rate was adjusted to obtain the required fluidisation velocity. Once the required velocity was achieved final adjustment of the coal feed rate was performed to maintain excess air levels within the selected range. After stabilising at each condition, tests were conducted for a period of 4 hours and data were collected.

6.0 Test Results & Analysis :

Free board combustion as a percentage of heat input was computed for each of the test data. Free board combustion ranged from 6 - 9% for bituminous coal depending on the superficial fluidisation velocity. The proposed mathematical model was used to predict the free board combustion under simulated condition of test runs. Figure shows the predictions from the model and the test values. It can be seen that the free board combustion computed from the test data generally tallies with the prediction. The free board combustion values are on the higher side compared to the values obtained by researchers for Western coals. Reason can be attributed to less fines and coal characteristics considered in the latters' experiments.

Also indicated are the variation of free board combustion with parameters like bed temperature,fines, fluidisation velocity and excess air. Prediction of free board combustion with variations in operating fluidisation velocity, average bed temperature, percentage fines (<1 mm) and excess air are commensurate with the operating experiece in fluidised bed combustion boilers over the ranges considered.

7.0 Conclusion :

A model has been developed to predict the free board combustion in fluidised bed boilers. This model has been validated for application to high ash Indian coals . The proposed model can be used for sizing the free board region of fluidised bed boilers in an optimum manner.

8.0 Acknowledgement :

The authors wish to thank the management of BHEL for permission to present the paper. The help rendered by the colleagues in BHEL in carrying out the work is gratefully acknowledged.

9.0 Abbreviations :

E	: Elutriation Rate Constant	di	: Size Fraction
μ_g	: Viscosity of gas	ρs	: Solid Density
ρg	: Density of gas	δ	: Bubble Voidage
U_o	: Superficial Gas Velocity	db	: Bubble Dia
dp	: Mean Particle Dia	ε_{mf}	: Voidage at Minimum Fluidisation Velocity

10 References :

1. Kunii,D and Levenspiel,O. Fluidization Engg, John Wiley & Sons inc.
2. Bing Song Xu, Elutriation Rate Constants of Fines from Fluidised Bed.'
3. Lee, Y.Y et al, Effects of Modes of Coal Feeding on Coal Volatile Release in Fluidized Bed Combustors, First Fluidized Bed Combustion & Applied Technology Symposium, Beijing, 1983.
4. Krishnan.R.P. et al, Combustion of High Ash Indian Coals in FBC, Fuel, Oct 1991.

BASIC MODEL FOR COMPUTING FREE BOARD COMBUSTION

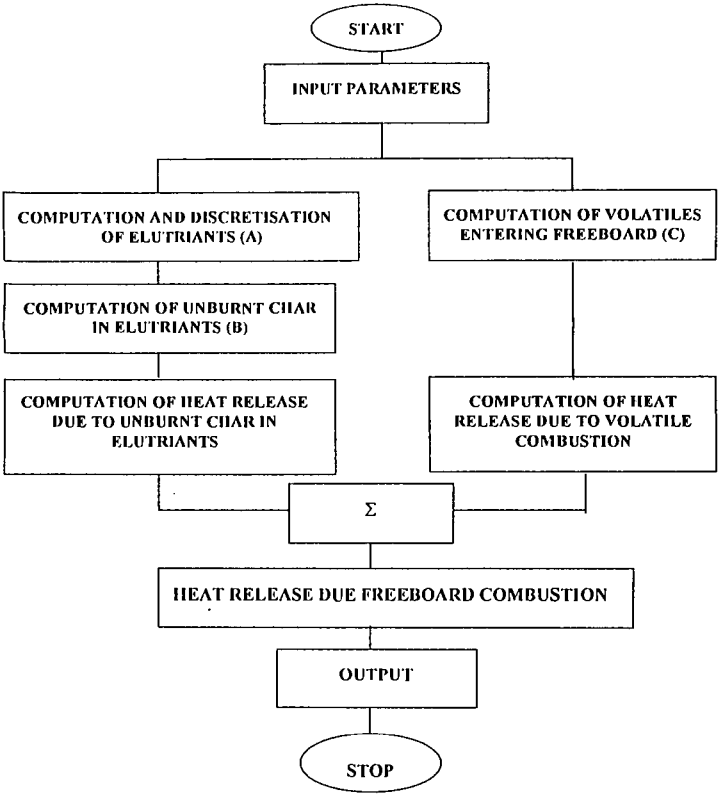

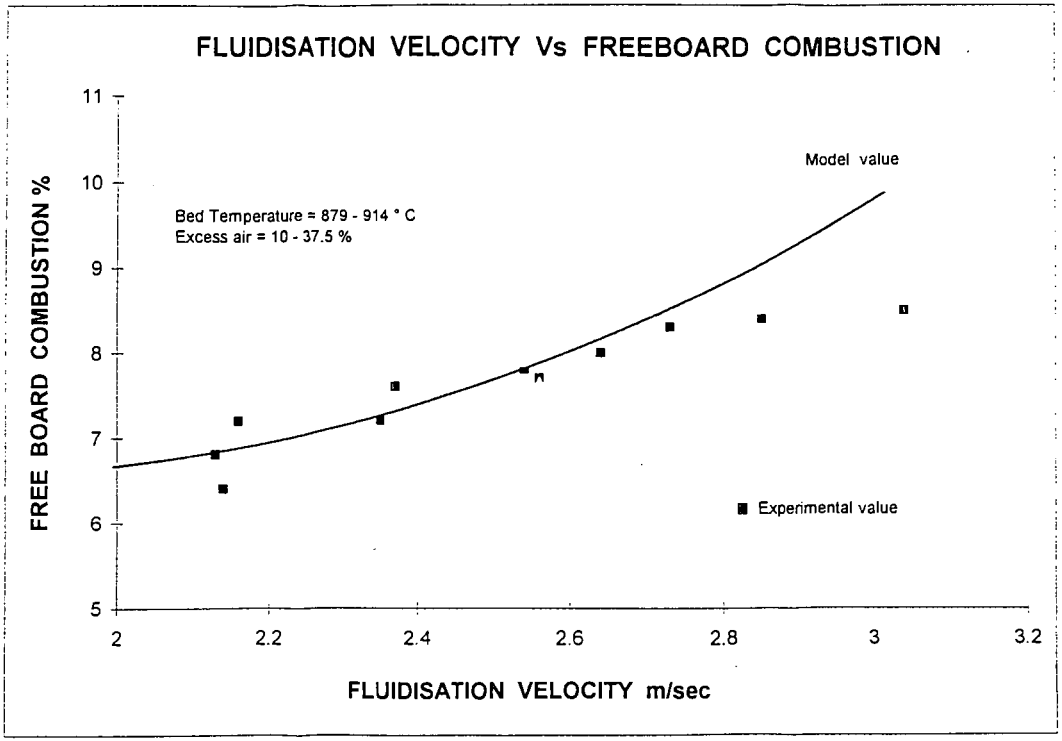
FLUIDISATION VELOCITY Vs FREEBOARD COMBUSTION
FREE BOARD COMBUSTION %
11
10
9
8
7
6
5
Bed Temperature = 879 - 914 ° C
Excess air = 10 - 37.5 %
Model value
Experimental value
2
2.2
2.4
2.6
2.8
3
3.2
FLUIDISATION VELOCITY m/sec

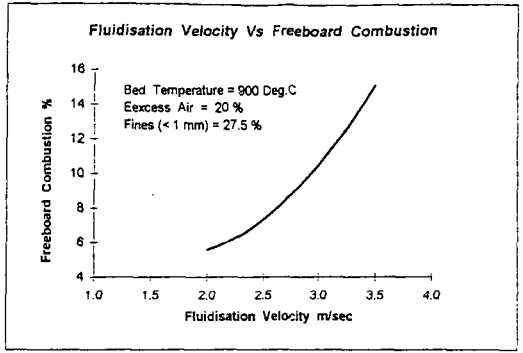

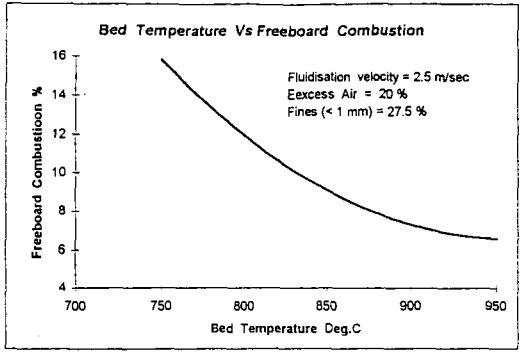

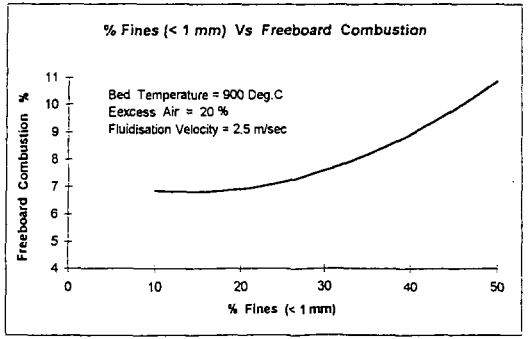

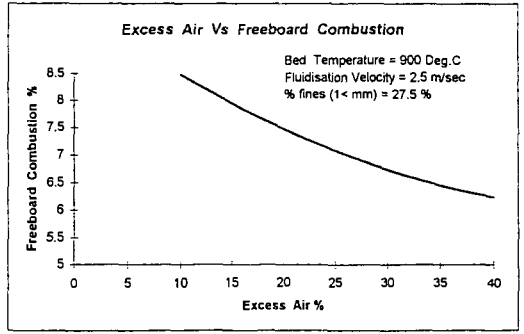

Model Predictions

THE EFFECT OF CHLORIDE ON EMISSIONS FROM ATMOSPHERIC FLUIDIZED BED COMBUSTORS

Jianghu Xu, Wei Xie, Wenjun Han, Laura Dicken, John T. Riley and Wei-Ping Pan
Materials Characterization Center, Department of Chemistry
Western Kentucky University
Bowling Green, KY 42101

Keywords: AFBC combustion, sulfur oxides, hydrogen chloride

ABSTRACT

The ability to capture SO_2 is one of the most important advantages of fluidized bed combustion. Also the capture of halogen species by limestone may help in the use of high chlorine coals. In order to clarify the affects of chlorine in the absorption of SO_2 and other emissions, experiments involving PVC addition have been carried out using the 12-inch laboratory AFBC system at Western Kentucky University. From the emission studies, the experimental results showed that SO_2 concentration in flue gases is dramatically reduced when PVC is fed into the combustor at a rate of 1% by weight of the fuel, and then leveled off when PVC feeding is 3.3%. These results are explained in terms of the interaction between SO_2 and HCl. Meanwhile, the addition of PVC resulted in decreases of CO_2 and increases in the O_2 level in the flue gas. This indicated that HCl, as a flame inhibitor inhibits CO oxidation. A mechanism involving the interaction between HCl and SO_2 in AFBC systems is proposed.

INTRODUCTION

It is well known that the emission of SO_2 from coal-fired power plants is one of the main reasons for acid rain, and SO_2 together with hydrogen chloride emitted from coal combustion may play roles in the corrosion of boiler components. Collectively, such emissions cause some operational and economic concerns.[1] In situ sulfur and halogen capture by limestone is a major advantage of fluidized bed combustion (FBC). Experimental work on the retention of sulfur and halogen species has been studied for decades. It has been found that sulfur and halogen capture by sorbents are interrelated.[2,3]

Incineration is an important waste-to-energy technology used for the disposal of municipal solid waste (MSW). However, it is necessary to reduce the possibility of the forming volatile organic compounds (VOCS) during combustion before incineration can reach its full potential. In previous work, the proposed mechanism for the formation of chlorinated organics and possibly polychlorinated dibenzo-p-dioxins (PCDDs) and polychlorinated dibenzofurans (PCDF) has been proposed as follows:[4]

PVC → HCl (undergoes thermal decomposition)	(1)
$4HCl + O_2 \rightarrow 2H_2O + 2Cl_2$ (Deacon Reaction)	(2)
$C_6H_5OH + Cl_2 \rightarrow$ chlorophenols	(3)
Condensation of chlorophenols → PCDDs and PCDFs	(4)

Chlorine gas is a key intermediate in the formation of chlorinated compounds. It is generally thought that it is molecular chlorine, but not HCl, that reacts with aromatic compounds such as phenols, to produce chlorinated aromatic compounds, such as chlorophenols and polychlorophenols, which are precursors to PCDDs and PCDFs. On the other hand, it is also believed that molecular chlorine, instead of HCl, that attacks metal in coal-fired combustion systems causing corrosion.

In previous studies, it was found that SO_2 emission decreases with an increase in the chlorine content of coal used for combustion in an AFBC system. Also, the sulfur content in ash (both fly ash and bed ash) increases in the same time. It was reported that the presence of halide species may help SO_2 capture.[2]

The main objectives of the study reported in this paper are to study the chlorine-sulfur interactions during coal combustion and to investigate new ways for using AFBC systems with high sulfur/high chlorine coal co-fired with MSW to minimize SO_2 emission and the emission of chlorinated aromatic compounds (such as PCDDs and PCDFs).

EXPERIMENTAL

All experimental work was conducted with the 0.3-meter (12-inch) laboratory AFBC system at Western Kentucky University. A full description of the AFBC system has been previously reported,[5] so only a brief description is given in this paper. In this project, an under-bed continuous feed

fuel/limestone system was installed in the AFBC system. This modification improved combustion efficiency to around 95%. Six movable bed heat exchangers in the bed area were added to the AFBC system. Typical operation involves setting the correct coal/limestone feed and air flows and then using the movable tubes to adjust the bed temperature to the desired setting. Another sixty-six gas heat exchanger tubes are in fixed position located approximately one meter from the top of the combustor. The hot gases from the combustor are allowed to enter a wet cyclone where they are met with a wall of water (which keeps the cyclone cool), which subsequently takes almost all solids to the bottom of the cyclone into a holding tank. The combustor's operating parameters (air/water flow, coal/limestone feed, fuel bunker weight, temperatures, and pressure) are controlled and logged to file with a Zenith 150 MHz computer utilizing the LABTECH software version 3.0. During the combustion runs any needed changes in the parameters can easily be entered into the computer, by accessing the correct control screen and making the necessary corrections on line.

Two coals were used in this study, an Illinois # 6 coal (0.28% Cl and 2.4% S) and an eastern Ky coal (95010). Analytical data for the two coals and the limestone used in the study are presented in Table 1. The limestone came from Kentucky Stone in Princeton, KY. The coal and limestone both were air dried before being crushed to -4 mesh (4.75 mm). The limestone also was used as the bed material in the AFBC system. The PVC was mixed with coal as a 0.1% by weight and 0.33% by weight. During combustion runs, limestone also was fed into the system at a constant rate dependent upon the fuel used.

A full description of the flue gas sampling system and procedure, as well as the fly ash and bed ash sampling procedures, has been presented elsewhere.[5-7] During combustion runs the flue gases at the gas heat exchanger region were analyzed continuously using on-line FTIR spectroscopy and gas chromatography.

The major operating parameters for the experiments were as follows: excess air level -- around 1.3; Ca/S ratio -- approximately 3; bed temperature was controlled between 1140 K and 1160 K.

RESULTS AND DISCUSSION

One of the objectives of this study was to illustrate that SO_2 emission decreases as the amount of chloride in the fuel mixture used in the AFBC system increased. PVC is the principal source of chloride in the fuels used in the study. Figure 1 shows that SO_2 emission decreases as the amount of PVC used in the fuel mixture increases. It can be clearly seen that the SO_2 emission decreases dramatically when a mixture of 1% by weight of PVC with coal is fed into the combustor, and then leveled off when the PVC content in the fuel mixture increases from 1% to 3.3%. The sulfur contents in the fly ash and bed ash increase with an increase in the amount of PVC used in the fuel. Figure 2 illustrates that the sulfur content in the fly ash increases as the PVC/fuel ratio increases. Likewise, Figure 3 shows that the sulfur content of the bed ash increases with an increase in the PVC/fuel ratio. One explanation of the increased capture of SO_2 by the limestone is that the transient formation of liquid calcium halide phases can modify the surface of the partially sulfated sorbent particles, leading to increased SO_2 capture.[2] However, a more complex mechanism includes the possibility that the SO_2 from fuel sulfur combustion would undergo reaction with Cl_2 to form HCl and SO_3. Molecular chlorine is a key organic chlorinating agent and is replaced by HCl, which is less likely to cause any chlorination of organic species. In the case of HCl emissions, both HCl concentration in the flue gas and the chlorine contents in fly ash and bed ash increase with the increase of amount of PVC in the fuel.

The results of the effect of limestone on the capture both SO_2 and HCl are shown in Tables 2 and 3. With the presence of limestone, there is a significant improvement in the sulfur capture from the flue gas. Likewise, the sulfur contents in both fly ash and bed ash increase. In contrast, there is no significant difference in the emission of HCl regardless of the amount of limestone used. These results are in agreement with previous studies in our lab,[8] as well as Liang's work,[9] in which it was reported that chlorine is not effectively captured by limestone sorbent in both bubbling and circulating fluidized bed combustors.

A possible mechanism for the interaction between SO_2 and HCl can be proposed from the combination of results from previous reports[9] and those given in this paper. Thermodynamic data[10] shows the Deacon reaction (Reaction 2, as previously given)

$$4HCl + O_2 \rightarrow 2H_2O + 2Cl_2 \text{ (Deacon Reaction)} \qquad (2)$$

is favored over the range of temperatures from 300 K to 1500 K and is exothermic at 25°C (ΔH = -114 KJ/mol, ΔG = -76 KJ/mol). An increase in temperature will cause the equilibrium to move toward the reactants, which will lower the conversion of HCl to Cl_2. Before the equilibrium is reached, however, the reaction is predominantly kinetically-controlled. A rise in temperature will

lead to more products. Yang[11] reported that in the case where the reaction takes place in a steady moving gas flow and no catalysts are present, the reaction is far from equilibrium. Consequently, a higher temperature will lead to a higher reaction rate, meaning more Cl_2 will be produced. Also it should be noted that the Le Chatelier principle indicates that the addition of oxygen to the system to enhance the combustion process would tend to form more Cl_2.

When SO_2 is present from coal sulfur combustion, a most interesting and important reaction is that SO_2 may be attacked by Cl_2 to form SO_3 and HCl:

$$Cl_2 + SO_2 + H_2O \rightarrow 2HCl + SO_3 \quad (5)$$

During atmospheric fluidized bed combustion, SO_3 will be absorbed by limestone, according to the reactions represented by the following equations:

$$CaCO_3 \rightarrow CaO + CO_2 \text{ (calcination)} \quad (6)$$

$$CaO + SO_3 \rightarrow CaSO_4 \text{ (sulfation)} \quad (7)$$

The use of limestone as the bed material and feeding coal and limestone mixtures in fluidized bed combustion will keep excess CaO in the combustor. It is believed that it is SO_3, not SO_2, that reacts with CaO to form $CaSO_4$. Reaction 7, therefore, will be favored. Consequently, this will promote SO_2 reacting with Cl_2 (reaction 5) to produce SO and HCl to minimize both SO and molecular chlorine emissions.

It has been well established that halogenated species are good flame inhibitors.[12] According to Bulewicz,[13] there is a phenomenon of halogen inhibition of oxidation of CO and other species in an AFBC system. Thus, it might be expected that the concentration of SO_2 may increase due to its incomplete combustion to SO_3 in the presence of chloride. Reaction 7, however, can promote the oxidation of SO_2 to SO in the different ways through the Deacon Reaction in the presence of chloride and oxygen-rich conditions. These two effects compete with each other during coal combustion. From our experimental results, it is clear that reaction 7 predominates over the presence of chloride as the flame inhibitor.

CONCLUSIONS

From experimental investigations in an atmospheric fluidized bed combustor system of the influence of chlorine on sulfur capture, it was shown that the presence of HCl will promote SO_2 capture. On the other hand, the presence of sulfur will lead to the reduction of the formation of molecular chlorine. As a result, a minimization of the formation of PCDDs and PCDFs results. However, the optimum Cl/S ratio for the mechanisms proposed above can not be decided from this study and further studies are needed.

ACKNOWLEDGMENTS

The authors wish to thank the United States Department of Energy for financial support of this study through grant number DE-FG-94PC 94211.

REFERENCES

1. Minchener, A.J.; Lloyd, D. M; Stringer J., *Corrosion Resistant Materials for Coal Conversion Systems,* (Ed. Meadowcroft, D.B. and Manning, M.I.), Applied Science Publishers, New York, 1996, p. 299.
2. Johnson, I.; Lence, J.F.; Shearer, J.A.; Smith, G.W.; Swift, W.M.; Treats, F.G.; Turner, C.B.; Jonke, A.A., *Support Studies in Fluidized-Bed Combustion,* Argonne National Laboratory Quarterly Report ANL/CEN/FE-79-8, 1979.
3. Griffin, R.D., *Chemosphere,* **1986**, Vol. 15, 1987-1990.
4. Li. H.; Yang, X.; Tomes, W.; Pan, W.-P.; Riley, J.T., *Journal of Thermal Analysis*, **1997**, Vol. 49, 1417-1422.
5. Orndorff, W.W.; Su, S.; Napier, J.; Bowles, J.; Li, H.; Li,D.; Smith, J.; Pan, W.-P.; Riley, J.T., Proceedings of 12th International Coal Testing Conference, Cincinnati, OH, 1996, 67-75.
6. Xie, W.; Su, S.; Li, H.; Pan, W-P.; Riley, J.T., *Prepr. Pap.-Amer.Chem.Soc., Div. Fuel Chem.,* **1997**, 42(1), 345.
7. Xie, W.; Pan, W.-L.; Shen, D.; Pan, W.-P.; Riley, J.T., *Prepr. Pap.-Amer.Chem.Soc., Div. Fuel Chem.,* **1997**, *42(1),* 364.
8. Pan, W.-P.; Riley, J.T., Behavior of Chlorine during Coal Combustion in AFBC Systems, Final Report, EPRI Contract No. W09002-13, April, 1997.
9. Liang, D.T.; Anthony, E.J.; Loewen, B.K.; Yates, D.J., 11th International Conference on Fluidized bed Combustion, Montreal, 1991, pp. 917-922.
10. Atkins, P.W., *Physical Chemistry* (4th ed.), Freeman, New York, 1990.

11. Yang, X.D., *A Chemical Pathway to the Formation of Chlorinated Compounds During Combustion,* M.S. Thesis, Western Kentucky University, 1996
12. Dixon-Lewis, G.; Simpson, R.J., Sixteenth Symposium (International) on Combustion, The Combustion Institute, Pittsburgh, 1976, pp.1111-1120.
13. Bulewicz, E.M.; Janicka, E.; Kanderfer, S., The Tenth International Conference on Fluidized Bed Combustion, San Francisco, CA, 1989, p.163.

Table 1. Analytical Data* for the Coals and Limestone Used in the Study.

	Coal 95010	Coal 95031	KY Limestone
Moisture	2.32	8.32	0.19
Ash	7.22	10.78	57.93
Volatile Matter	39.97	37.21	18.90
Fixed Carbon	52.82	52.02	22.98
Carbon	79.38	72.16	11.18
Hydrogen	5.31	4.82	0.16
Nitrogen	1.63	1.54	0.00
Sulfur	0.67	2.38	0.00
Oxygen	5.69	7.57	30.73
Chlorine (ppm)	1039	3070	36
BTU/pound	14077	12842	-----

* Moisture is as-determined, all other values are reported on a dry basis.

Table 2. The Effect of Limestone on the Distribution of Sulfur.

	Coal 95010 with 3.3% PVC		Coal 95031 with 3.3% PVC	
	with limestone	no limestone	with limestone	no limestone
SO_2 emission in the flue gas (ppm)	0.126	3.125	0.202	28.274
Sulfur content in fly ash (%)	0.739	n/a	1.295	1.271
Sulfur content in bed ash (%)	4.319	n/a	5.162	4.959

Table 3. The Effect of Limestone on the Distribution of Chlorine.

	Coal 95010 with 3.3% PVC		Coal 95031 with 3.3% PVC	
	with limestone	no limestone	with limestone	no limestone
HCl emission in the flue gas (ppm)	168.58	160.39	174.72	169.26
Chloride content in fly ash (%)	0.347	0.343	0.384	0.382
Chloride content in bed ash (%)	not determined	not determined	0.83	1.00

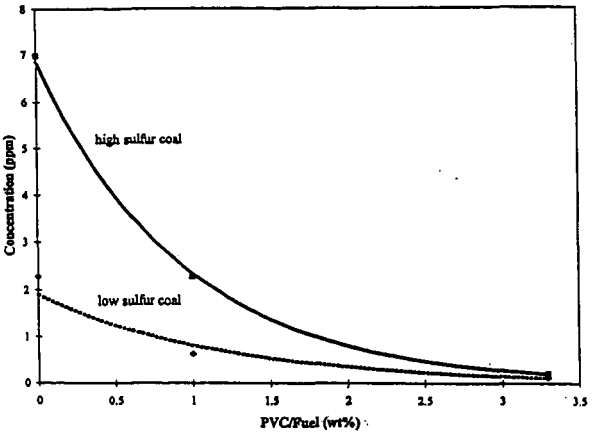

Figure 1. The effect of the PVC/fuel ratio on the emission of sulfur dioxide from the AFBC system.

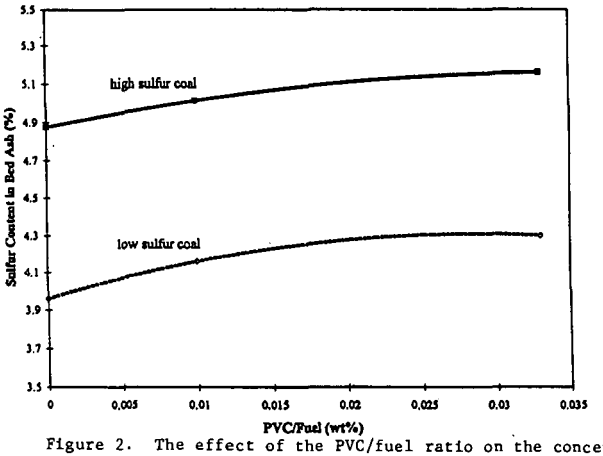

Figure 2. The effect of the PVC/fuel ratio on the concentration of sulfur in the fly ash of the AFBC system.

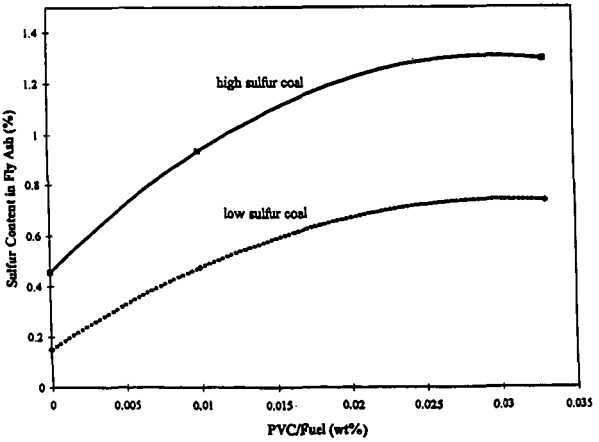

Figure 3. The effect of the PVC/fuel ratio on the concentration of sulfur in the bed ash of the AFBC system.

IGNITION BEHAVIOR OF PULVERIZED COALS: EXPERIMENTS AND MODELING

John C. Chen, Maurice D. Richardson, and Jianping Zheng
Department of Mechanical Engineering
North Carolina A&T State University
1601 East Market Street
Greensboro, NC 27411
tel: 910.334.7620; fax: 910.334.7417
email: jchen@ncat.edu

KEYWORDS: Coal ignition, coal reactivity, modeling

INTRODUCTION

This paper reports the ignition temperatures, measured directly using two-color pyrometry, for three coals under various combinations of oxygen concentration and particle size. The measurements show that a range of ignition temperatures is measured under nominally identical experimental conditions, showing that particle-to-particle variations in size and reactivity must be accounted for. Our Distributed Activation Energy Model of Ignition (DAEMI), modified to account for these variations, is applied to the results to extract ignition rate constants.

We present data from a laser-based experiment used to measure the ignitability of pulverized coals in a room-temperature gas environment. The absence of hot furnace walls surrounding the test section allowed for optical detection of the ignition process. The experimental parameters studied include the coal type, oxygen concentration, particle size, and the temperature to which particles are heated by the laser pulse. The results show clearly that ignition reactivity is strongly dependent on coal type, and that the ignition rate constants determined are consistent with published data for overall combustion reactivity. The data also show convincingly that particle-to-particle variation in physical and/or chemical property of the fuel must be accounted for in order to model the ignition data correctly, and to accurately describe their ignition reactivity.

EXPERIMENT

The experiment is similar to one described in detail elsewhere,[1] so only a brief description is given here. Figure 1 presents a schematic of the laser ignition experiment; the inset shows the details around the test section. Sieve-sized particles were dropped through a tube into a laminar, upward-flow wind tunnel with a quartz test section (5-cm square cross-section). The gas was not preheated. The gas flow rate was set so that the particles emerged from the feeder tube, fell approximately 5 cm, then turned and traveled upward out of the tunnel. This ensured that the particles were moving slowly downward at the ignition point, chosen to be 2 cm below the feeder-tube exit. A single pulse from a Nd:YAG laser was focused through the test section, then defocused after exiting the test section, and two addition prisms folded the beam back through the ignition point. Heating the particles from two sides in this manner achieved more spatial uniformity and allowed for higher energy input than a single laser pass. For nearly every case, one to three particles were contained in the volume formed by the two intersecting beams, as determined by previous observation with high-speed video.[2]

The laser operated at 10 Hz and emitted a nearly collimated beam (6-mm diameter) in the near-infrared (1.06 μm wavelength). The laser pulse duration was ~100 μs and the pulse energy was fixed at 830 mJ per pulse, with pulse-to-pulse energy fluctuations of less than 3%. The laser pulse energy delivered to the test section was varied by a polarizer placed outside of the laser head; variation from 150 to 750 mJ was achieved by rotating the polarizer. Increases in the laser pulse energy result in heating of the coal particles to higher temperatures. At the ignition point the beam diameter normal to its propagation direction was ~3 mm on each pass of the beam. An air-piston-driven laser gate (see Fig. 1) permitted the passage of a single pulse to the test section. The system allowed for control of the delay time between the firing of feeder and the passage of the laser pulse. Finally, ignition or non-ignition was determined by examining the signal generated by a high-speed silicon photodiode connected to a digital oscilloscope. Figure 2 shows typical signal traces from the photodetector for both ignition and non-ignition events. Features of the trace for the ignition case is similar to that described previously.[1]

Particle temperature was measured by two-wavelength pyrometry. A simple lens coupled to an optical fiber bundle collected light emitted by the igniting particles. The output from the fiber bundle is collimated and separated into two beams via a dichroic filter. Light of wavelengths below 0.75 μm (the dichroic filter's cut-off wavelength) was passed through a bandpass interference filtered centered at 0.7 μm with a optical bandwidth of 40 nm. The remaining light was passed through an interference filter centered at 0.9 μm with an optical bandwidth of 10 nm. Separate high-speed silicon photodiodes detected each beam following the optical filters. The pyrometer was calibrated using a 2-mm diameter blackbody source at 990°C. Figure 3 shows typical signals from the photodetectors for a representative run, and the resulting temperatures measured.

We have examined the ignition behavior of three coals: one subbituminous, and two high-volatile bituminous. All samples were obtained from the Penn State University Coal Sample Bank, and the reported proximate and ultimate analyses are shown in Table 1. The coals were sieve-sized using a Ro-Tap shaker, and dried at 70°C under vacuum for at least 12 hours prior to each day's experiment.

RESULTS

Each day's experiment was conducted as follows: After choosing the coal and oxygen concentration to examine, the coal was loaded into the batch-wise feeder. The delay time between the triggering of the feeder and the appearance of the coal batch at the feeder tube exit was measured by visual observation in conjunction with a stop watch; typical values were 2.3-2.9 s. The delay time was then programmed into the electronic trigger device that triggered the laser gate. The gas flow rate needed to achieve a drop distance of ~5 cm for the coal batch was also determined by visual observation. Finally, a laser pulse energy was chosen, and the experiment commenced. At each set of operating conditions (coal type and size, oxygen concentration, and laser energy), 20 attempts at ignition were made in order to measure the ignition frequency, or probability, which is the parameter sought from these studies. Mapping this ignition frequency over a range of laser pulse energy produces an ignition-frequency distribution.

Such a frequency distribution is shown in Fig. 4 for the Pittsburgh #8 coal. It can be seen that at each oxygen concentration, ignition frequency increases monotonically over a range of laser pulse energy. Below this range the ignition frequency is zero, and higher energies result in 100% ignition frequency. This behavior is due to the fact that, within any coal sample, there exists a distribution of reactivity among the particles.[3] Thus, in this experiment, in which a batch of perhaps several hundred particles of a sample is dropped into the test section but only a few are heated by the laser pulse, there is an increasing probability (or frequency) as the laser energy is increased that at least one of the heated particles is reactive enough to ignite under the given conditions.

Figure 4 also shows the effect of oxygen concentration: As oxygen level is decreased from 100% to 50%, the frequency distribution shifts to higher laser energies or, equivalently, higher particles temperatures, as expected. This is consistent with ignition theory since at decreased oxygen levels, higher temperatures are necessary for heat generation by the particles (due to chemical reactions) to exceed heat loss from the particles and lead to ignition. The shift in distribution can be viewed in two ways: First, for a fixed laser pulse energy, a decrease in oxygen level leads to a decrease in the ignition frequency, all else being the same; second, a decrease in oxygen implies that a higher laser pulse energy is needed, in order to achieve the same ignition frequency.

The variation in temperatures measured for separate runs under identical conditions show the existence of particle-to-particle variations in the sample. Ignition temperature variations of up to 300 K is observed from run to run. This variation is due to the combination of reactivity and/or particle size differences between runs.

DISCUSSION

Over the past three decades, many experiments have examined the ignition of pulverized coals under conditions which simulate pulverized fuel-firing conditions.[4,5,6,7,8,9] The common factor among these studies is the assumption of a single, average, kinetic rate-constant in describing the ignition reactivity of each coal. As we have shown previously,[3] it is necessary to account for the variation in reactivity among the particles within a sample in order to model the ignition distribution observed in this and nearly all previous ignition studies. Once such a

model is implemented, the parameters may then be adjusted to fit the data and produce the desired ignition rate constant and reaction order with respect to oxygen for each coal.

Our previous experience in modeling ignition distribution data[3] provides some insight to explain the results described earlier. The model details will not be described here, but it is sufficient to note that the model accounts for particle-to-particle variations in reactivity by having a single preexponential factor and a Gaussian distribution of activation energies among the particles within a sample. The distribution is characterized by two parameters, an average activation energy (E_o) and a standard deviation (σ) in the activation energy.

In light of this model, the differences in the range of laser energies over which the various coals achieved 100% ignition frequency is a direct result of the breadth of the distribution of activation energies: A narrow distribution (small standard deviation) leads to a small laser-energy range since most particles have similar activation energies and, thus, reactivities. Indeed, in the limit that the standard deviation is zero (all particles have the same activation energy), the ignition-frequency distribution would become a step function from 0 to 100% ignition frequency. Conversely, a broad distribution of reactivities (large σ) leads to a relatively larger range of laser energy needed to achieve 100% frequency. The effect of variations in the average value of the activation energy (E_o) in the distribution is to shift the ignition-frequency plot; higher E_o means lower ignition reactivity for a particular coal, which shifts the ignition distribution to higher laser energies.

Finally, with regard to the effect of oxygen concentration on the slope and shift of the ignition-frequency distributions observed for the Pittsburgh #8 coal, the model interprets such differences to be the result of the variation in the reaction order, n, with respect to oxygen concentration.

ACKNOWLEDGEMENT

The support of this project by the U.S. Department of Energy through Grants DE-FG22-94MT94012 and DE- FG22-96PC96221 is gratefully acknowledged.

REFERENCES

1 Chen, J.C., Taniguchi, M., Narato, K., and Ito, K. "Laser Ignition of Pulverized Coal," *Combust. Flame* 97, 107 (1994).

2 Chen, J.C., Taniguchi, M., Ito, K. "Observation of Laser Ignition and Combustion of Pulverized Coals," *Fuel*, 74(3), 323 (1995).

3 Chen, J. C. "Distributed Activation Energy Model of Heterogeneous Coal Ignition," *Combust. Flame*, 107, 291 (1996).

4 Essenhigh, R.H., Mahendra, K.M., and Shaw, D.W. *Combust. Flame*, 77, 3 (1989).

5 Cassel, H.M. and Liebman, I. *Combust. Flame*, 3, 467 (1959).

6 Karcz, H., Kordylewski, W., and Rybak, W. *Fuel*, 59, 799 (1980).

7 Fu, W. and Zeng, T. *Combust. Flame*, 88, 413 (1992).

8 Zhang, D., Wall, T.F., Harrie, D.J., Smith, I.W., Chen, J., and Stanmore, B.R. *Fuel*, 71, 1239 (1992).

9 Boukara, R., Gadiou, R., Gilot, P., Delfosse, L., and Prado, G. *Twenty-Fourth Symposium (International) on Combustion*, The Combustion Institute, Pittsburgh, PA, 1993, pp. 1127-1133.

Coal		Prox. Analy. (dry wt%)		Ultimate Analysis (dry, ash-free wt%)				
Penn State ID	Rank	Vol. Matter	Ash	C	H	N	S	O (diff.)
Wyodak (DECS 26)	Subbituminous	44.9	7.59	69.8	5.65	0.94	16.1 (O+S)	-
Pittsburgh #8 (DECS 23)	high-volatile A bituminous	39.4	9.44	82.0	5.63	1.49	4.27	6.66
Illinois #6 (DECS 24)	high-volatile C bituminous	40.8	13.4	66.1	4.59	1.14	14.8 (O+S)	-

Table 1: Ultimate and proximate analyses of coals used in this study.

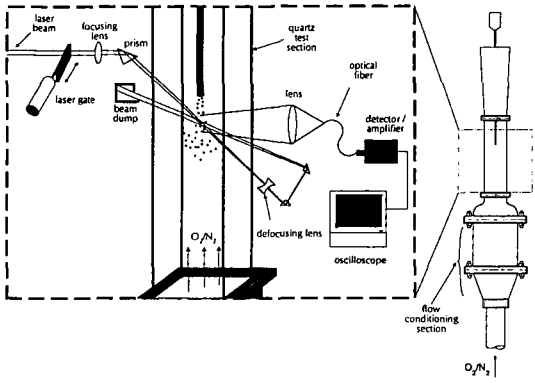

Fig. 1: Schematic of the laser ignition experiment.

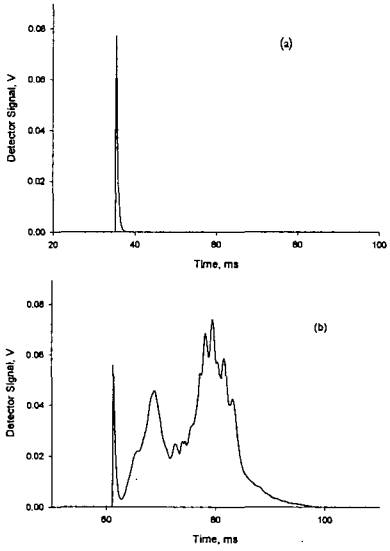

Fig. 2: Signal traces from photodetectors showing (a) non-ignition and (b) ignition events for the Pittsburgh #8 bituminous coal. Particle size was 125-158 μm, and oxygen concentration was 100%.The short-lived spike in both traces result from laser heating of the coal surface and subsequent cooling. Ignition and combustion of the coals causes the long-lived emission of (b).

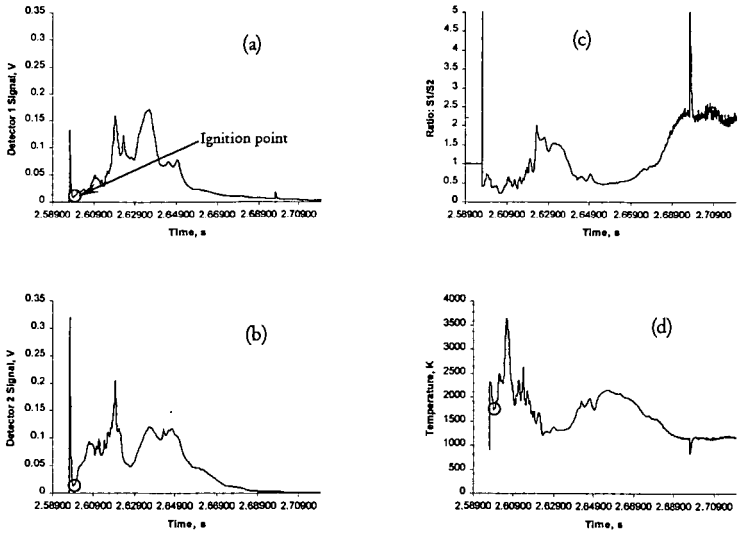

Fig. 3: Representative signal traces from experimental run with Pittsburgh #8 high-volatile bituminous coal showing (a) the signal at a wavelength of 0.9 μm, (b) the signal at a wavelength of 0.7 μm, (c) the ratio of signals, and (d) the interpreted temperatures. The ignition point is marked by circles in (a), (b) and (d).

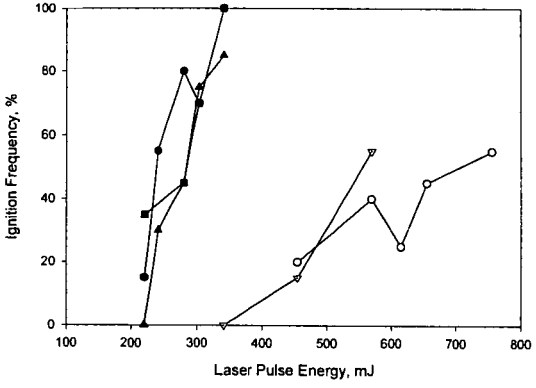

Fig. 4: Ignition-frequency distribution of Pittsburgh #8 (DECS-23) coal, 125-150 μm diameter. Solid symbols are data taken at 100% oxygen concentration, and open symbols are data for 50% oxygen concentration.

FOULING IN A 160 MWe FBC BOILER FIRING COAL AND PETROLEUM COKE

By E.J. Anthony[1], A.P. and J.V. Iribarne[2], and D.L. Granatstein[1]
1. CETC, Natural Resources Canada, Nepean, ON K1A 1M1
2. University of Toronto, Toronto, ON M5S 1A1

Keywords: FBC, Petroleum Coke, and Fouling

ABSTRACT

The 160 MW_e FBC boiler owned and operated by TVA, has recently been co-fired with coal and petroleum coke (up to 50%). However, it has suffered fouling problems. On examination of the deposits it became clear that, only in a few cases, could the fouling be partially attributed to alkali metals, and even in those cases the primarily limestone-derived materials were almost quantitatively sulphated to a level which was sufficient to cause agglomeration by itself. In other cases, it appeared that the fouling mechanism was carbonation of the free lime component of the deposit followed by sulphation. Finally, there were a few deposits, which were less sulphated than bed materials and fly ash, but where agglomeration appeared to have occurred by a conversion of the free lime in the deposits to Ca $(OH)_2$, followed by carbonation.

INTRODUCTION

Petroleum coke is a fuel of very high heating value, which is becoming increasingly available on the energy market in North America [1]. However, as fuel-grade petroleum coke contains significant amounts of sulphur in the ash, it must be burned in such as way as to minimize SO_2 emissions. One method is to burn it in a fluidized bed boiler (FBC) to take advantage of the ability of FBCs to capture SO_2 in situ, using limestone. Owing to petroleum coke's high heating value (typically 32-34 MJ/kg), co-firing with fuels such as coal or biomass is an option.

To take advantage of this relatively cheap fuel, the Tennessee Valley Authority (TVA) examined the co-firing of petroleum coke in their existing 160 MW_e CFBC boiler. However, in order to avoid re-permitting the unit, it was decided to keep the amounts of coke fired at or below 50%. A number of operational challenges had first to be resolved [2,3]. Despite their satisfactory resolution, a new problem, significant fouling in several regions of the boiler, was discovered.

Initially, it was supposed that the fouling was due either to V, which can be present at relatively high levels in petroleum coke ash, and/or to the alkali metal content of the coals used for co-firing. However, it appeared that fouling occurred over a wide temperature range, and consequently it was felt that there was, almost certainly, a number of fouling mechanisms. Hence, it was decided to carry out a detailed series of analyses to identify the most probable mechanisms for fouling and, in particular, to determine whether the V in the petroleum coke, or Na, K and Cl in the coal played a part.

EXPERIMENTAL

Five deposit samples were initially supplied by TVA (see Table 1), along with two coals, Warrior and Freeman, and one petroleum coke, Pine Bend, analyses of which are supplied in Table 2. These are the fuels used during the period preceding the collection of the deposits on shutdown of the boiler. The TVA limestone used for sulphur capture was 91.5% $CaCO_3$, with the bulk of the balance comprised of SiO_2 and Al_2O_3.

Subsequently, a number of other deposits were obtained from lower temperature regions of the boiler. These included samples from the water wall tubes, and a deposit from the multiclones, which are known to operate at about 370°C. These deposits were also examined using the same techniques described below.

The major components were analyzed by X-ray fluorescence (XRF), sulphur by Leco analysis and infrared determination, and sulphate determinations using wet chemistry. Elemental carbon was determined by Leco analysis and infrared absorption, while direct determination of carbonate content was by coulometry. All trace analyses were carried out by induced coupled plasma spectrometry, and as the total CaO content was considered a parameter of special importance, this was also checked by neutron activation, as was the V concentration.

In addition to the above, the total alkalinity (TA), and free lime (FL) were determined by wet chemical methods [4]. Some samples were subjected to phase analysis (i.e., density separation and analysis by X-ray diffraction) using special methods developed by the authors [5]. In this

way it was possible to build a complete description of the samples in terms of their constituent components. These analyses, together with those for the bed ash (BA) and fly ash (FA), are presented, along with the Ni and V data from the minor constituents, in Table 3. For comparison it should be noted that the Ni levels in the two coals are about 17 and 25 ppm, while the Ni and V levels in the Pine Bend coke are 306 and 870 ppm respectively.

RESULTS

Data from the various analyses can be used to develop the phase analysis for the deposits and this appears in Table 4. The difference (SUM-100%) in this Table is due to SiO_2, Al_2O_3, Fe_2O_3, and other calcium compounds (OCC) formed by reaction with the SiO_2 and Fe_2O_3, e.g., larnite and calcium ferrite, whose presence was confirmed by XRD.

Table 5 gives the composition of a number of samples from lower-temperature regions of the boiler. Finally, Table 6 gives the composition of two samples taken from very-low-temperature regions of the boiler (i.e., < 400°C). Unlike all other deposits examined, these were not highly sulphated. On examination with Thermogravimetric Analysis (TGA), it was shown that these deposits had substantial amounts of $Ca(OH)_2$.

DISCUSSION

The samples have been analyzed to determine the main constituent phases. As seen in Table 4, they are mainly (80%+) composed of Ca-based compounds. What is remarkable about these samples is that, with the exception of sample AD, all CaO in the deposits has been converted to $CaSO_4$. This is analogous to deposits, examined by the authors, from a Korean CFBC boiler firing 100% petroleum coke, which were almost entirely composed of $CaSO_4$ from the sorbent, with little or no CaO [6]. For comparison, it should be noted that the bed and fly ash are about 35 and 26% converted to $CaSO_4$, and contain 31 and 39% CaO respectively. Only in three cases are there significant amounts of carbonates; i.e., samples AD, NW and NNW, collected near access doors, presumably below 800°C, since $CaCO_3$ is unstable above that temperature under atmospheric FBC conditions. In the case of sample AD, the combination of $CaSO_4$ and $CaCO_3$ is probably sufficient to agglomerate the deposits, as they contain relatively low concentrations of alkali metals or V (see Table 3). It has also been shown in separate laboratory studies that carbonation is an even more effective method of agglomerating limestone-derived FBC materials than sulphation [7].

In samples NW and NNW, the conversion to $CaSO_4$ is well over 60%. This has been shown to be sufficient to agglomerate the TVA bed material by itself, when exposed to sulphating conditions in a laboratory oven [8]. It also corresponds to a situation in which limestone-derived particles must expand to allow the additional conversion, because the total pore volume produced by calcination is exceeded by this degree of sulphation [9]. A possible contribution by Na and K to the agglomeration on tubes TT and TB cannot be ruled out, but the levels of alkali metals are quite moderate compared with agglomerates formed when firing biomass, for example [10].

In the case of the samples described in Table 5, although these are more highly converted to $CaSO_4$ (varying from 45 to 66%), the presence of extremely elevated $CaCO_3$ levels is most likely the cause of the agglomeration, presumably initiated by carbonate formation with subsequent sulphation [6].

Some samples, although only slightly sulphated, were also agglomerated (see Table 6). In those samples, carbonation was clearly extremely high, and the agglomeration could be attributed to it. However, in the case of the multiclones, which were known to operate at about 370°C, it was initially difficult to explain the agglomeration, as our previous work had shown that carbonation effectively ceases below about 400°C [11]. On more careful examination it was found that significant amounts of $Ca(OH)_2$ were present in the samples, and in those from the multiclones, no CaO at all. Given that previous work showed carbonation was relatively fast down to ambient conditions if FBC ashes are first converted to $Ca(OH)_2$ (which is stable at FBC conditions up to about 450°C), it appears the free lime in the deposits is first converted to the hydroxide and then agglomerated by carbonation formation.

CONCLUSIONS

A number of deposit samples have been examined from the TVA boiler, co-firing coal and petroleum coke. All the deposits examined are primarily limestone derived, and those from higher-temperature areas of the boiler are almost quantitatively sulphated. This high degree of sulphation is sufficient to cause agglomeration, although Na and K are present in concentrations of a few percent, which may contribute to agglomeration. At boiler temperatures below 800°C,

deposits are found which, although more highly sulphated than the bed materials or fly ash, are also strongly carbonated; here the most probable cause of agglomeration is fast carbonation, followed by a slower sulphation process. Finally, some agglomerates have been found which are formed below 450°C, substantiated by the fact that any free lime in them is present as $Ca(OH)_2$, which is unstable at FBC conditions above that temperature. These samples are less sulphated than the bed material and fly ash, but are strongly carbonated. Here agglomeration is attributed to a two-step process, which involves conversion of the free lime in the sample to hydroxide followed by carbonation. To the authors' knowledge, this is the first instance of this type of agglomeration being reported in a FBC.

REFERENCES

1. Anthony, E.J., "Fluidized Bed Combustion of Alternate Solid Fuels; Status, Successes and Problems of the Technology", Progress in Energy and Combustion Science, **21,** 239-268, 1995.
2. Anthony, E.J., Carson, R., Anderson, K.D. and Lau, I., "Petroleum Coke and Coal Start Up Testing", Journal of Energy Resources Technology, **119**, 96-102, 1997.
3. Anderson, K.D., Manaker, A.M., and Stephens, E.A., "Operating Experience of the Tennessee Valley Authority's 160-MW Atmospheric Fluidized Bed Combustion Demonstration Unit, Proceedings of the 14th International Conference on Fluidized Bed Combustion, ASME, ed. F.D.S. Preto, Vancouver, B.C., May 11-14, 1997.
4. Anthony, E.J., Iribarne, A.P. and Iribarne, J.V. "Report on Analysis of FBC Ash Deposits from the Tennessee Valley Authority 160 MW_e FBC Boiler", Division Report ERL 96-01(IR), November, 1995.
5. Iribarne, A.P, Iribarne, J.V., Anthony, E.J. and Blondin, J., "The Phase Analysis of Coal Combustion Ashes", Journal of Energy Resource Technology, **116**, No. 4., 278-286, 1994.
6. Anthony, E.J., Iribarne, A.P., and Iribarne, J.V., "A New Mechanism for FBC Agglomeration and Fouling in a 100 Percent Firing of Petroleum Coke", Journal of Energy Resources Technology, **119**, 55-61, 1997.
7. Skrifvars, B.J., Hupa, M. and Anthony, E.J., Mechanism of Bed Material Agglomeration in the Cyclone and Return Leg of a Petroleum Coke Fired Circulating Fluidized Bed Boiler", Proceedings of the 14th International Conference on FBC, ASME, ed. Preto, F.D.S., pp. 819-843, Vancouver, B.C., May 11-14, 1997.
8. Anthony, E.J., Jia, L., Preto, F. and Iribarne, J.V. "Agglomeration and Fouling in Petroleum Coke Fired Boilers", Proceedings of the 14th International Conference on FBC, ASME, ed. F.D.S. Preto, pp. 839-846, Vancouver, B.C., May 11-14, 1997.
9. Couturier, M.F., "Sulphur Dioxide Removal in Fluidized Bed Combustion, PhD Thesis, Queen's University, Ontario, 1986.
10. Miles, T.R., Miles, T.R. (Jr), Baxter, L.L., Bryers, R.W., Jenkins, B.M. and Oden, L.L., "Alkali Deposits Found in Biomass Power Plants: A Preliminary Investigation of their Extent and Nature", National Renewable Energy Laboratory Report, April 15, 1995.
11. Anthony, E.J., Jia, L., Preto, F., Woods, J. and Rocque, W., "Pacification of High Calcic Residues Using Carbon Dioxide", CETC Division Report, ERL 96-20(CF), 1996.

Table 1: Sample Descriptions

Sample	Location and Description	Date Collected
AD – "B" COMPT	Access Door (Large pieces, light brown, and white. Shortly after being in contact with air and humidity, the pieces began to disintegrate into smaller pieces).	4/26/95
TT	Unground Piece of TVA-SH2, Top Tubes (Pieces of hard deposits with colored layers, dark brown, beige, reddish, which kept their form and shape).	
TTB	SH1, Near Tube Bends, Top Tubes (A dark brown powder).	4/24/95
NW	Convective Pass, SH-NW Door (A pinkish powder with some solid pieces).	4/26/95
NNW	Convective Pass, SH, Near NW Door (A pinkish powder).	4/26/95

Table 2: Fuel Analysis

Fuels	Warrior coal	Freeman coal	Pine Bend coke
Proximate analysis, wt %			
Moisture	6.56	10.03	0.63
Ash	11.00	10.17	0.48
Volatiles	31.65	33.93	10.17
Fixed carbon	50.79	45.87	88.72
Ultimate analysis, wt %			
Carbon	65.28	63.09	86.84
Hydrogen	4.57	4.36	3.42
Nitrogen	1.44	1.19	1.48
Sulphur	2.88	3.95	5.57
Oxygen (by difference)	8.27	7.21	1.58
Heating value (MJ/kg)	26.71	26.22	-

Table 3: Major Components (wt %)

Components	BA	FA	AD	TT	TTB	NW	NNW
SiO_2	3.27	4.44	3.20	8.39	4.99	7.74	8.74
Al_2O_3	0.61	1.13	0.75	4.29	2.58	2.47	2.37
Fe_2O_3	0.82	1.85	0.91	2.98	1.86	4.01	4.35
CaO	60.3	63.5	59.5	34.6	34.1	32.3	31.8
MgO	3.5	1.92	3.48	1.67	1.20	2.03	2.02
Na_2O	0.02	0.08	0.41	1.54	1.98	0.18	0.15
K_2O	<0.01	0.1	<0.01	1.02	1.04	0.34	0.33
TiO_2	0.042	0.048	0.05	0.37	0.28	0.13	0.12
MnO	0.01	0.02	0.01	0.03	0.02	0.02	0.02
Cr_2O_3	<0.01	<0.01	<0.01	0,02	0,03	<0.01	<0.01
P_2O_5	0.05	0.04	0.03	0.15	0.07	0.04	0.03
SO_3	30.70	23.5	28.3	46.5	49.3	46.3	46.5
LOI	1.05	4.62	4.6	-0.30	1.05	3.3	3.1
SUM	100.37	101.25	101.2	101.3	98.5	98.9	99.6
Ni (ppm)	69	30	-	-	831	155	119
V (ppm)	329	127	447	3034	3008	533	367

Table 4: Phase Composition of Deposits (wt %)

Component	AD	TT	TTB	NW	NNW
$CaSO_4$	48.0	79.0	80.3	75.6	75.2
CaO	28.5	0.8	0.2	0.1	0.0
$CaCO_3$	5.9	0.3	0.5	5.8	5.3
SUM	82.4	80.1	81.0	81.5	80.5
R[1]	33	94	97	96	97

1. R is the degree of conversion of Ca compounds to $CaSO_4$ on a % molar basis

Table 5: Phase Composition of Lower-temperature Deposits (wt%)

Sample/Component	$CaSO_4$	CaO[1]	$CaCO_3$	Δ^2
White coating on sloped walls	49.9	4.7	12.0	23.7
Light coat on waterwall tubes	40.9	9.9	19.0	22.7
Near Manway G on compt. waterwalls, 8 ft. from feed	51.4	9.7	25.7	9.4

1. Includes both CaO and OCC
2. Δ represents non-Ca-based components

Table 6: Phase Composition of Very-low-temperature Deposits (wt%)

Sample/Component	$CaSO_4$	OCC[1]	$Ca(OH)_2$	CaO	$CaCO_3$	Δ^2
Tenacious coat starting in compartment 8 ft. above feed	23.6	10.6	6.2	4.9	45.3	11.7
Multiclone deposits	14.5	16.3	16.3	0	32.9	18.5

1. OCC are expressed as CaO
2. Δ represents non-Ca-based components

CHARACTERIZATION AND PREPARATION OF BIOMASS FOR CO-COMBUSTION WITH COAL

Volker Siegle, Hartmut Spliethoff, Klaus R.G. Hein
University of Stuttgart, IVD, Pfaffenwaldring 23, 70569 Stuttgart, Germany
Tel. / fax: #49-711-685-3575 / #49-711-685-3491

INTRODUCTION

The reduction of the greenhouse gas CO_2 is the topic of many discussions in Europe. The substitution of CO_2 neutral fuels like biomass for coal in energy production could help to reach this aim. A fast attainable way for the use of biomass is to direct replace part of the coal in power plants. First, demolition and waste wood as well as wood residues from the forest and residual straw from agriculture should be used for co-combustion. In a second step specially cultivated energy plants like salix, poplar and also energy cereals should be taken into account. For the cultivation of salix and poplar farmers have only little experience. Cereal cultivation, however, is state of the art. Therefore the use of cereals as energy crops for co-combustion seems to be a promising technique.

BIOMASS ANALYSIS

In Germany, analyzing biomass for thermal use is subject to the problem that there are no generally valid guidelines for the method way of carrying out the analysis. Therefore the usual, and also reasonable, methods applied are the same as in solid fuel analysis. To a large extent, this way seems to be justifiable, yet might also arise difficulties. This problem shall be demonstrated by taking the determination of the ash content as an example.
That is, the incineration temperatures for wood fuels, according to the standards (Table 1), vary between 550 and 815°C. For strawlike fuels, there are no regulations at present. The dependence on the incineration temperature of the measured ash content in various fuels is presented in Figure 1. It can be seen that the ash content of all the examined biomass types decreases with rising incineration temperatures. This decrease, however, is particularly clear in the case of straw. The ash content at low temperatures most likely corresponds to content of mineral matter. The part of mineral matter in coal is usually 10% above the ash content. The "content of ash" of the straw sample incinerated at 500°C is 22% above its content at 800°C, the wood sample even shows a difference of 50%.
To find out the inert parts that escape from the ashes at the higher incineration temperature, the main ash components of the incinerated sample were analyzed.
Figure 2 exemplifies the concentrations of ash components, referring to the fuel, of samples of different incineration temperatures. It is evident in particular that the concentrations of calcium, potassium, and magnesium decrease with rising incineration temperatures.
In the case of potassium, a remarkable minimum can be noted in the temperature range of 700°C, both with straw and with wood, which means that the potassium escapes. At higher incineration temperatures, the 700°C range is passed quickly, hence, less potassium escapes because it can be bound to other ash components.
The decreasing ash contents with rising temperatures are of major importance for both pure biomass combustion and co-combustion of biomass in pulverized fuel firing at flame temperatures of 1300 to 1400°C and more, since the escaping substances may substantially contribute to slagging and corrosion. Furthermore, for the ash balance, the consequence arises therefore that the high volatile components have low recovery rates. For instance, by the ash balance of a pure straw flame only 50 per cent of the potassium could be recovered, yet almost 90 per cent of the less volatile sodium. Once the substance has volatilized, it not necessarily deposits again on ash particles when the condensation temperature is reached but on all the available surfaces and thus is lost for the balance, but contributes to slagging and corrosion.

Biomass Heating Value and its Components

For the investigation of natural biomasses, more than hundred different biomass types were analyzed with regard to their contents of carbon, hydrogen, nitrogen, sulfur and chlorine, and to get their heating value. In addition, analyses analogous to the proximate analysis of coal, were carried out on the biomasses to find out the contents of volatiles, fixed carbon and ash. The fuels investigated were various sorts of straw, wood, whole plants and grains. The volatiles content of

all the biomasses typically range from 76 to 82 per cent. Their fixed carbon content is between 15.5 and 19 per cent. The average carbon content reaches from 47.5 per cent in whole plants and grains over 49.2 in miscanthus to about 51 per cent in wood. Like the carbon content, the average heating value of the biomasses, too, rises from whole plants to wood, i.e. from about 17.6 MJ/kg of annual whole plants over miscanthus with 18 MJ/kg to 18.7 MJ/kg of wood. The mean values, referring to dry, of the investigated biomass components are summarized in Table 2.

The heating value can on the one hand be measured with a calorimeter or on the other be calculated with empirical formulae by elementary analysis. Boie has developed a formula for young fuels (younger than hard coal), which was tested to find out whether it would be applicable also to the youngest fuel, biomass. As a first step though, the expected standard deviations of the two determining methods were compared. To this end repeated determinations of the upper heating value (UHV) of different coals and biomasses were carried out with a calorimeter. The same was done to determine in addition the content of carbon, hydrogen, nitrogen and sulfur as well as the moisture and the ash content. The standard deviation with calorimeter determination method is 150 kJ/kg. From the element contents, the LHV can be evaluated with Boie's formula. With this method of heating value determination, the mean standard deviation was 200 kJ/kg. Thus, in the case of biomasses with their usual heating values between 16,000 and 20,000 kJ/kg, the deviation is about 1 per cent of the full-scale value for both determination methods. These deviations are the limits of accuracy of the analysis systems, and, first of all, they are independent of the fact whether Boie's equation holds or not.
In Figure 3, the lower heating values evaluated according to Boie are outlined above the measured values. The mean values are in the range given by Boie of +/- 420 kJ/kg. Wood, in this case, is rather found at the upper margin whereas the values of gramineous biomass such as straw, whole plants and cereals lie at the lower margin of this range, i.e. Boie's formula calculates the heating value of these fuels by 2.5 per cent too low. This corresponds to the experiences by STÜLPNAGEL ET AL. who obtained values of annual crops which were too low by 3.3 per cent. The scatter around the mean values is clearly lower with the homogeneous biomasses wood and miscanthus than with whole plants, grains, and straw. The conclusion to be drawn from this is that in establishing the heating value by ultimate analysis and Boie's formula, on average, sufficiently precise values will result but by single analyses greater deviations have to be taken into account.

Preparation of Whole Plants for Co-Combustion in Pulverized Fuel Firings

Whole cereal plants consist of a straw and a grain part. The weight percentage of these two component parts are more or less equal, and the same holds for their weight-related heating value. The density, however, of the two elements differ considerably. The grain's density is distinctly higher than that of straw, which entails a higher energy density of the grain. The measurement of the density is based on gas displacement. In this method, an empty reference sample vessel and another vessel filled with a weighed sample are filled at liquid-nitrogen temperature (-196°C) with the same amount of gas. The displaced volume is then evaluated by the pressure difference developing this way. Consequently, the weight data of the probe being given, the particle density can be calculated.
The particle density of straw, and of wood, too, depends on the grain size. Through the increasing size reduction by milling, inclusions of air in the cells and capillaries are opened and accessible for gases. In the coarse state, these inclusions are part of the solid volume. For particle sizes smaller than 300 µm, this means higher densities. Grains are denser in the state of rawness than straw. Their density, too, increases with smaller grain sizes.
The size reduction of straw and wood is done principally by cutting along the grain, i.e. elongated fibrous particles are produced. Grain milling results in rather compact spherical particles. Decisively important for the ignition and combustion of particles in a pulverized fuel firing is the proportion of surface to volume which, in turn, depends on the particle size.
Figure 3 demonstrates the dependence of surface on volume for different particle forms. The spherical form appears to be the most unfavorable whereas elongated particles show a better surface-to-volume proportion. This makes obvious that grains, in order to complete combustion within the given residence time in a pf firing, have to be ground to a finer size than straw. This could also be demonstrated by combustion experiments.

Combustion Experiments

For combustion experiments to compare straw and whole plants, straw was milled in a cutting mill with a 6 mm insert sieve, for the whole plants was used a 1.5 mm insert sieve. The obtained mean particle size was about 1 mm with straw, and 500 µm with whole plants. In order to obtain a yet finer grinding, one whole plant was milled several times which brought about a mean particle size of 110 µm. These fuels were combusted in varying thermal shares combined with hard coal in the IVD experimental pf firing facility and analyzed with regard to their burnout. In the case of a decreasing share of the coarsely milled whole plant in co-combustion, a drop in the burnout degree can be recognized whereas with straw and the very finely ground whole plant, the burnout degree stays constantly high. This means that straw in whole-plant preparation has to be ground much too finely in order to have the grain part burned out completely, too.
A complete burnout is the precondition for subsequent pollutant-reducing measures. Because of the high fuel nitrogen content of whole plants, increased NO_x emissions from combustion will have to be reckoned on. For this reason, primary NO_x-reducing measures in whole-plant utilization are especially important.
Primary measures for NO_x reduction should be interpreted as interventions in the combustion course in order to prevent formation of nitrogen oxides from the outset. This can be done either by staged air injection and reburning, respectively, or by an adequate injection of the fuels through the burner. Fig. 5 shows the different ways of fuel injection with a multi-fuel burner. In the case of the configuration "preblended", the fuels are blown in together via the annular orifice, each with 50 m3/h carrier air, and with "preblended central" both fuels are injected central. The configurations "coal central" and "biomass central" mean that one of the fuels is injected by the central orifice and the other one by the annular orifice. The effects of the different burner configurations on NO_x emissions with various shares of whole plants are represented in Fig. 6.

Cereal and Coal Preblended via Annular Orifice
In case of the annular-orifice injection, the fuel has already been well mixed with the swirled secondary air when entering the first reaction phase. This results in an increased oxidation of the fuel nitrogen into nitrogen oxide. If biomass and coal are injected through the annular orifice, the NO_x emissions slightly decrease with an increasing share of biomass despite the higher nitrogen input. The reason for this are the different ways nitrogen is captured in the two fuels and the lower tendency of the biomass nitrogen to convert into NO_x.

Cereal via Centre, Coal via Annular Orifice
In this configuration, the primary air is split into two even fractions: one injected through the annulus as coal transport air, the second injected through the centre to transport the biomass. The two fractions are the same for all the coal/biomass ratios. As a result, when a pure coal flame is fired, the coal enters the combustion chamber already mixed with only the half of the total primary air. This is the reason why for this flame the NO_x emissions are somehow lower with this configuration then with the previous one.
Then, taking small whole-plant shares, the NO_x emissions slowly rise until the biomass amount has consumed all its available primary air quantity. From a biomass share of 20% of the thermal input on, the NO_x emissions drop distinctly because the fuel is injected into the substoichiometric, inner recirculation zone and part of the fuel nitrogen becomes reduced to elementary nitrogen.

Cereal via Annular Orifice, Coal via Centre
The pure coal flame here emits the smallest amount of NO_x since the whole fuel nitrogen reaches the substoichiometric, inner recirculation zone. With larger shares of biomass, the NO_x emissions increase though this rise is less distinct than the drop of the curve in the above case. With a 35% share of biomass the input of nitrogen by biomass and by coal is the same amount each. Consequently, the curves of this configuration are supposed to cut those of the previous configuration in this area. Yet they only do so with a biomass share between 40 and 50%. The reason for this is again the lower tendency of the biomass nitrogen to oxidize into NO_x, even if there is enough oxygen available in the area of the biomass injection.

Cereal and Coal Preblended via Centre
In the fourth configuration, the fuel mixture of cereal and coal, and thus the entire fuel nitrogen, is centrally fed to the inner recirculation zone. The NO_x emissions, for biomass shares up to 40%, show the same behavior as in the previous configuration "cereal via annular orifice, coal via centre". However, with more than 40% of biomass, the NO_x emissions decrease. The reason for this is that more fuel nitrogen is entered by the biomass than by the remaining coal share. With this burner configuration, the lowest NO_x-emission level of the whole sequence of experiments is

achieved with a 100%-cereal flame. The fuel (with these flames) is injected into the inner recirculation zone with two times the primary air amount, i.e. with a high impulse. Due to the lacking oxygen in this zone, only little fuel nitrogen is oxidized into NO_x.

CONCLUSIONS

- Establishing the heating value of biomass by ultimate analysis and Boie's formula, on average, sufficiently precise values will result but by single analyses greater deviations have to be taken into account.
- Because of the different grinding character and particle structure of straw and grain the grain have to be ground finer than the straw to reach sufficient burnout.
- If in an existing swirl burner premixing of fuel is not possible or not desired because of other disadvantages, the fuel with the higher nitrogen contend should be injected through the centre into the inner recirculation zone.
- The fuel-N of biomass has a lower tendency to convert into NO_x than the fuel-N of coal.

REFERENZES

R. Stülpnagel et al.: Investigations for a cheap estimation of the net calorific values of different biomasses, 7th E.C. Conference, Biomass for Energy and Industry, S. 969 - 973, 5.-9.Oct.92, Florence, Italy

TABLE 1: Incineration temperatures of different standarts

	application	incineration temperature
ASTM D 3174	Coal, Coke	700 - 750 °C
ASTM E 830	RDF	750 ± 25 °C
ASTM D1102	Wood	580 - 600 °C
DIN 51 719	Coal, Peat,	815 ± 15 °C
DIN 51 749	charcoal	710 ± 15 °C
DIN 52 182	wood pellets	550 °C
Ö-Norm 1074	wood	815 °C

TABLE 2: Analysisdata of biomass, dry basis

	volatiles wt %	fixed C wt %	C wt %	H wt %	N wt %	S wt %	Cl wt %	LHV kJ/kg
cereals	79,5	16,0	47,6	5,3	1,13	0,13	0,41	17,6
grain	80,5	17,2	47,5	5,4	1,86	0,11	0,26	17,8
straw	79,5	14,5	46,8	5,4	1,0	0,1	0,5	17,4
Miscanthus	81,0	16,1	49,2	5,8	0,24	0,08		18,0
wood	80,5	17,4	50,9	5,7	0,5	0,09	0,1	18,7

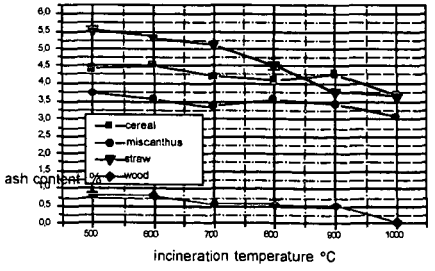

Fig. 1: ash content dependend on incineration temperature

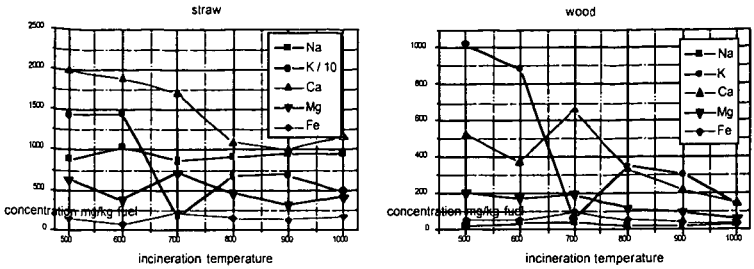

Fig. 2: Concentration of the ash components at different incineration temperatures

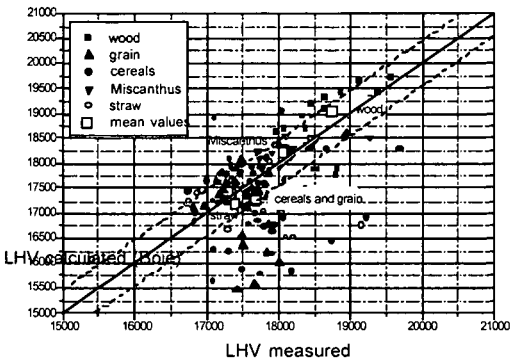

Fig. 3: LHV measured compared with LHV calculated

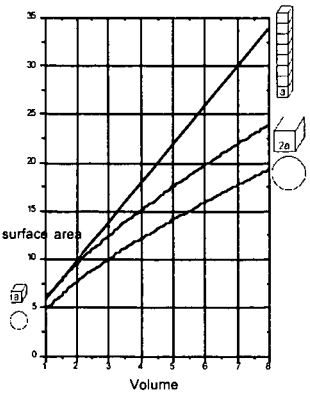

Fig. 4: Dependence of surface on volume

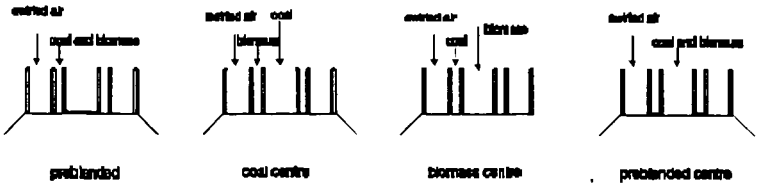

Fig. 5: Burner configurations

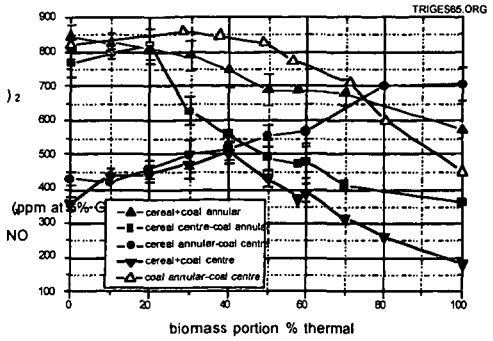

Fig. 6: NO_x emissions with different burner configurations

STUDIES OF THE MECHANISM FOR THE FORMATION OF CHLORINATED ORGANICS DURING THE COMBUSTION OF MSW AND COAL

Jianghu Xu, Ying Xie, Jeremy Bowles, Wei-Ping Pan and John T. Riley
Materials Characterization Center, Department of Chemistry
Western Kentucky University
Bowling Green, KY 42101

Keywords: Co-firing MSW, chlorinated organics, combustion mechanisms

ABSTRACT

Several kinds of coals and the major combustible components in MSW, such PVC and cellulose, were tested in this project. TGA/MS/FTIR analyses were performed on the raw materials and their blends, and the combustion profiles collected indicated various types of thermal behavior. The results indicated greater possibilities for the formation of organic compounds during co-firing at fast heating rates than at slow heating rates. Experiments in a tube furnace showed that molecular chlorine is a key intermediate for the formation of chlorinated organics during the combustion of MSW. A mechanism proposed for the formation of chlorinated organics includes the Deacon Reaction. Experiments conducted using pure organic compounds verified this reaction as a possible pathway. The effect of sulfur dioxide on the formation of molecular chlorine during combustion processes was examined. The results indicate the introduction of SO_2 does minimize the formation of molecular chlorine and subsequently chlorinated organics.

INTRODUCTION

The amount of municipal solid waste produced in the United States each year has risen to more than 200 million tons. According to a prediction by the Environmental Protection Agency (EPA) this amount will rise to 216 million tons by the year 2000.[1] Landfilling, which is the traditional way to deal with this waste, is becoming more and more impractical owing to the rapidly declining availability of landfill space and stricter environmental regulations. Incineration of the MSW is one of the alternative waste management technologies that has some advantages over the conventional methods. However, due to the concern over emissions of hazardous chlorinated organics, especially the harmful polychlorinated dibenzodioxins (PCDDs) and dibenzofurans (PCDFs), the development of technology for the incineration of MSW has slowed significantly.

Despite reports of significant amounts of PCDDs and PCDFs being found in the emissions of municipal waste combustors, they were not detected in the effluents from a combined coal/municipal waste plant, nor were noteworthy amounts found in the fly ash.[2] Several mechanisms have been proposed to explain the formation of PCDD or PCDFs during the combustion of MSW, and molecular chlorine has been recognized as a key intermediate. One of the possible pathways for the formation of PCDDs and PCDFs is associated with *de novo* synthesis from compounds within the flue gas and fly ash.[3] This synthesis involves the Deacon Reaction and is represented by the following steps:

$PVC \rightarrow HCl$ (thermal decomposition) (1)

$4HCl + O_2 \rightarrow 2H_2O + 2Cl_2$ (Deacon Reaction) (2)

$C_6H_5OH + Cl_2 \rightarrow$ chlorophenols (3)

Condensation of chlorophenols $\rightarrow$ PCDDs and PCDFs (4)

From the Deacon reaction, molecular chlorine is produced and subsequently chlorinates aromatic compounds through substitution reactions. In our study, the source of HCl has been confirmed as the thermal decomposition of chlorine-containing plastics. Chlorine gas may be generated in-situ from HCl and oxygen in the combustion gases of MSW incinerators via the Deacon Reaction.

The use of coal as a co-firing energy source for municipal wastes may inhibit the formation of chlorine-containing organic compounds. Some conclusions have suggested an inhibitory effect of increased SO_2 concentration with regard to PCDD/PCDFs formation. Scheidle and co-workers demonstrated that adding lignite coal as an auxiliary fuel to paper recycling residues decreased the levels of dioxins in fluidized-bed incinerator emissions.[4] Based on the thermodynamic evaluation and published test data, Griffin proposed that as long as the Cl/S ratio is high, chlorine formation for the elevated production of chlorinated aromatics and PCDD/Fs is prevalent, but in the presence of substantial amounts of sulfur, chlorine production and consequently, PCDD/Fs formation is suppressed.[5] Gullett and co-workers reported that high concentrations of a sulfur species (sulfur dioxide) are responsible for the apparent lack of PCDDs and PCDFs in the emissions from coal-fired combustors.[6] Lindbaurer showed that co-firing MSW with 60% coal drastically reduced the formation of PCDD/PCDF.[7] Co-firing coal and MSW seems to have the dual advantage of being

a source of energy and having the potential of reducing the formation of chlorinated species in combustor emissions.

There are several different mechanisms involving sulfur species proposed for limiting PCDD production, one of which suggested that in coal combustion, the role of sulfur interference with the chlorination step (and hence the formation of PCDDs) is critical. When sulfur is present in excess over chlorine, in any system, the forward reaction predominates:

$$SO_2 + Cl_2 + H_2O \rightarrow SO_3 + 2HCl$$

Thus the chlorinating agent, chlorine, is converted into HCl, which is very unlikely to undergo aromatic substitution reactions to form PCDD and PCDF precursors. In the project reported in this paper, this reaction was examined in a tube furnace. The results indicated an apparent inhibiting effect of sulfur on the Deacon reaction.

Municipal solid waste (MSW) varies considerably in composition. The noncombustibles of MSW, such as metals and glasses, were excluded from this study. Refused-derived fuels (RDF) are made from the combustible components of MSW. The combustion and thermal decomposition process of these individual materials and their blends were examined in this study using TGA/FTIR/MS and GC/MS techniques. The combination of TGA/FTIR and TGA/MS offers complementary techniques for detection and identification of the evolved gases. This kind of on-line analysis has advantages in providing the relationship between the combustion products and time/temperature.

EXPERIMENTAL

1. TGA/FTIR/MS System

Small amounts of tested materials were placed in the TGA and heated to 1000°C at different heating rates in a dynamic air atmosphere. The spectra and profiles of gas species flowing out of the TGA were recorded and analyzed by the TGA/FTIR/MS analytical system. The three key components of this system are as follows:

- Model 951 Thermogravimetric Analyzer (Dupont Instruments)
- Model 1650 Fourier Transform Infrared Spectrophotometer (Perkin Elmer)
- VG Thermalab Gas Analysis System (Fisons Instruments)

The TGA is interfaced to the FTIR using an insulated teflon tube heated to a temperature of 150°C by a Powerstat variable autotransformer. The 25 mm x 10 cm gas cell with KBr windows used with the FTIR is heated using a Barnant thermocouple controller. The tube and gas cell are heated to prevent possible condensation of the gaseous products. The TGA is also interfaced to the mass spectrometer using a fused silica capillary sampling inlet that is heated to approximately 170°C.

2. Studies with the Tube Furnace

To simulate the conditions used in the AFBC system, tests were performed in a concentric tube, quartz reactor inserted into the horizontally mounted electric Lindberg furnace. To study the combustion performance of the materials of interest, the furnace was preheated to the desired temperature before the sample was introduced. The composition of the process gases can be adjusted by the calibrated teflon flow meters before being introduced into the reaction system.

The reaction products were swept into a cold trap containing a chosen absorbent. After the reaction was completed, the solvent was concentrated, and the sample analyzed using the GC/MS system. A Shimadzu QP 5000 system with a NIST/EPA/NIH 62,000 compound database was used for GC/MS analysis. The identification of compounds was accomplished by using a computerized library search and by comparison with literature mass spectra. Moreover, comparing to the GC retention time of the pure compounds helped confirm the identification of the unknowns. Standard materials were tested to establish the detection limits of the experimental set-up.

3. Laboratory Fluidized Bed Combustion Tests

The laboratory scale (12-inch) atmospheric fluidized bed combustor at Western Kentucky University was used in this study. The active bed area is 125 in^2. The freeboard zone of the combustor is 10 feet high, providing adequate residence time for the combustion of fine fuel particles which may be entrained in the gases leaving the bed. The fuel is injected into the fluidized bed by using pneumatic injectors. The injectors used for these tests are located about 9 in above the air distributor of the combustor. The bed temperature is controlled by the fuel feed rate adjustment.

Evolved gases from the combustor were analyzed by gas chromatography and FTIR spectroscopy. To determine if any chlorinated organic compounds were formed during the combustion reactions, the combustion gases were collected in Tenax adsorption tubes. The collected samples were extracted separately with hexane (99.9%) for 24 hours using a soxhlet extraction apparatus. The samples were then analyzed using a GC/MS system.

a source of energy and having the potential of reducing the formation of chlorinated species in combustor emissions.

There are several different mechanisms involving sulfur species proposed for limiting PCDD production, one of which suggested that in coal combustion, the role of sulfur interference with the chlorination step (and hence the formation of PCDDs) is critical. When sulfur is present in excess over chlorine, in any system, the forward reaction predominates:

$$SO_2 + Cl_2 + H_2O \rightleftharpoons SO_3 + 2HCl$$

Thus the chlorinating agent, chlorine, is converted into HCl, which is very unlikely to undergo aromatic substitution reactions to form PCDD and PCDF precursors. In the project reported in this paper, this reaction was examined in a tube furnace. The results indicated an apparent inhibiting effect of sulfur on the Deacon reaction.

Municipal solid waste (MSW) varies considerably in composition. The noncombustibles of MSW, such as metals and glasses, were excluded from this study. Refused-derived fuels (RDF) are made from the combustible components of MSW. The combustion and thermal decomposition process of these individual materials and their blends were examined in this study using TGA/FTIR/MS and GC/MS techniques. The combination of TGA/FTIR and TGA/MS offers complementary techniques for detection and identification of the evolved gases. This kind of on-line analysis has advantages in providing the relationship between the combustion products and time/temperature.

EXPERIMENTAL

1. TGA/FTIR/MS System

Small amounts of tested materials were placed in the TGA and heated to 1000°C at different heating rates in a dynamic air atmosphere. The spectra and profiles of gas species flowing out of the TGA were recorded and analyzed by the TGA/FTIR/MS analytical system. The three key components of this system are as follows:

- Model 951 Thermogravimetric Analyzer (Dupont Instruments)
- Model 1650 Fourier Transform Infrared Spectrophotometer (Perkin Elmer)
- VG Thermalab Gas Analysis System (Fisons Instruments)

The TGA is interfaced to the FTIR using an insulated teflon tube heated to a temperature of 150°C by a Powerstat variable autotransformer. The 25 mm x 10 cm gas cell with KBr windows used with the FTIR is heated using a Barnant thermocouple controller. The tube and gas cell are heated to prevent possible condensation of the gaseous products. The TGA is also interfaced to the mass spectrometer using a fused silica capillary sampling inlet that is heated to approximately 170°C.

2. Studies with the Tube Furnace

To simulate the conditions used in the AFBC system, tests were performed in a concentric tube, quartz reactor inserted into the horizontally mounted electric Lindberg furnace. To study the combustion performance of the materials of interest, the furnace was preheated to the desired temperature before the sample was introduced. The composition of the process gases can be adjusted by the calibrated teflon flow meters before being introduced into the reaction system.

The reaction products were swept into a cold trap containing a chosen absorbent. After the reaction was completed, the solvent was concentrated, and the sample analyzed using the GC/MS system. A Shimadzu QP 5000 system with a NIST/EPA/NIH 62,000 compound database was used for GC/MS analysis. The identification of compounds was accomplished by using a computerized library search and by comparison with literature mass spectra. Moreover, comparing to the GC retention time of the pure compounds helped confirm the identification of the unknowns. Standard materials were tested to establish the detection limits of the experimental set-up.

3. Laboratory Fluidized Bed Combustion Tests

The laboratory scale (12-inch) atmospheric fluidized bed combustor at Western Kentucky University was used in this study. The active bed area is 125 in^2. The freeboard zone of the combustor is 10 feet high, providing adequate residence time for the combustion of fine fuel particles which may be entrained in the gases leaving the bed. The fuel is injected into the fluidized bed by using pneumatic injectors. The injectors used for these tests are located about 9 in above the air distributor of the combustor. The bed temperature is controlled by the fuel feed rate adjustment.

Evolved gases from the combustor were analyzed by gas chromatography and FTIR spectroscopy. To determine if any chlorinated organic compounds were formed during the combustion reactions, the combustion gases were collected in Tenax adsorption tubes. The collected samples were extracted separately with hexane (99.9%) for 24 hours using a soxhlet extraction apparatus. The samples were then analyzed using a GC/MS system.

RESULTS AND DISCUSSION

1. Characterization of Raw Materials and Their Blends

The thermal behavior of the raw materials of interest were investigated at a heating rate of 10°C/min. The purpose of these experiments was to understand the processes and mechanisms of thermal decomposition of different raw materials. To help accomplish this task, profiles for the evolution of different gaseous products were obtained and used to assess the relative thermal stability and temperature relationships of the materials. These results are important to the analysis of materials and control of the performance of an AFBC.

As observed from the FTIR and MS analyses, a common decomposition product from newspaper and cellulose was furfural. Upon interpretation of the MS spectrum obtained from the combustion of PVC one finds a very notable result. As shown in Figure 1, it appears that the production of molecular chlorine accompanies the release of a large amount of HCl during the combustion of PVC. Materials with masses 36 and 38 are formed at the same time, and strongly suggest the presence of isotopes of $H^{35}Cl$ and $H^{37}Cl$. The integrated ratio is close to the chlorine isotopic ratio. Furthermore, three additional m/z peaks appear at exactly the same point, with apparent masses of 70, 72, and 74 corresponding to $^{35}Cl_2$, $^{35}Cl^{37}Cl$, and $^{37}Cl_2$. This is strong evidence suggesting that some fraction of the abundant HCl may be undergoing a thermal Deacon Reaction to produce molecular chlorine. Following the in-situ generation of Cl_2, the aromatic compounds can be readily attacked to form chlorinated organics such as chlorobenzene, which correspond to masses of 112 and 114. It is a plausible starting point for the formation of chlorinated organics from the combustion of chlorine-rich fuel mixtures. When changing the atmosphere from air to nitrogen, chlorine is not identified in the products from the thermal decomposition of PVC. This can be attributed to the absence of oxygen, a necessary reactant in the Deacon Reaction. However, although there is no Cl_2 formed, HCl is still the major product from the combustion of PVC, even in air.

In order to study combustion performances under conditions similar to those for AFBC systems, a series of experiments were carried out at a heating rate of 100°C/min. The decomposition reactions of fuels occur at a much faster rate and at higher temperatures as the heating rate increases. As shown in the TGA/FTIR data, the chlorine and hydrocarbon species formed during the combustion of blends are released at the same time for the higher heating rate, whereas they evolved at different times for the slow heating rate. Also, more hydrocarbons are produced at the higher heating rate. In fact, the heating rate in an AFBC system is much higher than 100°C/min, whereby one can expect there are greater possibilities for yielding chlorinated organic compounds during co-firing coals with RDF in an AFBC system.

2. Studies of the Mechanism for the Formation of PCDD/Fs During the Combustion of MSW

The purpose of this series of experiments was to examine the proposed mechanism for the formation of PCDD/Fs during the combustion of MSW. Before the following study was conducted, a series of experiments was completed to obtain the optimum conditions for the operation of the furnace and establish the detection limits for GC/MS analysis.

Four gram samples of different raw materials were burned in air in a tube furnace. The furnace was preheated to a temperature of 850°C before the sample was introduced. The gaseous products were trapped in chilled CH_2Cl_2 and analyzed by GC/MS. As a summary of the results of replicated analyses, phenol is one of the major products that evolved during the combustion of coal, newspaper, cellulose, and RDF. One of the major products of PVC combustion is HCl. This is in accordance with the TGA/MS results and the proposed mechanism for the formation of polychlorinated phenols. It was shown in the GC/MS data that chlorophenol is a major product when blends are burned.

To examine the possibility of producing molecular chlorine via the Deacon Reaction over a temperature range of 400-800°C, a mixture of air and 10% HCl in nitrogen (air: HCl volume ratio of 2:1) was introduced into the quartz tube preheated to different temperatures in the furnace. The product gases were trapped in a phenol-methylene chloride solution and the solution analyzed for chlorophenols by GC/MS. Phenol has proven to be an effective absorbent for chlorine gas, therefore, the production of molecular chlorine through the Deacon Reaction can be monitored by the production of chlorinated phenol in the trapped solution. The results showed that the production of chlorophenols is enhanced as the temperature increases. This indicates that the Deacon Reaction is favored at higher temperatures.

The Deacon Reaction readily occurs, even at the room temperature, in the presence of a catalyst such as Cu compounds. Cu is one of the more abundant elements in MSW, consequently, under the co-firing conditions the Deacon Reaction may take place much more readily than under our test conditions.

To examine the gas phase chlorination of phenol, as expressed in the equation (2), 100 mg portions of phenol were place in a heated tube and evaporated in the presence of a constant flow of 0.5% Cl_2 in nitrogen. The products were cooled by liquid nitrogen and condensed upon exiting from the combustion tube, carefully washed by methylene chloride, and analyzed using the GC/MS system. The chlorination of phenol began at temperatures around 250°C and produced 2-chlorophenol, 4-chlorophenol and 2,4-chlorophenol. At higher temperatures, dibenzofuran was produced.

The combustion of chlorinated phenols, which may lead to the reaction illustrated in equation (3), was examined by heating 100 mg portions of 2,4-chlorophenol in the presence of air in the tube furnace. The GC/MS results shows that the condensation products from the combustion of 2,4-dichlorophenol include 2,4,6-trichlorophenol, tetrachlorodibenzofuran, and dichlorodibenzodioxin. The latter two compounds began to be formed below 400°C.

Based on the above information, the proposed mechanism seems to be a possible chemical pathway for the production of PCDD/Fs during the combustion of MSW under the specific temperature ranges studied.

3. The Effect of Sulfur Species on the Deacon Reaction

The following tests were designed to explore the negative effect of SO_2 upon the chlorine formation through the Deacon Reaction, subsequently, minimizing possible PCDD formation. In the previous studies, it was found that combustion of the chlorine-containing polymer PVC may produce chlorinated organic compounds. The most important of these compounds were chlorinated benzenes (the major products), naphtahalenes, styrenes, and biphenyls.

Tests conducted by Gullet and coworkers showed that the homogeneous reaction of Cl_2 with SO_2 to form HCl (a less likely chlorinating agent than Cl_2) is not measurable below 800°C.[8] This is not apparent from thermodynamic calculations of the free energy change. Although equilibrium calculations suggest that the reaction is favored over the full range of temperatures tested, the kinetics of reaction may prevent observation of measurable product until the higher temperatures are reached.

Therefore, the possible effect of SO_2 upon the formation of Cl_2 through the Deacon Reaction was examined at 800°C. The quartz tube reactor was preheated to the desired temperature before the gas was introduced. The flow rate of HCl (1% in nitrogen), SO_2 (4.86% in nitrogen) and air were adjusted by the calibrated teflon flowmeters. The evolved gas was trapped by a carefully chosen absorbent, which was prepared by dissolving 50 mg phenol in 25 mL methylene chloride. The amount of phenol in the trapping solution was accurately controlled to within +/-0.0001g. Then the trapped solution were concentrated to 1 mL and injected into the GC/MS system for analysis. In the quantitative study, the concentration of HCl and O_2 in the gaseous mixtures was fixed, and only changed the fraction of SO_2. At each condition, the results presented were based on at least three runs. It was shown that once SO_2 was introduced the production of chlorophenol decreased. The relationship between the S/Cl ratio and the production of chlorophenol is shown in Figure 2.

Griffin, in a study of co-incineration of coal and municipal solid wastes, postulated that dibenzodioxins would not form when the S/Cl ratio was greater than 10, and proposed increasing the sulfur of the wastes in co-combustion with coal in order to decrease dioxin formation.[5] However, in our experiments in which the S/Cl was less than 2.5/1, dramatic decreases in the major chlorine-containing products of combustion were observed. This could indicate that quenching effects of sulfur are even greater than those calculated by Griffin.

4. Co-combustion of PVC with coal in the AFBC system

The objective of this set of experiments was to evaluate the combustion performance when co-firing coal with MSW. PVC was selected for this study, since it is the major source of chlorine during the MSW incineration. The objective was to determine the emission of inorganic acid gases (HCl and SO_2), the extent of chlorinated organic compound formation, as well as to examine the effect of using coal as a co-combustion energy source with MSW.

The fuel used in this test was switched from coal alone to the mixture of coal, PVC and wood pellets. The experimental conditions were as follows:

Fuel compositions:	(1) 100% coal
	(2) 89% coal, 1% PVC and 10% wood pellets
	(3) 86.7% coal, 3.3% PVC and 10% wood pellets
Fuel feed rates:	~17.5 lb/hr
Limestone feed rates:	~1.26 lb/hr for coal 95010, ~4.48 lb/hr for coal 95031

Ca/S ratio:	~3.0
Air flow rate:	~3.25 lb/hr

Analytical data for the raw materials used in this study are shown in Table 1. The IC data showed that with the increase of PVC in the fuel mixture, the HCl emission increased and the SO_2 emission decreased. Compared with the results from the combustion runs of 100% coal, no chlorinated organics and PAHs were detected under our experimental conditions.

CONCLUSIONS

From the results of the study reported in this paper, the following statements and observations can be made:

- The major combustion product of PVC is HCl. With the release of large amounts of HCl, molecular chlorine can be generated through the thermal Deacon Reaction.
- The TGA/FTIR/MS results indicate that under high heating rates, there are more hydrocarbons released from the combustion of coal and other raw materials. Moreover, the concurrent evolution of HCl and the large amount of hydrocarbons may facilitate the formation of chlorinated organics.
- The proposed four-step mechanism involving the Deacon Reaction appears to be a possible chemical pathway for the formation of PCDD/Fs during the co-combustion process within specific temperature ranges.
- SO_2 is an effective inhibitor for the formation of molecular chlorine through the Deacon Reaction.
- No PAHs and chlorinated organics were detected in the fly ash and flue gas when co-firing PVC with coal in the WKU AFBC system.

REFERENCES

1. "Summary of Recent Literature Pertaining to the Incineration of Municipal Solid Wastes," Prepared by the Center for Environmental Information, Inc. ENYSEG Contract No. 87-372, 1988.
2. Junk, G.A.; Richard, J.J. *Chemosphere*, **1981**, *10*, 1237-1241.
3. Altiwicker, E.R.; Milligan, M.S. *Chemosphere*, **1993**, 27, 301-307.
4. Scheidle, K.; Wurst, F.; Kuna, R.P., *Chemosphere*, **1986**, 17, 2089.
5. Griffin, R.D., *Chemosphere*, **1986**, *15*, 1987.
6. Gullett, B.K.; Bruce, K.R. Beach, L.O., *Waste Manage. Res.*, **1992**, *8*, 203.
7. Lindbauer. R.L., *Chemosphere*, **1992**, 25, 1409.
8. Gullet, B.K.; Bruce, K.R. Beach L.O., *Environ. Sci. Technol.*, **1992**, 26, 1938-1943.

Table 1. Analytical Data for Raw Materials

Parameter	95010	95031	PVC
Coal Seam	Blend	IL#6	
Rank of Coals	A	B	
% Moisture*	2.32	8.32	0.00
% Ash	7.22	10.78	0.36
% Vol. Matter	39.97	37.21	99.64
% Fixed Carbon	52.82	52.02	0.00
% Carbon	79.38	72.61	38.71
% Hydrogen	5.31	4.82	4.2
% Nitrogen	1.63	1.54	0.07
% Sulfur	0.67	2.38	0.22
% Oxygen	5.69	7.57	0
Chlorine, ppm	1,039	3,065	56.45**
Cal.Value (Btu/lb)	14,077	12,842	8,556

* Moisture is as-determined. All other analyses are reported on a dry basis. The rank of each coal is high volatile A, B or C bituminous

** The unit for chlorine in PVC is percent.

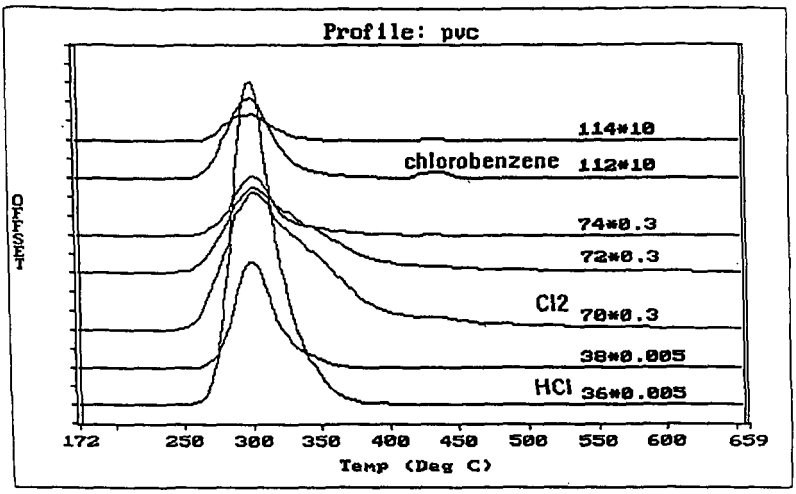

Figure 1. Mass profiles of HCl and Cl_2 evolved during the combustion of PVC.

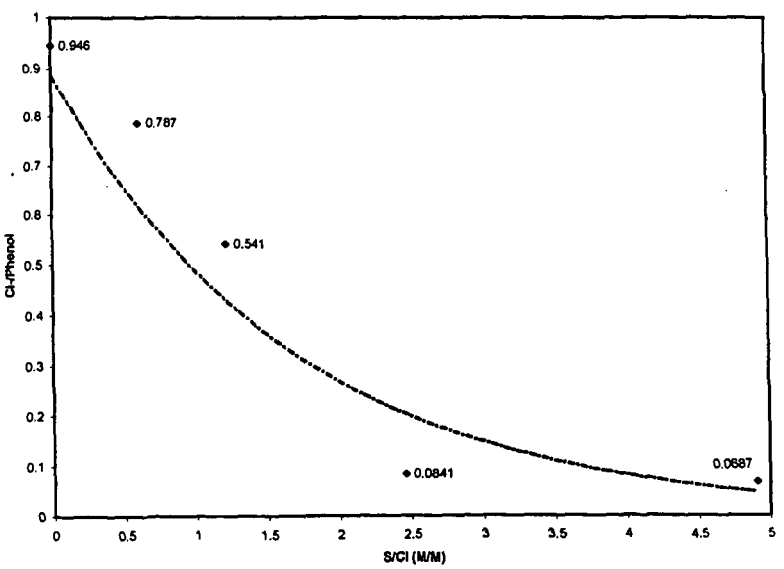

Figure 2. Production of chlorinated phenol as a function of the S/Cl ratio.

MODELLING AND SIMULATION OF TRANSIENT COAL COMBUSTION PROCESSES IN FIXED AND MOVING GRATES

F. CHEJNE ; W. F. FLOREZ ; J.P. HERNÁNDEZ.; E. ARENAS C; A. HILL and J.C. ROJAS

Energy and Thermodynamics Group. Universidad Pontificia Bolivariana.
A.A. 56006. Medellín, Colombia, S.A.

Abstract—A time dependent mathematical model and a computer program have been developed to simulate coal combustion on moving and fixed grates. The physical models for both, the combustion of a single coal particle and the combustion of continuos bed of coal, have allowed a better approach to reality. The partial differential equations of the model are solved using implicit collocation and relaxation techniques, with finite differences for time advance. The program MTCC can predict several important parameters that describe the coal combustion processes in fixed and moving grates, such as composition, heat of reaction and temperature profiles for gaseous and solid phases, in the bed and the particle's interior. In addition, the program can simulate non-isothermal particles with the exposed core and non-reactive core models. The basic structure of the model includes a system of six differential equations which represent the mass and energy balances for all phases at any point along the bed.

Keywords: Char, grate firing, heat transfer, mathematical model.

INTRODUCTION

Most of the commonly used models for coal combustion are stationary, isothermal in each particle,[1,2,3] and they also emphasize more on the reaction kinetics than on the heat transfer mechanism itself. The works published so far do not cover many important aspects and phenomena of the process like the thermal effects on the interphase between the unreacted coal core and the ash layer in the particles, and this fact justifies our work. This model considers simultaneously the devolatilization, drying and combustion rates in the bed,[3,4] as well as the gas production due to chemical reactions in the gaseous phase. The whole set of balances of the model can be used to assess an optimal grate velocity in the combustion equipment in order to achieve considerable energy savings. Another important fact to consider is the particle size distribution and how it evolves with time, since the heat conduction through the bed depends strongly on the particle's diameter at each point.

MATHEMATICAL MODEL FOR COAL COMBUSTION ON GRATE

A system of several chemical reactions for a wide set of carbonaceous material-gas reactions was taken into account in the solid phase as in gases. The mathematical model was built for both, a single particle and also for a continuos system formed by the solid and gas passing through the column.

Basic equations

The mass and energy balance equations consider the moisture, volatil material, oxygen and heat exchange inside a single coal and also, between the bed and the gases passing through it. It also expresses that the heat released during the reaction is dissipated by convection to the gas and by conduction to the particles around. The mass balance equations for the solid and gases are

$$dm_i = R_{\alpha,i}\frac{dA_L}{d\xi}d\xi \tag{1}$$

$$\frac{dF_i}{d\xi} = R_{\alpha,i}\frac{dA_L}{d\xi} + R_{\alpha,i}\frac{dVg}{d\xi} \tag{2}$$

respectively. Concerning the energy balance, the equations are,

$$F_g C_{pg} \frac{\partial \theta_g}{\partial \xi} = h\left(\theta_c - \theta_s\right)\frac{dA_p}{d\xi} + \sum_j R_{gas,j}\frac{\Delta H_j}{\left(T_{ref} - T_{gs}\right)}\frac{dV_g}{d\xi} \tag{3}$$

$$-\frac{\partial^2 \theta_g}{\partial \xi^2} - \frac{hZ_c\left(\theta_c - \theta_s\right)}{\lambda_c(1-\varepsilon)A}\frac{dA_p}{d\xi} + \sum_i R_{sol,i}\frac{Z_c \Delta H_i}{\left(T_{ref} - T_{gs}\right)\lambda_c(1-\varepsilon)A}\frac{dA_p}{d\xi} - \frac{\partial \theta_s}{\partial r_c} = 0 \tag{4}$$

Additionally, along the bed the conservation equations for every particle must be solved. The energy equation for $r < r_N$ is stated as:

$$\frac{1}{r^2}\frac{\partial}{\partial r}\left(r^2 \frac{\partial \theta_r}{\partial r}\right) + \frac{\sum \Delta H_i R_{sol,i}}{\lambda_r\left(T_{ref} - T_{gs}\right)r_N} = \frac{\rho_r C_{pr}}{\lambda_r}\frac{\partial \theta_r}{\partial t} \tag{5}$$

But for the case $r_N \leq r \leq r_p$ we must not consider the generation term. Finally, the mass equation within the particles is written as,

$$\frac{1}{r^2}\frac{\partial}{\partial r}\left(r^2 \frac{\partial \rho_v}{\partial \rho}\right) + \frac{R_{sol,i}}{r_N D_{ef}} = 0 \tag{6}$$

Boundary conditions

The gas temperature at the reactor's entrance does not vary with time and the coal temperature at the same point will be constant as well, when the coal feeding is continuous. Coal temperature at the reactor entrance will depend on time when it is a batch process. On the other hand coal temperature on the top of the bed is subjected to radiation conditions and the length of the coal bed depends upon the coal consumption rate. The boundary conditions for chemical species are known at the entrance of the reactor for air and they are also initial conditions for Carbon.

The computer program MTCC was developed for modeling both, reactive and non-reactive core particles. For the non-reactive model we have to apply a continuity condition between the core and the ash layer, however this is unnecessary for the exposed-core model. In addition, for both models we need to apply symmetry at the center and a Dirichlet condition on the surface to assess convection effects. Most physical properties were calculated using the Chilton-Colburn analogy,[5] while some expressions as the diffusion coefficient and specific area can be found in references 3,6,7,8.

Reaction kinetics

The model includes the set of chemical reactions from the references 8 and 9. Models for gas-solid reactions: These models deal with drying and devolatilization and in this work we modified and used them in transient stages of combustion including in the analysis the growth rate of the ash layers.

Drying and devolatilization processes: The non-reactive core model is analysed. For the devolatilization case it was necessary to perform a mass balance with the different gases being generated in this stage and the remaining mass in the coal bed.

Mass and heat transfer: There are many useful analogies that considers the effects of solid-fluid heat and mass transfer coeffients in the process, as presented by Bird, Stewart, Lightfoot, and others.[10,11,12] In the simulation program all these coefficients depend on the temperature, composition and flows along the solid bed, and therefore they are constantly changing with position and time.

DESCRIPTION OF THE SIMULATION PROGRAM

The basic necessary input data for the program are: Complete physical and chemical characterization of the fed coal, composition and temperature of the primary air at the entrance, basic geometry and dimensions, i.e. reactor diameter, bed length, flow parameters as bed porosity, pressure head and other physical properties.

The numerical method was a combination of collocation[13] and relaxation. In the collocation method, each variable is written as linear combination of a set of non-linear interpolating functions, which depend on the spatial coordinates. For example, in the present work the equations have the general form,

$$\frac{\partial f}{\partial t} = A\frac{\partial^2 f}{\partial z^2} + B\frac{\partial f}{\partial z} + C \tag{7}$$

where A,B, and C are functions of temperature , composition and time and with the variable f assumed to be,

$$f_j = \sum_{i=1}^{N} a_i F_{ij} \tag{8}$$

where f_j states for the variable f at node j, and N is the number of collocation points. The method has the advantages that the collocation points can be generated anywhere in the integration domain and a symmetric and well posed coefficient matrix is generated and easily inverted. The collocation method uses radial local functions between the collocation point and the other point in the domain.

Equation (8) is substituted into differential equation (7), and in this manner a set of N equations with N unknowns is obtained, where N is the number of nodes and the unknowns are the coefficients of the linear combination (8). On the other hand, the time term is discretized in finite differences using upwinding schemes.

The initial step is to transform the differential equations into a equivalent set of differential equations of first order by an adequate change of variable[14,15]. Thus the aspect of the final equations to be solved is,

$$\frac{\partial Y}{\partial t} = \{a\} Y = G(Y) \tag{9}$$

where $\{a\}$ is the coefficient matrix and Y_i is the vector of temperatures and heat fluxes at node i. Next, the first order derivatives are discretized in finite differences, and the resulting truncation error expands in Taylor series,

$$E_k(Y + \Delta Y) = E_k(Y) + \sum_{i=1}^{N} \frac{\partial E_k}{\partial Y_{i,k-1}} \Delta Y_{i,k-1} + \sum_{i=1}^{N} \frac{\partial E_k}{\partial Y_{i,k}} \Delta Y_{i,k} \tag{10}$$

E_k is the truncation error at the same node. By means of an iterative algorithm, the error is minimised based not only on the values of the position along the bed but also on the values of temperatures T_g and T_s and concentrations at each node.

RESULTS

In transient state, temperature rises due to energy transfer within the solid and gases plus the thermal energy generation by chemical reactions as shown in figures 1,2 and 3.

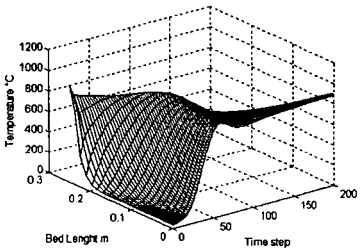

Figure 1. Temperature of the solid as function of time and position. Time step = 200 s

On the other hand, the composition of the gaseous mixture changes strongly with time. The oxygen O_2 decreases for the oxidation of Carbon to produce CO_2 and then it increases again because the air flow is constant while the Coal is consumed (figures 4,5).

In figure 6 the amount of water in combustion gases is depicted. Water and Oxygen play an important role influencing how much CO (figure 7) is obtained during combustion, however as a general rule the evolution of CO and CO_2 are alike.

Finally, during the entire process growing amounts of NO_x and SO_2 coming form the Coal were observed (Figures 8-9).

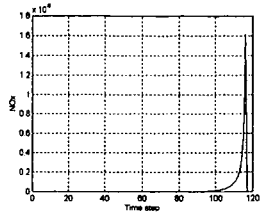

Figure 2. Fraction of NOx in gases growing with temperature and time.

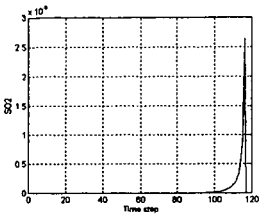

Figure 3. Fraction of SO2 in gases.

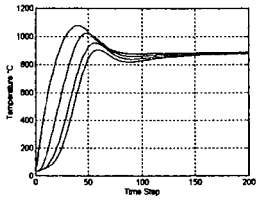

Figure 4. Coal temperature as function of time at different posotions along the bed. Time step =200 s

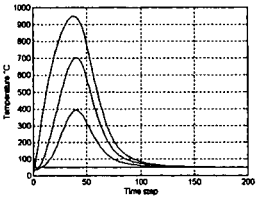

Figure 5. Gas temperature as fuctions of time at different positions along the bed. Time step= 200 s

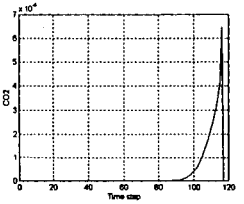

Figure 6. Carbon dioxide fraction in gases at the entrance of the reactor

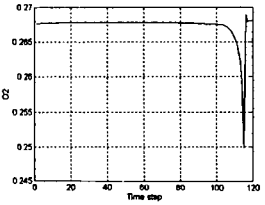

Figure 7. Oxygen fraction in gases at the entrance of the reactor

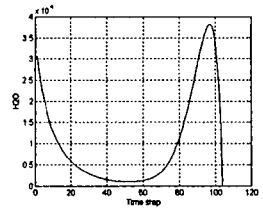

Figure 8. Fraction of water during combustion as function od time. Time Step =200 s

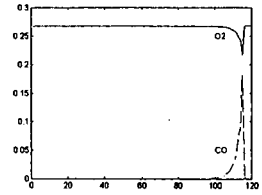

Figure 9. Relation between Oxygen and CO as time progresses. Time step=200 s

CONCLUSIONS

The computational model will allow us to predict the combustion stages and eventually the production of unburned material due to oxygen deficiency. The cases analysed here correspond to enough oxygen such that there is not unburned material

REFERENCES

1. Radovic, L. *Proc. Coal Cumbustion Course.*, Bogota, Colombia, 1995.
2. Kramer, F., Smoot, S., Balckman, D. *20th Symp. Of Combustion.* The Combustion Institute, USA, 1984. 139-154.
3. de Souza-Santos, M.L.,*Ph.D. Thesis* University of Shieffield, U.K.,1987.
4. Young,R.W., Cross, M., and Gibson, R.D.,"Mathematical model of grate-kiln-cooler process used for induration of Iron ore pellets",*Ironmaking and steelmaking.*1979, **1.**
5. Bartok, W., Sarofim, A del F. "Fossil Fuel Combustion",John Wiley & Sons, 1991.
6. Kūcūkada, K.,Thibault, J., Hodouin, D., Paquet, G. and Caron, S.*"Modelling of a pilot scale iron ore pellet induration furnace"*, Canadian Metallurgica Quarterly, 1994,**33**,1.
7. Incropera, F., *Fundamentals of heat and mass transfer.*,John Wiley & Sons, 1996.
8. Bryden, K.,Ragland,K., *"Numericol modeling of a deep fixed bed combustor"*,Energy Fuel,1996,**10**, 269.
9. de Souza-Santos, M.L.,*"Comprehensive modelling and simulation of fluidized bed boiler and gasifiers"*,Fuel, 1989, **68**, 1507
10. Bird, B.,*Transport Phenomena,* John Wiley & Sons, 1976.
11. Wakao, N. and T. Funazkri, *Chem. Eng. Sci.*1978, **13**, 1375.
12. Wakao, N. and S. Kaguei, " Heat and mass transfer in packed bed.", Gordon & Breach, 1982
13. Chen, C and Golberg, M. *"A bibliography on radial basis function approximation"*, Boundary Elem. Comm, 1996, 7, 155
14. Press, W., Flannery, B., "Numerical Methods", Cambridge University Press, 1987.
15. Lapidus, L. "Numerical Solution of Partial differential equations in science and engineering", John Wiley & Sons, 1982.
16. Press, W., *"Numerical recipes: The art of scientific computing"*,Cambridge university Press, 1986.

NOMENCLATURE

$[O_2]^*_{S,G}$ = Oxygen concentration in gas stream
ΔH_{rxn} = Carbon combustion enthalpy
$[O_2]$ = Oxygen concentration
$[O_2]_e$ = Oxygen concentration inside coal
a = Coal bed specific area
A_p = Particle area
C_{pg} = Gas specific heat
D_{O2} = Oxygen diffusion coefficient
f = Remaining coal fraction in the bed
F_g = Gas flow
G_g = Air flow mass
h = Convective heat transfer coefficient
K_{ef} = Coal thermal conductivity
K_m = Mass transfer coefficient
Kr = Reaction rate
M_c = Mass per unit volume of the coal particle
M_{mc} = Carbon molecular weight
M_o = Initial mass per unit volume of the coal particle
M_{O2} = Oxygen molecular weight.
N_p = Number of particles per unit volume
r = Radius of the non reactive particle nucleus
R_{gg} = Gas-gas reaction rate
R_{sg} = Solid-gas reaction rate
T_c = Solid temperature
T_{co} = Initial solid temperature
T_g = Gas temperature
T_{go} = Gas temperature at the entrance
V_g = Gas volume
Z = Axial bed distance
Z_o = Initial bed height

Greek letters

ρ_g = Gas density
ε_p = Coal porosity
α = Thermal diffusivity
ξ = Dimensionless axial coordinate
ρ = Dimensionless radius
θ_c = Dimensionless coal temperature
λ_{CZ} = Ash thermal conductivity
θ_g = Dimensionless gas temperature

PYROLYSIS KINETICS OF THE WASTE-TIRE CONSTITUENTS: EXTENDER OIL, NATURAL RUBBER, AND STYRENE-BUTADIENE RUBBER

Sylvie Charpenay, Marek A. Wójtowicz, and Michael A. Serio

Advanced Fuel Research, Inc., 87 Church Street, East Hartford, CT 06108-3742

Keywords: Waste Tires, Pyrolysis, Kinetics

ABSTRACT

In order to design tire pyrolysis and combustion processes, it is helpful to know the kinetics of thermal decomposition of tires. In this study, pyrolysis kinetics of tire constituents are reported. A thermogravimetric analyzer, coupled with a Fourier-Transform Infrared spectrometer for gas-product analysis, was used in a series of non-isothermal pyrolysis experiments. The heating rates were 1 K/min, 3 K/min, 30 K/min, and 100 K/min. The results are discussed in terms of single and distributed activation energy kinetics, and a comparison with the available literature data is made.

INTRODUCTION

It has been demonstrated by several studies that, to some degree, the decomposition of the organic part of tires can be related to the decomposition of its separate components, i.e., extender oil, natural rubber (NR), butadiene rubber (BR), and styrene-butadiene rubber (SBR) [1-3]. There exists, however, appreciable uncertainty about the value of the activation energy (E) corresponding to each decomposition process; a wide variation in the observed values of activation energies has been reported by several investigators [2-5]. Whether the differences between the results of various studies arise from differences in tire material components, experimental set-ups used, or methods of activation-energy determination is unclear, and we shall try to shed some light on this issue in this study.

In general, previous investigators used single activation energies which, in some cases, were found to vary with the heating rate [3,4].

KINETIC ANALYSIS

In what follows, it is implicitly assumed that the reaction rates to be determined follow first-order kinetics, which is a reasonable starting assumption for the polymers used in tires. While isothermal techniques are useful to determine kinetic parameters, their implementation is time-consuming. Non-isothermal techniques provide faster means to obtaining this kinetic information. The most common non-isothermal technique is the so-called Friedman method [6], in which the logarithm of the rate constant, k, is plotted at each point as a function of the inverse temperature. The rate constant, k, is calculated from the equation: $dw/dt = k\,(w_f - w)$, where w is the sample weight at time t, and w_f is the final sample weight. Since k is equal to $A\,exp(E/RT)$, (A is the pre-exponential factor, E is the activation energy, T is temperature in degrees Kelvin), the parameters A and E can be determined from the linear region(s) of the plot of $ln(k)$ versus $1/T$. A drawback of this method is the fact that it introduces a bias in the values of A and E when the reaction has a distribution of activation energies [7]. In such a case, the Friedman method is unable to differentiate between the effect of the distribution and the effect of the magnitude of the mean activation energy, and gives an erroneous value for the mean value of E. This value is usually lower than the "true" value [7].

Another non-isothermal method of determining the kinetic parameters involves the measurement of the temperature at which the rate of volatile evolution is maximum, T_{max} [5,8]. This technique was used in this study. The method has been shown to be applicable to the determination of E and an approximate value of A for wide distributions of activation energies [7]. In a typical sequence of experiments, thermal-decomposition rates are measured at different heating rates. The relationship between the heating rate, M, and the value of T_{max} is given by the following equation

$$ln(M/T^2_{max}) = ln(AR/E) - E/(RT_{max}),$$

from which the kinetic parameters A and E can determined [8]. While the value of E is accurately determined even for wide distributions, the value of A usually requires a slight adjustment (typically within a factor of two) [7]. The width of the distribution, σ, can then be determined from the width of the peak representing the rate of weight loss. In the T_{max} method, some difficulties can be encountered when peaks are not well resolved; in such cases, substantial shifts in T_{max} can occur. However, the same problem arises when using the Friedman method, unless deconvolution of the peaks is attempted [4]. Another limitation is associated with the presence of small, multiple maxima superimposed on a broader peak, i.e., when the assumption of the first-order kinetics is not fully supported. In this case, again, the applicability of both the T_{max} and Friedman methods is limited. The exact value of T_{max} may also be difficult to determine for large, broad peaks.

In the present study, the T_{max} method was employed, and an attempt was made to reduce the limitations of the T_{max} method by using: 1) a large number of heating rates; 2) very low heating rates for the improved peak resolution; and 3) in the case of noisy data, the measurement of T_{max} was made at the mid-point of the peak width in order to minimize the effect of noise on T_{max}.

MATERIALS AND EXPERIMENTAL

Samples of extender oil, natural rubber, polybutadiene rubber and poly-styrene-butadiene rubber were obtained from Pirelli-Armstrong, New Haven, Connecticut, and a sample of scrap-tire material was provided by Oxford Tire, Plainfield, Connecticut.

The weight loss and volatile-species evolution were monitored throughout the thermal decomposition of the sample using the TG-FTIR apparatus and technique described previously (a thermogravimetric analyzer coupled with a Fourier-transform infrared spectrometer for volatile-species analysis; see references [9,10]). Sample sizes used varied between 10 and 20 mg. The tire particles were sieved to 20×40 mesh. The following heating rates were used in the TG-FTIR experiments: 1, 3, 10, 30, 100 and 200 °C/min. In other thermogravimetric studies of tire pyrolysis, the heating rates were varied only by a factor of 6–50, with the data often reported for just one tire component. Thus, with regard to the range of the heating-rate variation and the number of tire components studied, our work seems to be most comprehensive to date.

RESULTS AND DISCUSSION

In general, TG-FTIR experiments showed that at least 90% of the weight loss was attributable to tar, the remaining 10% being H_2O, CO, CH_4 and CO_2. It was found that the gases evolved approximately in the same temperature range as the tar did, which is in agreement with our previous work [5]. In view of this result, it was decided that a comprehensive analysis of the gas-species evolution was unnecessary, and the value of T_{max} was determined from the weight-loss data. The rate of weight loss as a function of temperature is shown in Figure 1 for oil, NR, BR, and SBR heated in helium at 30 °C/min.

The T_{max} method was applied to the TG data for extender oil, NR, BR and SBR, as shown in Figure 2, where $ln(M/T_{max}^2)$ is plotted as a function of $1/T_{max}$. Wherever possible, the available literature data have been expressed in terms of $ln(M/T_{max}^2)$ and $1/T_{max}$, and they are included in the plot. It can be seen that the T_{max} method applies reasonably well to the experimental data, and fairly linear trends are obtained. It can be concluded that the activation energy, as determined using the T_{max} method, appears to be constant over the range of heating rates used. This result is in contrast with the study by Williams and Besler [3], in which the variation in the activation energy with the heating rate was reported when the Friedman method was employed.

It should be noted that only limited accuracy in the values of T_{max} reported in the literature is expected as T_{max} was not meant to provide kinetic information there, but was merely used as an approximate index of reactivity. In most studies, the Friedman method was utilized to determine the pyrolysis kinetics. The slight differences observed in Figure 2 between the data of this study and the literature data may be caused by several factors, including the use of somewhat different materials, differences in the temperature measurement, and differences in the way T_{max} was determined. A summary of the kinetic data obtained in this study is shown in Table 1.

Interpretation of the data for the extender oil presents an inherent difficulty associated with the accurate determination of T_{max} because the decomposition covers a wide range of temperatures. However, even with a significant uncertainty for T_{max} of ± 7 K, i.e., $1/T_{max} \sim \pm 0.015 \times 10^{-3}$ K^{-1}, the kinetics of this process can be estimated (see Figure 2a and Table 1). It seems particularly appropriate to use the T_{max} method to determine the pyrolysis kinetics for this material as a distribution of activation energies is likely to occur in the case of oil components having different molecular weights. If applied, the Friedman method would grossly underestimate the value of E, and the determined kinetics would apply only to a narrow range of heating rates. In fact, the literature values of the activation energy have been reported much lower than the value determined in this study (e.g., $E/R = 5.9 \times 10^3$ K reported by Yang *et al.* [2] versus $E/R = 10 \times 10^3$ K found in this study). Using the activation energy determined by the T_{max} method, the value of σ (the width of the distribution) was found by fitting the Gaussian-distribution model to the experimental data. The width of the Gaussian distribution function is reported in Table 1.

In Figure 3, the predicted and experimental oil-decomposition patterns are shown for two different heating rates. Predictions were made using both single- and distributed-activation-energy models. In the single-activation-energy model, a value of $E/R = 5.9 \times 10^3$ K was used, as reported in reference [2]. The pre-exponential factor was adjusted to provide the best fit for the low-heating-rate data (Figure 3a). It can be observed that the distributed-activation-energy kinetics fit the data at both heating rates, whereas the single-activation-energy model fails at the high heating rate (Figure 3b).

The activation energy found for natural-rubber decomposition (Table 1) appears consistent with literature data [2,3, 11–14]. Also, T_{max} values from the literature data are relatively similar (Figure 2b). From the shape of the decomposition peak (in particular the width of the peak) as a function of temperature, it was found that a single activation energy would fit the data fairly well.

The uncertainty in T_{max} for the NR has been estimated to be ± 3 K, i.e., $1/T_{max} \sim \pm 0.007$ 10^{-3} K^{-1}. In Figure 4, thermal-decomposition data are shown for two heating rates, as well as model predictions made using the kinetics derived from the T_{max} analysis. Good agreement between the data and model predictions can be seen. Data in Figure 4 also imply a change in the reaction mechanism that occurs between the low heating rate and the high heating rate. At the low heating rate (Figure 4a), a shoulder is observed at high temperatures, which is not present in the high-

heating-rate data (Figure 4b). This most likely represents the presence of a residue which forms only at the low heating rate, and which is more stable than the original rubber material. The residue readily decomposes at higher temperatures.

Previous studies showed that the decomposition of BR occurs in a two-step process: (1) depolymerization; followed by (2) the decomposition of the residue [15]. This behavior can also be observed in this study, since two weight-loss peaks were observed, as shown in Figure 5. It can also be seen in Figure 5 that the decomposition behavior changes with the heating rate: at the low heating rate, the low-temperature peak (related to depolymerization) is insignificant compared to the high-temperature peak (the residue-decomposition peak). At high heating rates, however, the low-temperature peak (depolymerization) becomes larger, and can account for as much as 50% of the weight loss. This change of mechanism occurs over a relatively narrow range of heating rates (1 to 100 °C/min), and illustrates the difficulty in the kinetic analysis applied within a range of process conditions. In previous studies [15, 16], the activation energy for the depolymerization process was reported, while this work provides values for the process of residue decomposition. The T_{max} data for the butadiene rubber (the residue-decomposition peak) appear in Figure 2c, and they show a fair agreement with the studies carried out under similar conditions. In particular, the three high-temperature points from the work by Williams *et al.* [3] lead to an activation energy similar to the one found in the present study. The difference observed with the low-temperature point may result from the fact that, in the present study, the T_{max} was measured at the mid-point of the peak width, slightly below the peak maximum, while it is not known how it was measured by Williams *et al.* This detail is particularly important because the BR peak is not completely "smooth," and exhibits some shoulders that were neglected here in order to provide more reliable kinetics. In addition, differences between various types of BR may account for the observed discrepancy.

As seen in Figure 1, the SBR decomposition occurs over a wide temperature range, with "shoulders", and is probably not accurately represented by a single activation energy. It is then expected that the T_{max} method (as well as any method based on the assumption of a single activation energy reaction) provides only approximate values for the kinetic parameters. As seen in Figure 2d, two values of T_{max} are reported, the main one referring to the center of the main peak, and the other to the shoulder observed in the weight-loss derivative curve, prior to the main peak. It can be seen in Figure 2d that the literature data fall along either one of the two curves. This result suggests that different types of SBR may have been used, which decompose differently depending, for example, on the methods used in rubber synthesis or on the co-polymer composition. The data from Figure 2d were used to determine activation energies that are shown in Table 1. Similar values of E/R were obtained by applying the T_{max} approach to our data and to the data of other investigators (E/R = 35–40 $\times$ 10^3 K). These values are found to be high compared to the literature values determined using the Friedman method with the assumption of a single activation energy (E/R = 17–25 $\times$ 10^3 K). Clearly, the assumption of a single activation energy is in this case inadequate. The thermal decomposition of SBR appears to involve a number of chemical reactions, i.e., a model with distributed activation energies is more appropriate. The T_{max} method may then be more accurate since it does not make any assumption about the width of the distribution. However, the large uncertainty in the value of T_{max} ($\pm$ 7 K, i.e., $1/T \sim \pm$ 0.015 $\times$ 10^{-3} K^{-1}), which is due to the wide and complex decomposition peak, leads to a large uncertainty in the activation energy.

CONCLUSIONS

The activation energy for the decomposition of oils, NR and BR was found to be independent of the heating rate. This result is in contrast to the results of some studies which found a variation of the activation energy with the heating rate. It is believed that this discrepancy is a result of the different kinetic analyses performed (the T_{max} method versus the Friedman method). It appears that a widening of the peak may occur at high heating rates, which would result in a lower activation energy determined by the Friedman method, whereas the value obtained from the T_{max} method would be unaffected.

A distributed activation energy was found to be more appropriate for the description of oil decomposition as compared with a single-activation-energy model.

A single-activation-energy model adequately describes the decomposition of NR and the BR residue. However, SBR decomposition cannot be easily represented by a single-activation-energy process. The SBR decomposition peak seems to consist of three components, and further work on the kinetic analysis of this peak is needed.

Changes in thermal-decomposition mechanisms have been identified for BR and NR pyrolysis. Caution is advised in extrapolating the kinetics to the heating rates appreciably different from the ones used in kinetic experiments.

The kinetics of waste-tire pyrolysis and its relationship with the kinetics of individual tire components will be a subject of a separate paper.

ACKNOWLEDGMENT

The support for this work came from the National Science Foundation under grant No. III-9215045.

REFERENCES

1 Brazier, D.W., and Nickel, G.H., *Rubber Chem. Technol.* **48**,661 (1975).
2 Yang, J., Kaliaguine, S., and Roy, C., *Rubber Chem. Technol.* **66**, 213 (1993).
3 Williams, P.T., and Besler, S., *Fuel* **74**, No. 9, 1277 (1995).
4 Kim, S., Park, J.K., and Chun, H.D., *J. Env. Eng.*, July, 507 (1995).
5 Teng, H., Serio, M. A., Wójtowicz, M. A., Bassilakis, R. and Solomon, P. R., "Reprocessing of used tires into activated carbon and other products," *Industrial & Engineering Chemistry Research* **34**, 3102–3111, 1995
6 Friedman, H.L., *J. Polym. Sci.*, Part C, **6**, 183 (1963).
7 Braun, R.L., and Burnham, A.K., *Energy & Fuels* **1**, 153 (1987).
8 Van Heek, K.H., Juentgen, H., *Ber. Bunsenges. Phys. Chem.*, 72, 1223 (1968).
9 Carangelo, R.M., Solomon, P.R. and Gerson, D.J., "Application of TG-FTIR to Study Hydrocarbon Structure and Kinetics," *Fuel* **66**, 960 (1987).
10 Whelan, J.K., Solomon, P.R., Deshpande, G.V., Carangelo, R.M., *Energy & Fuels* **2**, 65, (1988).
11 Bhomick, A.K., Rampalli, S., Gallagher, K., Seeger, R., and McIntyre, D., *J. Applied Polym. Sci.*, 33, 1125 (1987).
12 Chien, J.C.W., and Kiang, J.K.Y., *Eur. Poly. J.* **15**, 1059 (1979).
13 Madorsky, S.L., Strauss, S., Thomson, D. and Williamson, *J. Res. Natl. Bur. Std.* **42**, 499 (1949)
14 Freeman, E.S. and Carroll, B., *J. Phys. Chem.* **62**, 394 (1958).
15 Brazier, D.W., and Schwartz, N.V., *J. Appl. Polym. Sci.* **22**, 113 (1978).
16 Hausler, K.G., Schroder, E., and Scwartz, A., *Plaste und Kautschuk* **25** (4), 212 (1978).

Table 1 The kinetic parameters for the thermal decomposition of tire components: extender oil, natural rubber (NR), butadiene rubber (BR) and styrene-butadiene rubber (SBR). E is the activation energy, R is gas constant, A is the pre-exponential factor and σ is the width of the Gaussian distribution function.

Material/Peak	$E/R \times 10^{-3}$ (K)	A (s^{-1})	$\sigma/R \times 10^{-3}$ (K)
extender oil	10	5.2×10^{5}	0.5
NR	25.6	8.2×10^{14}	0
BR: 1st peak	23 → 76		
2nd peak	34.4	1.15×10^{18}	0
SBR: main peak	35.1		
shoulder	40.1		

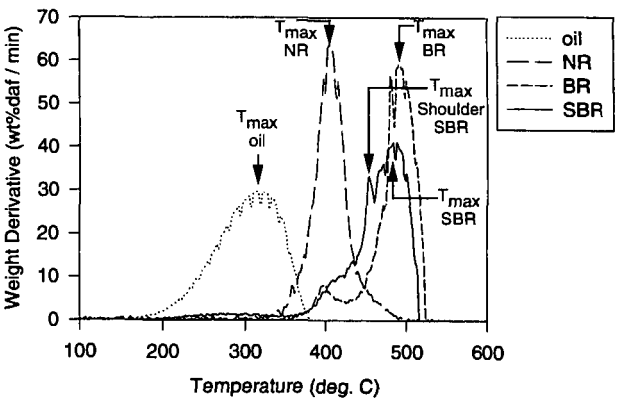

Figure 1 Rate of weight loss from the TGA experiment for extender oil, natural rubber, butadiene rubber and styrene-butadiene rubber.

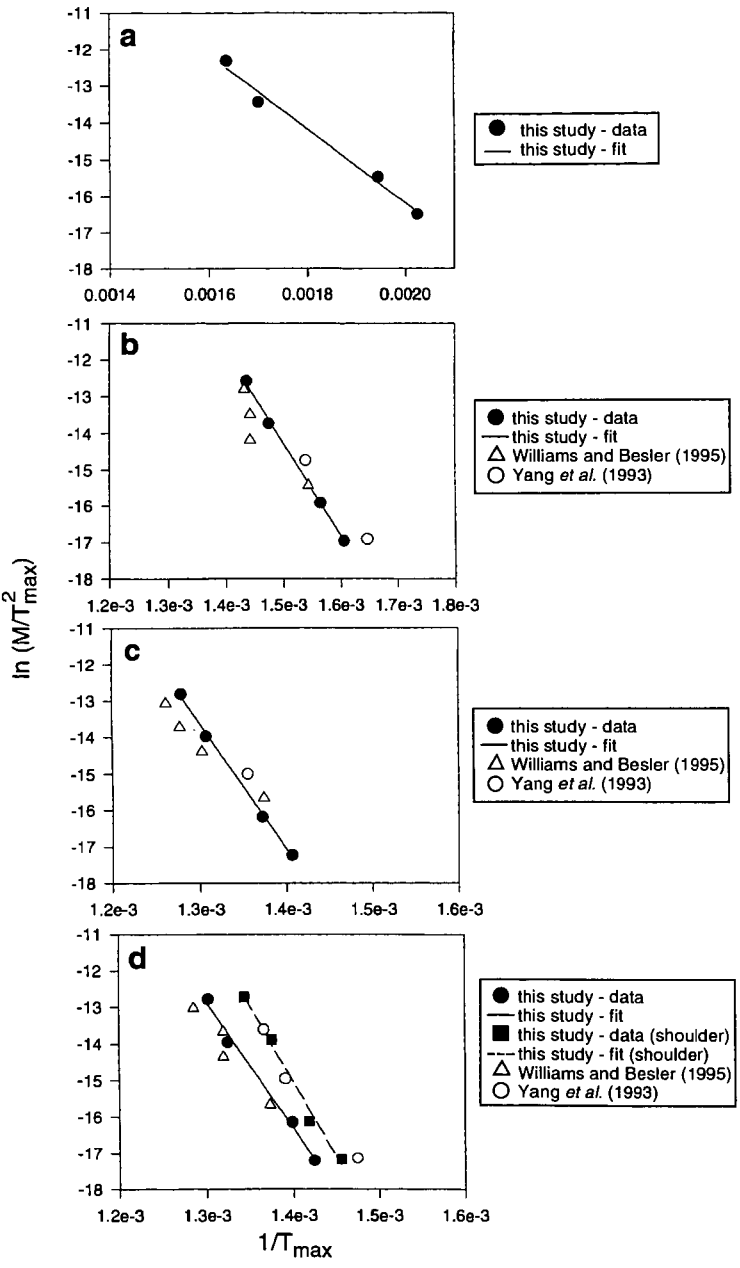

Figure 2 Determination of kinetics using the T_{max} method for a) extender oil, b) natural rubber, c) butadiene rubber, and d) styrene-butadiene rubber. The figure includes data from this study as well as literature data [2,3].

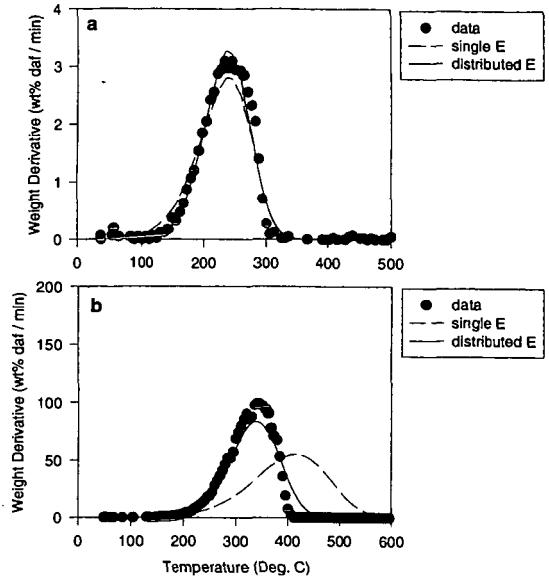

Figure 3 The comparison of data and model predictions for the decomposition of oils at a) 3 °C/min; and b) 100 °C/min. The solid lines represent predictions made by using a distribution of activation energies. The value of the mean activation energy was taken from Table 1, and the width of the distribution was fitted to match the data. The dotted lines represent predictions made by using a single activation energy and the pre-exponential factor that was adjusted to fit the 3 °C/min data.

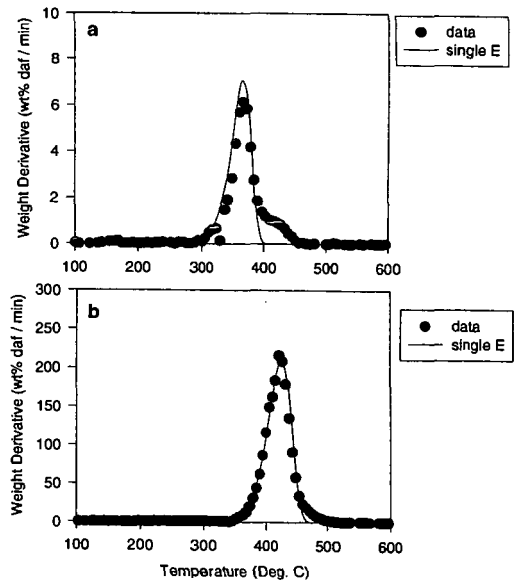

Figure 4 The comparison of data and model predictions for the decomposition of natural rubber at a) 3 °C/min; and b) 100 °C/min. The solid lines represent predictions using a single activation energy, the value of which was taken from Table 1.

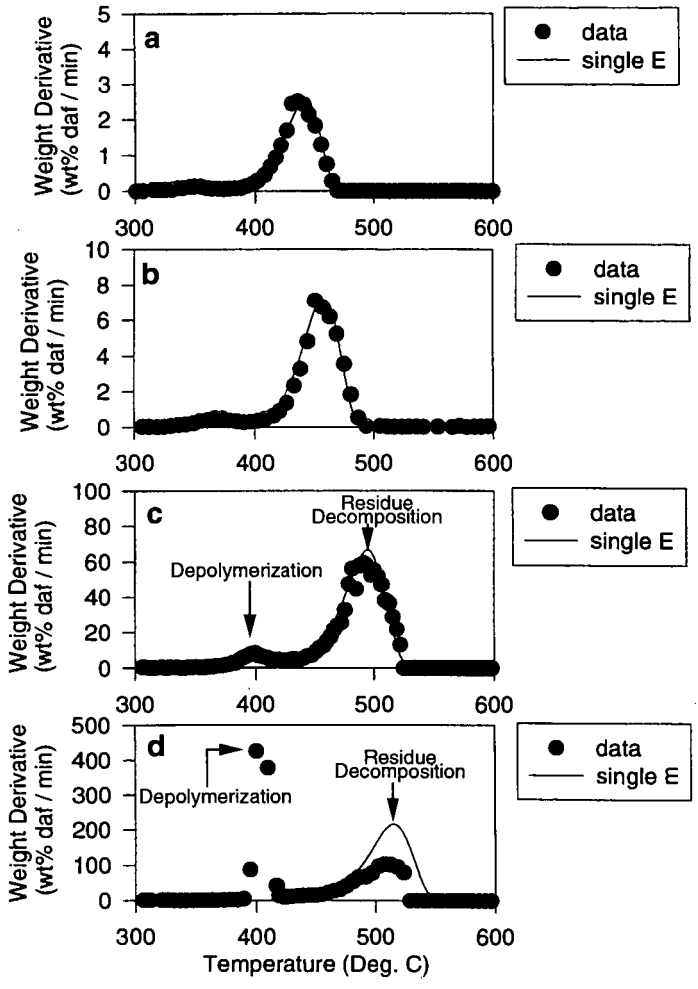

Figure 5 The comparison of data and model predictions for the decomposition of butadiene rubber at a) 1 °C/min; b) 3 °C/min; c) 30 °C/min; and d) 100 °C/min. The solid lines represent predictions made by using a single activation energy, the value of which was taken from Table 1. The low-temperature peak corresponds to depolymerization, while the high-temperature peak corresponds to the decomposition of the residue.

A STUDY ON THE INFLUENCE OF FUEL PROPERTIES ON NO_x EMISSION BEHAVIOR

Sarma V. Pisupati

The Combustion Laboratory
404 Academic Activities Building
University Park PA 16802 USA

Key words; Coal, blends, combustion, NO_x emissions, cleaning

INTRODUCTION

Coal combustion in the recent past has been a challenge not from the burning point of view but from meeting emission standards point of view. Coal cleaning is used as a method to reduce sulfur and to some extent even hazardous air pollutants such as heavy metals. Mineral matter in coals can also be reduced by coal cleaning. Sulfur dioxide emissions have been correlated with the sulfur content of the coals. It is also known that there are no practical methods to reduce nitrogen by cleaning. Coals with very similar nitrogen content can vary widely in the NO_x emissions. A lot of attention was paid in understanding the effect of design and operating conditions of the combustor on the NO_x emissions. However, there seems to be a lack of clear understanding on the influence of fuel properties on the NO_x emission behavior. Although fuel switching is a solution to reduce SO_2 emissions, it is not a viable option for NO_x emissions. Cleaning changes the composition of coals (usually reduces the mineral matter, increases the heating value and alters the volatile matter). Volatile matter content has shown to influence the NO_x emissions. Higher volatile matter is reported to lower the NO_x emissions.

OBJECTIVE

The objective of this paper is to examine the influence of volatile matter and coal cleaning on the NO_x emission behavior. Tests were conducted to evaluate the NO_x emission characteristics of blends of an Indonesian coal (low ash, low sulfur, high moisture content), a Powder River Basin (PRB) coal and a Colorado (CO) subbituminous coal with a non-compliance coal from Pennsylvania in various proportions in a 1000 lb/h (steam) Research Boiler. The effect of coal cleaning was examined in a 0.5 MMBtu/h Down- Fired Combustor (DFC). Coal from the Upper Freeport seam was cleaned by CQ Inc., PA for evaluation of the effect of coal cleaning on hazardous air pollutants emissions.

EXPERIMENTAL

Sample Preparation for the Research Boiler Tests

Two tons of each coal were received in 55 gallon drums for the study. The as received samples (2 x 0") were mixed gravimetrically in the required proportion for each test. The mixtures were crushed and ground to approximately 70% passing though a 200 mesh screen, with no more than 0.5% retained on a 50 mesh screen. The particle size distributions of the pulverized coals was determined using a Malvern Particle Size Analyzer (Series 2600). The compositional analysis of the as-fired coal was determined using Leco proximate and ultimate analyzers. Calorific values of the fuels were determined using a Parr Adiabatic Calorimeter.

Description of the Equipment Used

The combustion tests were conducted in a 1,000 lb steam /h water tube research boiler with a maximum thermal input of 2 million Btu/h. The boiler is a standard Cleaver Brooks "A-frame", water-tube boiler. A schematic diagram of the boiler and auxiliaries is given in Figure 1. The boiler operates at a maximum steam pressure of 200 psig. The combustion chamber is 3 ft wide, 3 ft high and 7' ft long.

To promote evaporation and ignition of difficult-to-burn fuels, a ceramic quarl extends the length of the combustion chamber by two feet. The quarl and the boiler are preheated by burning natural gas prior to introducing of the test fuel. The preheated quarl acts as a source of radiant heat to help support the flame. Pulverized coal was fed from a two foot diameter hopper to an eductor via a 1.5-inch diameter screw feeder. The pulverized coal was entrained into an annular section and then through a swirler. The feed rate of pulverized

coal was monitored by load cells. The products of combustion (O_2, CO_2, CO, NO_x and SO_2) are monitored at the economizer outlet with a series of on-line gas analyzers. The baghouse, used for particulate collection, contains sixteen 5 inches diameter by 8 ft long high-temperature fiber glass bags with out-to-in flow and pulse- jet cleaning. Details on the boiler are found elsewhere (Pisupati et al., 1996).

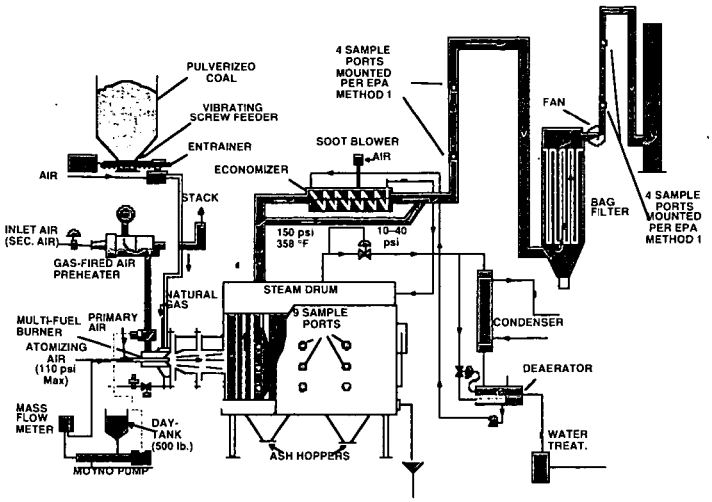

Figure 1. Schematic Diagram of the 1,000 lb/h Research Boiler

The Down Fired Combustor (DFC) has a 20 inch internal diameter, and is 10 feet high. A multifuel burner, capable of firing coal oil and natural gas, was installed at the top of the combustor. Coal was conveyed to the buner pneumatically. All combustion air streams (primary, secondary, and tertiary) were introduced at the same height in the burner. A firing rate of approximately 350,000 BTU/h was used in this study. Details on the combustor are provided elsewhere (Pisupati et al., 1997a)

RESULTS AND DISCUSSION

Table 1 provides the compositional analysis of the coals used in the study.

Table 1. Compositional analyses (Wt.%, dry basis)

	Coal Sample			
	100% PA	100% Indonesian	100% Colorado	100% PRB
Volatile Matter	20.47	46.20	38.11	45.22
Fixed Carbon	67.19	52.14	51.48	48.41
Ash	12.34	1.66	10.41	6.37
Moisture (as-fired)	1.69	21.44	6.81	25.86
Higher Heating Value (BTU/lb as fired)	13,680	10,098	11,668	9,072
Carbon	74.90	72.95	70.9	71.22
Hydrogen	4.45	5.18	5.09	5.37
Sulfur	0.81	0.12	0.46	0.46
Nitrogen	1.25	1.06	1.71	0.94
Oxygen	6.25	19.03	11.43	15.64
Ash	12.34	1.66	10.41	6.37

The ASTM volatile matter content of the coals tested in the Research Boiler ranged from 20 to 46 wt.% on a dry basis. Table 2 shows the operating conditions for the tests. The combustion efficiency reported in the Table was calculated using Ash Tracer Technique. NO_x emissions in lb/MMBtu were calculated per the 40 CFR, Part 75.

Table 2. Summary of the test conditions and flue gas emissions

Parameter	Test 1	Test 2	Test 3	Test 4	Test 5	Test 6	Test 7	Test 8	Test 9	Test 10
Firing Rate (MMBtu/h)	1.71	1.6	1.6	1.5	1.57	1.63	1.61	1.6	1.6	1.6
Combustion Air Flow (lb/h)	794	699	716	681	655	773	863	757	667	665
Tertiary Air Flow (lb/h)	420	278	320	301	420	411	420	420	420	419
Coal Transport Air Flow (lb/h)	108	118	144	118	108	108	113	111	108	120
Flue Gas Composition (O_2)	5.98	5.25	6.29	5.54	6.73	6.55	6.72	6.07	6.12	5.83
CO (ppmv)	111	93	85	53	103	90	70	111	92	42
CO_2 (%)	12.67	13.27	12.7	13.67	12.4	12.6	12.6	13.09	13.06	13.17
SO_2 (ppmv)	400	290	227	45	344	348	249	364	329	45
NO_x (ppmv)	612	616	635	551	556	604	662	554	506	394
SO_2 @ 3% O_2 (ppmv)	480	331	277	53	434	433	314	439	398	295
NO_x @ 3% O_2 (ppmv)	734	705	777	642	702	753	835	668	612	467
NO_x emissions (lb/MMBtu)	0.96	1.03	1.23	1.08	0.98	1.07	1.22	0.97	0.96	0.87
Combustion Efficiency (%)										

* Test1-100% Indonesian coal; Test #2-80% PA coal/20% Indonesian coal; Test #3-50% PA coal/50% Indonesian coal; Test #4-100% Pennsylvania Coal; Test #5-80% PA coal/20% Colorado coal; Test #6-50% PA coal/50% Colorado coal; Test #7-100% Colorado coal; Test #8- 80% PA coal/20% PRB coal; Test #9-50% PA coal/50% PRB coal; Test #10-100% Powder River Basin coal

It can be seen from Table 2 that most the tests were conducted with similar air staging. It has been reported that for conventional unstaged combustion, an increase of NO_x emission with an increase of the amount of volatile matter, whereas, for low- NO_x configuration, NO_x decreased with increase in volatile matter. Several other researchers also established the importance of parameters like volatile content and Fuel Ratio (Fixed Carbon to Volatile matter Ratio) (Carpenter, 1995; Monroe et al., 1997; Rozendaaal et al., 1997). In addition to the NO_x emissions, carbon burnout was also correlated with volatile matter and Fuel Ratio. Figure 2 shows the influence of volatile matter on the NO_x emissions (lb/MMBtu) of the parent coals. In another current study being conducted in The Combustion Laboratory, it was observed that for a suite of five bituminous coals (with unstaged and staged air) the NO_x emissions decreased with increase in volatile matter (Pisupati, 1997b).

It can be seen from the Figure that the ASTM volatile matter content is not a good indicator of NO_x emissions for this suite of coals. The NO_x emissions for the Colarado coal and Indonesian coals are higher than the Pennsylvania coal inspite of the higher volatile matter content. However, for the PRB coal the NO_x emissions were lower than the Pennsylvania coal. Figure 3 shows the NO_x emissions of parent coals and blends with PA coal.

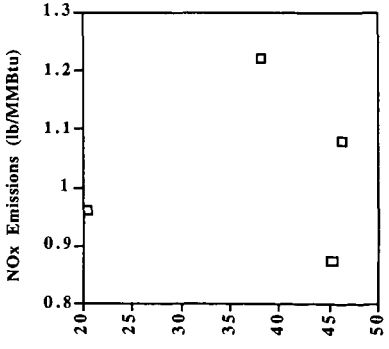

Figure 2. NOx Emissions as a function of volatile matter of the parent coals

It can be observed from Figure 4 that the NO_x emissions in general tend to increase with the nitrogen content in the fuel. Nitrogen content of the fuels appears to be an important property for predicting NO_x emissions. To study the distribution of nitrogen between the volatiles and char

phases, chars were generated from the parent coals at 950 °C and were analyzed for the nitrogen content and heating value. Table 3 provides the analysis of the chars of the four coals. From the data, the fraction of nitrogen in the volatiles and the calorific value of the volatiles was computed.

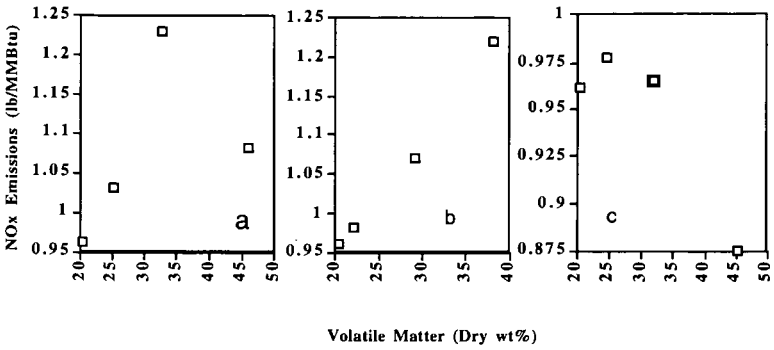

Figure 3. NOx emissions of the parent coals and blends a) Indonesian and PA coals; b) Colorado and PA coals; c) PRB and PA coals

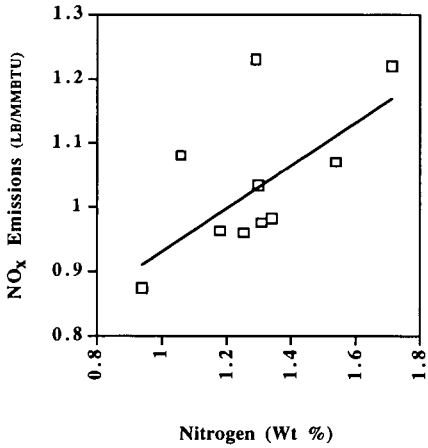

Figure 4. NO_x emissions as a function of fuel nitrogen content

Figures 5 shows the nitrogen content and the calorific value of the volatiles as a function of the volatile matter. It can seen from the plot that higher the amount of volatiles released, higher is the amount of nitrogen associated with the volatiles and lower is the calorific value of the volatiles. Lower calorific value of the volatiles is due to the higher oxygen and moisture content of the coals. This also implies that the volatile are leaner in combustible hydrocarbons capable of reducing the nitrogen oxides to nitrogen. The volume of the inert species increases the velocity and thereby the residence time in the ceramic quarl used in the study. The higher nitrogen content of the volatiles (especially lower rank higher moisture fuels) therefore, results in higher NO_x emissions. Data in Table 2 show that as the percent Indonesian or Colorado or PRB coal is increased there is an increase in the combustion efficiency of the blend. The results also showed, as expected, that the average SO_2 emissions are also lower for the blends with increasing percent Indonesian or Colorado, or PRB coals.

Table 3. Properties of the chars produced from the parent coals

Parameter	PA Coal	Indonesian Coal	Colorado Coal	PRB coal
Nitrogen (Wt.%)	1.30	1.34	1.61	1.37
Higher heating value of the char (Btu/lb)	11,463	13,482	11,467	12,055
Calculated HHV of the Volatiles (Btu/lb)	12,803	8,630	10,521	7,761

Effect of Coal Cleaning

A Pennsylvania coal with high ash content was cleaned by CQ Inc., to study the influence of cleaning on HAPs emissions. The ash content was reduced from 26.00 to 7.69% and sulfur from 1.87 to 1.47% on a dry basis. The cleaning process resulted in higher nitrogen content in the clean coal from (1.38% as opposed to 1.10% in the raw coal). Volatile matter contents of the raw and clean coals were 26.47 and 32.41%, respectively. Coals being of the same rank, the effects of nitrogen increase and volatile matter increase resulted in a marginal decrease in NO_x emissions from 1.00 lb/MMBtu to 0.9 lb/MMBtu.

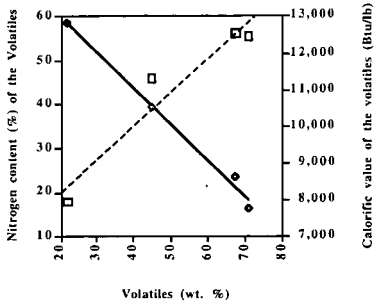

Figure 5. Nitrogen content and the calorific value of the volatiles of the parent coals

SUMMARY

NO_x emission behavior of a bituminous and three lower rank coals, and blends in various proportions was characterized. The results showed that the NO_x emissions vary significantly with volatile matter. Volatile phase nitrogen increased with the volatile matter. The calorific value of the volatiles was observed to decrease for coals with higher volatile matter (particularly high moisture, low rank coals). The study revealed that the quality of volatile matter is important than the quantity of volatile matter in predicting the influence of volatile matter on NO_x emissions particularly low rank coals. The results indicated that the average SO_2 emissions are lower for the blends with increasing percent low sulfur coals. The effect of coal cleaning on NO_x emissions was not significant because of the two opposing effects of higher fuel nitrogen and volatile matter contents in the clean coals.

ACKNOWLEDGMENT

The author thanks the Pennsylvania Electric Company for supplying the coal samples for the Research Boiler tests. The work on the DFC was performed for the Department of Energy under the cooperative agreement DE-FC22-92PC92162. The staff of The Combustion Laboratory generated some of the data.

REFERENCES

Carpenter, A. M., (1995) "Coal Blending for Power Stations" IEA Coal Research Report, IEA Coal Research, London, IEACR/81, July 1995, pp. 64-66.

Maier, H, Spliethoff, H., Kircherer, A., Fingerle, A., and Hein, K. R. G., (1994) "Effect of Coal Blending and Particle Size on Nox Emission and Burnout" Fuel, **73**, pp. 1447-1452.

Monroe, L.S., Clarkson, R.J., Stallings, J. W., (1997) "Reduced emissions from certain coal blends for utility boilers" EPRI-DOE Combined Utility Air Pollutant Control Symposium "The Mega Symposium, August 25-29, 1997; Washington, D.C.

Pisupati, S. V., Sharifi, R., Liu, Y., Scaroni, A.W. (1996) "Measurements of Temperature, Particle Size Distribution and Particle Speed in an Industrial Boiler" Proceedings of the Thirteenth Annual Pittsburgh Coal Conference, Pittsburgh, PA, Sept. 3 - 6, 1996, University of Pittsburgh, pp. 1297 - 1302.

Pisupati, S. V., Simons, G. A., Oehr, K. H., Zhou, J., (1997a) "Use of Biomass-based Product for Simultaneous NO_x and SO_2 Capture in Pulversized Coal Combustion Systems", Proceedings of the 9th International Conference on Coal Science, Essen, Germany, Vol. II, pp. 1791-1794 , 7-12 September 1997.

Pisupati, S.V. (1997b), unpublished data.

Rozendaaal, C. M., Witkamp, J.G., van Vliet, H. N., Vissers, A.M.C., (1997),"Impact of Coal Quality and Coal Blending on NOx Emissions for Two Pulverized Coal Fired Units", EPRI-DOE Combined Utility Air Pollutant Control Symposium "The Mega Symposium, August 25-29, 1997; Washington, D.C.

FUEL CHARACTERISTICS OF SEWAGE SLUDGE AND OTHER SUPPLEMENTAL FUELS REGARDING THEIR EFFECT ON THE CO-COMBUSTION PROCESS WITH COAL

Th. Gerhardt, R. Cenni, V. Siegle, H. Spliethoff, K.R.G. Hein
University of Stuttgart, IVD, Pfaffenwaldring 23, 70569 Stuttgart, Germany
Tel. / fax: #49-711-685-3395 / #49-711-685-3491

ABSTRACT

In the European countries, and especially in Germany, the co-combustion of biomass and waste materials together with coal in the power plants is expected to find wide application in the near future. At the IVD several kinds of supplemental fuels are tested to find out their combustion behaviour in different firing systems together with the regular fuels hard coal and lignite coal. The investigations were done in bench scale facilities for basic research but also up to pilot scale combustion rigs. In order to get information about destruction and formation of hazardous matter multiple variations of the combustion parameters were applied under conditions like those in industrial furnaces. In this paper characteristics of the fuels are compared according to immediate analysis, elementary analysis and analysis of the ash components. Combustion experiments were carried out with various portions of thermally dried municipal sewage sludge. The by-products of the combustion process were collected and balanced.

INTRODUCTION

The conversion of energy from fossil fuels into heat and electricity involves unavoidably the emission of CO_2 which is known as a greenhouse gas. The intention to reduce the amount emitted to the atmosphere leads first of all to the reduction of energy consumption. The next objective is to increase the efficiency of the energy conversion process which is successfully done by power plant development for a long time and up to a high standard in todays combustion systems. We can use now this high efficient facilities and substitute part of the coal input by CO_2-neutral biomass like straw and wood.
Also with co-fireing waste material similar effects can be obtained. Waste incinerator plants have to be prepared for various hazardous matter coming along with the inhomogeneous mixed waste material. The expenses to cover all possible compositions of waste in the combustion system and especially in the flue gas cleaning system lower the efficiency far below the standard of the power plants. For special kinds of waste which occur separately and show constant and homogeneous properties the co-combustion with coal equivalent to biomass can achieve higher yield of energy compared to the usual waste incineration systems. To ensure a disposal without higher risks for environment the composition of this waste materials has to be carefully checked regarding the contents of hazardous matter. Another reason to treat waste material in existing combustion facilities for power generation is the cost saving aspect. Additional equipment to co-fire the supplemental fuels can be limited to the storage, transport and dosing devices.

FUEL CHARACTERISTICS

At the IVD several research projects with a wide variety of experiments were carried out on this topic in the last years. Having started the co-combustion with biomass like straw and fresh cut wood the supplemental fuels changed to waste material like waste wood, municipal sewage sludge and plastic granulate etc. The main fuels were in principal German hard coals and in several places also German low rank coals (brown coal) have been used. **Table 1** shows an overview on the average fuel properties of supplemental fuels compared to those of the regular fuels and the mixed waste. The results of immediate analysis and elementary analysis are calculated to the base of dry substance in order to be comparable.
The typical municipal household waste delivered to the incineration plant has about 30 % moisture. The dry substance consists of nearly 50 % volatiles which is almost the complete amount of combustibles. Besides a small amount of fixed carbon the rest of the waste material is mineral substance determined as ash. The fuel called RDF is an abbreviation for refuse derived fuel and means a fraction of normal household waste where recyclable material is sorted out and which is ground to a homogeneous particle size for better handling in different combustion systems. The portion of ash decreased compared to the normal waste to a level of 14 % and therefore the lower heating value (LHV) is nearly double. This difference is even enlarged by lower moisture contents of about 15 % of the RDF.

A material normally included in the municipal waste is plastic. Due to separate waste collection or in industrial production processes this material sometimes occurs separately Known to have big energy content combustion can be a reasonable possibility to dispose mixed or minor quality fractions which are not worth to recycle into new products. The different kinds of plastic are very similar regarding their combustion properties. The high density polyethylene is taken as a sample to show them. Noticeable is that the complete dry substance consists of only volatile matter. Ash is missing totally except some reinforced materials with fibreglass [1].
As a by-product of the coke oven process the tar oil of hard coals was tested in the IVD furnace concerning its ability to reduce nitrogene oxides as a reduction fuel by fuel staging. Being a liquid fuel it offered best possibilities to optimize the mixing conditions in the reaction zones. So it showed very good results in minimization of hazardous matter with the primary measure, fuel staging [1]. On the other hand combustion under high temperature is a suitable method to dispose this carcinogenic organic substance.
Coming to the sewage sludge we see a supplemental fuel which is very similar in the fuel characteristics to straw and wood regarding only the organic share. The analysis shows the typical data of sludge from municipal waste water treatment. An obvious difference to straw and wood is the high ash content also responsible for the reduced LHV. As a product of a cleaning process the variation of single properties can be high and so the values shown in table are an average from 15 different sludges. Even if extreme deviations are possible the standard deviation is mostly in between ± 10 %. In the waste water treatment the sewage sludge is separated with a content of dry substance about 5 %. Mechanical dewatering by centrifuge or filter press are increasing that up to range between 20 and 45 %, according to a reduction of volume and weight of 80 to 90 %. For a longer storage and a better suitability to handle the sludge an additional thermal drying up to 90 % of dry substance is carried out in more and more cases.
The analysis for straw and wood are on behalf of a data base with more than 100 different kinds of biomass which can be roughly devided in this two groups. A closer description is given in a publication of V.Siegle in this conference [2]. As well these materials are the origins of the regular fossil fuels discussed as the main fuels in this context. During the coalification the biomass turned first to peat than to lignite and brown coal before hard coal and anthracite are formed. Due to this process the big content of volatile matter in biomass is transformed more and more into fixed carbon and the water content, about 50 % in the brown coal, is reduced by high pressure and temperature in the mines.
Figure 1 shows the energy content of the organic part of the fuels. At first sight an increasing fixed carbon content (waf) corresponding to a decreasing share of volatile matter in the combustibles as shown in **figure 2** increases also the lower heating value. This is correct for the group of biomass based fuels starting from straw going further to brown coal, hard coal, anthracite and char. If the origin of the organic substance however is different from the biomass deviations are noticeable. For the sewage sludge for example the higher content of volatile matter compared to the biomass is coming along with a higher energy content. The plastic material is totally different in its behaviour consisting 100 % of volatile matter it shows the maximum heating value of more than 40 MJ/kg.

EXPERIMENTAL

The IVD operates a 500 kW pilot scale test facility for pulverized coal combustion. It is a vertical furnace with an internal diameter of 0.7 m and an active length of 7 m. The chamber is completely water cooled and the first 4m beginning with the position of the burner on top are refractory lined. In the tests to be described in this paper especially the ash removal system is of interest. According to the industrial plants there is a bottom ash hopper for coarse particles and slag drops. The air preheater with the need of small flow rates to realize the heat transfer is the next step where particles are separated from the flue gas. The range of particle size collected here is starting from 10 µm up to 1 mm. Operation temperature therein is about 500°C on the side of the flue gas. The first separation of fly ash is done in a cyclone collecting particles in the range between 5 µm and 100µm at the temperature about 350°C. The fly ash in here has similar properties to that of electrostatic precipitators (ESP) in the power plant. Finally the flue gas passes a bag filter with an adjustable temperature up to 200°C. The fine dust found in this device is in several ways comparable to scrubber residues of large scale plants.
The purpose of the tests was to obtain knowledge about the changes in operation of the plant and in quality of the solid combustion residues by adding thermally dried municipal sewage sludge into the pulverized coal combustion system. Starting from the pure coal combustion sewage sludge was added in increasing share of 5, 10, 15, 20, and 25 % of the thermal input. The experiments were carried out for a duration of 10 to 20 hours at each adjustment and ash

balances were performed every 4 hours. Due to the high ash content, which is nearly 5 times that of the coal, and only one third of the energy content, every MW produced by sewage sludge causes 15 times the ash of the coal combustion. **Figure 3** shows the relation between the share of fuel mass flow and ash mass flow in dependence on the share of thermal power produced by the sewage sludge in the given combination of fuels.

RESULTS AND DISCUSSION

Figure 4 shows the 10 main elements in the ash of the coal in comparison with the contents of them in the sewage sludge ash. To find an influence of the co-combustion it is reasonable to look at those elements with a higher concentration and what is even more important with a difference in concentration between the two fuels. As a first example the iron was chosen because it is expected to show only small deviation from the theoretically calculated average concentrations in the ash fractions. Even no enrichment of iron species in dependence on particle size or separation temperature in the collecting devices are assumed. The results drawn in **figure 5** demonstrate this. The increasing line represents the theoretical average concentration of iron the combustion residue should have and the scattered points are showing the measured concentrations. The symbols distinguish between bottom ash, air preheater residue and fly ash out of the cyclone and the bag filter. It is obvious that there is no significant enrichment or volatilization of this element and the deviation characterizes the reliability of the measured data.
Two elements which are typically higher concentrated in the sewage sludge ash than in the coal are the calcium and the phosphorus. In order to avoid a higher risk of slagging and fouling these new components for the plant are of major interest. Thc calcium described in **figure 6** follows as well the line of theoretical average concentration. The triangles representing the bag filter concentrations are clearly below the average and the bottom ash together with the air preheater retains most of the calcium in the front part of the flue gas path. In theory the calcium is known to lower the ash melting point which can give an explanation for agglomeration of particles with enriched Ca-contents in the hot part of the facility. A different behaviour is determined for phosphorus which occurs only in sewage sludge. As we can see in **figure 7** the measurement of the filter samples clearly show an enrichment in the colder end of the flue gas way. Furthermore the calculated average concentration is not achieved. A possible explanation for the missing phosphorus can be given by species which are volatilizing during the combustion and condensate in any part of the pipe system. In cases like that the time to reach a steady condition regarding input and output may be much longer than the 20 hours maximum of the tests. To confirm this assumption concentrations of phosphorus will be measured in dependence on the duration of one experimental adjustment.
The strongest effect of enrichment in the colder part of the flue gas path is observed, as expected, with the mercury. Also the effect of volatilizing is clearly proofed by this example shown in **figure 8**. About 50 % of the mercury fed into the plant with fuels is leaving it as elementary Hg in the flue gas. The boiling point of Hg at 358°C is higher then the flue gas temperature in the stack, but in the range down to -39°C it is liquid and therefore it vaporizes partly into the flue gas atmosphere. A maximum saturation of mercury in air is given at 100 g/m3 if the temperature is 200°C. So there is no limitation caused by this effect. The 50 % of mercury captured in the fly ash are mainly bound in HgS and HgCl. The enrichment on the surface of the small particles in the bag filter is higher than that of any other measured component. Even so the biggest amount of the Hg in the residues was captured in the cyclone ash because there was found the biggest share of the ash mass flow.
Figure 9 shows an overview of the enrichment behaviour in the bag filter of the IVD plant for all substances measured in the solid residues. They are sorted in order of the calculated enrichment factor which compares the element concentration in the bag filter to the average concentration of every flame adjustment. The concentration in the bag filter is devided by the average concentration and 1 is substracted. So 0 means no enrichment, positive numbers are standing for a higher concentration in the filter and negative for a lower one. Finally the mean values over all of the adjustments are calculated and drawn in the diagram. The range of ± 20 % (-0.2 to0.2) can not proof a significant enrichment because of the scattering of the measurements. But especially the heavy metals found as trace elements in the fuels are determined to be found in higher concentrations in the filter. Some of the main ash components do also show any enrichment however not so distinct. Potassium, phosphorus and sodium concentrate in the filter and the calcium as mentioned is found more in the front of the flue gas path.
The distribution of ash between the various hoppers was about 20 % in the bottom ash hopper, 9 % in the air preheater and 16 % in the bag filter. The biggest amount was found in the cyclone

with 54 % of the whole ash. This distribution was constant even if the ash flow with the highest share of sewage sludge was almost five times that of the coal combustion.

CONCLUSIONS

The analysis of various materials intended to be used or disposed as supplemental fuels in coal fired power plants has shown that there is always a range of the results sometimes with a big gap between minimum and maximum. This is consistent especially with the natural products like biomass or any mixed waste material. Nevertheless the investigated fuels, biomass and municipal sewage sludge showed quite constant and homogeneous properties excepting some loads coming from any special treatment. A decreasing content of volatile matter in the organic part was coming along with an increasing heating value at least for the group of biomass originated fuels, peat and coal.

Most noticeable for the sewage sludge was the highest share of ash, nearly 50 % of the dry substance, compared to all the other fuels. In that score attention was turned to the behaviour of the compounds in ash during the combustion process. The increasing share of sewage sludge up to a level of 25 % of the thermal input, corresponding to 80 % sewage sludge ash in the whole ash, had no significant effect on the distribution between the different ash removal systems. Even if the ash amount is 5 times bigger than that of the coal combustion. The heavy metals Hg, Zn, Pb, Ni, Cu and Cd showed an enrichment in the bag filter at the end of the flue gas path which was only for the mercury clearly proportional to the sewage sludge share. The concentrations of the main ash-components are more consistent. The biggest difference between the ashes of sewage sludge and coal are the elements calcium and phosphorus which are found only or at least in a higher share in the sewage sludge. Only potassium, phosphorus and sodium are enriched in the fine ash of the filter. The calcium however is found in higher concentrations in the hoppers of the hot part of the facility.

For some elements significant amounts could not be measured in the solid residues. In case of the high volatile trace element mercury it is obvious that about 50 % of the input is leaving the plant in an elementary form via the stack with the flue gas. In case of the phosphorus vaporization and condensation of some species are suspected to hold back this element in the pipe system until a steady condition is achieved. Further measurements will have to confirm that.

REFERENCES

[1] Th. Gerhardt, R. Cenni, H. Spliethoff, K.R.G. Hein, University of Stuttgart, IVD: Combustion Behaviour of Coal-Waste Flames in Pulverized Fuel Firing Systems. Inflame-Measurements in a Pilot Scale Facility with Hard Coal and Dried Sewage Sludge; International Technical Conference on Coal Utilization and Fuel Systems; March, 1997, Clearwater, Florida, USA

[2] V. Siegle, H. Spliethoff, K.R.G. Hein, University of Stuttgart, IVD: Characterisation and Preparation of Biomass for Co-Combustion with Coal; American Chemical Society Division of Fuel Chemistry, Spring 1998 Meeting March 29 - April 2, Dallas, Texas, USA

Table 1: Analysisdata of biomass and waste material in comparison with German hard coal and brown coal

dry	Waste Samples								Coal Samples	
basis %	Munic. Waste	RDF	Plastic HDPE	Tar Oil	Sewage Sludge	Straw	Wood	Activ. Carbon	Hard Coal	Brown Coal
volatiles	48.6	80.4	100	87.5	46	79.5	80.5	6.2	34.7	49.4
ash	43.1	13.7	0	0.2	47.2	6	2	9.2	8.3	5
fix. C	8.3	5.9	0	12.3	6.8	14.5	17.5	84.6	57.1	45.9
LHV MJ/kg	12.3	22.9	42.9	37.7	11.3	17.4	18.7	30.3	30.2	25.6
C	31.9	58	86	85.5	27.5	46.8	50.9	89.5	72.5	67
H	4.12	7	14	5.93	3.8	5.4	5.7	0.7	5.6	4.9
N	0.4	0.8	0	0.64	3.3	1	0.5	0.5	1.3	0.7
S	0.6	0.2	0	0.6	1.4	0.1	0.1	0.2	0.9	0.4
Cl	1	1.1	0	n.a.	0.14	0.5	0.1	< 0.1	0.16	0.1
$O_{calculated}$	18.9	19.2	0	7.3	16.8	40.2	40.7	0	11.2	21.9

Figure 1: Energy content of fuels (waf)

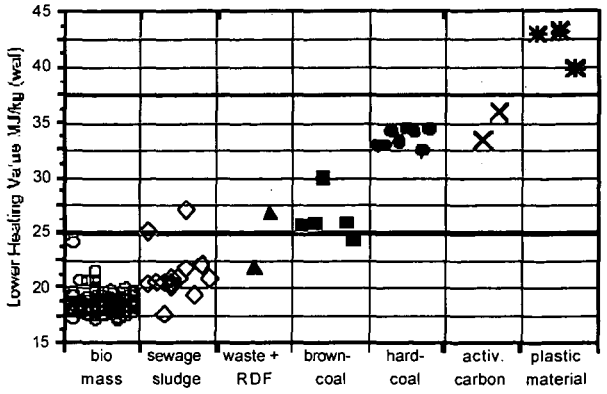

Figure 2: Content of volatile matter in the organic substance

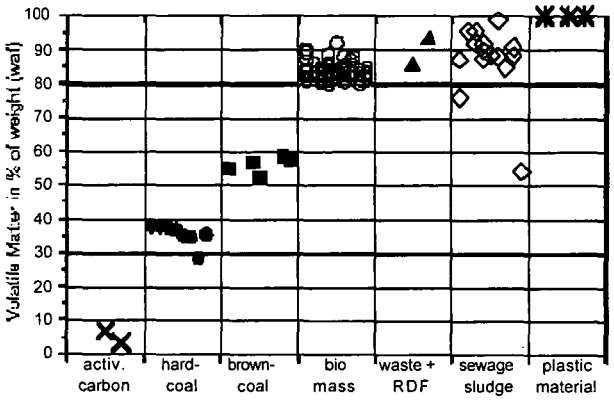

Figure 3: Relation between share of fuel mass, ash amount and share of thermal power

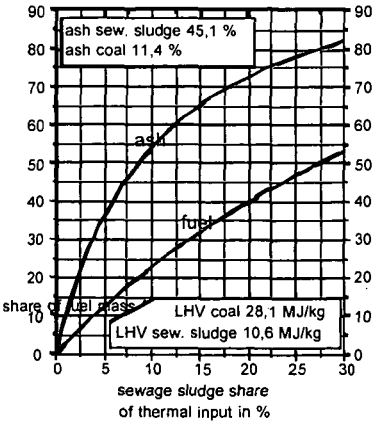

Figure 4: Elements in the ash of sewage sludge and hard coal.

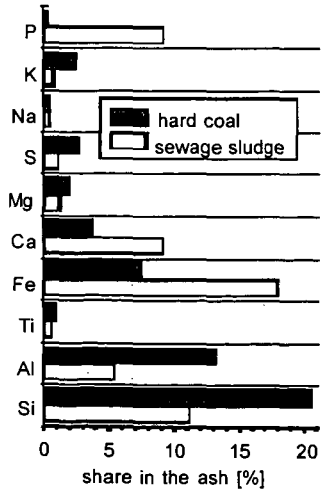

Figure 5: Iron concentration in the ash

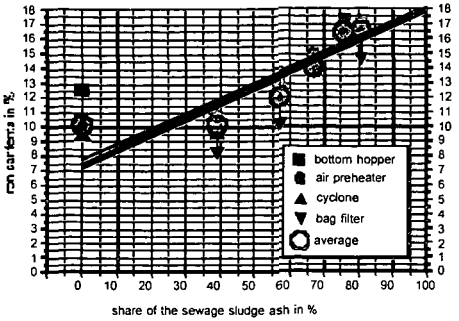

Figure 6: Calcium concentration in the ash

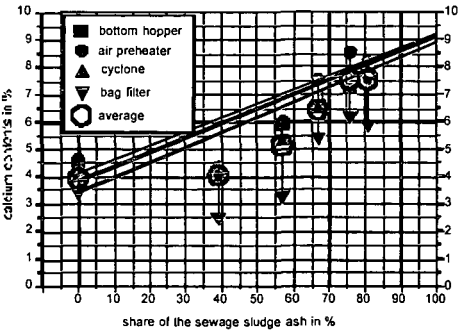

Figure 7: Phosphorus concentration in the ash

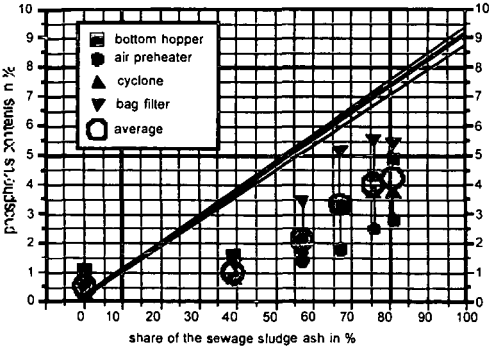

Figure 8: Mercury concentration in the ash

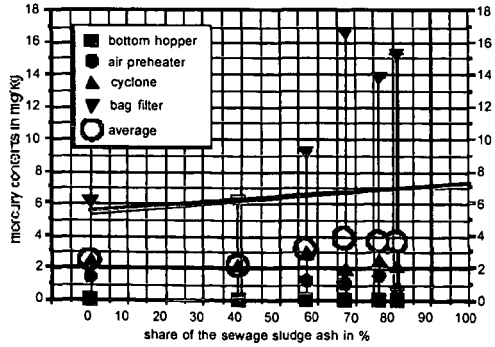

Figure 9: Enrichment of elements in the bag filter

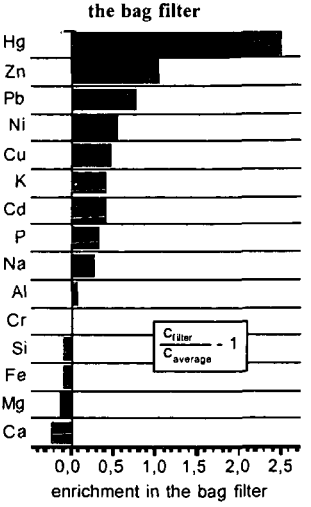

CHEMICAL STRUCTURE OF COAL TAR DURING DEVOLATILIZATION USING SOLID-STATE ^{13}C NMR

E. M. Hambly[1], T. H. Fletcher[1], M. S. Solum[2], and R. J. Pugmire[3]

[1]Department of Chemical Engineering Brigham Young University, Provo, Utah 84602
Departments of Chemistry[2] and Chemical and Fuels Engineering[3], University of Utah, Salt Lake City, Utah 84112

Keywords: coal, pyrolysis, ^{13}C NMR

Introduction

Recent advancements in chemical analysis techniques have allowed quantitative investigations of the chemical structure of both coal and its pyrolysis products.[1-2] Solid-state ^{13}C NMR spectroscopy has proven particularly useful in obtaining average values of chemical structure features of coal and char, while liquid phase ^{1}H NMR spectroscopy has been used to determine some of the chemical features of coal tar.[3-6]

Watt et al.[7] performed pyrolysis experiments on 3 coals at 930 K, and reported solid-state ^{13}C NMR analyses of the coals and chars and liquid ^{13}C NMR analyses of the corresponding tars. Tars were dissolved in deuterated methylene chloride (CD_2Cl_2) prior to analysis. The non-soluble tar portion was analyzed with standard solid-state ^{13}C NMR techniques.[7] The soluble tar portion was analyzed using a high resolution ^{13}C NMR technique developed for liquid phases.[7] The liquid ^{13}C NMR data, as well as the composite tar data, indicated that the chemical structure of the tar was significantly different from the original coal. The number of bridges and loops per cluster in the tar was found to be much lower than that of either the coal or the char. Additionally, the number of aromatic carbons per cluster in the tar was found to significantly lower than that of the coal or char. These data were in major disagreement with key assumptions in current network devolatilization models. Watt's data were subject to question based on (a) the use of a solvent prior to analysis of the tar, and (b) collection of tar at such low temperatures where devolatilization was not complete (e.g., ~38% mass release for an Illinois #6 coal). The experiments reported here were performed at a higher temperature (and hence higher degree of pyrolysis). The resulting tars were analyzed as received with standard solid-state ^{13}C NMR techniques.

Experimental Apparatus

Samples of tar and char were produced at atmospheric pressure in a laminar flow drop tube reactor similar to that used by Watt.[7-8] The tars and aerosols are collected on polycarbonate filters so that tar samples can be scraped from the filters rather than removed using a solvent. Coals were pyrolyzed at atmospheric pressure in 100% nitrogen at a gas temperature of 1080 K with a residence time of 282 ms. This temperature has chosen since it provides a high degree of pyrolysis while minimizing secondary reactions of the resulting tar. Five coals of different rank were examined, with properties listed in Table 1. The 63-75 μm size fraction was used in all of these experiments, resulting in heating rates of approximately 10^4 K/s. The "D" on the Penn State coal identification number signifies coals from a suite selected by the DOE Pittsburgh Energy Technology Center's Direct Utilization/AR&TD program. These coals have been well characterized and studied by many other researchers.[4,7-12]

Results and Discussion

A summary of the pyrolysis yield data and elemental composition of the tar is provided in Table 2. As expected, the volatiles yields are high; the coals are nearly completely devolatilized. In addition, the shape of the total volatiles and tar yield curves versus rank are as expected, with relatively constant values from lignite through the high volatile bituminous coal, then dropping for the low volatile bituminous coal.[3-5,11-12,13-16] Elemental analyses of the corresponding chars are currently under way.[17]

Solid state ^{13}C NMR techniques (CP/MAS and dipolar dephasing) were used to determine the chemical structural features of coals and coal tars.[3,18] The solid-state ^{13}C NMR data for the tars are presented in Tables 3 and 4, along the corresponding analyses of the coals. The composite tar data from Watt[7-8] are also presented for comparison. Comparing the NMR data for the tar and the coal provides insight into the nature of the structural changes that occur during pyrolysis. The carbon aromaticity (f_a) of the tar is 14 to 53 percent higher than in the parent coal (on a relative basis). In general, the aromaticity of the tars seems to increase slightly with coal rank.

The values of the average number of aromatic carbons per cluster (C_{Cl}) in the tar range from 9 to 16 (see Figure 1). With the exception of the lignite, the value of C_{Cl} in the tar is similar to that of the corresponding parent coal. The data reported by Watt et al.[7] are also shown here, with C_{Cl} values of the composite tar ranging from 8 to 11. The solid-state tar data reported here

are thought to be less prone to error than the data from the liquid-phase analysis. Based on these new data, it appears that errors may be generated in using a solvent. These new data on tar help to confirm the assumption that the values of C_{Cl} in the tar are equal to those in the parent coals, an assumption that is used extensively in the network coal pyrolysis models.[19]

The number of side chains per cluster (S.C.) in the tar is much lower than in the corresponding coals (see Table 4). In the parent coals, the values of S.C. decrease with rank, while this trend is not seen in the resulting tars. The values of S.C. from the liquid-phase analysis were slightly higher than the values from the solid-state analysis, but still much lower than in the parent coal. The fact that the number of aromatic carbons per cluster are similar for both coal and tar and that the number of side chains per cluster is greatly lower in the tar is consistent with the increased aromatieity in the tars.

The number of attachments per cluster (σ+1) in the tar is less than in the parent coal, as shown in Table 4. The liquid-phase analysis yielded values of σ +1 that were slightly lower than observed from the solid-state analysis. Interestingly, while σ+1 varies with coal type for the parent coals, σ+1 is nearly constant with coal type for the tars. The number of bridges and loops per cluster (B.L.) in the tar is higher than in the corresponding coal, as shown in Table 4, although the increase is slight for the Illinois #6 coal. In contrast, the liquid phase analysis reported values of B.L. that were much lower than in the parent coal. For all coals, the average cluster molecular weight (MW_{Cl}) in the tars is lower than in the parent coals (see Figure 2). This was also seen in the liquid-phase analysis. The values of MW_{Cl} in the coals decrease with increasing rank; this trend is not seen in the tars. Except for the Beulah Zap lignite, the MW_{Cl} in the tars is relatively constant with rank. Several sets of data indicate that tar molecular weight distributions peak in the range of 250 to 400 daltons.[11,20-21] The tars in this study have molecular weights per cluster in the range of 170 to 240 daltons. This discrepancy seems to indicate the presence of species in some of the reported tar data that contain more than one cluster (i.e., dimers and trimers rather than monomers); whereas the data reported in this work is based on the average molecular weight of monomer units. The slight increase in the number of bridges and loops per cluster (B.L.) in the tar may indicate that some form of polymerization may have occurred in the tars. This result would be consistent with the presence of dimers in the tar and would rationalize the differences in the mass of the monomer units defined by the NMR data and that reported by other investigators using different analytical techniques that do not define the basic monomer unit.

As seen in Figure 3, the average molecular weight of side chains (MW_δ) in the tar is much lower than that found in the parent coals. This result is different than that reported with the liquid-state analysis. While MW_δ decreases steadily with rank, in the coals, MW_δ in the tars is relatively constant with rank, within the experimental error of the data.

The main difference between the solid-state analysis and the liquid phase analysis seems to be in the number of side chains per cluster, which influences the aromaticity as well as the number of attachments per cluster. The fact that the liquid-phase analyses of tars dissolved in solvent produced NMR results that were quite different from the solid-state analyses seems to indicate that the use of solvents (such as CH_2Cl_2) prior to other types of tar analysis may give misleading results.

The chemical structure of these tars, as determined from solid-state ^{13}C NMR spectroscopy, do not vary greatly with coal rank. The greatest differences seem to be in the tars from the lignite. However, large differences in tar yield are seen as a function of coal rank, as expected. The similarity in chemical structure of the coal tars is somewhat surprising since large differences are seen in the elemental composition of these tars. Additional experiments are underway to determine the chemical structural features of tars obtained at different temperatures and to compare the results with the corresponding chars.[21]

Conclusions

Standard solid-state ^{13}C NMR techniques were used to analyze coal tar from five coals of different rank. This is the first set of solid-state data for coal tar. Tar was produced at atmospheric pressure in a drop tube reactor at a temperature of 1080 K and a residence time of 282 ms. The parent coals were also analyzed for comparison using solid-state ^{13}C NMR.

The tars analyzed in this study represent a nearly completely devolatilized coal. Previous data from liquid-phase ^{13}C NMR analyses of tars of partially devolatilized coals were compared with new solid-state analyses. These new tar data indicate that there may be significant errors associated with using solvents to study tar structure. Since tars from the two experiments were not obtained at the same temperature, it is recommended that low temperature pyrolysis experiments be performed and the tars analyzed with solid-state ^{13}C NMR techniques.

These new ^{13}C NMR data on coal tars indicate that the average chemical structure of tar does not vary greatly with coal type under the conditions used in this study, with the largest differences found in lignites, even though the variation in the chemical structures of the parent coals is much more significant.

Table 1
Coal Properties

Coal	PSOC ID	Rank	%C (daf)	%H (daf)	%N (daf)	%S (daf)	%O (daf) (by diff.)	%Ash (dry)
Beulah Zap	1507D	ligA	64.16	4.78	0.94	1.81	28.32	13.92
Blue #1	1445D	subA	74.23	5.48	1.30	0.65	18.35	3.29
Illinois #6	1493D	hvCb	74.81	5.33	1.48	4.85	13.54	9.65
Pittsburgh #8	1451D	hvAb	82.77	5.61	1.74	0.98	8.90	4.29
Pocahontas #3	1508D	lvb	90.92	4.51	1.34	0.82	2.41	11.92

Table 2
Pyrolysis Yields and Tar Elemental Composition

Coal	Vol. (% of daf coal)	Tar (% of daf coal)	%C	%H	%N
Beulah Zap	54.36	1.51	78.71	4.90	1.30
Blue #1	57.67	10.92	83.61	4.85	1.68
Illinois #6	59.91	12.47	85.23	4.89	1.80
Pittsburgh #8	46.24	19.92	87.68	4.94	1.96
Pocahontas #3	24.89	7.33	92.13	4.87	1.34

Table 3
^{13}C NMR Analysis of Coals and Tars[a]

Coal	Sample	f_a	f_a^C	$f_{a'}$	f_a^H	f_a^N	f_a^P	f_a^S	f_a^B	f_{al}	f_{al}^H	f_{al}^*	f_{al}^O
Beulah Zap	coal	65	8	57	19	38	7	14	17	35	24	11	11
Beulah Zap	tar	88	7	81	36	45	11	22	12	12	7	5	2
Blue #1	coal	60	5	55	19	36	8	13	15	40	29	11	7
Blue #1	tar	88	4	84	35	49	8	18	23	12	6	6	1
Watt Blue #1	tar*	64	7	57	27	31	8	16	7	36	27	10	na
Illinois #6	coal	66	3	63	21	42	7	16	19	34	24	1	8
Illinois #6	tar	88	2	86	36	50	7	19	24	12	6	6	1
Watt Illinois #6	tar*	74	3	71	35	36	6	16	14	26	17	9	na
Pittsburgh #8	coal	65	3	62	23	39	5	16	18	35	24	11	7
Pittsburgh #8	tar	86	2	84	36	48	5	18	25	14	7	7	2
Watt Pitt #8	tar*	73	2	70	37	33	6	16	12	28	18	10	na
Pocahontas #3	coal	78	1	77	32	45	2	15	28	22	15	7	7
Pocahontas #3	tar	89	1	88	38	50	3	18	29	11	7	4	2

[a] Percentage carbon (error): f_a = total sp^2-hybridized carbon (±3); $f_{a'}$ = aromatic carbon (±4); f_a^C = carbonyl, $\delta > 165$ ppm (±2); f_a^H = aromatic with proton attachment (±3); f_a^N = nonprotonated aromatic (±3); f_a^P = phenolic or phenolic ether, δ = 150-165 ppm (±2); f_a^S = alkylated aromatic δ = 135-150 ppm(±3); f_a^B = aromatic bridgehead (±4); f_{al} = aliphatic carbon (±2); f_{al}^H = CH or CH_2 (±2); f_{al}^* = CH_3 or nonprotonated (±2); f_{al}^O = bonded to oxygen, δ = 50-90 ppm (±2). *Composite values reported by Watt et al.[7]

Table 4
Derived Properties of Coal and Tar[b]

Coal	Sample	χ_b	C_{Cl}	σ+1	P_o	B.L.	S.C.	MW_{Cl}	MW_δ
Beulah Zap	coal	0.246	14	5.2	0.48	2.4	2.8	440	52
Beulah Zap	tar	0.148	9	3.7	0.85	3.2	0.5	170	16
Blue #1	coal	0.270	13	5.0	0.48	2.4	2.6	371	42
Blue #1	tar	0.274	13	4.0	0.77	3.1	0.9	222	15
Watt Blue #1	tar*	0.112	8	3.2	0.58	1.8	1.4	205	35
Illinois #6	coal	0.300	15	5.5	0.52	2.9	2.6	368	35
Illinois #6	tar	0.279	13	3.9	0.77	3.0	0.9	213	13
Watt Illinois #6	tar*	0.197	11	3.4	0.56	2.0	1.3	228	30
Pittsburgh #8	coal	0.290	14	4.8	0.48	2.3	2.5	323	32
Pittsburgh #8	tar	0.298	14	3.8	0.70	2.7	1.1	228	14
Watt Pitt #8	tar*	0.163	9	2.8	0.52	1.5	1.3	178	25
Pocahontas #3	coal	0.364	18	4.0	0.59	2.3	1.7	316	23
Pocahontas #3	tar	0.330	16	3.8	0.81	3.1	0.7	237	10

[b] χ_b= fraction of bridgehead carbons, C_{Cl}= aromatic carbons per cluster, σ+1 = total attachments per cluster, P_o = fraction of attachments that are bridges, B.L. = bridges and loops per cluster, S.C. = side chains per cluster, MW_{Cl} = the average molecular weight of an aromatic cluster, MW_δ = the average molecular weight of the cluster attachments. *Composite values reported by Watt et al.[7]

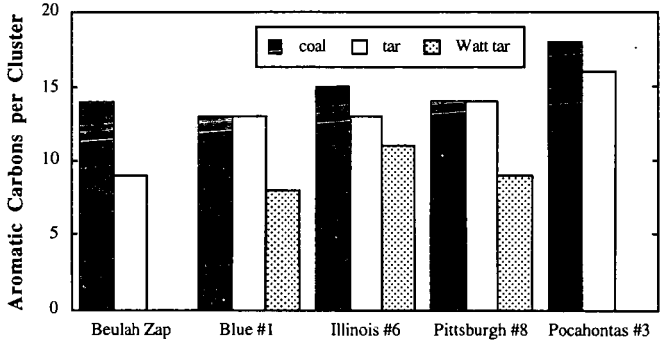

Figure 1. Aromatic carbons per cluster (C_{Cl}) in coal and tar. Previously reported data from Watt et al.[7] are shown for comparative purposes.

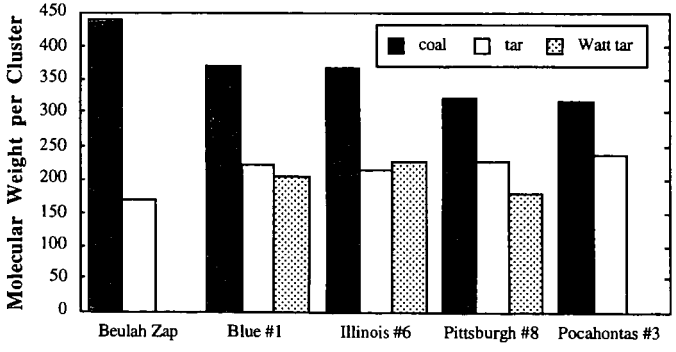

Figure 2. Molecular weight per cluster (MW_{Cl}) in coal and tar. Previously reported data from Watt et al.[7] are shown for comparative purposes.

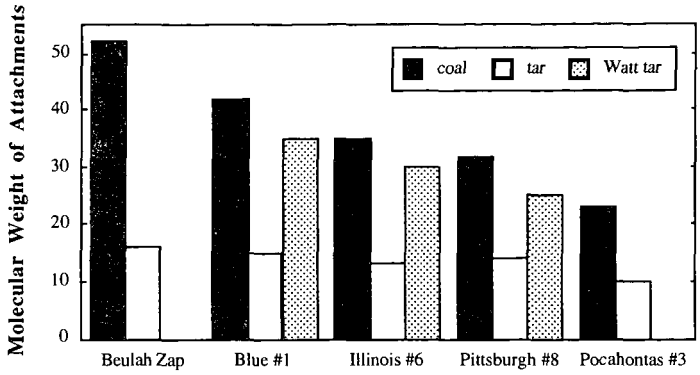

Figure 3. Molecular weight of cluster attachments (MW_δ) in coal and tar. Previously reported data from Watt et al.[7] are shown for comparative purposes.

References

1. Miknis, F. P., Turner, T. F., Ennen, L. W. and Netzel, D. A., *Fuel* 67:1568-1577 (1988).
2. Vasallo, A. M., Wilson, M. A., Edwards, J. H., *Fuel* 66:622-626 (1987).
3. Solum, M. S., Pugmire, R. J. and Grant, D. M., *Energy and Fuels* 3:187 (1989).
4. Fletcher, T. H., Solum, M. S., Grant, D. M., Critchfield, S. and Pugmire, R. J., *23rd Symposium (International) on Combustion*; The Combustion Institute, Pittsburgh, PA, **1990**; pp 1231.
5. Pugmire, R. J., Solum, M. S., Grant, D. M., Critchfield, S. and Fletcher, T. H., *Fuel* 70:414 (1991).
6. Fletcher, T. H., Solum, M. S., Grant, D. M. and Pugmire, R. J., *Energy and Fuels* 6:643-650 (1992).
7. Watt, M., Fletcher, T. H., Bai, S., Solum, M. S., and Pugmire, R. J., *26th Symposium (International) on Combustion*, The Combustion Institute, Pittsburgh, PA, **1996**.
8. Watt, M., The Chemical Structure of Coal during Devolatilization, M. S. Thesis, Chemical Engineering Department, Brigham Young University (1996).
9. Chen, J. C. "Effect of Secondary Reactions on Product Distribution and Nitrogen Evolution from Rapid Coal Pyrolysis," Stanford University, HTGL Report No. T-280 (1991).
10. Freihaut, J. D. and Proscia, W. M., *Energy & Fuels* 3:625 (1989).
11. Freihaut, J. D., Proscia, W. M. and Seery, D. J., *Energy and Fuels* 3:692-703 (1989).
12. Fletcher, T. H. and Hardesty, D. R., "Milestone Report for DOE's Pittsburgh Energy Technology Center," contract FWP 0709, Sandia Report No. SAND92-8209, available NTIS (1992).
13. Solomon, P. R., Fletcher, T. H. and Pugmire, R. J., *Fuel,* 72: 587-597 (1993).
14. Fletcher, T. H., *Combust. Sci. Tech.* 63:89 (1989).
15. Fletcher, T. H., *Combust. Flame* 78:223 (1989).
16. Fletcher, T. H., Kerstein, A. R., Pugmire, R. J. and Grant, D. M., *Energy and Fuels* 6:414 (1992).
17. Hambly, E. M., The Chemical Structure of Coal during Devolatilization, M. S. Thesis (in progress), Chemical Engineering Department, Brigham Young University (1997)).
18. Orendt, A. M., Solum, M. S., Sethi, N. K., Pugmire, R. J. and Grant, D. M., *^{13}C NMR Techniques for Structural Studies of Coals and Coal Chars,* In Advances in Coal Spectroscopy, H. L. C. Meuzelaar, Ed., Plenum Press, New York , pp 215-254 (1992).
19. Smith, K. L., Smoot, L. D., Fletcher, T. H., Pugmire, R. J., *The Structure and Reaction Processes of Coal*, Plenum, New York (1994).
20. Solomon, P. R., Serio, M. A., Despande, G. V. and Kroo, E., *Energy and Fuels* 4:42-54 (1990).
21. Simmleit, N., Yun, Y., Muezelaar, H. L. C. and Schulten, H. R., *Thermochemical Analysis of U.S. Argonne Premium Coal Samples by Time-Resolved Pyrolysis Field Ionization Mass Spectrometry,* In Advances in Coal Spectroscopy, Plenum, New York (1992).